INFORMATION TO USERS

This manuscript has been reproduced from the microfilm master. UMI films the text directly from the original or copy submitted. Thus, some thesis and dissertation copies are in typewriter face, while others may be from any type of computer printer.

The quality of this reproduction is dependent upon the quality of the copy submitted. Broken or indistinct print, colored or poor quality illustrations and photographs, print bleedthrough, substandard margins, and improper alignment can adversely affect reproduction.

In the unlikely event that the author did not send UMI a complete manuscript and there are missing pages, these will be noted. Also, if unauthorized copyright material had to be removed, a note will indicate the deletion.

Oversize materials (e.g., maps, drawings, charts) are reproduced by sectioning the original, beginning at the upper left-hand corner and continuing from left to right in equal sections with small overlaps.

Photographs included in the original manuscript have been reproduced xerographically in this copy. Higher quality 6" x 9" black and white photographic prints are available for any photographs or illustrations appearing in this copy for an additional charge. Contact UMI directly to order.

ProQuest Information and Learning
300 North Zeeb Road, Ann Arbor, MI 48106-1346 USA
800-521-0600

UMI®

Université d'Ottawa · University of Ottawa

The Role of C-S-H Microstructure and Calcium Hydroxide on Creep and Shrinkage of Hardened Portland Cement Paste

Basile Tamtsia Tamboue

B.A.Sc. (Moncton), M.A.Sc. (Sherbrooke)

A Dissertation submitted to

School of Graduate Studies

In partial fulfillment of the requirements for the degree of

Doctor of Philosophy in Civil Engineering

Department of Civil Engineering

Faculty of Engineering

University of Ottawa

Ottawa, Canada, K1N 6N5

The Doctor of Philosophy in Civil Engineering is a joint program between Carleton University and the University of Ottawa, which is administrated by Ottawa-Carleton Institute for Civil Engineering

© Basile Tamtsia Tamboue, Ottawa, Canada, January 2001

National Library of Canada
Acquisitions and Bibliographic Services
395 Wellington Street
Ottawa ON K1A 0N4
Canada

Bibliothèque nationale du Canada
Acquisitions et services bibliographiques
395, rue Wellington
Ottawa ON K1A 0N4
Canada

Your file Votre référence

Our file Notre référence

The author has granted a non-exclusive licence allowing the National Library of Canada to reproduce, loan, distribute or sell copies of this thesis in microform, paper or electronic formats.

L'auteur a accordé une licence non exclusive permettant à la Bibliothèque nationale du Canada de reproduire, prêter, distribuer ou vendre des copies de cette thèse sous la forme de microfiche/film, de reproduction sur papier ou sur format électronique.

The author retains ownership of the copyright in this thesis. Neither the thesis nor substantial extracts from it may be printed or otherwise reproduced without the author's permission.

L'auteur conserve la propriété du droit d'auteur qui protège cette thèse. Ni la thèse ni des extraits substantiels de celle-ci ne doivent être imprimés ou autrement reproduits sans son autorisation.

0-612-68002-9

Canada

Dedicated to my beloved parents

ACKNOWLEDGEMENTS

The author is indebted to Dr. Jim Beaudoin, Principal Research Officer at National Research Council-Institute for Research in Construction and Adjunct Professor at University of Ottawa, Department of civil Engineering, under whose supervision of the work described herein was conducted.

Technical help from Messrs. Robert E. Myers, Gordon Chan and Garry Polomark is also gratefully acknowledged. The author would also like to express appreciation to the team of research and technical officers at the Materials Laboratory, Institute for Research in Construction, National Research Council Canada, where this research was conducted.

Thanks also belong to Dr. Franz Josef Ulm, associate professor at MIT for his helpful discussions in the course of this research.

The financial support of the Natural Sciences and Engineering Research Council of Canada (NSERC) is gratefully acknowledged.

Abstract

The thesis provides new research related to the mechanisms of creep and shrinkage of hardened Portland cement paste. The emphasis is put on the role of calcium silicate hydrate (C-S-H) microstructure and calcium hydroxide the most important phases in hydrated Portland cement paste.

Specially designed specimens were used for creep and shrinkage measurements. These were well hydrated and very thin in order to avoid the occurrence of moisture gradients during the drying process. Length change of specimens following organic solvent exchange was used as a microstructural probe. Length change data of compacted CH powder, pre-conditioned from 11% to 85% relative humidity, are presented in order to support inferences on the role of CH in cement paste. Similar measurements were conducted on Portland cement and tri-calcium silicate pastes. It is suggested that the length change on removal of water may be related to surface energy changes not always specific to the C-S-H phase alone. Mass change measurements versus time during exchange were carried out to support the interpretation of the length change behavior.

The re-saturation of Portland cement paste systems with synthetic pore solution after several drying pre-treatments was adopted to facilitate electrical measurements in order to investigate the shrinkage, creep, and creep recovery behavior. The state of the water in each pre-treated specimen was characterized using the DTGA methods. The coupling of a.c. impedance spectroscopy (ACIS) and creep and shrinkage measurements established ACIS as an effective method for evaluating pore structure modification as well as the nature of changes to the pore network of cement paste during creep and shrinkage experiments. Cement paste specimens from which all evaporable water was completely removed were found to creep a significant amount contrary to the hypothesis that they should not creep at all. The compacted calcium hydroxide specimens were found to creep with a creep coefficient less than one. This suggested that calcium hydroxide makes a contribution to the overall deformation of cement paste systems.

TABLE OF CONTENTS

PAGE

LIST OF TABLES

PAGE

LIST OF FIGURES

PAGE

GLOSSARY

hcp	hydrated cement paste
C-S-H	calcium silicate hydrates
CH	calcium hydroxide
C/S or c/s	calcium to silicate ratio
w/c	water cement ratio
C_3S	tricalcium silicate (alite)
D-dry	drying at 105°C for 3 hours
DTA	differential thermal analysis
TGA	thermogravimetric analysis
DTGA	differential or derivative thermogravimetric analysis
DSC	differential scanning calorimetry
TEM	transmission electron microscopy
SEM	scanning electron microscopy
MIP	mercury intrusion porosimetry
SA	surface area
GPC	gas permeation chromatography
GA	gas adsorption
LAXRS	low-angle X-ray scattering
TMS	trimethylsilylation
RH or rh	relative humidity
I85	compacts pre-conditioned at 85% RH then immersed in isopropanol
M85	compacts pre-conditioned at 85% RH then immersed in methanol
CH20	compacts prepared at 20 kilo-lbs. loading
CH60	compacts prepared at 60 kilo-lbs. loading
CH100	compacts prepared at 100 kilo-lbs. loading
DMSO	dimethylsulfoxide
DDAL	diallyldimethylammonium
E_o	initial modulus of elasticity
ε_{co}	initial creep strain
ε_c	total creep strain
ε_{cc}	creep strain induced by sustained load only

ε_{sh}	shrinkage strain
α_{do}	degree of hydration at loading
α_d	degree of hydration
$f_{\alpha d}$	fractional increase in degree of hydration
σ	applied load or stress
J_o	initial compliance of the hardened cement system
$J(t, t_o)$	compliance of the hydrated cement system at age t when loaded at t_o
$\tau=t-t_o$	elapsed time under loading
$dJ(t,t_o)/dt$	compliance rate
$\Phi(t, t_o)$	creep coefficient of the material at age t when loaded at t_o
ACIS	Alternating Current Impedance Spectroscopy
R_Ω or HFR	high frequency resistance
R_2, ϕ or HFA	high frequency arc diameter
n	depression angle parameter
K_p	bulk stiffness of the hydrated cement paste
K_{CH}	stiffness of calcium hydroxide
$K_{C\text{-}S\text{-}H}$	stiffness of calcium silicate hydrate
η_{CH}	viscosity of calcium hydroxide
$\eta_{C\text{-}S\text{-}H}$	viscosity of calcium silicate hydrates
a_L	lower coefficient limit of the compliance rate
a_U	upper coefficient limit of the compliance rate

DEFINITIONS

Bangham effect:	The length change associated with the change in surface free energy of a material.
Intercalation:	The process wherein water or other fluids e.g. methanol enters the interlayer spaces of C-S-H.
Perturbation:	This refers to an interaction of an adsorbate e.g. methanol with the solid surfaces of C-S-H. This can be the result of processes involving adsorption, chemisorption, intercalation or chemical reaction.
"Preserve":	This refers to the minimization of the effects of drying on the microstructure of C-S-H through the use of various solvents.

Part 1: Introduction

CHAPTER 1

INTRODUCTION

1.1 General

Creep and shrinkage of Portland cement systems (paste, mortar and concrete) are known to be phenomena of huge complexity. The operative mechanisms, after almost a century of wide investigation and despite several plausible theories, still remain obscure. They are, however, generally believed to be very sensitive to the process of curing, the surrounding environment, the specimen size, and especially the composition of concrete. These variables vary widely among different countries and laboratories.

Most of the current design methods for prediction of creep and shrinkage are based on tests combined and carried-out from different laboratories over many years. The use of short-term data to predict long-term creep and shrinkage of concrete may be suitable and it is of great interest for the design engineers. Such predictions assume a good knowledge of the behavior of cement paste binders and their constituents. New approaches for studying creep and shrinkage that minimize the moisture gradients within the specimen may provide insights and resolve uncertainties with respect to deformation mechanisms.

The recent knowledge of the calcium silicate hydrated (C-S-H) microstructure obtained from various techniques (TGA/DTA, IR Spectroscopy, NMR etc.) has led to a better understanding of the distribution of water within the C-S-H. It is suggested that depending on its location in the C-S-H microstructure, water can considerably affect the creep and shrinkage of Portland cement paste subjected to sustained load or a drying regime.

The literature review is presented in Part 2 and places emphasis on a synthesis of the existing knowledge of the deformations in hardened Portland cement paste. A brief description of the AC impedance spectroscopy method is provided to illustrate the potential application of this technique for short-term creep and shrinkage investigations. Electrical methods have been found to be useful for the rapid characterization of the microstructure of microporous materials. Their relatively recent application to concrete has initiated activity in three centers (NRC, Canada; Northwestern University, USA and Heriott-Watt University, UK). These methods provide a non-

destructive means of investigating changes in basic properties of hydrated cement-based materials. Details of these methods are provided in Part 3 through experimental study and methodology. The candidates on-going investigations consist of a coupling of a.c. impedance and creep and shrinkage of hardened Portland cement paste. Creep and length change data of partially or totally saturated specimens following organic solvent exchange (a microstructural probe) complement the coupled measurements. The role of calcium hydroxide on creep behavior and its interaction with organic solvent-based microstructural probes was also investigated. The analysis of results and corresponding discussion are presented in Part 4. Some remarks and recommendations will follow the conclusion.

1.2 Definitions

Shrinkage and creep believing to be the manifestation of the same phenomenon are generally characterized by some useful terms illustrated in Figures 1.1 and 1.2, and defined as follows.

Instantaneous strain — also referred to as the initial strain is that occurring immediately on loading. It consists of a reversible and an irreversible component.

Elastic strain — this is the reversible component of the instantaneous strain. It is not necessarily proportional to stress and becomes progressively nonlinear at higher stress levels.

Permanent set — this is the irreversible component of the instantaneous strain. It is the result of innumerable minute plastic deformations or ruptures, perhaps due to inhomogeneities in the material and is analogous to permanent set exhibited by steel loaded beyond its yield point.

Drying shrinkage — loss of water from concrete stored in unsaturated air gives rise to drying shrinkage. It is partially irreversible.

Creep — the total time-dependent deformation of concrete due to sustained stress. It consists of a reversible and an irreversible component. In order to eliminate

the effect of varying stress, creep is normally referred to a constant stress level or defined in term of strain per unit stress (specific creep).

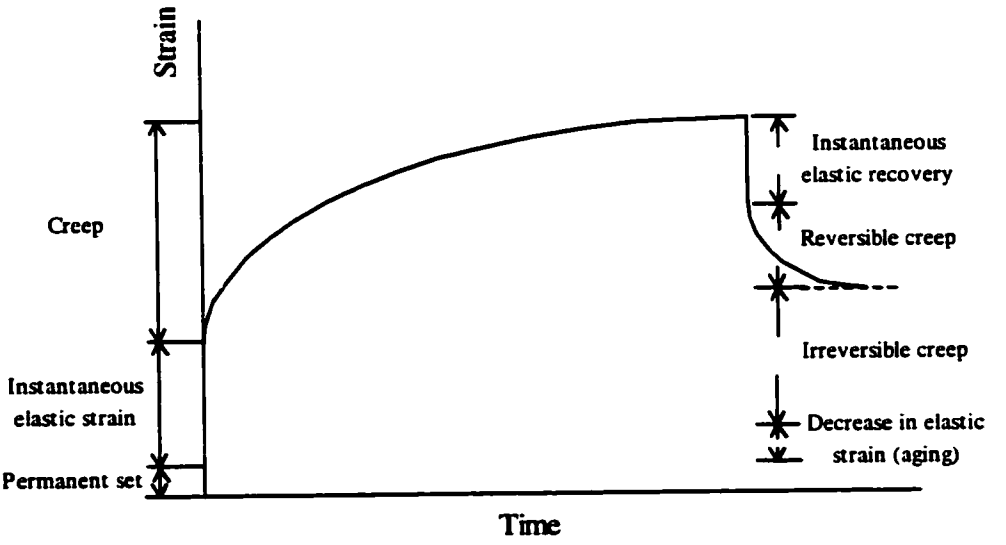

Figure 1.1: Deformation in concrete

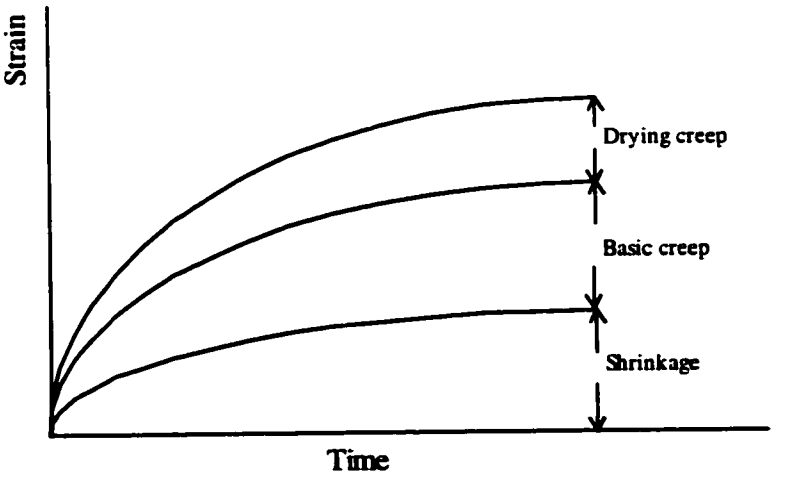

Figure 1.2: Time-dependent strains in a specimen drying under load

Instantaneous Elastic recovery	On removal of load the initial elastic strain is only partially reversible. The partial instantaneous elastic recovery is usually attributed to the increase in modulus of elasticity, which occurs with time.
Reversible creep	the instantaneous recovery is followed by a time-dependent decrease in strain or reversible creep the magnitude of which depends on the length of time under load.
Irreversible creep	the incomplete recovery of total strain leads to a residual deformation known as irreversible creep. Irreversible creep increases with time at a decreasing rate and is thought to be slow viscous flow.
Autogeneous volume changes	these arise from the natural process of hydration when no moisture exchange takes place with the surroundings. The volume of the solid increases with hydration and decreases with self-desiccation as the available water is utilized. This volume change is small, however.
Basic creep	creep which occurs in the absence of moisture exchange between the specimen and surroundings, i.e., without attendant shrinkage or swelling.
Drying creep	creep is usually increased when a stressed member is subjected to variations in humidity. A precise estimation of the magnitude of the variation in creep is complicated by the existence of concurrent drying shrinkage.
Stress-strength ratio	the applied stress expressed as a proportion of the ultimate stress. This parameter is useful at engineering level, where creep has been observed to be proportional to stress and inversely proportional to strength.

1.3 Strains and AC impedance measurements

1.3.1 Optical strain gage system

The type of gage used for the present study is unique in that it incorporates a specially designed prism, which permits readings of a gage secured to a remotely located specimen by an autocollimating telescope. Using this method, the position of the gage with respect to an autocollimator is not critical and errors of gage mounting are reduced to 0.1 percent. It has high sensitivity and because of its lightweight, it is well adapted to measuring strains accurately to 1×10^{-6} mm/mm in many materials.

1.3.2 Frequency response analyzer

The application of AC impedance spectroscopy (ACIS) techniques in the concrete science field is relatively recent even though it has been used extensively in the electrochemical field. Impedance spectra recorded over a wide range of frequencies (from 15 MHz to 1 Hz) have provided new information and insight on cement paste microstructure and hydration. Interpretation of an impedance spectrum is usually through modeling with an equivalent circuit until the electrical response of the elemental microstructure of the cement paste is well simulated. The characteristics of the electrolyte in hardened cement paste observed through real-time measurements of quantitative changes to the high frequency arc diameter under various loading and drying pre-treatments and environmental changes may affect creep and shrinkage.

1.4 Objectives and strategic elements of investigation

1.4.1 Objectives

Given the dominant role played by the deformation of the paste component in creep and shrinkage of concrete, the present research is mainly focused on the behavior of hydrated cement paste and/or hydrated cement minerals e.g. C_3S. In order to contribute to a better understanding of the creep and shrinkage mechanisms previously proposed, our multi-level objectives are to:

1 Validate the hypothesis that cement (or hydrated C_3S paste) specimens from which all the evaporable water has been removed will not creep.
2 Establish the dependence of creep and shrinkage to the state of the water in cement paste samples under equilibrium conditions at different relative humidity positions along the desorption isotherm.
3 Ascertain the relevance of the role which water plays in the creep and shrinkage process by exchanging it with organic solvent-based microstructural probes and subsequent re-saturation with a synthetic pore solution.
4 Determine the role of $Ca(OH)_2$ in hydrated cement systems through an investigation of the processes involved in the removal of water by solvent exchange.
5 Attempt to determine the creep characteristics of phase pure $Ca(OH)_2$ and hydrated C_3S.
6 Develop a new test method based on the application of AC impedance spectroscopy for characterizing and monitoring short-term microstructural changes in hydrated Portland cement systems caused by the surrounding environment and/or by a sustained load.

1.4.2 Strategic elements of the investigation

Historically several practical difficulties have hindered the investigation of the central role which water plays in the creep and shrinkage of cement pastes. A primary difficulty rests with the detection of the small volume and weight changes involved in specimens at equilibrium with the surrounding environment. The thermodynamically irreversible character of the hydrating Portland cement paste and the unstable nature of the hydration products (C-S-H) are believed to constantly change the chemical and physical properties of the material. The use of mature, very thin specimens, rigid and consistent procedures and environmental control should be applied in order to minimize gradients and to work under true equilibrium conditions. Most of the theories explaining one or more creep mechanisms are based on water movement through the microporous hydrated cement systems. In the proposed work particular attention will be given to the relationship between the creep of hydrated cement paste and its water content determined from differential thermogravimetric analysis in a controlled environment.

Specially designed "T-shaped" paste specimens (that meet the requirements for hygral equilibrium and structural stability) were subjected to a sustained compressive load or to a drying regime. They were fabricated from paste cylinders and were about 1 mm thick with a height of 25.4 mm and a flange width of 5.72 mm. Compacted calcium hydroxide ($Ca(OH)_2$) powder,

tricalcium silicate (C_3S), and Portland cement pastes were used in the experiments. The water solid ratios of the samples varied from 0.35 to 1.0.

Creep specimens were loaded at ages of 18, 24 and 30 hours (young specimens) and at ages of 2 and 30 years (mature specimens) and subjected to different hygrometric conditions ranging from 96% relative humidity to the D-dried state (equivalent to drying to the vapor pressure of dry ice at –78°C).

Differential thermogravimetric mass change was monitored on specimens conditioned at different humidities in a controlled environment. Mass and length changes, degree of hydration, surface area and porosity measurements were performed on samples subjected to various drying regimes. These results provided a reasonable indication of the state of water in the material. This is important for assigning a mechanistic argument to various aspects of the creep process.

Shrinkage, creep and creep recovery as well as the coupled a.c. impedance spectroscopy spectra were monitored simultaneously in real time in order to evaluate the microstructural changes taking place during the shrinkage and/or creep process. The coupled a.c. impedance spectroscopy experiment involved fitting the "miniature" creep frames with appropriately shielded electrodes. Such tests were utilized to establish relationships between pore structure, pore solution, electrical resistance and strain due to short-term creep and shrinkage.

Part 2: Literature review

CHAPTER 2

STRUCTURE AND STRENGTH OF HARDENED CEMENT PASTE

2.1 Structure of hardened cement paste

2.1.1 Introduction

The cement paste consists of grains of unhydrated cement embedded in a matrix of cement hydration products. These products are comprised primarily of a cement gel with a semi-continuous system of water-filled or empty capillary pores. Diamond (1976) emphasized three basic levels of microstructure: (a) the atomic level, which is concerned with crystal and molecular structure; (b) the particle level, which is principally concerned with the morphological aspects of crystals and particles; and (c) the micromorphological level, which describes how all the components fit together. However, following Young (1982), in considering creep and shrinkage phenomena another useful approach is to consider the microstructure in terms of its individual components as given in Table 2.1.

Table 2.1. Component of hardened Portland cement paste (Young, 1982)

Component	Remarks
C-S-H	Includes micropores (<2.6 nm diameter)
Capillary pores	Mesopores and macropores
Calcium hydroxide	Only crystalline material
Calcium aluminate hydrates	Ettringite and monosulphoaluminate
Anhydrous residues	Unhydrated remnants of cement grains

In the following review these five components will be considered and described chemically and/or physically. The relative proportions of all of these components change with duration of curing and degree of hydration, but all of them must be included in any description of hardened cement structure.

2.1.2 Hydration products

2.1.2.1 Calcium silicate hydrate gel (C-S-H gel)

C-S-H gel (the abbreviation of Calcium Silicate Hydrates) is one of the products of the chemical reaction between water and the silicates in of cement clinker. The cement gel adheres to the unhydrated cement particles and fills some of the space existing between these particles prior to hydration. But there are also some crystals formed. The water in excess of that required for hydration fills the remainder of space between the original grains of cement, known as capillary voids, about two orders of magnitude larger than the gel pores. Unfortunately C-S-H is essentially a semi-amorphous material. It is therefore a difficult task to try to elucidate its basic structure. However, C-S-H can be considered as the continuous solid matrix of the hydrated system. An understanding of its properties (Young, 1982 and Xi and Jennings, 1992) is central to a successful physicochemical explanation of the fundamental origins of creep and shrinkage.

a) Chemical and physical characterizations

Although the composition of C-S-H gel is quoted as $C_{1.5}SH_{1.5}$, the C/S and H/S mole ratios of this hydrate are variable and still under investigations by several researchers (Beaudoin and Brown, 1992; Massazza and Daimon, 1992; Richardson and Groves, 1992). In Portland cement paste compositional variations are much greater because of the ability of C-S-H to incorporate large quantities of oxide impurities, alumina and sulphate in particular. This was shown by Kalousek (1957) and Lachowski (1979) and recently the presence of both aluminum and sulphur has been confirmed by microanalysis (see Lachowski et al., 1980). The C/S mole ratios of C-S-H gels depend on several factors such as water/solid ratio, surrounding temperature and degree of hydration, and may typically vary between 1.2 and 2.3 if determined by transmission electron microscopy (Richardson and Groves, 1993) or by electron probe microanalysis (Rayment and Majumdar, 1982; Richardson and Groves, 1993; Taylor and Newbury, 1984; Uchikawa et al., 1987).

Silicate polymerization

C-S-H gel is nearly amorphous. It follows that X-ray diffraction has given only very general indications of its structure. The most significant development in recent times with regard to chemical composition has been the characterization of C-S-H as a silicate polymer. Several

researchers have found the degree of silicate polymerization to be of great importance with regard to the deformation properties of hardened cement paste (Parrott, 1977a, 1977b; Parrott and Taylor, 1979; Parrott and Young, 1980). The amount of irreversible shrinkage or creep decreases with an increase in polysilicate content of a paste while the recoverable portion is unaffected. The nature of the silicate anions has been determined from the kinetics of the reaction with molybdate, and, in greater detail, by trimethylsilylation (TMS) and ^{29}Si nuclear magnetic resonance (NMR). The molybdate complexing method involves controlled hydrolysis and complexing of the silicic acids; the kinetics of complexation being analyzed spectrophotometrically (Young, 1982; Parrott and Taylor, 1979). The polysilicate fraction is then determined by measuring the concentration of silica which remains unreacted in a mixture of silicic acids after 300 seconds of complexing (Parrott and Taylor, 1979), and the proportion of polysilicate is linearly proportional to the measured concentration with a given polysilicate. In TMS methods, the sample is treated with a reagent that converts the silicate anions into the corresponding silicic acids, which then react further with replacement of SiOH by $SiOSi(CH_3)_3$. The resulting TMS derivatives can be identified and semi-quantitatively determined by various procedures (Dent Glasser et al., 1981; Lachowski, 1979a, 1979b; Taylor, 1990) of which the most widely used have been differential evaporation to isolate the higher molecular weight species, gas liquid chromatography (GLC) and gel permeation chromatography (GPC). After reporting that the analysis of molybdate complexing method gives reliable estimated proportions of silicates in mixtures of monosilicate, disilicate and polysilicate with a degree of condensation exceeding four, Parrott and Taylor (1979) concluded that this analysis is more preferable than the TMS method. The use of ^{29}Si "magic angle" NMR complements after Taylor (1990) the trimethylsilylation method in two ways. First, it is a purely physical technique, in which there is no possibility of altering the structure through side reactions. Except with very young samples, no preliminary drying is needed. Second, it gives slightly different data, relating not directly to the fractions of the silicon present in different anionic species, but to the fractions present in different environments. The terms $Q^0 \ldots Q^4$ refer to the connectivity, Q^0 thus denoting an isolated tetrahedral, Q^1 an end group tetrahedral (and thus including silicon present as Si_2O_7), Q^2 middle groups, and so on.

Surface area

The physical characteristics of C-S-H are also diverse and these are dependent on the technique of measurement, the sample preparation procedure and the environmental condition. Table 2.2 shows the variation of the specific surface area measured by different techniques using different

drying methods (Young 1982). For example, the surface area as measured by adsorption of water vapor is usually reported to be 5 to 10 times greater than that measured by the adsorption of nitrogen or organic molecules. According to more recent work the "surface area" of C-S-H cannot be considered as a unique property since its value depends on the choice of technique used for its characterization.

Table 2.2: Surface Area of C-S-H Materials Measured by different Techniques and under Different Conditions of Drying (Young, 1982)

Condition	Area (m^2/g)	Method of test	Reference
Saturated	~1000	Nuclear magnetic resonance	Barbic et al.
Saturated	~750	Low angle X-ray scattering	Winslow and Diamond
D-dried	200-300	Low angle X-ray scattering	Winslow and Diamond
D-dried	250-300	Water vapor adsorption	
Solvent replacement	150-200	Nitrogen adsorption	Litvan
Oven-dried	~150	Low angle X-ray scattering	Lawrence et al.
D-dried	20-100	Nitrogen adsorption	Winslow and Diamond

In a D-dried paste, the interlayer space is reopened by exposure to 42% relative humidity (Ramachandran et al. 1981). After this treatment, helium can on re-drying below 11% RH fully enter the interlayer space within 40 hours of flow time so that the volume of interlayer space can be measured in the partially open or fully open state, depending on the relative humidity of exposure.

In contrast to values for fully hydrated pastes obtained using water, the N_2 areas tend strongly to increase with w/c ratio, but are also significantly affected by the drying conditions under which the sample has been dried (Young, 1982; Taylor, 1990). It would appear that the value obtained using water, whatever its precise significance, is dominated by the structure at or near the individual layer level and is thus relatively insensitive to coarser features of the structure. With a possible reservation regarding material dried by solvent replacement, Taylor (1990) reported that N_2 cannot penetrate the interlayer spaces and can therefore only give information about structural features at a somewhat coarser level.

Porosity

The measurement of the porosity of C-S-H also faces similar difficulties. Parrott (1981) and Parrott et al. (1980) after drying and rewetting experiments as well as solvent replacement

treatments concluded that the porosity of the paste is significantly changed as water is removed. Young (1982) indicated that the pore structure of a saturated paste is more open than previously thought and that the microporosity may only be created during drying. Therefore, it was concluded that the nature of the interaction of water with C-S-H gel is the major concern (Ramachandran et al. 1981; Wittmann, 1976).

b) Structural models of C-S-H

Some idea of the chemical structure of C-S-H gel would be helpful in trying to deduce its role in creep and shrinkage phenomenon. Kalousek (1957) and Lachowski (1979) have shown the thin sheets or foil-shaped C-S-H structures in the saturated state from TEM (Transmission Electron Microscope) observation. However, Lachowski et al. (1980) have suggested several morphological types of C-S-H structures based on SEM (Scanning Electron Microscope) observation. The discrepancy between these observations may be due to strong drying conditions for SEM specimen preparation, which might result in the SEM morphologies being artifacts. Even though it is quite common to consider the basic elements to be derived from layered structure, there are substantially different interpretations of experimental results in terms of structural models, which have been proposed by a number of researchers (Daimon et al., 1977; Feldman and Sereda, 1970a, 1970b; Ishai, 1968; Kondo and Daimon, 1974; Powers, 1962, 1965; Power and Brownyard, 1967; Wittmann, 1976). Mainly, these differ on how the assumed structural degeneracy is considered to be manifested and the way in which evaporable water is associated with the gel. It is not surprising that several different interpretations exist as recalled from the difficulty in measuring the physical characteristics.

According to Powers (1962, 1965) and Power and Brownyard (1967) C-S-H gel is a rigid substance made up of colloid-size particles, and has a characteristics porosity of 28%. C-S-H gel in a saturated paste is believed to consist of randomly arranged laminae consisting of 2 or 3 elementary calcium silicate layers, or sheets, as distinct structural units. The average width of the pores involved is about 1.5 nm and they are known as "gel pores". Much bigger "capillary pores", form another component of the hardened cement paste. These are the remains of the original water-filled spaces that have not become filled with gel. Their volume thus decreases, and that of the gel pores increases, as hydration proceeds. This model is essentially based on water-vapor adsorption isotherms and on a somewhat arbitrary classification of the types of water held in the paste (evaporable and non-evaporable). The mechanical properties of the hydrated gel are described using this model. The particles are presumed to be held together by Van der Waals

forces. Swelling on exposure to water is explained by the individual particles separating due to layers of water molecules existing between them. This model also includes the existence of some chemical bonds between the particles to explain the limited swelling nature of the materials.

According to Feldman and Sereda's model (1970a, 1970b), C-S-H gel in saturated cement pastes is considered to consist of a completely random arrangement of single calcium silicate layers. When two layers (sheets) approach closely together, local ordering will create an interlayer environment for water, which is termed interlayer or zeolitic water and is regarded as part of the solid. Gel pores do not exist in this model. There is no clear-cut size distinction between interlayer regions and micropores. The presence of interlayer water, and the importance of this type of water in explaining the properties and behavior of cement pastes, are two of the main features of this model. It is thought that only water can enter the interlayer regions as opposed to nitrogen, methanol, and other molecules. Swelling on wetting is not due to separation of the primary aggregations or breaking of these bonds, but to the net effect of several factors: (i) the Bangham effect due to reduction of solid surface energy; (ii) water molecules penetration effect; (iii) menisci effects due to capillary condensation; (iv) an aging effect, which results in decreased surface area, and increase in solid volume and a net shrinkage.

According to the Munich model (Wittmann, 1976), the explanation of the mechanical properties of hydrated Portland cement gel is a major concern. It assumes that the water adsorption isotherm is reversible and free of aging, intercalation effects and other forms of specificity and that shrinkage forces are result of meniscus formation. It is concluded that above 2% and below 42% relative humidity, the length change is due to surface free-energy changes, and at higher relative humidity the length change is ascribed to the disjoining pressure of water separating surfaces held together by Van der Waals bonds.

In an attempt to unify these diverging views Kondo and Daimon (1974) and Daimon et al. (1977) proposed a similar model to both Feldman-Sereda's model and Powers-Brownyard's model, and they suggested that some relatively large pores are accessible to water only through interlayer spaces. In this model, there is a distinct difference between intergel particle pores, intercrystallite pores, and intracrystallite pores. On the surface of gel particles within intercrystallite pores there is physically adsorbed water which may influence the properties of C-S-H gel in a way as suggested by Powers (1968). Moreover, the interlayer water between layers of crystallites may be removed or it may re-enter as predicted by Feldman and Sereda (1970b).

Ishai (1968) proposed another structural model of C-S-H essentially based on Powers-Brownyard's model. This model was developed mainly to explain the volume changes in the paste due to variations in its moisture content (swelling and shrinkage) and due to continuous

loading (creep). The classification of the water held in hardened paste is the main difference between Ishai's model, which distinguishes four types of evaporable water, and Powers-Brownyard's model in which there are only two types. In addition to chemically bound water within the C-S-H gel, the four types of evaporable water are: (i) pore water in the capillary and gel voids, at a distance of 1.0-2.0 nm from the solid surfaces; (ii) water which is adsorbed on the surface of the crystallites in layers 1-2 molecules deep, i.e. 0.4-0.8 nm thick; (iii) adsorbed water which is confined between adjacent crystallite surfaces in narrow spaces two molecules wide (about 0.8 nm). This type of intercrystalline water is subjected to two sets of forces, and consequently is adsorbed more strongly than types 1 and 2; (iv) a water layer, one molecule thick, which is between layers of C-S-H crystallites. This type of intracrystalline (zeolitic) water is strongly bound to the solid and cannot be removed during normal drying. At the micro-level, Ishai (1968) suggests that the structure of cement gel can be represented as an aggregation of anisotropic crystal clusters randomly oriented in a solid matrix.

Whatever model has been proposed, the exact nature of the C-S-H microstructure determination is still uncertain, due mainly to the lack of a direct structure determination technique (Young, 1982; Wittmann, 1976). Also, it is now believed that the removal of water by any drying process will more or less change the C-S-H structure (Parrott, 1978; Parrott et al., 1980), and that the dried paste will be different from the saturated paste. The various morphologies and composition of C-S-H can also cause problems in obtaining a clear understanding.

Although purely physical models based on treating C-S-H as a gel have proved to be useful (Taylor, 1990; Wittmann, 1976), there is increasing experimental evidence that the chemical nature of the material cannot be completely ignored and must be taken into account in more precise models (Young, 1982).

2.1.2.2 Calcium hydroxide

Crystalline calcium hydroxide, usually called portlandite is the second most abundant product in hydrated Portland cement pastes. It is present in the form of relatively large crystalline aggregates and occupies about 20% to 25% of the hydrated cement paste volume. It is a well-crystallized solid containing hydroxyl ions, but no water molecules (Young, 1974, 1982). Dehydration occurs rapidly on strong heating at 400~500°C. Calcium hydroxide, in hydrating cement pastes, may vary in morphology, being found as small equidimensional crystals; large flat, platy crystals; large, thin, elongated crystals; or variations of these forms (Berger and McGregor, 1972; Diamond, 1976). Its morphology is particularly affected by admixtures, water-

cement ratio, temperature of hydration, or by the type of silicate (Berger and McGregor, 1972, 1973). CH crystals are not completely pure (Diamond, 1972; Lachowski et al., 1980; Young, 1974; Moore, 1980). Microanalysis studies have indicated the existence of some quantities of silica as well as occluded C-S-H products. Berger (1972) suggests that CH can act as a rigid in-situ restraint for deformation, although it was found that changing CH contents do not appear to affect the shrinkage behavior of calcium silicate paste (Hwang, 1983; Parrott and Young, 1982; Young, 1974). Creep characteristics of CH are not known, but Young (1974) suggests that they would probably be similar to other inorganic materials, with creep potentially arising from plastic deformation and slip between atomic planes.

2.1.2.3 Calcium aluminate hydrates

Gypsum ($C\bar{S}H_2$) is generally added to Portland cement clinker in order to control the setting. The 6-calcium aluminate trisulfate-32-hydrate usually termed ettringite (AFt) and calcium aluminate monosulfate-12-hydrate (AFm) are both found in cement pastes but apparently in smaller proportions compared to the C_3A and C_4AF contents of the cement clinkers. Although ettringite forms first during the reaction between C_3A and $C\bar{S}H_2$, and is present in young cement pastes, it is a transient phase which is converted to monosulphoaluminate ($C_4A\bar{S}H_{12}$). Both calcium aluminate sulfate hydrates are quite well crystallized in cement pastes (even though they are likely to have significant substitution of iron for aluminum, and carbonate or chlorides for sulfate that may be introduced into cement paste as chemical admixtures) (Diamond, 1976; Taylor, 1990; Young, 1980). In ordinary Portland cement, the ratio of SO_3 to Al_2O_3 is typically 0.6, suggesting that the final products will be AFm and C_4AH_{13}, but some AFt phase nevertheless often persists (Taylor, 1990).

It may not be entirely justified, to generally ignore the hydrated calcium aluminate phases due to their correspondingly minor role in the microstructure of the hydrated cement paste. These compounds do contain relatively large amounts of quite labile water as shown for ettringite (AFt) and the hexagonal hydrates of general formula C_4AXH_{12} where X can be various anions (Moore and Taylor, 1970; Taylor, 1990; Young, 1982; Uchikawa et al., 1970). Therefore, in Portland cement paste their contribution to shrinkage and creep may not be insignificant (Young, 1982; Beaudoin and Brown, 1992). However, the contribution by calcium sulfoaluminate hydrates will depend on the cement composition and sulfate (SO_3) content (Alexander et al., 1979; Hobbs, 1978). The ettringite morphology can be "needle-like", "wall-like", or an "amorphous" structure

depending on time of curing and amount of AFt formation (Ogawa and Roy, 1982; Regourd et al. 1976). According to Young (1982), the hexagonal hydrates are all based on calcium aluminate layer structures (Figure 2.1) with the anions occupying into layer positions, along with water molecules, in order to balance the net positive charges of the layers. In cement pastes the basal reflections are much broader and the morphologies are less distinct, indicating considerable disorder. Hydrated calcium aluminates without a definite hexagonal morphology can be clusters ("rosettes") of small, platy crystals instead of well hexagonal crystal (Young, 1982; Ogawa and Roy, 1982).

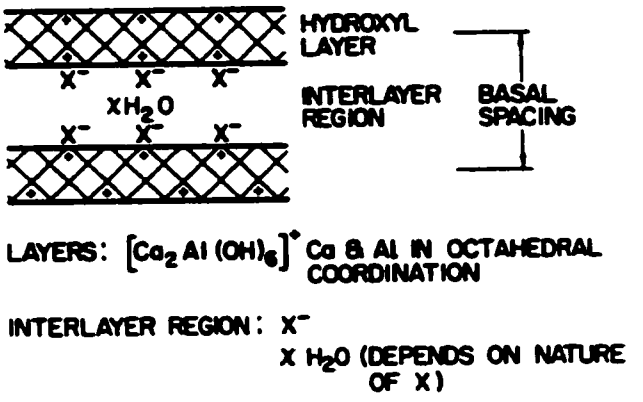

Figure 2.1: Schematic representation of the hexagonal calcium aluminate hydrate phases (Young, 1982)

There are conflicting results concerning behavior of ettringite on drying. It is quite possible that about 15 molecules of water in ettringite may be lost, without changing the X-ray diffraction pattern. Stronger drying, below 10% RH, was observed to collapse the lattice spacing and to destroy the X-ray pattern entirely (Diamond, 1972). Dehydrated, amorphous ettringite can be rehydrated above 85% RH. In the layer structure of the hexagonal hydrates, water molecules are loosely held between the "negatively-charged clay" layers. Drying can remove some of the water between the layers forming new hydrates (Young, 1974). Thus, loss of water might possibly cause a bulk contraction of the crystal and collapse to a smaller basal spacing. During drying, and even under pressure, phase changes can happen.

2.1.3 Capillary pores

The capillary porosity includes all pores greater than 2.6 nm diameter and decreases as hydration proceeds. This means that for a given paste system, the C-S-H gel which includes micropores

will increase with hydration while capillary pores decrease in order to achieve the same total porosity. The porosity and pore size distribution of the hardened cement paste are very important characteristics in determining the magnitudes of time-dependent deformation (Young, 1974; Ramachandran et al., 1981). The characteristics of porosity are quite complex and as difficult to study as the C-S-H gel. Mainly, it is because the drying process that is required before measurements can be made, changes the pore structure (Bentur et al., 1979; Parrott, 1981; Parrott et al., 1980). Also, pore dimensions extend over a range of four orders of magnitude and cannot be measured accurately by a single method (Young, 1974). Pore size distributions are affected by experimental parameters such as degree of hydration, temperature of curing, admixture, water-cement ratio, and type of cement (Bentur, 1980a; Bentur et al., 1978; Feldman and Swenson, 1975; Parrott, 1978). Pore sizes of porous materials have been classified in different ways by several authors: Powers and Brownyard (1967), Feldman and Sereda (1970a, 1970b), Daimon et al. (1977), and Bentur et al (1979). But using the IUPAC classification (1972), these are divided into mesopores (between 2.6 and 50 nm) and macropores (greater than 50 nm). Water (diameter around 0.33 nm in pure bulk water) occupies and penetrates all size ranges of pores structure within the paste, but a substantial volume of porosity cannot be intruded by organic liquids after the paste has been dried (Feldman and Sereda, 1970a, 1970b). Mills (1969) has suggested that cement hydrate can act as a molecular sieve when drying. Generally, organic molecules are substantially larger than the water molecule (for example: diameter of methanol is around 0.44 nm). Even the nitrogen molecule (N_2), which has a smaller size of 0.41 nm, is also denied access too much of the pore space. The reason is believed to be the fact that the water, by virtue of its small molecular size and high dipole moment, can occupy the smaller pore spaces where surface forces play a dominant role.

The solvent replacement method to remove the water from specimens without the problems which are inherent in direct removal of water by evaporation as described above have been suggested by Litvan (1976). When the pore size distribution is determined by gas adsorption (GA) on samples after drying by solvent replacement, a more satisfactory measure of porosity is obtained than that by mercury intrusion porosimetry (MIP) because collapse of pores during the measurement is minimized (Bentur, 1980a, 1980b).

The traditional methods of measuring pore size distribution employ the physical adsorption of gases and mercury intrusion porosimetry (MIP). Physical adsorption of gases (either water or nitrogen) utilizing BET theory are used to measure pore sizes below 30 nm. MIP has been used to measure the whole spectrum of pore size down to about 2.0 nm (Bentur, 1980b; Daimond,

1971). Unfortunately, in the area of overlap (3.0 nm-30 nm) there is not very good agreement (Diamond, 1971).

The disadvantage inherent in these methods originates in the assumptions: that there is regular pore geometry, that all pores are interconnected; that the pore size distributions do not change on drying. All these assumptions have been proved to be incorrect. It should be noted that it is impossible to measure the pore dimensions in saturated pastes. Due to the lack of a direct method to determine the pore size distributions, a suitable approach might be trying to deduce pore characteristics from studies of length and weight changes during drying and from solvent replacement experiments.

2.1.4 Anhydrous residues

Anhydrous residues in hydrated cement paste are also well crystallized compounds that would be expected to show low shrinkage and minimal creep similar to the rigid restraints caused by aggregate to mortar deformation in concrete (Young, 1974). This may in part explain the small shrinkage of low w/c ratio pastes. The minimum size of grain required to ensure that anhydrous grains persist in a paste will depend on the degree of hydration and the water-cement ratio (Young, 1982; Yudenfeund et al., 1972).

2.2 Strength of hardened cement paste

2.2.1 Introduction

Compressive strength might be the most significant property of hardened cement paste. Not only is it important in most structural applications, but it can be related to other properties are performance characteristics of cementitious systems, such as the elastic modulus and durability, which are more difficult to measure directly. When water is added to Portland cement, several chemical reactions occur. The final product of these reactions is the hardened cement paste for which, the strength characteristics depend on the mass ratio of the various minerals in the cement. This dependence also affects the increase of strength with time. The strength of reaction products from C_3A and C_4AF is considerably lower than that of the C_2S and C_3S hydration products (Beaudoin and Ramachandran, 1992; Odler, 1991). However, not only is the cement composition

of importance for strength, but also the pore size and the amount of water available for the hydration are of major importance.

2.2.2 *Bond between gel particles*

Generally speaking, the mechanical properties of the cement paste may be attributed to two types of bonds: The ***primary bonds*** result from the inter-growing of crystallites and the formation of chemical bonds at the points of contact, and the ***secondary bonds*** are due to van der Waals forces (cohesion forces) acting between the gel particles (Wittmann, 1973, 1976).

The chemical bond generally means a solid to solid contact similar to that existing at the grain boundary of a polycrystalline material, where some of the atoms approach the spacing of the atoms in the crystals, and a close fit exists between the lattice of the neighboring crystals (Soroka, 1979; Sychev, 1974). According to Sychev (1974), this bond can be strong only when most of the free water has been removed, resulting in a low concentration of water at the contact faces. The number of bonds, in turn, is dependent on the shape and size of the crystals involved. In any case such bonds are strong and when broken would not be remade under normal circumstances. The secondary bonds are much weaker. It is generally assumed that the cohesion forces in cement paste systems act across the adsorbed water, and that the adsorbed water is a constituent part of the bond between the gel particles (Feldman and Sereda, 1970a, 1970b). If the relative humidity is raised above a certain level disjoining pressure of water separates surfaces which are exclusively held together by van der Waals bonds (Wittmann, 1973).

The magnitude of cohesion forces is also dependent on size of the particles involved, i.e. on their specific surface area; larger forces (stronger bonds) are to be expected for higher specific surface areas (Soroka, 1979). Given the very high specific surface area of C-S-H gel, the strength of cement paste may be attributed to cohesion forces. However, it is difficult to estimate the relative importance of these two types of bond and Wittmann (1973) suggested that the contribution of both types to the strength of the cement paste is more or less the same. Later Setzer and Wittmann (1974) considered the strength of the hydrated paste to originate partly from chemical bonding with no influence from water vapor, and partly from physical forces, constituting about 50% of the total bond strength.

Consideration of a mature, low water-cement ratio cement paste as a continuous matrix surrounding a pore network, rather than particles joined by specific bonds might be a more useful approach for formulating a model of cement paste. Therefore, the area and type of solid to solid

contact might be the critical factor determining mechanical properties (Ramachandran et al., 1981).

2.2.3 Failure process

The intermolecular spacing and cohesion forces of the hydrate product pore characteristics and micro-cracks are all involved in the theoretical strength of an elastic material. The cohesive forces increase with increase in intermolecular spacing reaching a maximum when the spacing, brought about by tensile stress, is about twice the normal intermolecular distance (Soroka, 1979). With further increase in spacing cohesion forces rapidly decrease and fracture occurs. Critical flaws occur largely at regions of non-homogeneity, and this factor should be taken into account when relating the measured strength of such a body in terms of the strength of a specific bond (Ramachandran et al., 1981). The presence of cracks and other flaws within the material have been attributed to the difference between observed and theoretical strengths of brittle materials (Griffith). The latter were calculated from atomic theory and found to be 1000 times larger than their observed strengths. According to Griffith's theory, the presence of such cracks initiates failure as a result of high stress concentrations induced at, or near to, the crack when the material is loaded. The decrease in the specific surface energy, T, when such a crack is formed in a plate of unit thickness, was shown to be as follows:

$$T = \pi\sigma^2 c/(2E) \qquad (2.1)$$

where σ is the applied tensile stress normal to the plane of the crack; E is Young's modulus; and c is half the crack length. The equation 2.1 can be rewritten in the following form known as Griffith equation.

$$\sigma = \sqrt{2ET/\pi c} \qquad (2.2)$$

The Griffith's theory may be applicable to cement paste and concrete because the capillary pores in paste and the existing cracks at the paste-aggregate interface constitute such flaws.

The failure mechanism under compression is much more difficult to explain. It can be shown that, under compressive load, localized tension zones are formed around the tips of already existing cracks, in which stress intensity depends on the direction of the crack with respect to the direction of the load and its length to width ratio. As a result of tensile stresses the crack grows in

a plane, parallel to the direction of the compression, and not in the plane containing the initial crack, and subsequently causes failure (see Figure 2.2). In fact, all compression cracking is parallel to the direction of the load because this is the only direction that has no compression component normal to it.

There are basic differences between failure under tension and failure under compression. In tension the rate of energy release increases with crack length, c, whereas in compression, because crack growth only slightly affects the stress field, the rate of energy release is constant, and independent of crack length. Consequently, in tension, the first crack to grow is the critical crack which leads to failure. In compression, cracks that start to grow are often stabilized when they reach a harder phase. In this case, a substantial increase in stress is required to enable the crack to grow into the harder phase. However, before such an increase takes place, other cracks, next in order of weakness, begin to grow until they are stabilized. This progressive cracking serves as a mechanism of energy dissipation, and constitutes an alternative to fracture. Consequently, fracture is delayed and strength increased. This mechanism explains why cement paste and concrete are much stronger in compression than in tension.

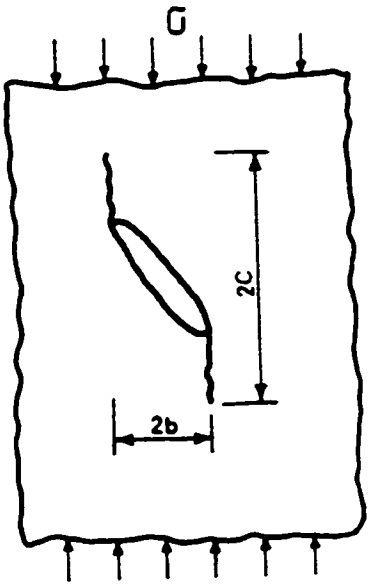

Figure 2.2: Crack growth in a compressive field (Soroka, 1979)

2.2.4 *Factors affecting strength*

2.2.4.1 Effect of porosity

Hardened cement pastes are porous solids and simple empirical relationships between strength and porosity have been found to represent data for a wide range of materials, including hardened cement pastes (Lawrence, 1973). The porosity and strength relationship is not unique for all cement pastes, and different curves, of the same general form, can be obtained for Portland cement pastes cured under different temperature/pressure combinations, or for pastes containing pulverized fuel ashes (Feldman and Beaudoin, 1976). This indicates some differences in the microstructure of the hydration product in different circumstances, explaining, for example, the different long-term strengths with different curing temperatures mentioned earlier.

More recent research has demonstrated the importance of the relative proportion of different pore sizes, and not just the overall porosity, in controlling strength. The pores of cement paste have an adverse effect on strength and above a certain porosity the strength drops to zero. In general, it is the larger pores that are the most important; at any given porosity, the strength increases with the relative proportion of fine pores (Domone, 1994; Odler and Rossler, 1985; Parrott, 1985). Strength and porosity measurements often show good correlation, some typical data are illustrated in Figure 2.3 after Roy and Gouda (1973).

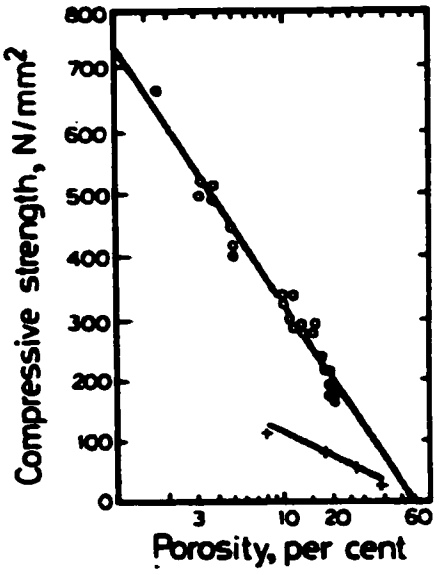

Figure 2.3: The relation between compressive strength and porosity for hardened cement Paste (Roy and Gouda, 1973)

The total porosity values in this figure include both gel and capillary porosity; only the latter can be reduced to near zero with low water-cement ratio mixes cured at normal temperatures and pressures, and the solid data were obtain in this way.

The linear relation between the logarithm of strength and the porosity of cement pastes has also been found by Feldman and Beaudoin (1976) to not necessarily satisfy all the available data as demonstrated in Figure 2.4 where a deviation from linearity is quite marked in the lower porosity range.

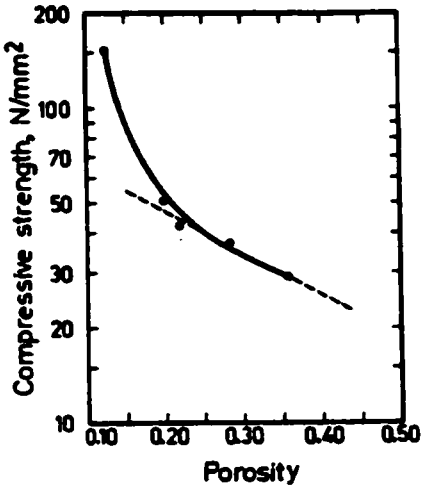

Figure 2.4: The relation between compressive strength and porosity for hardened cement Paste (Feldman and Beaudoin, 1976)

In any case, it is generally agreed that porosity constitutes the most important single factor in determining strength. It follows that any factors, which affect porosity of the paste, would also affect its strength. In this context, the most important ones are the water-cement ratio and degree of hydration, which directly affect porosity. Other factors, however, affect porosity indirectly mostly through their effect on the degree of hydration.

2.2.4.2 Effect of water-cement ratio

The effect of water-cement ratio on hydration of cement is limited in the first 24 hours but thereafter it becomes more significant. For ordinary Portland cement (opc) mixes, the water-cement ratio determines the initial porosity of the hydrated paste, i.e. the relative water content in the paste. Abrams first recognized the increase of strength with decreasing water-cement ratio at

any particular age in 1918. This effect, provided that the fresh cement paste or concrete mix is compacted sufficiently, has been validated by several research investigations (Feldman and Beaudoin, 1976; Soroka, 1979; Spooner, 1972) as showed in Figure 2.5. Given that the volume of the cement paste is equal to the sum of the volumes of the anhydrous cement and the mixing water, it can be expressed as follows:

$$V = Cv_c + \omega C \tag{2.3}$$

and its initial porosity, p_i, by

$$p_i = \omega/(v_c + \omega) \tag{2.4}$$

where C is the weight of the cement, v_c is its specific volume, and ω is the water-cement ratio. The total porosity of the cement paste also depends on the degree of hydration, meaning that in pastes of the same degree of hydration, the total porosity of the paste can be characterized by the water-cement ratio.

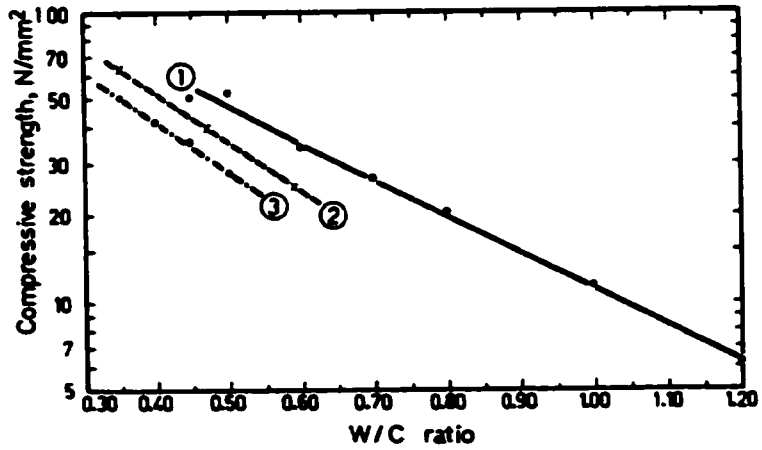

Figure 2.5: Relation between compressive strength of cement pastes and their W/C ratios after [(1) Soroka and Sereda, 1979; (2) Spooner, 1972; (3) Feldman and Beaudoin, 1976]

2.2.4.3 Effect of degree of hydration and moisture content

Continuous availability of moisture from the environment surrounding the fresh cement paste is necessary to sustain the hydration reactions and prevent drying shrinkage; only then will the full potential strength be developed. The first few days are the most critical and so good curing practice is of particular importance during this time. As the volume of hydration products is greater than that of the reacting cement, the porosity of paste decreases as hydration proceeds. Powers' (1958) suggested that this can be demonstrated quantitatively by assuming that the volume of the gel is 2.2 times the volume of the anhydrous cement and that it has a characteristic porosity of 28%. Also, it is assumed that no bulk volume changes occur during hydration. Therefore, the volume of the paste is constant, and equal to the volume of the original water-cement system.

Soroka (1979) showed that total and capillary porosity decrease with increase in the degree of hydration, Figure 2.6. Given the relation between strength and porosity, the expected similar relation between strength and degree of hydration has been confirmed by the data of Figure 2.7, in which the strength of the paste is plotted again parameter V_m/W_o. V_m is the amount of water required to cover the surface of the gel with a monomolecular layer and W_o is the original amount of mixing water. In a given cement paste W_o is constant and V_m/W_o is therefore a measure of the degree of hydration.

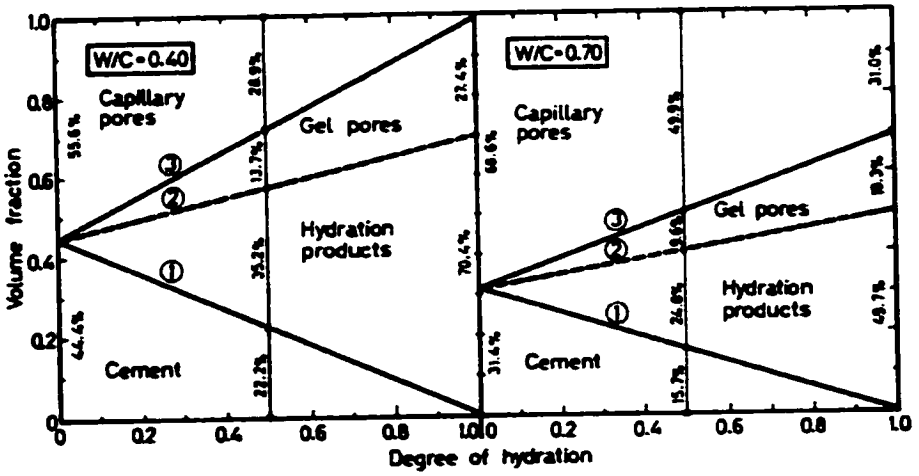

Figure 2.6: Relation between porosity and degree of hydration for cement pastes having W/C ratios of 0.4 and 0.7 (Soroka, 1979). Volume fraction of (1) unhydrated cement, (2) solids, and (3) unhydrated cement+gel

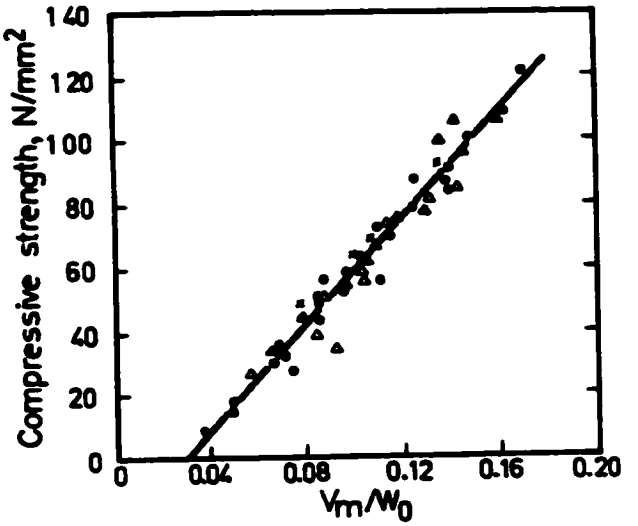

Figure 2.7: Relation between compressive strength of cement pastes and parameter V_m/W_o (Powers and Brownyard, 1967)

According to Griffith's theory, strength is expected to decrease with increase in the moisture content of a material because the presence of adsorbed water reduces specific surface energy. Applying this to cement pastes, Sereda and Feldman (1970a) found the effect to be more pronounced at the lower range of moisture content as shown in Figure 2.8. Feldman and Sereda (1970b) also suggested the decrease in strength to be due to the change in environment and not to the change in the state of the solid. It is also suggested that silicate bonds can be strained by concentration of stress around the cracks. Thus, in the presence of water, the breaking of these bonds will occur more readily. When the concentration of the water molecules is sufficient to maintain a rate of diffusion that will deliver the minimum required amount of water into an extending crack, no further decrease in strength will occur on further water addition. The decrease in strength can also be attributed to the decrease in cohesion forces, which results from the presence of adsorbed water.

2.2.4.4 Effect of mineral and chemical admixtures

The most common partial cement replacement materials are natural pozzolanas, pulverized fuel ash, ground-granulated blast furnace slag and condensed silica fume, sometimes call microsilica. The composition and properties of these materials modify to some extent the hydration processes

as well as the microstructure of the hardened pastes. They consequently, affect the engineering properties of cement paste.

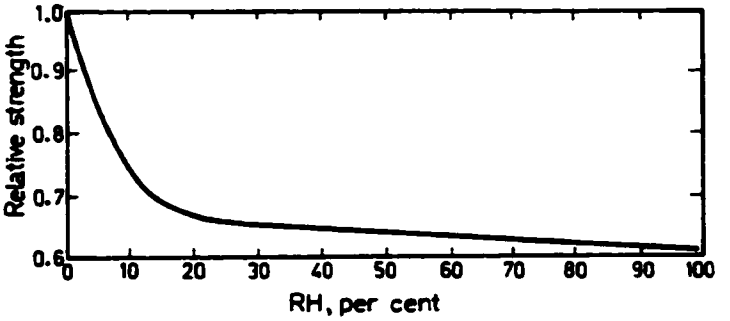

Figure 2.8: Effect of moisture content on compressive strength of cement paste (Feldman and Sereda, 1970a)

Partial replacement of mineral admixtures for Portland cement generally reduces the initial rate of cement hardening, but at advanced ages these cement-based systems can attain the same or even a higher strength than the corresponding control Portland cements. The initial reduction occurs with natural pozzolanas (Abdul-Maula and Odler, 1981; Delvasto, 1986; Massazza and Costa, 1979; Metha, 1981), fly ashes (Abdul-Maula and Odler, 1981; Hooton, 1986; Sybertz, 1989) and silica fume (Asgeirsson and Gudmundsson, 1979; Kohno et al., 1989; Nelson and Young, 1977). A typical example of this behavior is given in Figure 2.9 after Massazza and Costa (1979). The Portland blast furnace cements are mostly used for seawater and underground foundations because of their resistance to sulfate attack and lower heat of hydration (Regourd, 1998). With cements of higher slag content the fineness of slag is of major importance at all ages, as shown in Figure 2.10. In cements of lower slag content, the influence of slag fineness is expected to be rather less. The clinker fineness is more pronounced at early ages.

Chemical admixtures, which are used to alter the workability of the fresh mix (plasticizers and surperplasticizers), generally, do not in themselves have a major effect on the subsequent strength. The minor effects are described by Domone (1994). These are;

- a small (up to 10%) increase in strength at early ages resulting from the dispersion of the cement particles giving a greater surface area of fresh cement exposed to the mix water
- a reduction in strength due to a small amount of air entrainment with some surperplasticizers

- some retardation of strength gain with some admixtures.

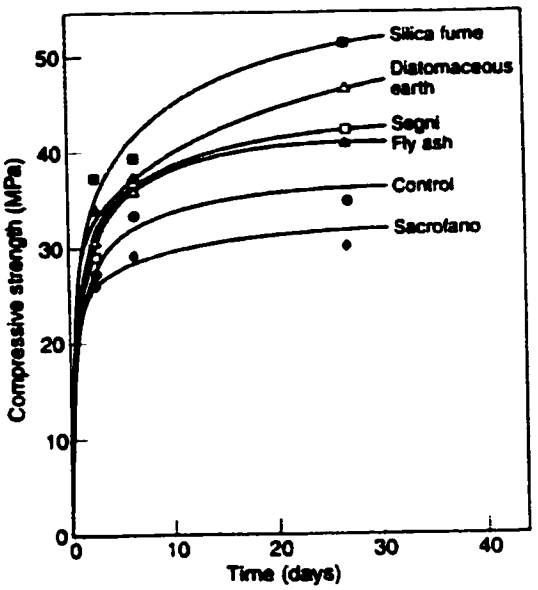

Figure 2.9: Strength development of different 20 per cent mineral admixture-cement mixes. Paste with w/c=0.5; 40x40x160 mm specimens cured for 72h in water and then In 65 per cent relative humidity at 20°C (Massazza and Costa, 1979)

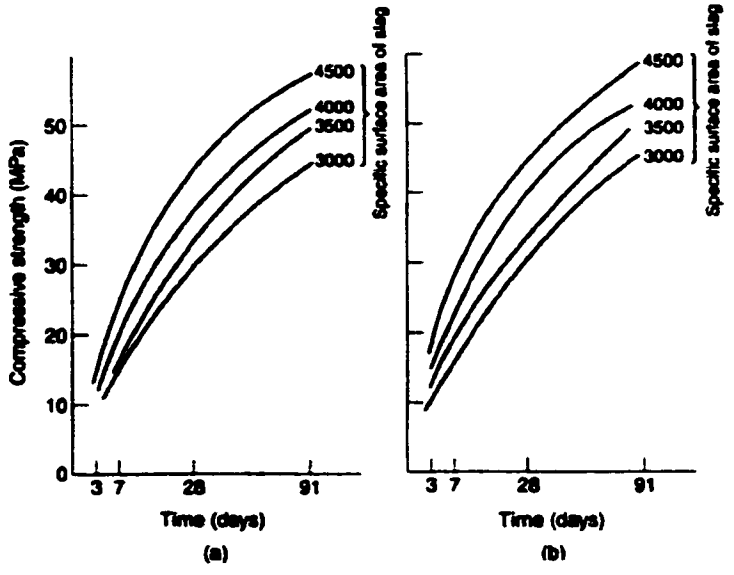

Figure 2.10: Compressive strength of mortars: cements CEM III/B with 75 per cent slag of specific surface areas (a) 3000 and (b) 4000 cm^2/g (Regourd, 1998)

These admixtures are commonly used to increase strength by achieving equivalent fluidity at lower water contents and hence lower water-cement ratios.

Retarders and accelerators are used to control the setting time of the cement paste mixtures. Accelerators decrease this and increase the subsequent rate of gain of strength. Retarders increase the setting time and hence delay the onset of hardening; the subsequent rate of gain of strength is normally not altered.

2.2.4.5 Effect of temperature

Low ambient temperatures reduce the rate of strength gain, but can result in significantly higher long-term strength. Therefore, in discussing the effect on strength of temperature, a distinction should be made between temperatures in the range of 0 to 100°C (i.e. above the freezing point and below the boiling point of water) and those exceeding 100°C. Only the lower range in which the paste is exposed to water vapor at atmospheric pressure will be presented here.

Soroka (1979) showed that an increase in temperature up to, say, 90°C, increases the rate of cement hydration. This increase in rate is believed to be effective mainly during the early stages of the hydration. The final degree of hydration was only slightly affected by curing temperature. In other cases, however, a higher degree of hydration has sometimes been found for the hydration at lower temperature (Idorn, 1968).

Since temperature has only a limited effect on the ultimate degree of hydration, essentially the same ultimate strength is to be expected in pastes of the same W/C ratio irrespective of curing temperature. This is not generally the case and a lower curing temperature is usually associated with a higher strength as illustrated in Figure 2.11.

This behavior suggests that the temperature effect involves two opposing factors and the final strength is dependent on which one is dominant at the time. Apparently, at early ages, the increased amount of hydration is the predominant factor and, consequently, the strength of the paste is greater when hydration takes place at higher temperature.

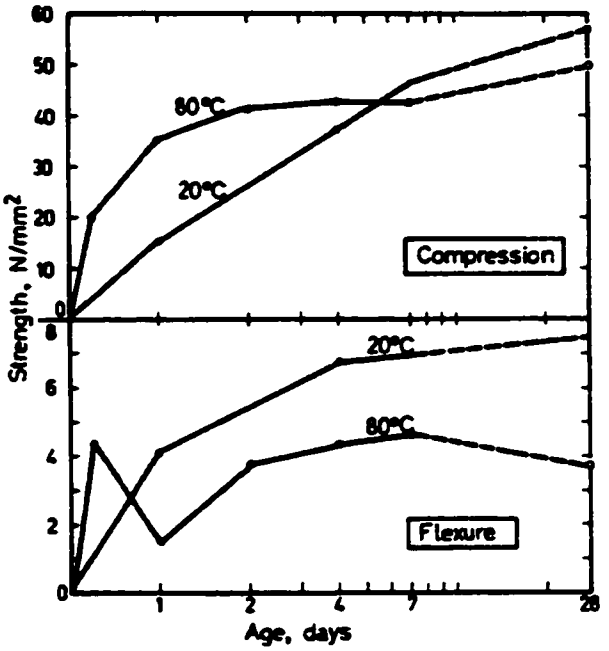

Figure 2.11: Effect of curing temperature on compressive strength of cement paste (Soroka, 1979)

CHAPTER 3

CHARACTERIZATION OF CEMENT PASTES FOR INVESTIGATING SHRINKAGE AND CREEP BEHAVIORS

3.1 Introduction

The investigation of hardened cement paste microstructure requires the measurement of its characteristic features. Theoretically, any techniques used to measure a particular parameter should give similar results, but unfortunately this is not true for cement paste. Different techniques have inherent limitations due to assumptions, which may be biased or over-simplified. There is also the limitation of instruments, either due to lack of resolution or to the state of the sample. The cement paste has unstable hydration products. Therefore any pretreatment of the paste can change its microstructure and conclusions based on the results of the pretreated sample may vary from one test to another. This is the reason why different hypotheses are proposed. Although the shortcomings are known, an existing technique must be selected until a better technique is developed. The following measurements and techniques are often used to investigate the microstructure of hardened cement paste.

3.2 Silicate polymerization

Following Young (1982), the use of silicate polymerization analysis to predict potential creep of a paste after any predetermined history appears to be a promising approach. The degree of silicate polymerization appears to be a significant parameter with regard to the deformation properties of the hardened cement paste (Young, 1982; Parrott, 1970a, 1970b; Parrott and Taylor, 1979; Parrott and Young, 1981). A high degree of silicate polymerization appears to result in a more stable, less deformable C-S-H, better able to resist stresses imposed during drying. It could be regarded as increasing the overall bonding of C-S-H and raising the energy needed to activate creep centers (Bentur et al., 1980; Gamble and Illston, 1976). Increasing the polysilicate content of a paste decreases the amount of irreversible creep or shrinkage, but did not affect the recoverable portion. Parrott (1978) however, suggested that silicate polymerization of a cement paste, while under load, will cause creep to occur, and this concept can be used to explain transitional thermal creep

(raising the temperature raises the rate of polymerization) and age effects (the rate of polymerization decreases with time). Both gel permeation chromatography (GPC) and gas chromatography of the trimethylsilyl (TMS) derivatives (Bentur and Young, 1981; Parrott, 1970a, 1970b; Lachowski, 1979; Power, 1961) and the molybdate complexing method (Parrott and Taylor, 1979) have been used to determine the polysilicate content of a paste.

The polysilicate fraction using GPC method is determined by separating the TMS derivatives, in which the side elements are attached to the backbone chains or skeletons of the silicates. Then the silicate structure is separated by correcting the ratio of the silicate fraction to the TMS derivatives. The "polysilicate" fraction was defined by Bentur et al. (1979) as the residues after heating at 180°C which represented the higher molecular weight species (Bentur and Young, 1981). This is different from the meaning used by Lentz (1966). His definition included all species of higher molecular weight than that of four silicate tetrahedral joined linearly (Collepardi and Marchese, 1972).

The polysilicate fraction using the molybdate complexing method is determined by measuring the concentration of silica which remain unreacted in a mixture of silicic acids after 300 seconds of complexing (Parrott and Taylor, 1979). The amount of polysilicate is linearly proportional to the measured concentration with a given polysilicate. The "polysilicate" fraction is defined as those species that have higher molecular weight than that of the di-silicate. Parrott and Taylor (1979) report that the analysis gives reliable estimated proportions of silicates in mixtures of monosilicate, disilicate and polysilicate with a degree of condensation exceeding four. They suggested that this analysis is more preferable than TMS method.

3.3 Pore structure

Pore size distribution (as measured by nitrogen adsorption) is a very important parameter that will indicate the change in pore size under different conditions. It will then be affected by experimental parameters such as degree of hydration (Bentur, 1980a); curing temperature of concrete (Bentur, 1980b); admixtures (Berger and McGregor, 1972; Feldman and Swenson, 1975; Hooton, 1986); aging (Bray and Sellevold, 1973; Collepardi and Marchese, 1972; Lankard, 1972); w/c ratio and cement composition. A knowledge of changes in pore size distribution may give a clearer idea as to what mechanism controls the shrinkage when the experimental parameters are changed.

The common techniques used for studying pore structure are the same as those for determining specific surface area. Therefore they bear the same kind of problems, e.g., gas adsorption with BET methods depends on the adsorbate. MIP and gas adsorption (GA) can only be measured on dried specimens, as discussed earlier. Also, it is thought that MIP may destroy some of the pore structure when intruding mercury at high pressure, and that not all porosity is intruded. Furthermore, both GA (either using H_2O or N_2) and MIP methods give a different pore size distribution curve (Bentur, 1980a), Figure 3.1. Normally, MIP can be used to measure large capillary pores (greater than 10 μm or down to 4.0 nm diameter). H_2O adsorption and N_2 adsorption measure the capillary pores smaller than 30 nm (Bentur, 1980a). The difference between the pore volume detected by MIP, and that measured by GA is large at low degrees of hydration because the pores larger than 30 nm can only be detected easily by MIP (Figure 3.1a), and the difference decreases with increasing hydration, Figure 3.1b (Bentur et al., 1978; Bentur et al., 1979).

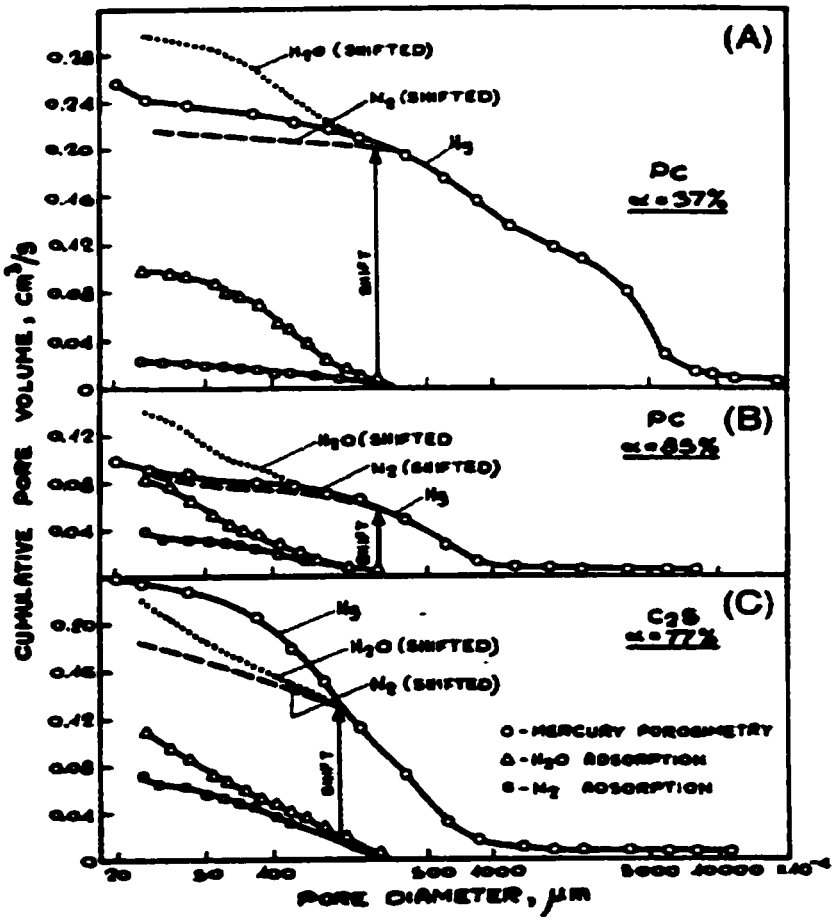

Figure 3.1: Comparison of pore size distribution determined by mercury porosimetry and H_2O and N_2 adsorption (Bentur, 1980)

In Figure 3.1, the H_2O adsorption and N_2 adsorption curves were shifted to coincide with the 0.03 μm diameter (30 nm) point of MIP curve, so that the measurements may be compared in the range where they are all theoretically effective. It seems that N_2 adsorption and MIP curves are similar, but not identical. Also, the shifted H_2O curve shows a higher porosity than the shifted N_2 curve (Bentur, 1980a).

3.3 Surface area

The range of specific surface area can vary widely depending upon the particle size and shape, and also the microporosity (Lowell, 1979). The surface area is dominated by smaller pores. Surface imperfections will create real surface area greater than the corresponding geometric area. The techniques used to measure the surface area are gas adsorption (GA) (Bentur, 1980b; Soroka, 1979), mercury intrusion porosimetry (MIP) (Bentur, 1980a, 1980b; Daimond, 1971), low-angle X-ray scattering (LAXRS) (Winslow and Daimond, 1974). However, the GA and MIP methods cannot be used to measure the surface area in a saturated paste. MIP can only measure area attributed to the large pores. Before measurements can be performed the specimen needs to be dried and this will significantly reduce the measured surface area (see Table 2.2). Solvent replacement is believed to be the best method of drying but the time of outgassing is fairly important (Orr and Dalla Valla, 1959). Also, the adsorbate, which is used in gas adsorption, will change the resulting surface area, Figure 3.2 (Mikhail and Selim, 1966). The lower surface areas obtained when organic vapors are used in the adsorption tests, are attributable to the greater diameter of the organic molecules, as described in Section 2.1.2. The surface area determined by water vapor adsorption is considerably greater because it includes some of the internal surface of the C-S-H sheets. Thus Feldman and Sereda (1970a, 1970b) claim that the "true" surface area of gel is the one determined by nitrogen adsorption. Kalousek (1957) thought that the small difference in diameter between water vapor and nitrogen gas that produces great differences in surface area results might be due to the fact that the water molecule can penetrate the micropore region.

LAXRS may be able to yield the surface area of saturated hardened cement paste. However, it does not give any information about pore size distribution and the change in pore systems other than the gel pores. Therefore, the gas adsorption of water or nitrogen is generally used although the method is inappropriate for use in a quantitative model for microstructure of cement paste as exists in concrete (Winslow and Daimond, 1974). It appears that different methods detect

different kinds of surface and reflect different states of the C-S-H at the time of measurement. No one method can be said to measure the "true" surface area. All values of surface area have some significance.

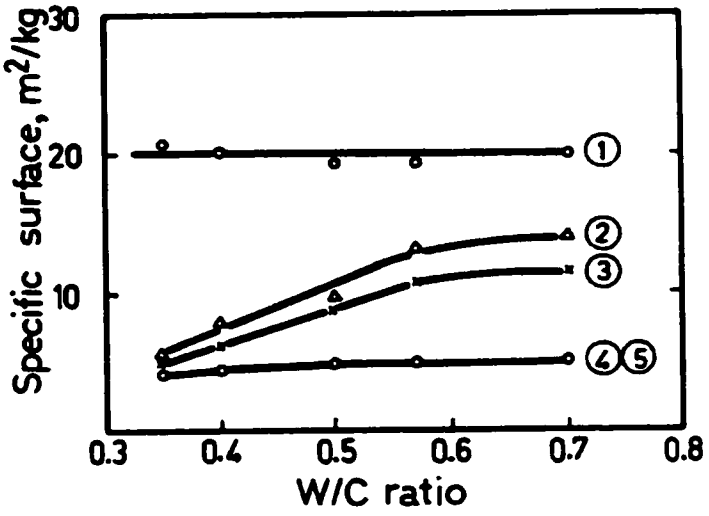

Figure 3.2: Surface area of cement paste determined by different adsorbents at different w/c: (1)Water vapor, (2) Nitrogen, (3) Methanol, (4) Isopropanol, and (5) Cyclohexane (Mikhail and Selim, 1966)

3.5 Micro-cracks

The fact that the permeability coefficient of a dried paste was found to be 70-fold greater than that of saturated paste (Powers et al., 1954) has been explained as the effect of microcracking (Chatterji, 1976, 1979). Bazant and Raftshiel (1982) indicated that even in a specimen as thin as 1 mm thick suddenly exposed to a lower RH, microcracking would happen. Microcraking also may even occur at high relative humidities as a result of shrinkage stresses developed in the vicinity of the CH crystal (Kawamura, 1978), and it may offset drying shrinkage (Lachowski, 1979). However, Bentur et al. (1979) claimed that such kinds of cracking would not affect the measured shrinkage. Helmuth and Turk (1967) indicated that specimen thickness as well as drying rate had no effect on the magnitude of shrinkage when specimens were dried to equilibrium at 47% RH. Recently, Day and Illston (1983) confirmed that not only recoverable but also irrecoverable shrinkage were not affected appreciably by rate of drying, therefore, they concluded that miniature specimens can be used to measure the unrestrained response of the material as long as the equilibrium condition is met.

3.6 AC impedance spectroscopy

Microstructural investigation of hydrating Portland cement paste by means of AC impedance technique is relatively new but continues to gain wide recognition. It is known to be able to provide useful information related to both ion concentration in the pore solution and microstructural changes in the hydrating cement paste (McCarter and Brousseau, 1990; McCarter et al., 1988; Gu et al., 1998). Its application to creep studies has not yet been reported even though there is a significant biographical review with regard to cement paste properties as well as shrinkage and moisture content of porous material (Beaudoin et al., 1996; McCarter and Curran, 1984; Norberg, 1999). One of the main parameters obtained from AC impedance spectroscopy - the high-frequency arc diameter - is dependent on the ionic concentration of the pore solution, pore-size distribution, and total porosity.

CHAPTER 4

DEFORMATIONS IN HARDENED CEMENT PASTE

4.1 Introduction

The volume of the hydration products of cement paste has been shown to be smaller than the combined volumes of the reacting cement and water by approximately 25% of the water volume. Under normal conditions this reduction in the volume of the cement-water system increases the porosity of the paste and is not reflected in the bulk dimension (Soroka, 1979). Under various conditions most engineering materials will exhibit time dependent deformations. In case of crystalline materials the phenomenon has been related to inter-crystalline slip. For hardened cement paste and/or concrete which is more complex, however, the problem is much more complicated and still under investigation by several researchers. Even though some volume changes take place due to chemical changes in the cement paste, the following sections, however, will be limited mostly to volume changes caused by physical factors such as external loading and changes in moisture content and temperature involving no chemical changes.

4.2 Elastic volume changes

4.2.1 Modulus of elasticity

Theoretically, elastic action involves displacement of atoms (or molecules in the case of complex materials) from their normal equilibrium positions, just enough to develop resistive forces. This displacement results in a change in volume. For complex and disordered molecules the elastic stress-strain curve may be nonlinear. In either case, the deformation is recoverable. If the cohesive strength of the material is exceeded at local imperfections, bonds will be broken. If the broken bonds propagate rapidly through the material, brittle fracture results.

Within the elastic range, the modulus of elasticity *(E)* of a material is defined as its strength per unit strain. For the cement paste, the modulus of elasticity is related to its compressive strength, increasing with an increase in the latter as shown in Figure 4.1 after Feldman and Beaudoin (1974). Consequently, all factors, which affect strength, will also affect the modulus of elasticity

of the hardened paste. An exception to this is the moisture content of the paste, which affects the two properties differently.

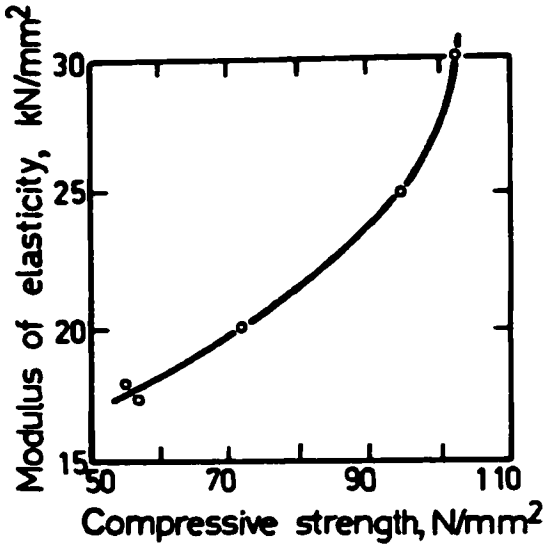

Figure 4.1: Relation between modulus of elasticity and compressive strength strength of cement paste (Feldman and Beaudoin, 1974)

Like strength, the modulus of elasticity can be related to the porosity of the paste using a similar expression,

$$E = E_o \exp(-bp) \qquad (4.1)$$

where E_o is the modulus of elasticity of a paste of zero porosity (p=0) and b is a constant which depends on the specific test conditions. This expression, which is based on statistical curve fitting, is generally valid for porous solids (Spriggs, 1962). Other expressions have been suggested, some of which were developed analytically from physical and geometrical considerations (Hashin, 1962). Powers (1961), for example, suggested the following expression.

$$E = E_g (1 - \varepsilon_c)^3 \qquad (4.2)$$

where ε_c is the capillary porosity, E is the modulus of elasticity of the paste, and E_g is the modulus when ε_c=0, i.e. E_g represents the modulus of elasticity of the gel.

Generally speaking, the strength of cement paste decreases with a decrease in moisture content, whereas its modulus of elasticity increases. It can be seen from Figure 4.2 that the modulus of elasticity attains its maximum on saturation, and decreases considerably on drying at 47 % relative humidity. On re-wetting the modulus increases, and on re-drying at 7% relative humidity it decreases again. The effect of moisture content, however, is not completely reversible due to irreversible changes in the structure of the paste. These changes are discussed later in relation to irreversible drying shrinkage of cement paste.

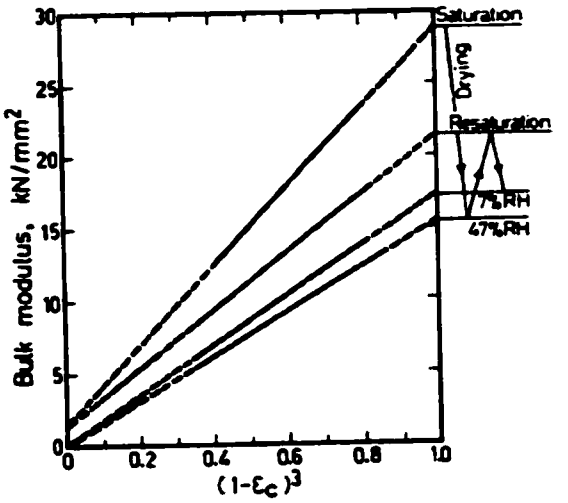

Figure 4.2: Effect of moisture content and capillary porosity on bulk modulus of elasticity of cement paste (Verbeck and Helmuth, 1968)

The effect of moisture content on the modulus of elasticity of cement paste is also demonstrated in Figure 4.3 after Sereda et al. (1966). It can be seen that drying of the saturated paste at 0% relative humidity decreases considerably the modulus of elasticity. Re-wetting, however, starts to affect the modulus only at a moisture content corresponding to a state of equilibrium at approximately 55% relative humidity, and on re-drying the modulus is affected only at the very low end of relative humidity scale. This relation between modulus of elasticity and moisture content may be noted to resemble the interlayer-water isotherm of Feldman and Sereda's model. Indeed, this model attributes the variation in the modulus of the cement paste with change in moisture content to movement of interlayer water.

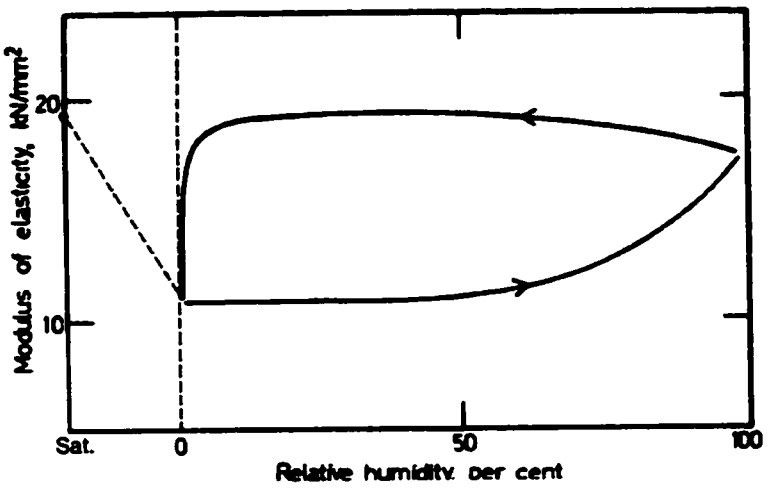

Figure 4.3: Effect of moisture content on modulus of elasticity of cement paste (Sereda et al., 1966)

Feldman and Sereda (1970b), furthermore, modeled the layer structure of the gel particles simply by two parallel short lines as can be observed on Figure 4.4. The water between the two lines, marked x in the figure, is interlayer water. The right hand part of the figure describes the variation in modulus of elasticity of the paste with the change in its moisture content, and the left-hand part is the weight change isotherm for the interlayer water. The letters A to G represent the same stages in all parts of the figure.

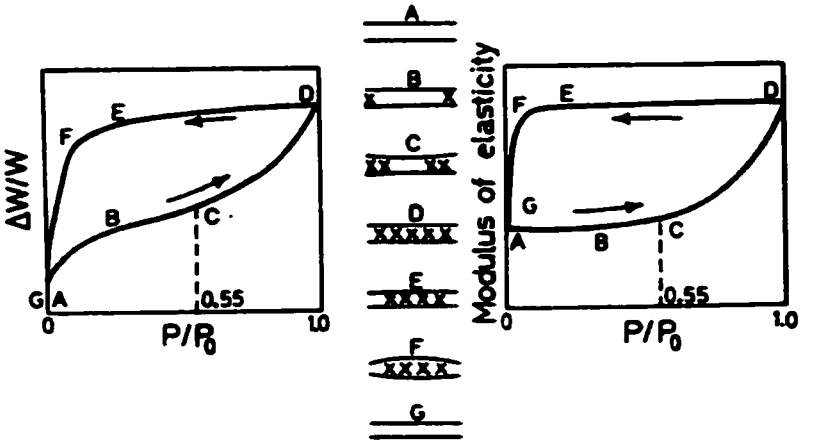

Figure 4.4: Effect of exit and re-entry of interlayer water on modulus of elasticity of cement paste (Feldman and Sereda, 1970b)

On increasing the relative humidity, water starts to enter the structure from the edge causing expansion by opening up the layers (stages A to C). It will be shown later, as is also implied by Figure 4.4, that the greater part of the swelling of the cement paste takes place at this stage. On the other hand, there will be no significant increase in the modulus of elasticity until the middle starts to fill, and the water molecules begin to act as webs or cross links in a sandwich-type construction. This stiffening effect, and the associated increase in the modulus, takes place from C to D and reaches a maximum when the layers are saturated (stage D). On drying from D to E, virtually no interlayer water is lost, and therefore the modulus is hardly affected. From E to F a small amount of interlayer water is lost from the edges, and the modulus, again, is hardly affected. Only when the interlayer water is removed from the middle (i.e. F to G) is the modulus of elasticity considerably decreased.

4.2.2 Poisson's ratio

Poisson's ratio is, by definition, the ratio of the lateral to the longitudinal (axial) strain in a loaded specimen. In a study by Helmuth and Turk (1966) the ratio in a saturated paste was found to vary from 0.26 to 0.31. In a paste dried at 7% and 47% relative humidity the ratio was 0.18.
The w/c ratio apparently does not affect Poisson's ratio. In one study the ratio averaged 0.25 independent of w/c ratio (Anson, 1964), and in another 0.21 (Soroka, 1979).

4.3 Shrinkage and swelling of cement paste

4.3.1 Introduction

The volume of a cement paste varies with its water content. Drying causes volume decrease (i.e. "drying shrinkage" or simply shrinkage), and wetting causes volume increase (i.e. swelling). Maximum shrinkage occurs on first drying of the paste, and a considerable part of this shrinkage is irreversible. That is, part of the volume decrease is not recovered on subsequent re-wetting. Further cycles of drying and wetting result in additional, usually smaller, irreversible shrinkage. After some time, however, the process becomes more or less completely reversible. Hence, the distinction between "reversible" and "irreversible" shrinkage. A schematic description of the preceding volume changes, in which irreversible shrinkage is assumed to take place on first

drying only, is presented in Figure 4.5. It may also be noted from the figure that continuous immersion in water causes swelling of the paste.

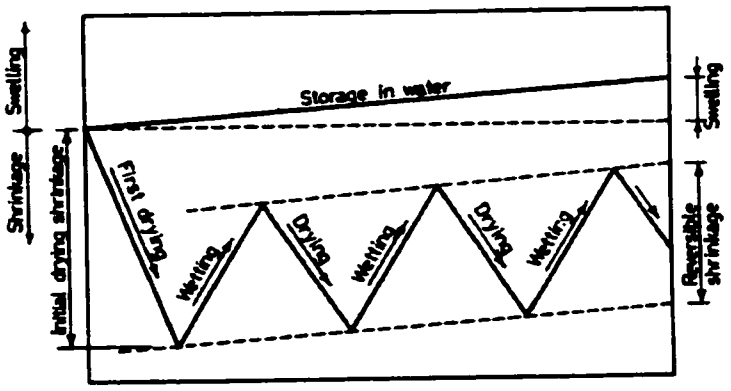

Figure 4.5: Schematic description of volume changes in cement paste due to alternate cycles of drying and wetting (Soroka, 1979)

The shrinkage of a cement paste, which was subjected to drying at the relative humidity indicated (Verbeck and Helmuth, 1968), is plotted in Figure 4.6 against the corresponding water losses. The resulting plot is linear with a distinct increase in the slope of the line at a water loss corresponding to drying at about 10% relative humidity. Accordingly, a water loss of approximately 17% in the high humidity region results in a shrinkage of about 0.6%, an additional loss of only 6% in the lower region doubles the shrinkage to 1.2%. It seems, therefore, that the water lost during the last drying stages affects shrinkage to a much greater extent than the water lost during the early stages.

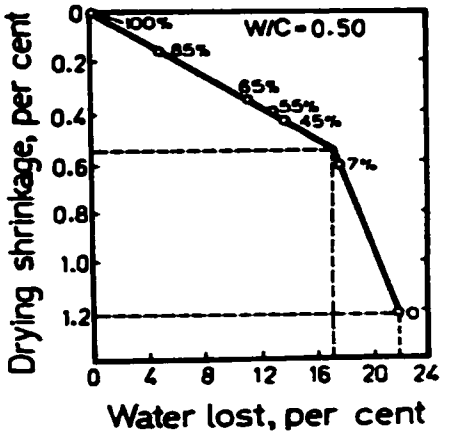

Figure 4.6: Effect of water-loss on shrinkage of cement paste (Verbeck and Helmuth, 1968)

Similar conclusions were reported by Young (1974) and data in Figure 4.7 show that one can have two or three different shrinkage regions while a specimen is drying.

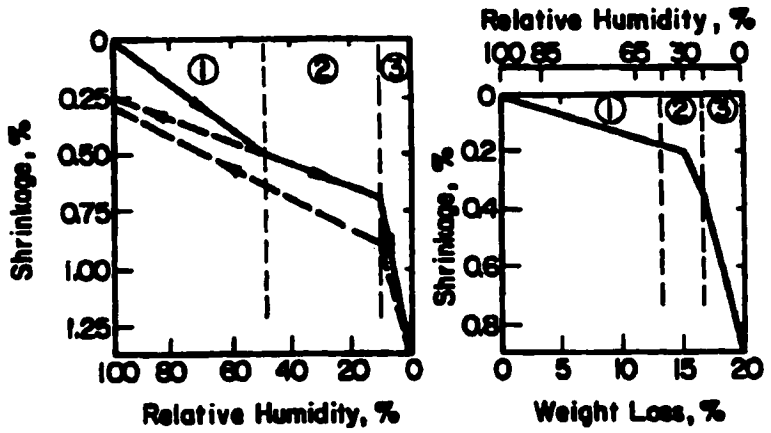

Figure 4.7: Shrinkage and swelling of typical cement paste as a function of (a) relative humidity and (b) weight loss (Young, 1974)

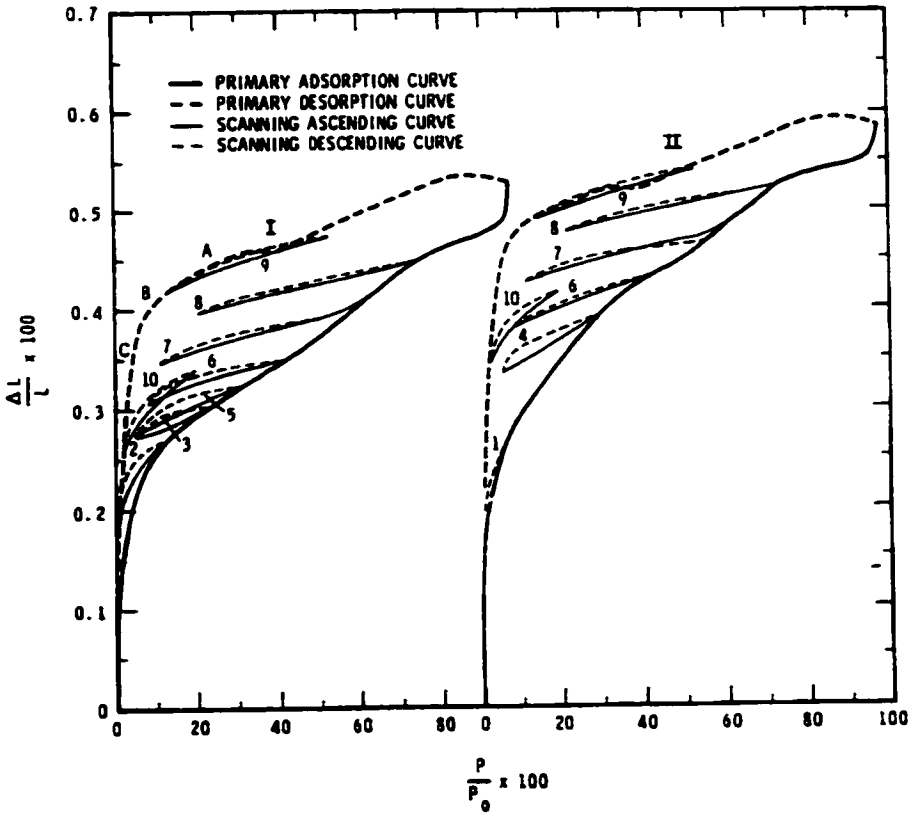

Figure 4.8: Length change isotherms and scanning loops for Portland cement pastes (Feldman, 1968)

The same conclusion is also apparent from Figure 4.8, which presents length change isotherms for cement pastes after Feldman (1968). On desorption in the relative humidity range from 100 to 10%, the slope of the curve is fairly gentle, whereas from 10 to 0% it becomes almost vertical. It can be seen, both in this case and from the data of Figures 4.6 and 4.7, that most of the shrinkage is associated with water loss in the low-humidity range. It is also evident from the scanning loops that length change isotherms, like the adsorption isotherms, are irreversible over the whole region.

The change in slope in Figure 4.6 and/or Figure 4.7 implies that shrinkage may be attributed to more than one mechanism. Moreover, in some tests of the same series the slope changed twice while in tests by others the slope changed three times (Roper, 1966; Verbeck and Helmuth, 1968; Young, 1974). Again, this pattern implies that more than one mechanism is involved. It should be noted, however, that the relation between shrinkage and water loss has not been found to be linear in all tests and that the breaks in the relevant curves have not always been observed. Nevertheless, in all tests shrinkage was found to be related to water loss and this relation was more pronounced at the later stages of drying. From thermogravimetric methods, Sabri and Illston (1982) identified two types of water as A; free and adsorbed water and B; water associated with the structure of ettringite and C-S-H gel. They attributed the reversible shrinkage to the movement of type B water, while irreversible shrinkage is thought to derive from the movement of type A water leading to the permanent closing of spaces between hydrate particles.

4.3.2 Factors affecting shrinkage

Since shrinkage of the cement paste is related to water loss, all the factors, which affect drying (i.e. temperature, humidity, pressure, and air movement) will also affect shrinkage. Shrinkage is also affected by cement composition, and by the factors associated with the structure of hardened cement paste such as w/c ratio, porosity, etc. There is a considerable effect of specimen size on the rate of drying shrinkage; in thin paste specimens, approximate weight and dimensional equilibrium can be reached in a very short time (Helmuth and Turk, 1967). In comparison to drying shrinkage measurements made on larger specimens, this shrinkage response clearly shows that the rate of shrinkage is controlled not by the basic phenomena causing shrinkage, but instead, by the concurrent process of water diffusion through the mass of the specimen. Day and Illson (1983) found that the magnitude of shrinkage strains when the cement paste specimens reached equilibrium at intermediate relative humidity were independent of the rate of drying.

4.3.2.1 Water-cement ratio

The effect of water-cement ratio on shrinkage was clearly demonstrated by Haller (1940). Indeed, at earlier stages, when the shrinkage rate is high, the w/c ratio has no significant effect on shrinkage. However, later shrinkage decreases with the decrease in the water-cement ratio and possibly ultimate shrinkage is reached sooner for cement with a low w/c ratio. Figures 4.9 and 4.10 show these general trends for cement pastes. Figure 4.10 shows that up to an age of 28 days shrinkage is essentially the same for all pastes regardless of differences in the amount of water lost, but at later ages, the differences become significant. Although the amount of water lost from 28 to 365 days is nearly the same for all pastes, the shrinkage varies considerably and increases with the w/c ratio.

This phenomenon of variation in shrinkage with w/c ratio might be explained by the difference in types of water lost at the various stages of drying, i.e., possibly at early stages water is lost from capillary pores and later water will be removed from the micropores. Bentur et al. (1978) also predicted results for C_3S pastes (see Figure 4.11) which agree well with experimental data in Figure 4.12 after Roper (1968).

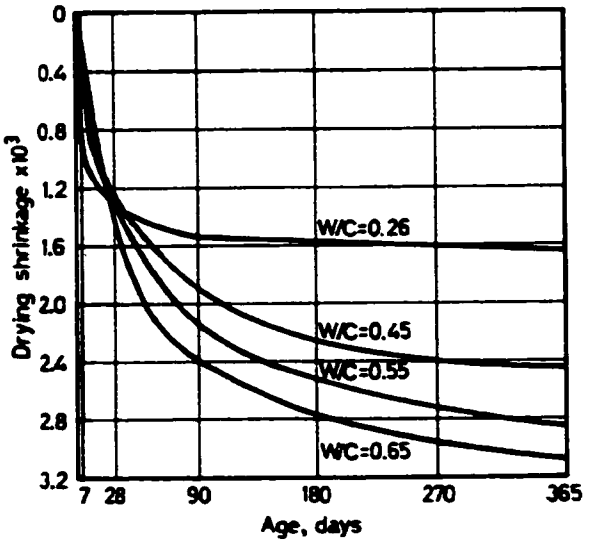

Figure 4.9: Effect of water-cement ratio on shrinkage of cement pastes (Haller, 1940)

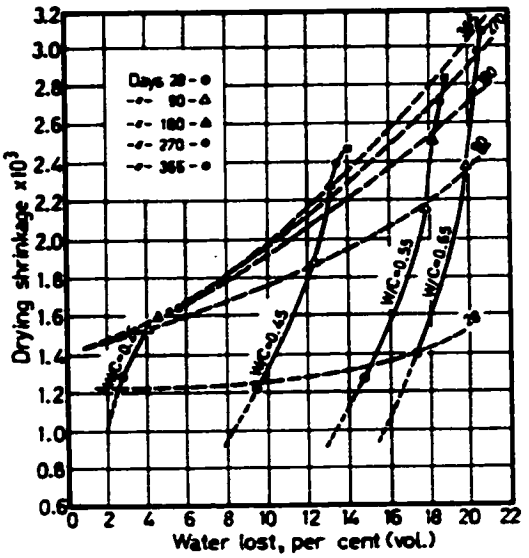

Figure 4.10: Effect of water-loss on shrinkage of cement pastes of different w/c ratios (Haller, 1940)

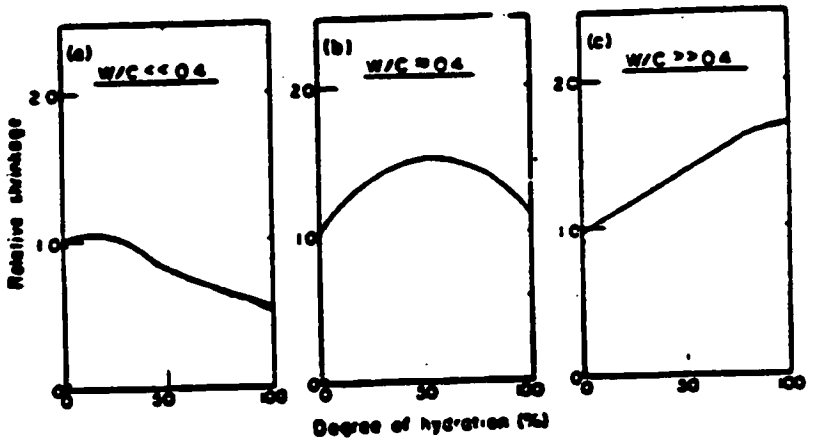

Figure 4.11: Predicted shrinkage behavior of C_3S pastes at different w/c ratio and α (Bentur et al., 1978)

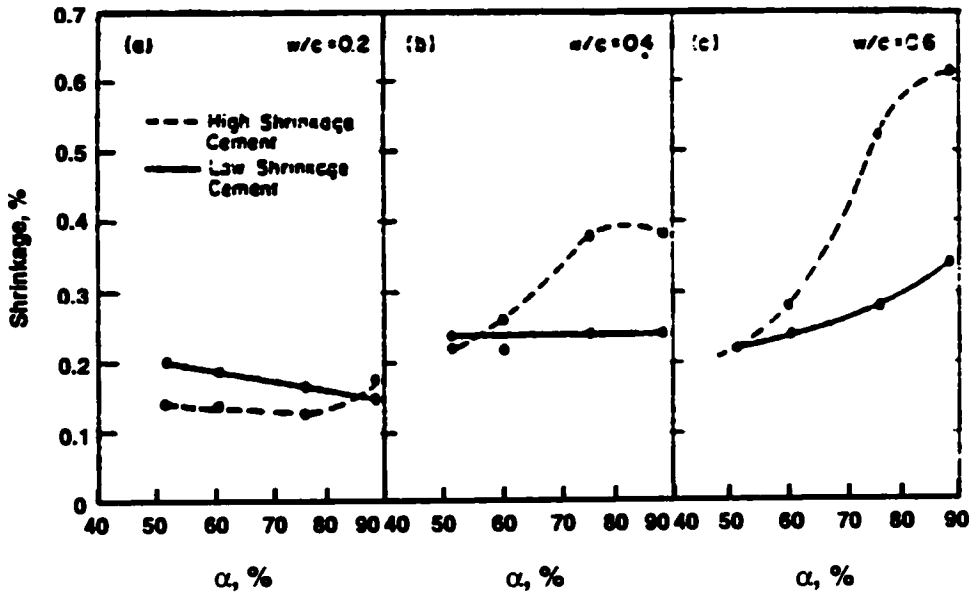

Figure 4.12: Observed effect of degree of hydration α and w/c ratio on shrinkage of Portland cement paste (Bentur et al., 1978)

4.3.2.2 Degree of hydration

The higher the degree of hydration, the higher the gel content of the paste (Soroka, 1979). The increase of C-S-H content increases the volume of gel pores at the expense of capillary pores. Greater shrinkage is expected in pastes with a higher C-S-H gel content, since, recalling the brief explanation of effect of w/c ratio, the drying from micropores (gel pores) is assumed to cause greater shrinkage than that from capillary pores. The data in Figures 4.12 and 4.13 (Bentur et al., 1978) and Figure 4.14 (Verbeck and Helmuth, 1968) support this conclusion; which compare the shrinkage of cement pastes for different periods of moist curing. In Figure 4.13, stage A is assumed to be the result of moisture loss from capillary pores and stage B is due to moisture loss from gel micropores. This will be discussed later. However, both Bentur et al. (1978) and Verbeck and Helmuth (1968) reported that there is a maximum shrinkage somewhere in the 60% to 80% range of degree of hydration (α) as shown in Figure 4.15c. The change in experimental conditions, such as temperature and additions of admixtures, will modify the influence of degree of hydration upon shrinkage as demonstrated by the data in Figure 4.15 (a) and (b). Therefore, the effects of degree of hydration in the range of 60% to 80% and at different mixing conditions should be further investigated and interpreted.

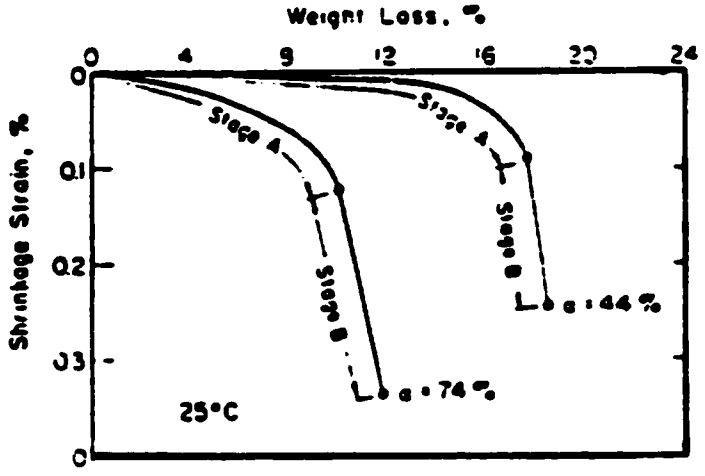

Figure 4.13: Effect of degree of hydration α to shrinkage-weight loss curve of C_3S pastes (Bentur et al., 1978)

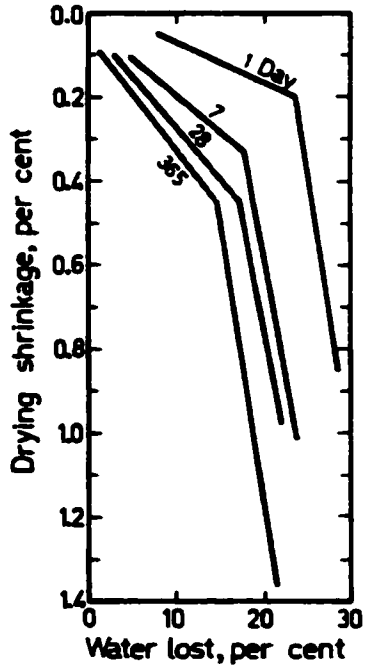

Figure 4.14: Effect of water-loss on shrinkage of Portland cement pastes cured for different periods (Verbek and Helmuth, 1968)

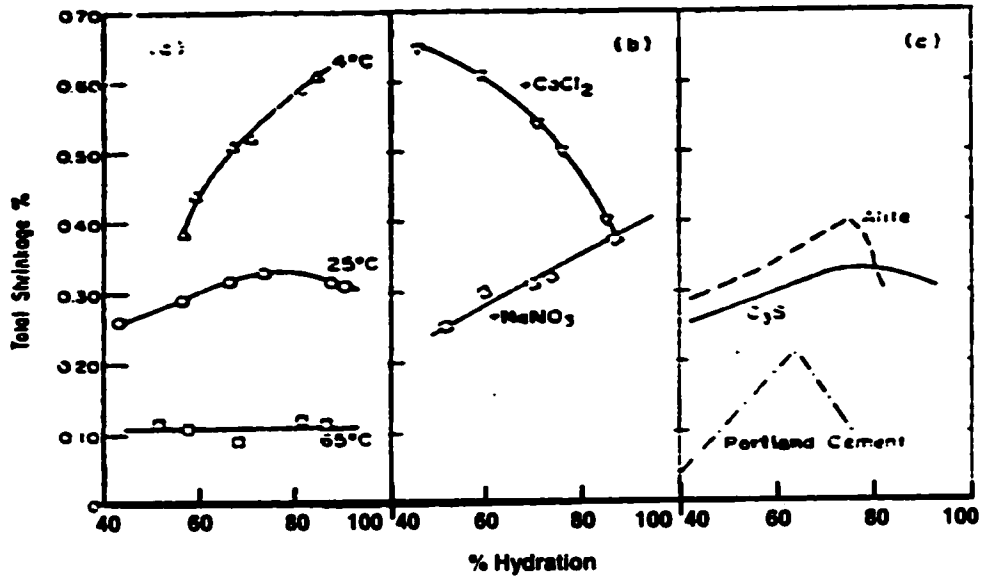

Figure 4.15: The effect of degree of hydration α on shrinkage at different conditions (a) Temperature, (b) Admixture, and (c) Composition (Bentur et al., 1978)

4.3.2.3 Capillary porosity

The capillary porosity of the paste depends both on the w/c ratio and the degree of hydration or the curing condition (Soroka, 1979). Porosity decreases with a decrease in the w/c ratio and with an increase in the degree of hydration as shown in Figure 4.16.

The study of well-matured cement pastes after Helmuth and Turk (1967) presented in Figure 4.17, demonstrates the effect of porosity on shrinkage. The data clearly indicate that shrinkage increases linearly with porosity. However, this conclusion may not be valid under all experimental conditions. Wittmann (1982) reported that both the total porosity as well as the pore size distribution influence shrinkage as they depend on the water/cement ratio and on the degree of hydration. He concluded that the drying process and, as a consequence, shrinkage of a porous material is governed essentially by the pore size distribution.

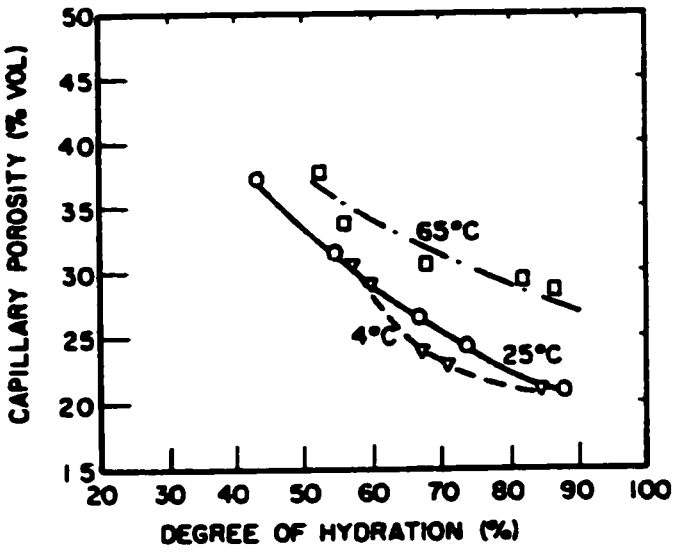

Figure 4.16: Capillary porosity versus degree of hydration α for C_3S, C_2S, C_3S/C_2S blend, and Portland cement pastes (Berger et al., 1976).

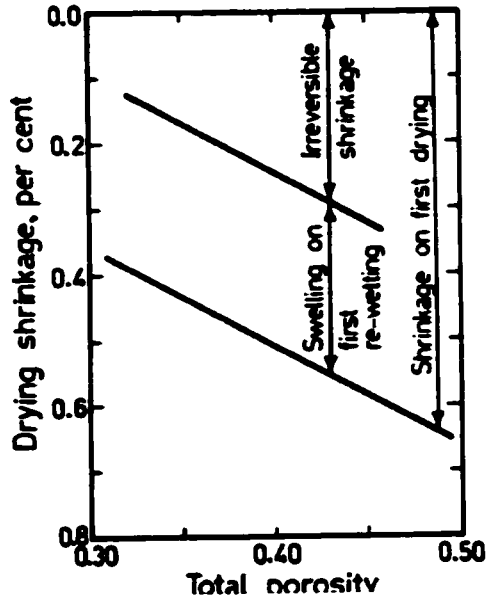

Figure 4.17: Effect of total porosity on shrinkage of cement paste (Helmuth and Turk, 1967)

4.3.2.4 Admixtures

Most of the chemical admixtures are generally believed to increase the magnitude of shrinkage, and it has been suggested that they were linked to the microstructural and porosity changes (Young, 1982). Berger et al. (1976) reported that shrinkage of pastes with $CaCl_2$ which is an accelerator that increases early hydration, decreases with increasing hydration, whereas in pastes without $CaCl_2$ shrinkage increases with increasing hydration as shown by data in Figure 4.18.
The porosity changes presented in Figure 4.19 show that after addition of $CaCl_2$ the pore size distribution tends to shift to a smaller value, and it is reported that it is accompanied with a change in external C-S-H morphology due to the presence of $CaCl_2$ (Berger et al., 1976). Feldman and Swenson (1975) suggested that the effect of an admixture is mainly one of the degree of dispersion in terms of alignment of sheets and displacement of the ends of sheets. It seems that the effect of admixtures on shrinkage of cement pastes depends on the specific admixture and the conditions concerning its use.

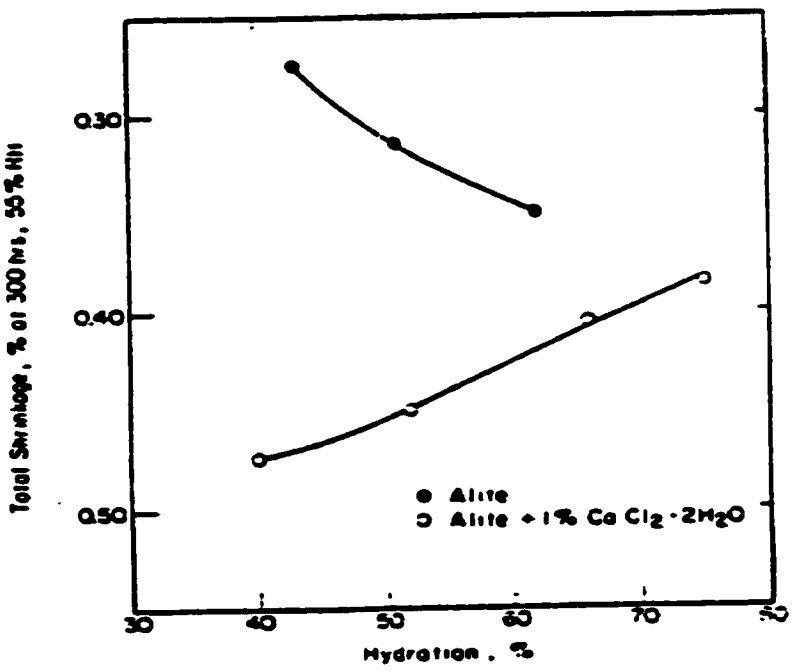

Figure 4.18: Effect of C_aCl_2 addition on drying shrinkage of alite paste (Berger et al., 1976)

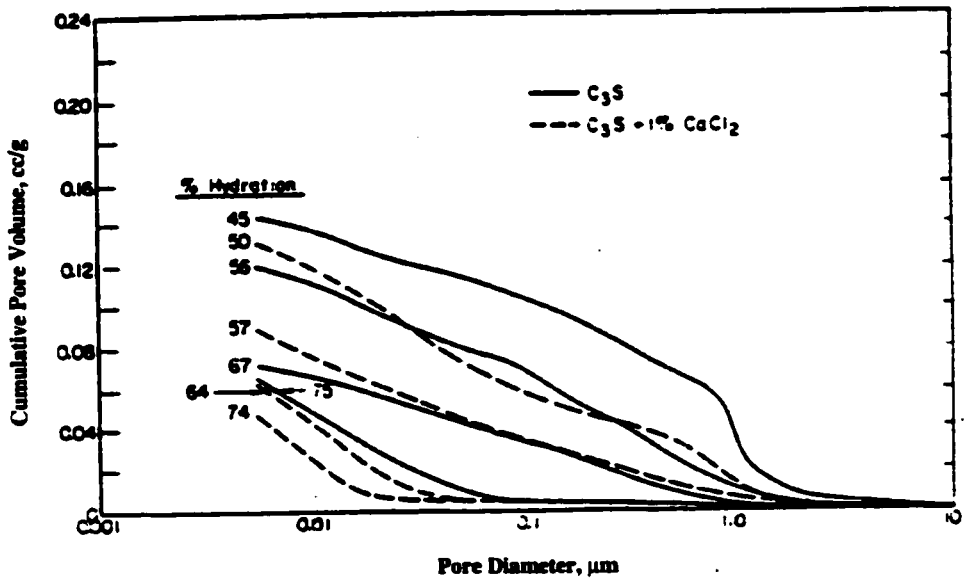

Figure 4.19: Effect of $CaCl_2$ addition on pore size distribution of alite paste (Berger et al., 1976)

4.3.2.5 Curing temperature

Increasing curing temperature primarily decreases the irreversible portion of the shrinkage (Parrott, 1977a). Even an exposure to high temperature for short periods may be effective. The effect of temperature may be mainly due to the formation of different pore size distributions. Figures 4.15 and 4.20 to 4.22 show the effect of curing temperature on shrinkage (Bentur, 1980; Bentur et al., 1978; Parrott, 1977a). High temperature curing, at 65°C, tends to develop a coarse capillary pore structure as the hydration proceeds. Therefore, the shrinkage apparently decreases as the volume of smallest pores in the range 2.5 nm-6.0 nm become smaller. For paste cured at low temperature, say 4°C, shrinkage increases with the increase of the degree of hydration (see Figure 4.20), which is in accord with a shift in pore size distribution towards smaller pores, Figure 4.22.

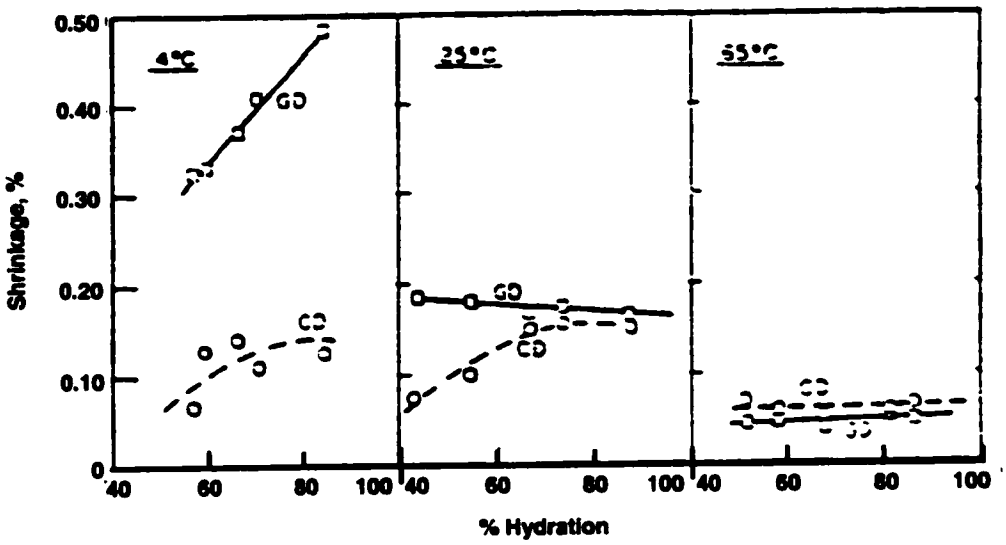

Figure 4.20: Effect of curing temperature on shrinkage of alite paste CE and GD is shrinkage caused by the capillary pores and gel pores respectively (Bentur et al., 1978)

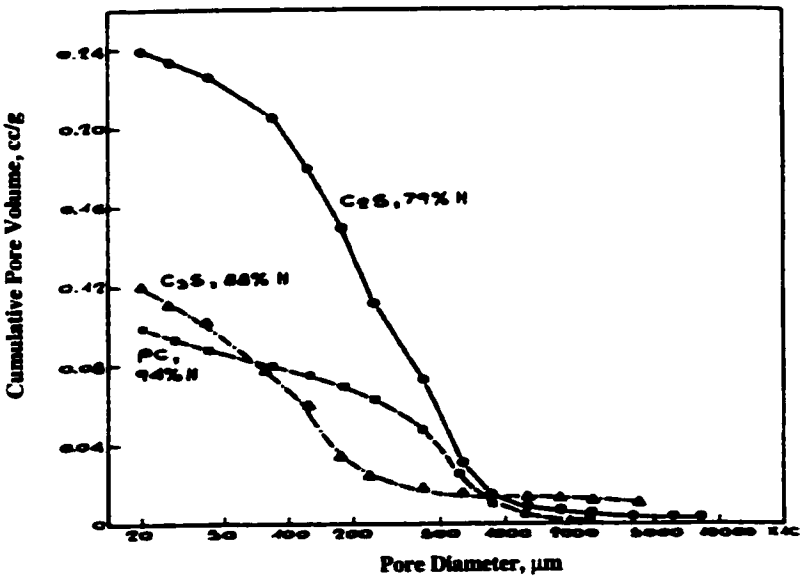

Figure 4.21: Cumulative N_2 pore size distribution for C_3S pastes cured at 25°C (Bentur, 1980)

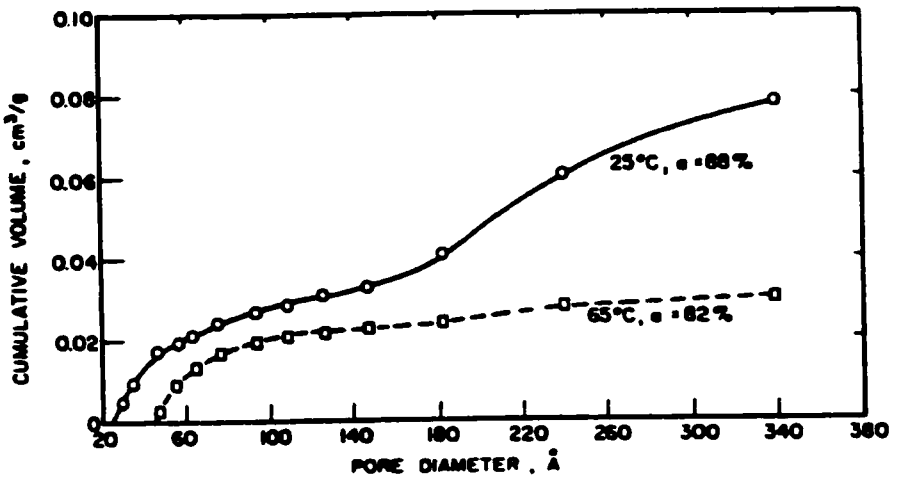

Figure 4.22: Effect of curing temperature and degree of hydration on N_2 pore size distribution (Bentur et al., 1978)

4.3.2.6 Cement composition

The composition of the cement can influence the shrinkage of the paste, and hence the concrete, although the effect is not large. Since most of the shrinkage is believed to originate in the C-S-H gel and its associated porosity, it might be because in a cement paste the presence of minor components changes the properties of C-S-H gel. There is some correlation between shrinkage and C_3A content (Alexander et al., 1979; Hobbs, 1978; Roper, 1968) that could be due either to the formation of sulfoaluminates or to A or $\overline{S}$ substitution in CSH. The contributions of the minor components appear to depend on the fineness of the cement and alkali content, which determine the effective amount of gypsum (Hobbs, 1978; Roper, 1968). Hence, there is an "optimum gypsum content" of minimum shrinkage for each cement type. Most characteristics of the effect of cement composition have been pointed out in Chapter 2, but the exact relationship is still uncertain.

4.3.3 Mechanisms of reversible shrinkage

As previously said variations in moisture content of the cement paste are accompanied by volume changes. The decrease in the volume of the paste on drying is referred to as "shrinkage", and its

increase on rewetting as "swelling". Generally, shrinkage and swelling are described by more than one mechanism. Opinions differ, however, with respect to the relative importance of each mechanism, as one would found in the following sections.

4.3.3.1 Capillary tension

Saturation vapor pressure or simply vapor pressure of a liquid is the pressure at which the liquid and vapor coexist at equilibrium, meaning that when the number of molecules leaving the liquid into the space above it (evaporation) is equal to the number returning to the liquid at any given time. When the vapor pressure over a liquid is lower than the saturation pressure, the number of molecules leaving the liquid (vaporization) is greater than the number returning (condensation), then the amount of liquid is gradually reduced, i.e. evaporation takes place. The vapor pressure for water that forms curved meniscus (such as forms in capillary pores greater than 2.6 nm diameter) is lower than the vapor pressure of pure bulk water. Thus lower vapor pressures are required for evaporation from pores. The relationship between the radius of curvature, r, of the meniscus and the corresponding vapor pressure, P_r, is given by Kelvin's equation, equation (4.3).

$$\ell n\frac{(P_r)}{(P_o)} = \frac{2\gamma M}{RT_o\rho r} = k\frac{2\gamma}{r} \qquad (4.3)$$

where P_o is the saturation vapor pressure over a plane surface, γ is the surface tension of the liquid, R is the gas constant, T is the temperature in kelvin (°K), ρ is the density of the liquid at T°K, and M is the molecular weight of the gas. This is shown in Figure 4.23; once the vapor pressure drops below the vapor pressure corresponding to the minimum possible radius, P_r, evaporation continues until the capillary is empty. Therefore, on exposing the cement paste to a gradually decreasing relative humidity, the pores gradually become empty in the order of their size, i.e., the bigger pores lose water first, then the smaller pores. During this exposure process, the capillary water is subjected to a tensile stress, P_{cap}, which is equal to ρh_1, where h_1 is referred to height of the capillary tube, as shown in Figure 4.23. The maximum stress, P_{cap}, can be expressed by equation (4.4) as follows.

$$P_{cap} = \frac{2\gamma}{r} \qquad (4.4)$$

Consequently, as the radius decreases with the decrease in vapor pressure, the tensile stress in capillary water decreases. This induced tensile stress, P_{cap}, in the capillary water must be balanced by compressive stresses in surrounding solid. Hence, the evaporation of capillary water and the formation of a meniscus will subject the paste to compressive stresses, which, in turn, will cause elastic volume decrease, i.e., shrinkage.

This mechanism can explain why, at the early stages of drying, which corresponds to region 1 in Figure 4.7, the amount of water lost is large compared to the resulting shrinkage (Helmuth and Turk, 1967; Verbeck and Helmuth, 1968). This is because at region 1 a large amount of water is lost from relatively large diameter pores, which is under a very small capillary tension. At later stages, water evaporates from the smaller pores and the small loss of water results in a significant shrinkage. The mechanism of capillary tension is thought to be valid when relative humidity exceeds 50 % according to Powers (1962, 1965), 35% according to Feldman and Sereda (1970a, 1970b), or 40 % after Ishai (1968), although there is some debate about the relative importance of this mechanism. However, the capillary stresses may not exist below about 40 to 45% RH since menisci are no longer stable (Young, 1974).

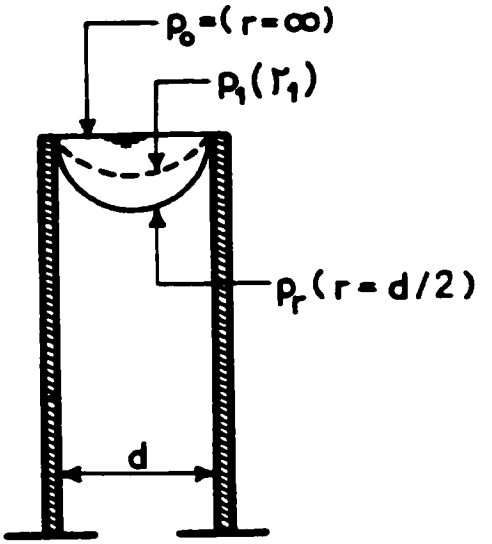

Figure 4.23: Relation between radius of curvature and vapor pressure (After Soroka, 1979)

4.3.3.2 Disjoining pressure (swelling pressure)

Adsorption of gas molecules onto the surface of a solid is a result of a mutual attraction between the molecules on the surface of the solid and the molecules of the gas. At a given pressure and temperature, a dynamic equilibrium is set up in which the number of molecules being adsorbed at any given time equals the number of molecules escaping the surface. The adsorbed water is considered to be compressed perpendicular to the surface with a tangential pressure (spreading pressure) along the surface. At a given temperature, the thickness of the adsorbed water layer is determined by the ambient relative humidity. The thickness increases with relative humidity reaching a maximum equivalent to a layer about 5 molecules deep (about 1.3 nm), and, in some situations when the distance between two adjacent particles is less than 2.6 nm, then swelling or disjoining pressure will build up (Powers, 1965; Soroka, 1979). A model as presented in Figure 4.24 has been developed by Powers to explain such mechanism. This mechanism is based on the tendency of adsorbed water to push the adjacent surfaces apart to achieve thermodynamic equilibrium. Resistance of the solid generates a compressive stress in the water. This situation has also been called "hindered adsorption water" or "load bearing water".

The disjoining pressure mechanism is enhanced at high relative humidity, region 1 in Figure 4.7, and requires weak cohesion. At 100% RH surfaces closer than 2.6 nm will promote hindered adsorption, 1.0 nm at 50% RH and 0.5 nm at 10% RH is probably the lower limit. As the vapor pressure is lowered disjoining pressures will diminish and surface can approach more closely with the process being reversible. Wittmann (1968) considers this mechanism to be important at relative humidity greater than 50%. Feldman and Sereda (1970a, 1970b) completely reject this mechanism on the assumption that interparticle bonds will never be broken due to adsorption of water. Parrott and Young (1982) pointed out two results suggesting that shrinkage does not simply derive from a reduction in disjoining pressure. First, the small expansion rate at lower relative humidity ranges would not be expected. Second, exchange of water for methanol followed by exchange of the methanol for n-pentane did not cause any significant shrinkage. Derjaguin and Churaev (1974) suggested that a considerable change in disjoining pressure should result from the replacement of a polar molecule (water or methanol) with a non-polar molecule (n-pentane).

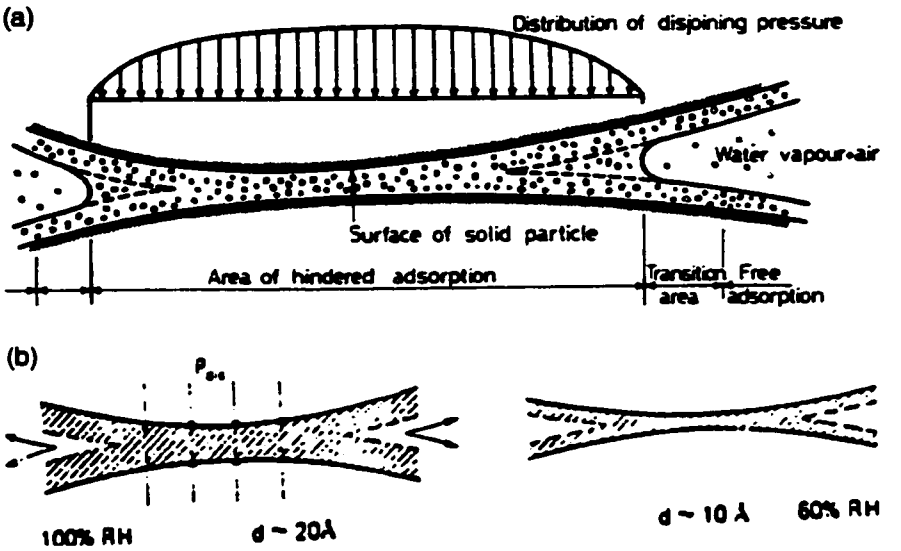

Figure 4.24: (a) Area of hindered adsorption (After Soroka, 1979) and (b) Disjoining pressure mechanism (After Mindess and Young, 1981)

4.3.3.3 Surface free energy (Surface tension)

Adsorption of water occurs on solid surfaces through interaction with the force fields on the surface atoms. Adsorption thus lowers the surface free energy of the solid. This is illustrated in Figure 4.25 (Soroka, 1979) the surface point B is under anisotropic force, because of force lacking in the BC direction. Therefore, the surface tends to contract and behaves like a stretched elastic skin. The resulting tension in the surface is known as "surface tension" and is a result of a higher energy level.

The drying increases surface tension and the induced compressive stress results in a volume decrement, i.e., shrinkage (Figure 4.26). Conversely, on adsorption the compressive stress will be relaxed and thus result in expansion, or swelling. This surface tension mechanism becomes significant only below 50% relative humidity, region 2 in Figure 4.7, where less than 2 molecular layers (about 0.6 nm) of water exist, and the effects become largest when the last monolayer of adsorbed water is removed below 30% RH. The change in surface free energy with relative humidity is described by the Gibbs free energy equation, equation (4.5) as follows.

$$\Delta\gamma = -\frac{RT}{S}\int_0^p n\frac{dP}{P} \qquad (4.5)$$

where $\Delta\gamma$ represents the change in surface free energy (tension) of pure adsorbent from its initial state under its own vapor pressure to its combining state provided that the integral represents a path of thermodynamic reversibility. The term *n* represents the number of moles of adsorbate on a fixed mass of adsorbent. S is surface area, P is the equilibrium vapor pressure, R is gas constant, and T is absolute temperature.

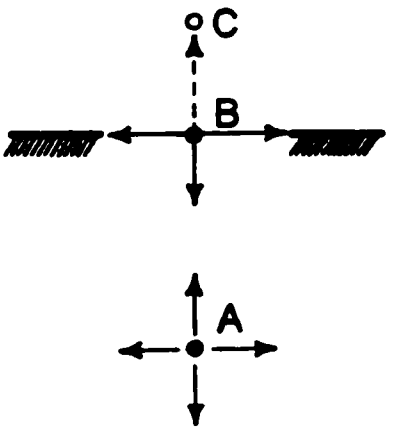

Figure 4.25: Schematic representation of surface tension (After Soroka, 1979)

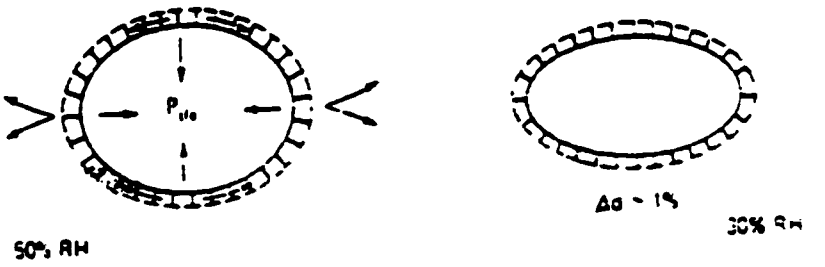

Figure 4.26: Surface tension mechanism (After Mindess and Young, 1981)

The Bangham equation, equation (4.6), is an empirical, linear relationship between length change and change in surface tension.

$$\frac{\Delta\ell}{\ell} = \lambda(\gamma - \gamma_o) = \lambda\Delta\gamma \qquad (4.6)$$

where $\Delta\ell/\ell$ is the length change, and λ is constant. Although Wittmann (1968) has used this equation quite successfully, Powers (1965) did not consider this mechanism valid above 30% RH and demonstrated a similar linear relationship from a thermodynamic treatment of hindered adsorption.

4.3.3.4 Movement of interlayer water

Reversible movement of water with respect to the layered C-S-H particles could cause volume changes because such movement would affect the spacing of the layers. Feldman and Sereda (1970a, 1970b) assumed that such reversible movement of water occurs, whereas in other models it is assumed that interlayer water may be removed but will not re-enter the structure. Therefore, the idea that the movement of interlayer water is the main mechanism of shrinkage and swelling after Feldman and Sereda is contradictory to those of Ishai (1968), Powers (1965), and Wittmann (1968). According to these latter mentioned authors, movement of interlayer water may account only for the irreversible part of shrinkage.
The recapitulation of difference of opinion described above is clearly presented in Table 4.1.

Table 4.1: Shrinkage mechanisms after various authors

Authority	*Relative humidity, %* 0 10 20 30 40 50 60 70 80 90 100
Powers (1965)	← Variations in swelling pressure →
	← Augmentation by capillary effects →
Ishai (1968)	← Variations in surface energy → ← Capillary tension →
Feldman and Sereda (1970a, 1970b)	← Movement of interlayer water → ← Capillary tension and variations in surface energy →
Wittmann (1968, 1977)	← Variations in surface energy → ← Variations in swelling pressure →

4.3.4 Mechanisms of irreversible shrinkage

Some of the shrinkage, which occurs in the first cycle of drying, and wetting is irreversible (Feldman, 1968; Helmuth and Turk, 1967; Mindess and Young; 1981). The Figure 4.17 shown previously and the Figure 4.27 after Feldman demonstrate the existence of non-recoverable

portion of shrinkage. This happens mainly in region 1, but also occurs in region 3 defined in Figure 4.7. Drying and re-wetting cycles continue at a relative humidity down to 50% and also induce irreversible shrinkage (Young, 1974), but at a much smaller extent than after first drying, as shown in Figure 4.7 (a). Prolonged drying of pastes dried after one day showed considerable irreversible shrinkage and water loss (Helmuth and Turk, 1967), Figure 4.28.

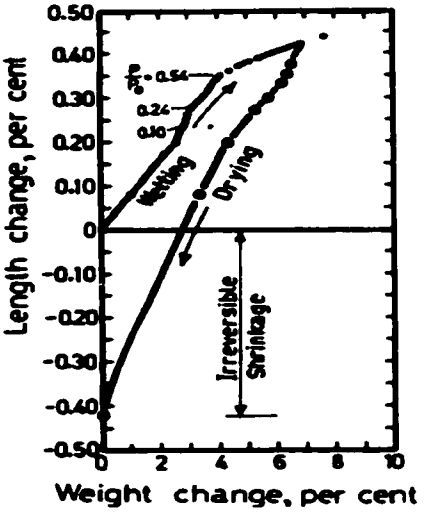

Figure 4.27: Effect of interlayer water loss on length changes of a cement paste (Feldman, 1968)

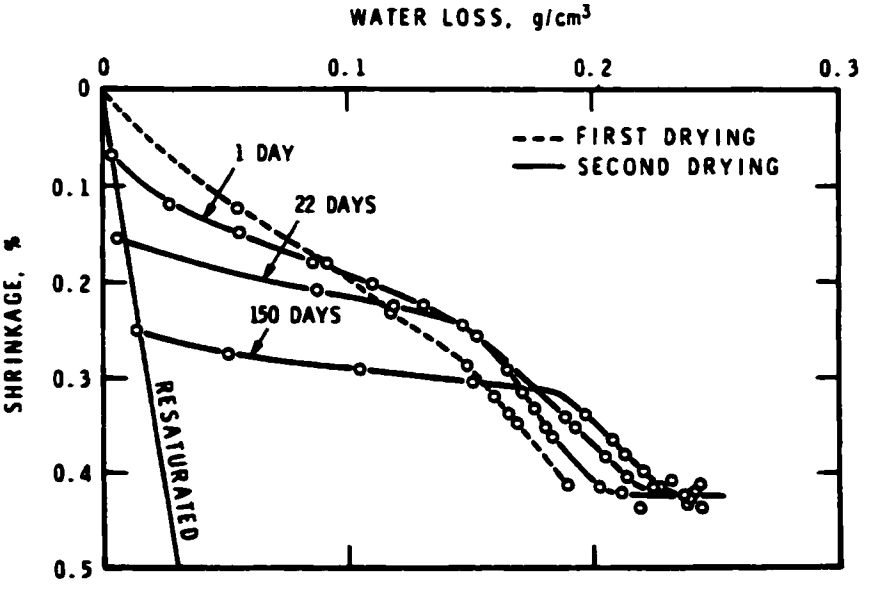

Figure 4.28: Drying shrinkage at 47% RH and water loss of cement paste of 0.5 water cement ratio (Helmuth and Turk, 1967)

Helmuth and Turk (1967) indicated that the magnitude of irreversible shrinkage depends on many factors, i.e., w/c ratio (reversible shrinkage is independent of this), drying period, curing period, etc. Irreversible shrinkage occurs slowly as aging progresses (Hunt et al., 1960) and may increase with an increase in total shrinkage. Parrott (1977b) reported that heating might reduce irreversible shrinkage primarily due to silicate polymerization. Therefore, some kind of structural change must be occurring within the solid, depending on such factors as stress, relative humidity, time, temperature, and porosity. The following explanations of irreversible shrinkage have been suggested, but it is quite possible that irreversible shrinkage might be the result of more than one mechanism (1968).

a. The removal of interlayer water below 11% RH may create interlayer space (Feldman, 1972) which will contribute to irreversible shrinkage or creep. Irreversible shrinkage may also occur above 11% RH to a lesser extent, see Figure 4.7, region 3.
b. Changes in capillary pore size distribution may also contribute to irreversible shrinkage based on the observation that loss of surface area, measured by nitrogen adsorption, occurs on drying (Hunt et al., 1960).
c. Changes in chemical bonding between C-S-H particles have also been suggested to be a cause of irreversible shrinkage, but the evidence is contradictory.

4.4 Creep of hardened cement paste

4.4.1 Introduction

Hardened cement paste and concrete can deform inelastically as well as in a time independent and reversible elastic manner. In addition, creep is also observed as a function of the magnitude and the duration of the external load, and is partly irreversible. The deformation caused by irreversible changes in the structure of the paste such as cracking is known as "permanent set". Also, the elastic deformation decreases with time due to the increase in the modulus of elasticity of the paste.

Under sustained loading the deformation of the paste increases at a gradually decreasing rate, see Figure 4.29, approaching a value several times larger than the elastic deformation. If the paste is allowed to dry when under load, shrinkage occurs simultaneously. Creep is, therefore, the

increase in deformation under a sustained stress excluding drying shrinkage as demonstrated in Figure 4.29 for a paste loaded under compression.

According to the strain terms illustrated in Figure 4.29, creep and shrinkage are assumed to be independent of each other and are superimposed. Strictly speaking, such an assumption is not correct because creep and shrinkage are mutually dependent, and the simultaneous shrinkage of the paste is associated with the increased creep. Accordingly, a distinction is made between "basic creep" and "drying creep". Basic creep is the creep observed in specimens, which reached equilibrium with the surrounding medium with respect to water content, i.e., it is creep which takes place when no simultaneous drying of the paste is involved. Drying creep is the additional creep induced by simultaneous drying and it's believed to be the most complicated and the least understood phenomenon sometimes called the "Pickett effect". Hence, the difference between the total time-dependent deformation and shrinkage is the sum of basic creep and drying creep as shown in Figure 4.29.

The explanation of the drying creep effect offered by Pickett (1956) is based on the fact that creep rate increases progressively nonlinearly with stress. When stresses resulting from load are superimposed on stresses caused by non-uniform shrinkage, the total stress becomes higher and the specific creep (creep per unit stress) should thus increase. Bazant and Moschovidis (1973) found this explanation to be at variance with other creep properties because if the total stress were actually in the nonlinear creep range, creep strain would also exhibit a strongly nonlinear dependence on stress. However, knowledge of the hygrometric properties of creep has been considerably improved by experiments on small specimens (Gulcklich and Ishai, 1962; Mullen and Dolch, 1964; Wittmann, 1970).

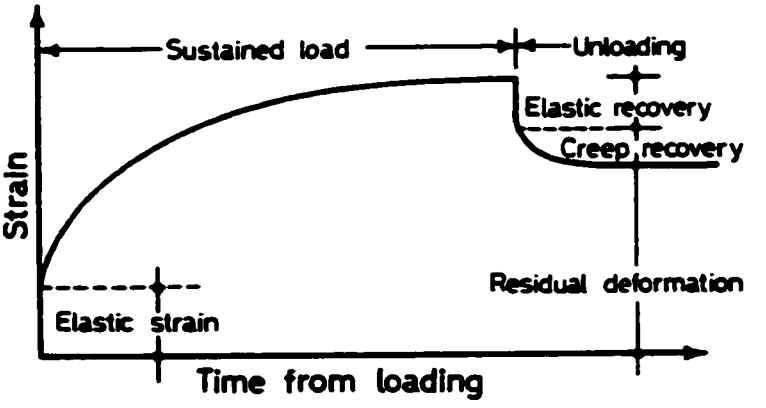

Figure 4.29: Deformation with time of cement paste under sustained loading (Neville, 1970)

Powers (1965) argued that creep is caused by the diffusion of the load bearing water; an external load changing the free energy of adsorbed water. Feldman (1972) has suggested that creep occurs through the gradual crystallization, or aging process, of layered silicate material leading to an increase of the extent of layering; water movement is not considered a major mechanism. Wittmann (1970) suggested that in the Powers and Feldman models creep should be zero, if the hydrated cement paste is dried out fully. However, his own measurements show significant creep even of the fully dried specimen. This is contrary to the results of Mullen and Dolch (1964) who reported that oven-dried specimens of cement paste exhibited no creep at all. They concluded that water movement was the dominant mechanism in the creep of concrete.

As with shrinkage, creep is partly irrecoverable. On unloading, an immediate decrease of the deformation will be observed due to elastic recovery. The instantaneous recovery is followed by a gradual decrease in deformation due to "creep recovery". Creep recovery is not complete, approaching with time a limiting value, which is smaller than the previous creep. As illustrated in Figure 4.30, the remaining residual deformation is either irreversible creep or the algebraic sum of the latter and shrinkage (or swelling), depending on whether or not loading has been accompanied by moisture exchange.

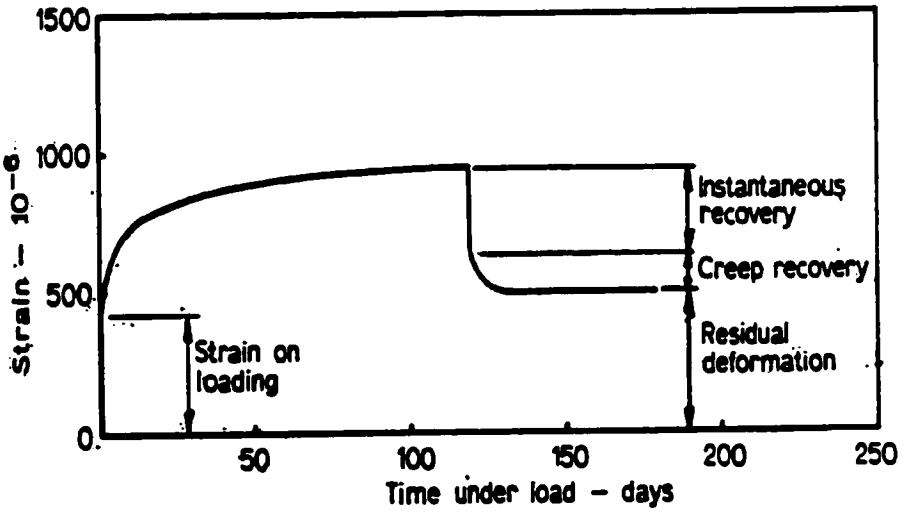

Figure 4.30: Creep and creep recovery of cement paste in hygral equilibrium with the surrounding medium

4.4.2 Factors affecting creep

4.4.2.1 Drying condition

The simultaneous drying of the paste increases the amount of creep and this increase is referred to as drying creep. Therefore, drying conditions would affect total creep through their effect on drying creep. Generally speaking, drying creep, and the resulting total creep, increases with the intensity of drying conditions, i.e. with the increase in temperature, decrease in relative humidity, etc.

The influence on creep of the relative humidity of the air in which the cement paste and/or concrete is stored has been known for several years. It was observed that a drying specimen creeps at a higher rate and achieves higher ultimate creep than specimen, which remains wet or remains dry. It is thus important to realize that, when we consider the influence of the relative humidity on creep, this implies that the equilibrium relative humidity within the cement paste is higher than the ambient humidity.

The effect of simultaneous drying and loading on creep described in Figure 4.31 after Ruetz (1968) demonstrates the difference between basic and drying creep. Some of the specimens were simultaneously allowed to dry at 40% relative humidity and others were tested under saturated conditions. It can be seen that, under the chosen conditions, the creep of the specimens, which were allowed to dry, is about twice the basic creep. Several researchers (Hannant, 1968; Nasser and Neville, 1965; Wittmann, 1970) have confirmed this result.

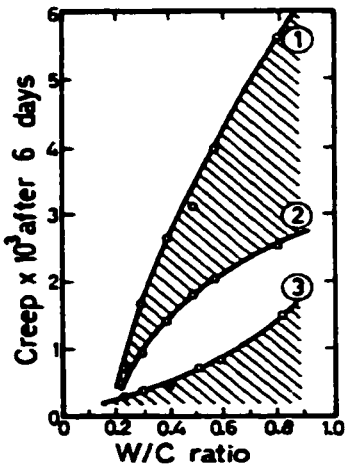

Figure 4.31: Effect of simultaneous drying and loading on creep of cement paste (Ruetz, 1968): 1, creep with simultaneous shrinkage; 2, shrinkage only; 3, basic creep

4.4.2.2 Strength, stress level and Stress-strength ratio

After investigation of the influence of the type of cement on creep, Neville (1970) established an approximate stress-strength ratio rule, which states simply that, for a constant mix proportions, creep is proportional to the applied stress and inversely proportional to the strength at the time of application of load. Ruetz (1968) also found the same conclusion by showing the evidence that creep increases with w/c ratio (see Figure 4.31). He argued that under otherwise similar conditions, the strength of the paste is related to the w/c ratio. Hence, it may be concluded that creep decreases with the increase in strength. Given that the modulus of elasticity of the paste is related to its strength, a similar conclusion may be reached with respect to the effect of this modulus on creep.

The effect of strength on creep implies that all factors, which affect the former, will also affect creep. For example, the effect of age is shown in Figure 4.32 after Ruetz (1968). Strength increases with age, so lower creep is to be expected with increase in the age of the paste at the time of loading, and such a trend is clearly evident from Figure 4.32. In engineering applications, the effect of strength on creep is of practical importance. It has been stated that in the manufacture of prestressed concrete, the loss of prestress due to creep can be reduced by delaying the prestressing operation and by using high strength concrete (Soroka, 1979).

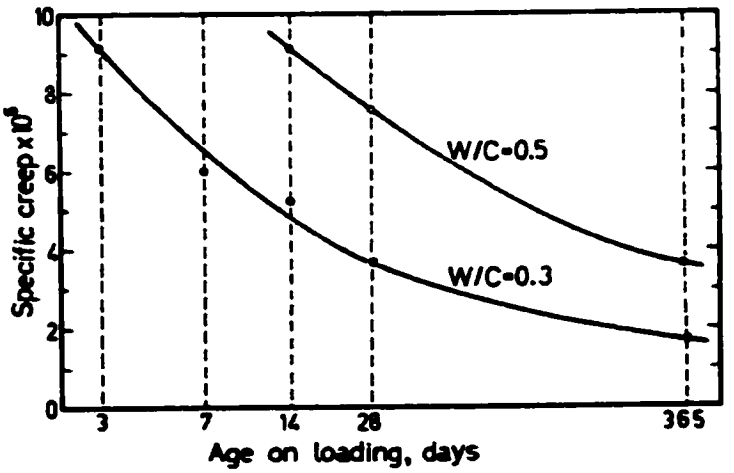

Figure 4.32: Effect of age at loading on basic specific creep of cement paste (Ruetz, 1968)

Wittmann (1968) found that creep of the cement paste increases with the increase in stress level (see Figure 4.33). His finding was confirmed in the tests summarized in Figure 4.34 after Neville (1970). The tests in question also indicated that a linear relation between creep and stress-strength ratio holds up to a ratio of 0.85. The maximum value of this ratio varies from 0.3 to 0.75 according to one source (Neville, 1970) and from 0.25 to 0.40 according to another (Roll, 1968). In considering the effect of stress level on creep, reference is sometimes made to "specific creep". Specific creep is defined as creep strain per unit stress. Accordingly, and recalling the linear relation between creep and stress-strength ratio, the same specific creep is to be expected for different stress levels in pastes of the same strength.

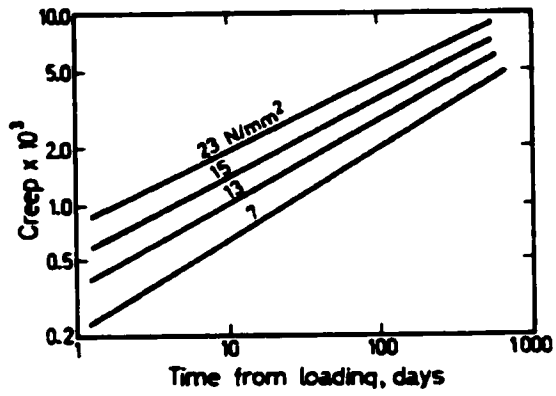

Figure 4.33: Effect of stress level on creep of cement paste (Wittmann, 1968)

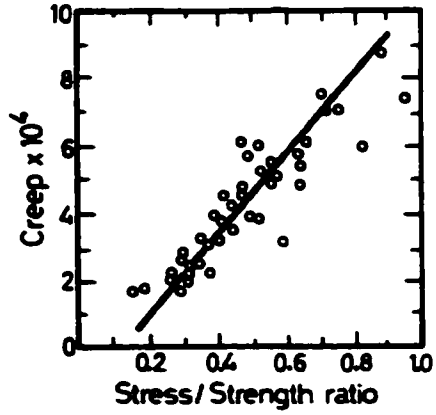

Figure 4.34: Effect of stress-strength ratio on basic creep of cement mortars (Neville, 1970)

4.4.2.3 Temperature

As it will be shown later, some of the proposed mechanisms of creep are associated with the movement of water within the paste. Accordingly, creep depends on the viscosity of the water, which decreases with rise in temperature. The reduced viscosity, in turn, accelerates creep and creep is therefore expected to increase with rise in temperature. This conclusion is confirmed in Figure 4.35 for a temperature range up to about 60°C. However, any further rise in temperature resulted in lower creep. Such a reversed trend can be attributed to the accelerating effect of temperature on the hydration process. A higher rate of hydration implies a higher rate of strength development, and a higher strength result in lower creep. Apparently, in this particular case, the effect of the increased hydration on creep over the lower temperature range was less than the effect of the decreased viscosity. Hence, that will be followed by a net increase in creep (Ruetz, 1968).

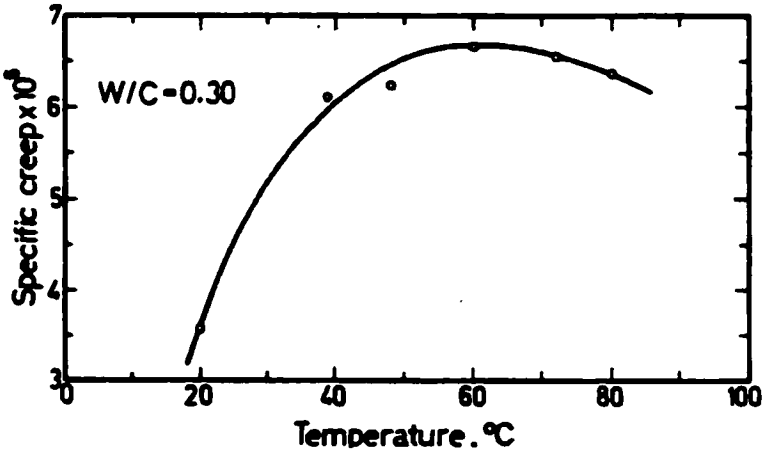

Figure 4.35: Effect of ambient temperature on basic creep of cement paste (Ruetz, 1968)

In the higher temperature range the relative magnitude of the two opposing effects was reversed resulting in a decrease in creep with rise in temperature. This explanation may not be valid for well-matured pastes or for those, which contain insufficient water to allow hydration to continue. In such pastes creep steadily increases with the rise in temperature up to 80°C (Ruetz, 1968).

4.4.2.4 Moisture content

The effect of moisture content on basic creep of cement paste is demonstrated in Figure 4.36 after Wittmann (1970). The data relate the cement paste (w/c=0.4) samples loaded to a stress-strength ratio of 0.2 to the moisture equilibrium as indicated in the figure by the relative humidities.
It is clearly evident that creep increases with increase in the ambient relative humidity, i.e. with the increase in the moisture content of the paste. The very low creep of the paste dried at 0% relative humidity may be noted. Even after this result Wittmann expressed the view that creep should be zero if the hydrated cement paste is fully dried. Several researchers have also reported that the specimens from which all evaporable water has been removed exhibit no creep or permanent set (Brown and Hope, 1976; Glucklich and Ishai, 1962; Mullen and Dolch, 1964). These results imply that creep may be conditional on the presence of moisture in the paste.

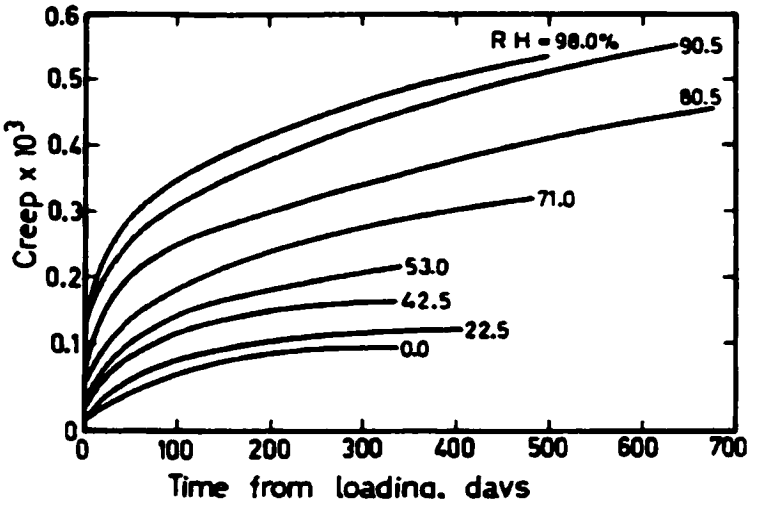

Figure 4.36: Effect of ambient humidity on basic creep of cement paste (Wittmann, 1970)

L'Hermite (1960) reported that, although dried concrete creeps little or not at all, its creep capacity can be restored by re-wetting and creep recovery of dried concrete could also be restarted or increased by re-wetting. It will be seen later that all mechanisms, which have been suggested to explain creep, are based on movement of water within the paste as a result of external loading. It should be noted that, although moisture loss affects deformation under load, the presence of load and the process of creep do not influence the moisture loss (Neville, 1970).

4.4.2.5 Admixtures

Logically, cement is the most important factor in creep because the hydrated cement paste is at the "heart" of the phenomenon. The influence of the cement can be seen first as that arising from the physical and chemical properties of the cement, and second as that due the variation in the amount of the hydrated cement paste. The influence is affected by the presence of admixtures as they can interact with cement phases and alter morphology, particle dispersion and other properties. It is possible that a part of the influence of the type of cement on creep also arises from differences in the fineness of the unhydrated cement. Such an influence in the case of shrinkage has been a subject of controversy for some time (Neville, 1962).

In 1954, Davis and Troxell (1954) cautioned that accelerators and water-reducing admixtures do not behave in the same way with different cements and mixes because the admixtures generally contain organic compounds whose effect is influenced by some of the minor constituents in cement. They recommended therefore, that before any admixture is used in a particular construction project its effects be experimentally established. It can only be concluded that admixtures affect creep of cement pastes with the exact nature of this effect varying with the specific admixture and test conditions.

4.4.2.6 Shape, size and isotropy of specimen

The shape and size of the concrete member are intrinsic properties of that member but the practical significance of these factors lies usually in making a transition from the results of creep tests on laboratory specimens to the behavior of the full-size members. In some practical cases, the difference in creep between members of different proportions is of significance.

Several investigators have indicated an influence of the size of the specimen on creep: the measured creep decreases with an increase in the size of the specimen but when the specimen thickness exceeds about 90 centimeters the size effect becomes negligible (Neville, 1970). Bazant et al. (1976) pointed out that when the standard 6-inch diameter test cylinders are used their core takes over 10 years to dry to a constant humidity. Consequently creep as well as shrinkage in the core is entirely different from that near the surface of the specimen, which produces internal self-equilibrating residual stresses of non-homogeneous distribution within the specimen, and so the observed creep as well as shrinkage is not directly associated with any simple stress state. These difficulties were found to be eliminated by a drastically reduction of the size of the specimen. When thin-walled specimen of 1-mm wall thickness is used the drying

process reaches in one day the same stage as a 6-inch cylinder reaches in about 16 years (Bazant et al., 1976). One objection against using a specimen so thin is that it cannot be made of concrete, even not of mortar, but only of pure cement paste. Thus, the specimen is not exactly representative of concrete. However, it has been well documented in the literature on creep that the creep responses of cement paste and of concrete are completely similar over the entire service stress range provided that the contribution of microcracking to concrete creep is negligible (Bazant, 1975). The difference between the creep of concrete and that of cement paste then consists merely of the elastic restraining effect of the aggregate, which reduces the relative magnitude of the creep but does not appreciably alter the time response. In the light of this, the use of very thin pure cement paste specimens gives information, which is also relevant for concrete. A related problem is the possible influence on creep of a lack of isotropy in concrete. If the structure of the hydrated cement paste is isotropic (proportionally well mixed), the direction of a sustained load relative to the direction of casting would not be expected to influence creep (Neville, 1970).

4.4.3 Creep mechanisms

Various mechanisms have been suggested to explain creep in cement paste. According to Wittmann (1982) mechanisms of creep can be divided into real and apparent mechanisms. The real creep mechanisms were subdivided into those termed short-time creep caused by water movement and redistribution in the porous structure of hardened cement paste; and those termed long-time creep far more complex, caused by displacement of gel particles and to some extent creep within particles under high concentrated stress. The apparent creep mechanisms are those caused by the surrounding environment and/or the changes of the internal structure of concrete. The most obvious and probably the most important apparent creep mechanism is drying creep. Creep due to thermal and/or hygral gradients, as well as cracking are all the consequence of apparent creep mechanisms. The mechanisms described here will be based on the models of hardened cement paste previously presented in Chapter 2.

4.4.3.1 Powers' model

This model assumes that the cement gel is similar to the hydrated product of C_3S and β-C_2S and that it is a poorly crystallized version of the mineral tobermorite. Since the structure of

tobermorite is layered, it is considered that hydrated Portland cement gel is also layered.
This model assumes that the cement gel is similar to the hydrated product of C_3S and β-C_2S and that it is a poorly crystallized version of the mineral tobermorite. Since the structure of tobermorite is layered, it is considered that hydrated Portland cement gel is also layered.
The volume changes in the cement paste which accompany the variations in its moisture content, were attributed by Powers to corresponding variations in swelling pressure. Essentially, the same mechanism induced by external loading and not by ambient humidity, was suggested by Powers to explain the reversible part of creep. According to his model, the load-bearing water in areas of hindered adsorption exerts the swelling pressure. Due to external loading, some of this water is squeezed out into areas of unhindered adsorption by a time-dependent diffusion process. The swelling pressure gradually decreases bringing about a decrease in the volume of the paste (i.e. creep) as the spacing of the particles in the gel is reduced. Unloading causes a drop in the pressure in the load bearing water. Consequently, the reverse process takes place and water gradually diffuses from adjacent unhindered areas bringing the swelling pressure to its proper value in relation to the ambient humidity. The resulting gradual increase in swelling pressure causes volume increase, i.e. creep recovery.
The suggested mechanism can be used to explain most of the factors affecting creep, which were discussed previously. Ambient temperature affects creep through its effect on the viscosity of the water. A rise in temperature decreases viscosity; hence the diffusion rate and the resulting creep are correspondingly increased. Also, the higher the stress level, the greater the diffusion rate and an increased rate of creep is therefore to be expected.
The load-bearing water is part of the gel water. The gel content, and associated gel water, increase with the degree of hydration, i.e. with the strength of the paste. At the same ambient humidity, the gel water content will therefore be greater in the stronger than in the weaker paste. Consequently, for the same load, the stress in the load-bearing water will be lower in the stronger paste and the resulting creep will therefore be smaller.
The irreversible creep is attributed by Powers, partly at least, to the formation of new bonds between surfaces when they are pressed together for the first time.

4.4.3.2 Glucklich and Ishai's model

This model is based on Powers, the main difference between the two being in the classification of the water held in the hardened paste. The model was developed mainly to explain volume changes in the paste due to variations in its moisture content (swelling and

shrinkage) and due to continuous loading (creep). On application, the external load is distributed between the liquid and the solid phases of the cement paste. Under sustained loading the compressed liquid begins to diffuse from higher to lower pressure areas. A gradual transfer of load accompanies this mechanism from the liquid to the surrounding solid phase. The stress in the solid thus gradually increases causing a gradual volume increase, i.e. creep. Accordingly, creep may be regarded as a delayed elastic deformation, and a lower creep is to be expected in stronger pastes because such pastes have a higher modulus of elasticity. Also, greater creep is to be expected in pastes of higher moisture content. The higher the moisture contents the greater the part of the load, which is taken initially by the liquid phase. Hence, the greater the load which is subsequently transferred to the solid phase. The greater the load transferred the higher the resulting creep. It is self-evident that creep will also increase with the intensity of the stress level. Again, creep will increase with temperature due to its effect on the viscosity of water.

When the load is removed, the stresses in the solid phase are relieved and creep recovery takes place. Owing to the viscous resistance of the confined water, the process is not completed immediately but continues over a period of time. Hence, the time-dependent nature of creep recovery (see Figure 4.30).

The irreversible creep is attributed to the migration of inter- and intra-crystalline water induced by the imposed load. As a result of this migration the inter- and intra-crystalline spacing is reduced and the volume of the paste decreases. This volume decrease is not recoverable because it involves a reduction in the energy level of the system.

4.4.3.3 Feldman and Sereda's model

This model also assumes that the cement gel is a poorly crystallized version of a layered silicate. It supposes, however, that the role of water is much more complex than it is in the Powers' model. In this model creep is attributed to exit of interlayer water resulting from the imposed external loading. On unloading, some of the water re-enters the structure; this accounts for the reversible part of the creep. The irreversible part is associated with the displacement of one C-S-H layer in relation to another or involves a process of breaking and remaking of interparticle bond (Feldman and Sereda, 1970b).

In a later study, Feldman (1972), however, suggested a modified mechanism in which he concluded that 'creep is a manifestation of the gradual crystallization or aging process of the layered material, resulting in further layering. Water movement, although occurring, is not

the major mechanism. Other processes, such as slippage and micro cracking, are also present.

4.4.3.4 Munich model

This model is primarily concerned with the explanation of the mechanical properties of the hydrated Portland cement gel. It assumes that the water isotherm is ideal and free of aging, intercalation effects other forms of specificity and shrinkage forces on meniscus formation. Even though the preceding mechanisms differ considerably, they all three, attribute creep, one way or another, to movement of water within the paste. According to Wittmann (1971), on whose studies the Munich model is mostly based, it is difficult to imagine that squeezing out of the load-bearing water as suggested by the Powers' model can play such an important role in the creep mechanism. Moreover, considering the mobility of adsorbed water, diffusion processes cannot account for the creep of the cement paste after periods as long as a few years. Accordingly, Wittmann suggested that the water affects creep only indirectly through its effect on swelling pressure which, in turn, weakens interparticle bonds. The weakening effect facilitates sliding of the gel particles with respect to each other and creep is, therefore, increased (Wittmann, 1973).

The role of swelling pressure in the creep mechanism may be indicated in Figure 4.37 after Wittmann (1970). In this figure, the creep rate is plotted against the equilibrium relative humidity. It can be seen that the rate of creep increases when the ambient relative humidity exceeds, about 50%. It was suggested (Wittmann, 1973) that in about the same humidity region, swelling pressure may overcome van der Waals attraction and separate the gel particles. As such separation weakens the structure, increased creep is to be expected. The suggested mechanisms described above to explain creep are summarized in Table 4.2. It can be seen that opinions differ considerably with respect to the exact mechanism involved. In any case, it seems that creep in cement paste is attributable to more than one mechanism.

4.4.3.5 Other models

Various other mechanisms have been invoked to account for creep phenomena in cement paste. These include microcracking, which may even occur at high relative humidity as a result of shrinkage stress developed near non-shrinking CH crystals (Ishai, 1968; Slate and Meyers, 1971). Recrystallization under load (Feldman, 1972; Ali and Kesler, 1972),

sometimes referred to as aging, reflected by the changes in surface area measurement at different degrees of reaction and different loading and drying conditions and slip between paste and aggregate (Ishai, 1968) are other possible considerations.

Table 4.2: Creep mechanism after various authors

Author	*Reversible creep*	*Irreversible creep*
Powers (1965)	Diffusion of water from areas of hindered to unhindered adsorption reduces swelling pressure, and thereby causes reduction in the inter-particles spacing.	Formation of new bonds between gel particles brought into close contact the first time.
Glucklich and Ishai (1962, 1968)	Diffusion of water from high to low pressure areas causes gradual load transfer from liquid to solid phase, causing a delayed elastic volume decrease.	Removal of inter- and intra-crystalline water reduces inter- and Intra-crystalline spacing.
Feldman and Sereda (1970b, 1972)	Exit and re-entry of Interlayer water.	Displacement of CSH layers in relation to each other and formation of new interparticle bond.
Wittmann (1970, 1971, 1973, 1977)	Weakening of the paste structure due to separation of gel particles by the swelling pressure at relative humidities exceeding 50%.	

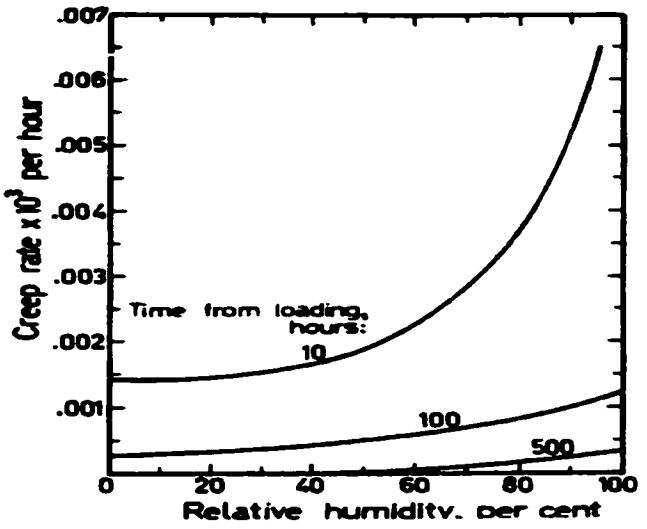

Figure 4.37: Effect of ambient humidity on basic creep of cement paste after different periods of loading (Wittmann, 1970)

A mechanism proposed by Ruetz called the adsorption theory suggests that creep occurs through slip between C-S-H particles in a shear process in which water acts as a lubricant. The sliding process takes place in the very thin, multi-molecular layers of adsorbed water. As the distance of any liquid molecule from the surface of a solid particle increases, the degree of orientation of the liquid molecule will change, depending upon the interaction between the liquid molecule and the solid surface. Such an orientation of liquid molecules will be disturbed by increasing temperature until at sufficiently high temperatures, the thermal inelasticity becomes so great that a viscous flow occurs (Ruetz, 1968). The adsorbed water molecules are oriented with respect to the surface and the effective rigidity of the film is thereby increased. Loss of water from the adsorbed films, on drying, will disturb the orientation of the films and hence result in an increased drying creep.

Ishai (1968) suggests that, whereas the diffusion of inter and intra-crystalline adsorbed water is the principal creep mechanism, even in immersed bodies, this moisture movement is not connected with the drying shrinkage that occurs in the normal range of relative humidity. The creep process, which takes place in the inter- and intra-crystalline spaces and the respective adsorbed water, is different both in type and origin. The applied load causes a decrease in those interparticle spaces within the range of the physical forces reducing the energy level of the system. The process is therefore irreversible.

More recently, Bazant et al. (1997) proposed another creep mechanism referred to as the microprestress-solidification theory, which appears to be an improvement, by the authors of the solidification theory. The microprestress is generated by the disjoining pressure of the hindered adsorbed water in the micropores and by very large and highly localized volume changes caused by hydration or drying.

Bentur et al. (1979) suggested that irreversible creep might be related to aging due to silicate polymerization of the C-S-H, induced by loading or drying.

4.5 Organic solvent exchange

4.5.1 Introduction

The use of solvent exchange has been applied for several purposes in cement and concrete science. A number of researchers have investigated the possible application of organic solvents such as methanol, ethanol or isopropanol to remove the evaporable water from the specimen prior to the determination of the pore structure of hardened cement paste (Feldman, 1987; Hughes, 1988; Marsh, 1985; Parrott, 1980). The advantage being that solvent replacement can quickly and simply be determined using inexpensive apparatus. The use of organic solvents had also been found to be an alternative method for determining bound water in C_3S pastes (Taylor and Turner, 1987).

The normal drying required for the removal of the evaporable water from samples before testing is believed to result in considerable alteration to the fine pore structure (Parrott, 1980, 1981). These changes are due to the stresses generated by the surface tension of the receding water menisci causing a collapse of some of the fine pores and resulting in an increased volume of larger pores.

Solvent replacement techniques, using solvents such as methanol and isopropanol, have been shown to reduce pore structural damage to cement paste samples during drying (Marsh, 1985; Parrott, 1980). However, recent evidence has suggested that some solvents may react with the hydration products of cement during solvent replacement, which casts doubt on subsequent microstructural determinations (Beaudoin, 1985, 1987; Day, 1981; Feldman, 1987; Taylor and Turner, 1987). Day (1981) showed that samples of hardened cement paste or calcium hydroxide that had been soaked in methanol had different weight loss characteristics from non-immersed samples during thermal decomposition. He suggested that

these differences might be explained by a reaction between methanol and calcium hydroxide, with calcium methoxide as possible product. These conclusions were disputed, and later studies found no difference in the thermogravimetric curves of cement paste samples due to methanol soaking provided that, either the samples were vacuum-dried before thermal analysis (Parrott, 1983), or oxygen was excluded from the furnace atmosphere (Dollimore, 1981). Taylor and Turner (1987) extended the finding of Day by including isopropanol and concluded that both solvents are strongly sorbed within the structure of mature C_3S pastes and unsuitable for use as a drying agent prior to thermal analysis. Beaudoin (1987) identified the reaction product, calcium methoxide, in calcium hydroxide and methanol mixtures by X-ray diffraction and infrared spectroscopy.

Feldman (1987) after measuring length change of Portland cement pastes during solvent exchange process suggested that while methanol is capable of entering interlayer space, the same does not occur with isopropanol. He proposed that isopropanol may be a suitable medium for establishing the diffusion characteristics of pastes and concrete. This does not negate the value of intentionally using methanol in creep investigations designed to determine the effects of microstructural perturbation on behavior under sustained load.

4.5.2 Counter diffusion process

Parrott (1984) showed that several organic solvents could replace a large portion of water in cement paste and suggested that the process of exchange of water from the saturated specimen was a simple physical process of counter diffusion with the rate of exchange depending upon drying history.

Generally, molecular transport of vapor, air and water proceeds simultaneously in a capillary-porous body and is referred to as diffusion. For a system consisting of a capillary-porous body and a substance bounded with it, the mass transfer or diffusion theory states that; at a positive temperature ($t>0°$ C) the bound substance consist of a liquid, vapor and inert gas, and that at a negative temperature ($t<0°$ C) it consists of ice, supercooled liquid (water), vapor and gas. Depending on the energy of binding between moisture and a body, the freezing temperature of water changes over a wide range. Thus, in most cases, there is always some amount of a supercooled liquid in capillary-porous bodies at the negative temperature.

The second particularity of mass transfer in capillary-porous bodies is the partial filling of pores and body capillaries with a gas and moisture (vapor, water or ice) i.e. a part of a

capillary is filled with water or ice and the remainder, with a vapor-gas mixture (humid air) (Luikov, 1997).

During the drying of concrete, the rate of diffusion of water may be characterized by the flux $\vec{J}$ denoting the mass of water passing through a unit area perpendicular to $\vec{J}$ per unit time. At uniform temperature, $\vec{J}$ is a function of the gradient of the Gibbs' free energy μ per unit mass of evaporable water. This function must be linear for sufficiently small gradients. Thus

$$\vec{J} = -\tilde{c}\, grad\mu \tag{4.7}$$

where $\tilde{c}$ = coefficient characterized the permeability of material, which is a function of temperature T and of the water content, w_e, of evaporable water per unit volume of porous material. Assuming water vapor as an ideal gas, the following well-known Gibbs relation applies:

$$\mu = (R/M)\, T \ln H + \mu_{sat}(T) \tag{4.8}$$

where R = gas constant, M = molecular weight of water, T = absolute temperature; RT/M = 1360 atm.cm^3/g at temperature T = 298° K; H = pore humidity = $P_v/P_{sat}(T)$ where P_v = vapor pressure; $P_{sat}(T)$ and $\mu_{sat}(T) = P_v$ and μ at saturation.

Considering the case of quasi-uniform temperature T (i.e., grad T = 0), and expressing μ in terms of T and H, equation (4.7) can be rewritten as follows:

$$\vec{J} = -c\ grad\ H \tag{4.9}$$

where

$$c = (R/M)\, T\tilde{c}/H \tag{4.9a}$$

Coefficient c, called permeability, depends on H and T. It probably also depends on grad H if grad H is large (Bazant and Najjar, 1997).

Diffusion through concrete is believed to be so slow that various phases of water in each pore (vapor, capillary water and adsorbed water) remain almost in thermodynamic

equilibrium at any time. Thus the relationship between H and w at a constant T and a fixed degree of hydration is given by the well known desorption or sorption isotherms (Powers and Brownyard, 1967). These may be written in a differential form as $dH = k\,dw$, where $(\partial H/\partial w)_T$ = function of H = cotangent of the slope of the isotherm w = w (H). When variable temperature T and the progress of hydration (aging, maturing) are taken into account, additional terms must be included (Bazant, 1970, 1971):

$$dH = k\,dw + \kappa\,dT + dH_s \qquad (4.10)$$

where $\kappa = (\partial H/\partial T)_w$ = hygrothermic coefficient = function of H = change in H due to one degree change in T at constant w and a fixed degree of hydration; dH_s = change (drop) in H caused by hydration during time interval dt at constant w and T = self-desiccation (166); $H_s(t)$ = pore humidity which would arise in time t in a sealed , initially wet specimen; w is understood as the total water w_e and the combined (non-evaporable) water w_n per unit volume of material ($w = w_e + w_n$).

The rate of change of the mass w of water per unit volume of porous material is determined from the flux field by the relation

$$\partial w/\partial t = -div\ \vec{J} \qquad (4.11)$$

expressing the condition of conservation of mass. Eliminating $\vec{J}$ and w from equation (4.7), (4.9), and (4.10), it follows:

$$\frac{\partial H}{\partial t} = k\ div\ (C grad\ H) + \frac{\partial H_s}{\partial t} + \kappa\ \frac{\partial T}{\partial t} \qquad (4.12)$$

which represents the diffusion equation governing drying of concrete at variable, but almost uniform temperature. Self-desiccation H_s and coefficient k, c, and κ depend on the degree of hydration of cement paste.

4.5.3 Length and mass changes variability

4.5.3.1 Length change on immersion in organic solvent

Feldman (1987) found that the length response of hardened cement paste (w/c=0.8) specimen immersed in isopropanol is a shrinkage while that of specimen immersed in methanol is an expansion (see Figure 4.38). It was found that the pore water could apparently be fully exchanged with methanol and that during the process, and during subsequent methanol sorption experiments length changes were small (Parrott, 1981).

From length change isotherm performed on hydrated Portland cement, Feldman (1968) found a large desorption but a very little contraction on the desorption curve for methanol. Given the similarity of the length change plot to the constructed irreversible plot for water, he suggested that interlayer penetration is taking place and that the penetration is less than that of water because of the respective sizes of the molecules. It is precisely these differences between water and methanol that make methanol an excellent candidate (as an adsorbate) to further understanding the effects of microstructure on creep behavior in cement paste.

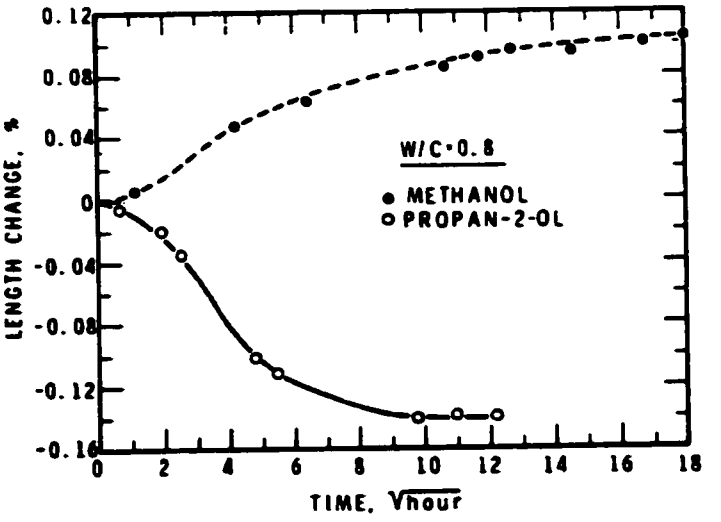

Figure 4.38: Length change versus (time)$^{1/2}$ on immersion of water saturated paste specimens in methanol and isopropanol respectively (Feldman, 1987)

The rate of change of length change of water-saturated paste specimens when immersed in organic solvent increases as the specimen thickness decreases probably because it is subjected to lesser restraining influence than the thicker specimens.

From studies of the length change of compacted samples of $Ca(OH)_2$ immersed in methanol, Beaudoin (1987) pointed out that length change observed may have been due to the formation of $Ca(OCH_3)_2$ resulting from the release of water as a reaction product. The released water may then interact with unreacted $Ca(OH)_2$, thereby contributing to the length change. The length change of $Ca(OH)_2$ in water is attributed to physical adsorption at low humidity, and dissolution and recrystallization at points of solid contact when the humidity is higher (Ramachandran and Feldman, 1967). Expansion may also be attributed to the pressure resulting from the increase in specific volume of the reaction products. The larger surface area of the reaction products could also result in increased length change due to physical adsorption. Another factor may be the release of strain energy from the $Ca(OH)_2$ particles after interaction with methanol (Beaudoin, 1987).

4.5.3.2 Mass change on immersion in organic solvent

It has been shown that the water-saturated specimen of cement paste loses weight when immersed in water-free methanol or isopropanol (Feldman, 1987). Results in units of weight of isopropanol entering the pores per unit volume of sample as a function of square root time are presented in Figure 4.39.

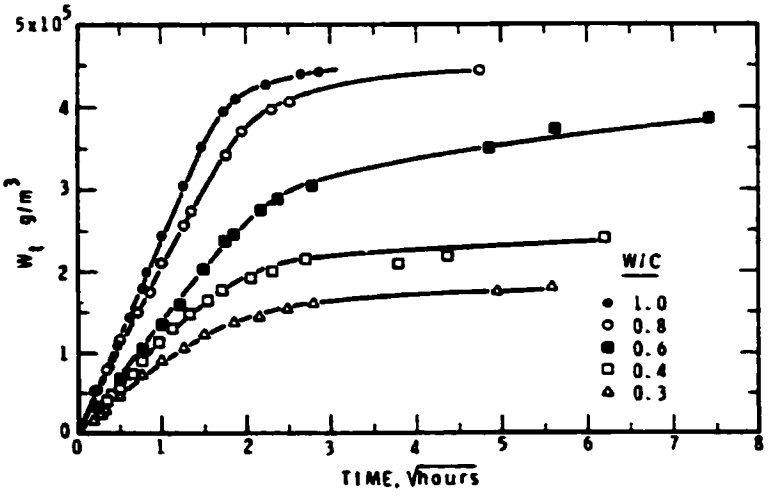

Figure 4.39: Diffusion of isopropanol (g/m3) into water-saturated pastes versus (time)$^{1/2}$ as a function of water-cement ratio (Feldman, 1987)

Samples of hardened cement paste or calcium hydroxide that had been soaked in methanol had different weight loss characteristics from unsoaked samples during thermal decomposition (Beaudoin, 1985, 1987; Day, 1981; Taylor and Turner, 1987; Thomas, 1989). Day (1981) suggested that these differences might be explained by a reaction between methanol and calcium hydroxide, with calcium methoxide as a possible product. Despite the contradictory conclusions pointed out by Parrott (1983), Taylor and Turner (1987) reported that methanol could not be completely removed from tricalcium silicate paste by normal drying methods, and their thermal analysis results for vacuum-dried specimens heated in an oxygen-free atmosphere supported the findings of Day (1981). Beaudoin (1987) as stated previously identified the reaction product, calcium methoxide, in calcium hydroxide and methanol mixtures by X-ray diffraction and infrared spectroscopy.

Hughes (1988) showed that the methanol exchange of ordinary Portland cement (OPC) paste takes place at a rate faster than that of isopropanol with a marked difference occurring with the OPC-silica fume paste. In this case the isopropanol apparently exchanges at the faster rate, exhibiting a maximum in the weight loss before gaining weight until equilibrium is achieved (see Figure 4.40). A possible explanation for the anomalous behavior of OPC-silica fume pastes was found to be due to the refinement of pore structure. It appears that even if the isopropanol may be suitably used to monitor the diffusion and durability characteristics of ordinary Portland cement paste (Feldman, 1987; Parrott, 1981, 1984), there is serious doubts about using it to characterize OPC-silica fume pastes (Hughes, 1988).

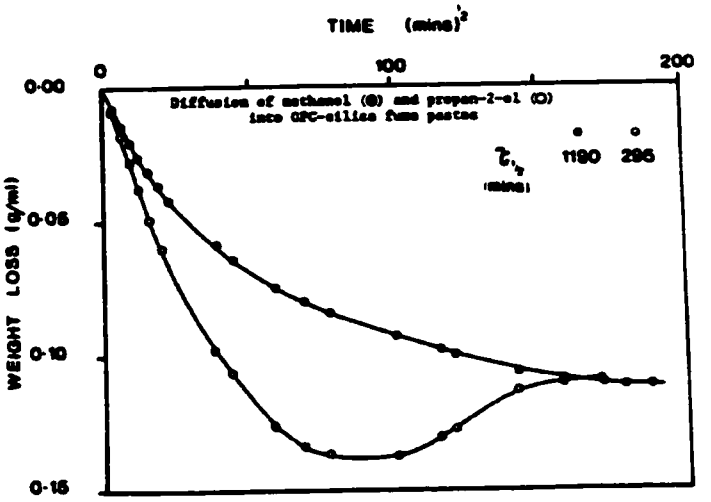

Figure 4.40: Diffusion of methanol and isopropanol (g/ml) into OPC-silica fume pastes versus (time)$^{1/2}$ (Hughes, 1988)

4.5.4 Modification of cement paste structure and properties

4.5.4.1 Pore structure and surface area

After pointed out the limited length changes that resulted from exchange of pore water with methanol at the completeness of the exchange and the low surface tension of methanol relative to water, Parrott (1981) suggested that methanol sorption measurements after completion of the exchange could be helpful in studying the original pore structure of hydrated alites samples. He also found that there was no effect of exchange time upon total porosity although methanol adsorption experiments indicated a change in pore size distribution (Parrott, 1963). The large hysteresis observed in the low-pressure region between methanol or isopropanol first adsorption and second desorption cycles led Day (1981) to suggest that the two solvents adsorption caused a change in the pore structure of cement paste.

Hughes (1988) suggested that the true entry size is not determinable since the high-pressure access is likely to be gained only at the expense of physical damage to the very fine pore structure of the blended paste. The entry of isopropanol into pores of such a restricted entrance may thereby be a function of the character of both the pore structure and isopropanol molecule and the interaction between isopropanol pore solution and the hydrated structure as modified by sorbed isopropanol.

Gimblett et al. (1978) from studies on the influence of pretreatment on the microstructure of C-S-H gels found that isopropanol treated samples can exhibited high percentage of smaller pores as well as nitrogen surface areas substantially closer to those measured by water sorption. Parrott (1981) suggested that the pore structure of the alite paste will not be excessively disturbed during the exchange process and that subsequent methanol desorption and adsorption cycles rather than nitrogen might be used to study pore structure. It is believed that the reduction of surface tension forces after removal of solvent is associated with the high range of surface areas of solvent replaced specimens up to 250 m^2/g compared to that of normally dried specimens ranging around 80 m^2/g (1981).

4.5.4.2 Microstructural development

Parrott (1983) found that exchanging the pore water for methanol had no significant effect upon thermogravimetric decomposition for exchange times in the range 0 to 14 days.

However, It is very important to note that the monohydric alcohols and especially methanol are reactive. Methanol is highly polar, forms alcohols of crystallization with many compounds, and can form methoxides with calcium, sodium and potassium (Day, 1981). Taylor and Turner (1987) concluded from methanol and isopropanol exchanges study that both solvents are strongly sorbed within the structure of mature C_3S pastes and unsuitable for use as a drying agent prior to thermal analysis. Subsequent thermal analysis produces CO_2 from the methanol at temperatures above 200°C, and the CO_2 in turn carbonates both $Ca(OH)_2$ and calcium silicate hydrates. In contrary to Beaudoin (1987) who found the reaction between $Ca(OH)_2$ and methanol to take place at 22°C, Thomas (1989) findings support the theory of solvents being physically sorbed by cement paste with subsequent reactions during thermal analysis, rather than a chemical reaction occurring between the solvent and $Ca(OH)_2$ before thermal analysis.

4.5.4.3 Strength development

It as been pointed out by Feldman (1968) that inter-layer water plays a role in both the length change and sorption isotherms, and in the variation of Young's modulus with relative humidity. He suggested that even if it is apparent that the methanol isotherm is more complicated, it is consistent in every way with the results obtained from water sorption.
Compressive strength results for Portland cement paste saturated in organic liquids were obtained by Robertson and Mills (1960), and found to generate a weakening effect when originally dry specimens were tested in water and alcohols. Beaudoin (1985) has pointed out the same conclusion from flexural strength experiments and explained the effect of alcohols on flexural strength of Portland cement paste to be possibly due to the dependence of Si-O bond fission energy on dielectric constant of the test fluid. Chemical attack of Si-O bond may thereby weaken the cement paste.

CHAPTER 5

AC IMPEDANCE SPECTROSCOPY

5.1 Introduction

Various electrical fields have been shown to be useful in the processing, the characterization, and even the rehabilitation of cement-based products and structures. The observation of a strong electromechanical response in hardened cement pastes by Wittmann (1973), recently confirmed by Li et al. (1995) and Yuan et al. (1995), attests to the fact that substantial microstructural changes can occur in hardened pastes when a electric field is applied. AC impedance spectroscopy has also shown promise as a tool for characterizing microstructural development in cement-based materials (Gu et al., 1995). Analysis of the spectra provides pore structure information. The bulk conductivity is governed by the amount of capillary porosity, its conductivity (pore fluid conductivity) and its connectivity. However, the geometry and concentration of adsorbed ions due to different surface conditions, may not be the same in each micropore (the relaxation time has a spread of values) and the interface resistance and capacitance are not ideally frequency independent (Iseki et al., 1972; Tien Chao-wen, 1984).

5.2 Impedance behavior of cementitious materials

5.2.1 AC impedance methods

The methods are characterized by the application of a small-amplitude sinusoidal potential perturbation to the working electrode at a number of discrete frequencies. At each one of these frequencies, the resulting current waveform will exhibit a sinusoidal response that is out of phase with the applied potential signal by a certain amount. Impedance spectra recorded over a wide range of frequencies (from 15 MHz to 1 Hz) have provided new information and insight on cement paste microstructure and hydration. An idealized impedance spectrum for a cement system is plotted in the real versus imaginary plane (Figure 5.1(a)). A single arc in the high-frequency range with a small part of a second arc in a relatively low-frequency

region is shown. It is suggested that the high-frequency arc (HFA) is attributed to the bulk paste impedance behavior and the second arc is due to the cement-electrode surface capacitance contribution. The intercepts R_1 (at the high-frequency end, at c. 20 MHz-7 MHz) and R_1+R_2 (at the minimum between the electrode arc and bulk arc, at frequency c. 100 kHz) are important parameters providing information related to cement paste microstructure. Interpretation of an impedance spectrum (IS) is usually through modeling with an equivalent circuit (Figure 5.1(b)) until the electrical response of the elemental microstructure of the cement paste is well simulated.

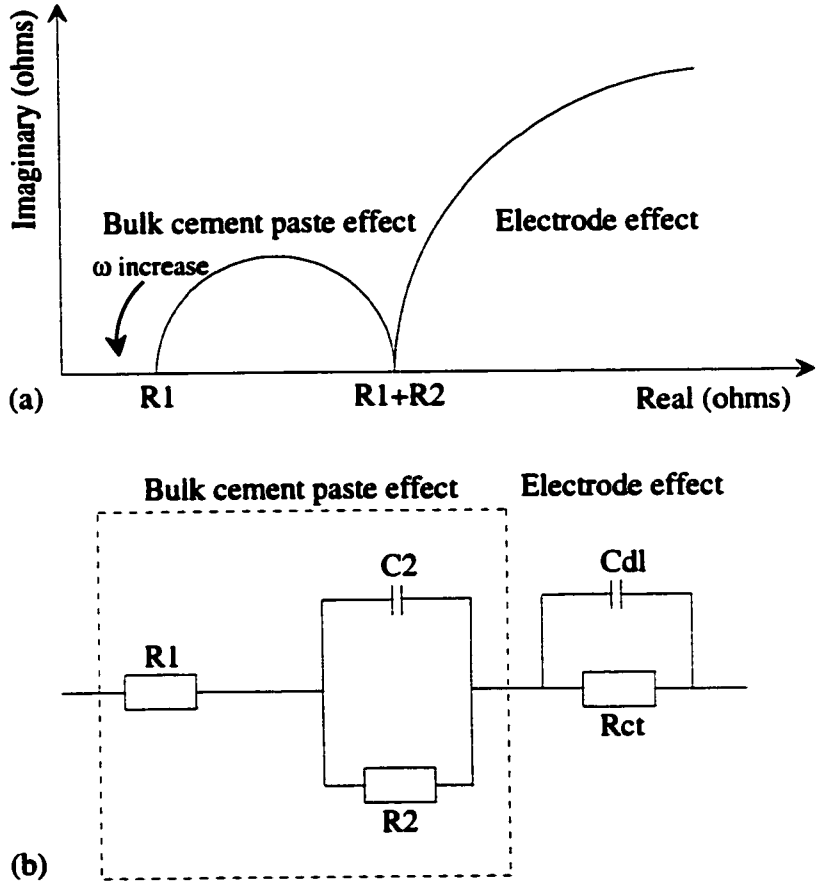

Figure 5.1 : (a) Schematic plot of a high frequency arc in the impedance complex plane obtained for cement paste systems. (b) A simplified electrical equivalent circuit for hydrating cement systems. R_1, R_2, and C_2 are high-frequency resistance, solid-liquid interface resistance and capacitance. R_{ct} and C_{dl} are cement-electrode interface charge transfer resistance and double layer capacitance.

Ideally, the value of R_2 should be equivalent to the diameter of the high-frequency arc if the HFA is a perfect semicircle. However, an ideal response is rarely observed. Most materials exhibit an inclined semicircle with the center depressed below the real axis by an angle θ_d (Figure 5.2). The angle depression is the most common phenomenon in a. c. impedance studies and the HFA diameter is then equal to $R_2/\cos(\theta_d)$. There may be several causes for the inclination of semi-circle including factors associated with "a spread of relaxation times" of the ions adsorbed on the solid-liquid interface (McCarter and Curran, 1984; McCarter et al., 1988), surface roughness (De Levie, 1965; Iseki et al., 1972) and uneven current distribution at the interface. This dispersion behavior may usually be described by presence of a non-trivial frequency-dependent element in the measured spectrum referred to as constant phase element (CPE) (Iseki et al., 1972).

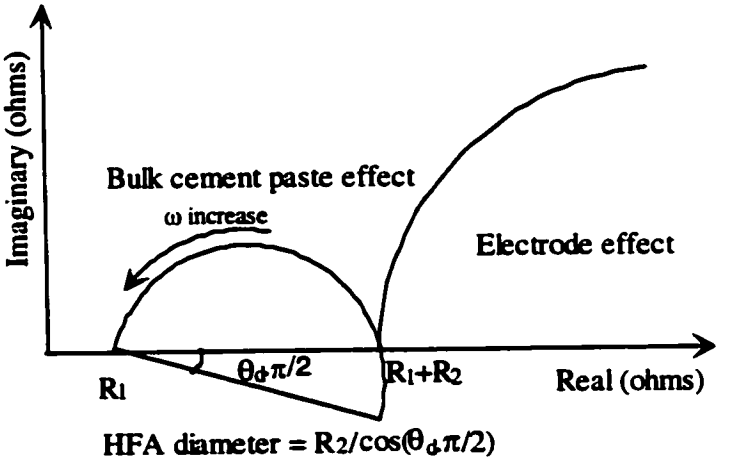

Figure 5.2 : An inclined semicircle showing its center depressed below the real axis by an angle θ_d.

5.2.2 *AC impedance as a tool for characterization of cement systems*

A. C. impedance spectroscopy has been demonstrated to be a useful tool for studying factors that influence pore structure in cement systems. Previous investigations (Gu et al., 1993; McCarter and Curran, 1984; Xu et al., 1993) have indicated that impedance behavior of the hydrating cement system depends upon ion concentration of the pore solution and porosity. The high-frequency arc diameter, R_2, can be expressed by:

$$R_2 = \frac{k_1}{\sigma_f}\left(\delta_{st} + \frac{k_2}{\sqrt{[C]}}\right)\left(\frac{1}{P.r_o}\right) \qquad (5.1)$$

where:

- σ_f is the ionic conductivity of the interface.
- [C] is the concentration of ions in the bulk pore solution.
- δ_{st} is the thickness of the Stern layer.
- k_1, k_2 are special constants related to pore geometry and ionic strength of pore solution and temperature respectively.
- P is the porosity of the cement matrix.
- r_o is the mean pore size, determined from a pore size distribution curve obtained by mercury intrusion porosimetry.

According to equation (5.1), the high-frequency arc diameter (or chord), R_2, is an inverse function of porosity, mean pore size and ionic concentration of the pore solution. In practice, an ideal semi-circle is generally not observed in most materials. It is normally an inclined semi-circle with its center depressed below the real axis by an angle $\theta_d\pi/2$. This behavior is normally associated with a spread of relaxation times and cannot be described by the classical Debye equation employing a single relaxation time. A dispersive, frequency-dependent element or so-called constant phase element (CPE) (Sluyters-Rehbach and Sluyters, 1990; Cole and Cole, 1941) can be introduced to account for the shape of the depressed complex plot. The impedance contribution of this element can be expressed as follows:

$$Z(CPE) = A_o^{-1}(j\omega)^{-n} \qquad (5.2)$$

where n=1-θ_d and $\theta_d\pi/2$ is the depression angle. Therefore, n can be used to represent the degree of perfection of the capacitor and represents a measure of how far the arc is depressed below the real impedance axis.

Disturbed circuit elements are associated with two types of physical interpretation. The first is associated directly with a nonlocal process, for example, diffusion. The other arises because microscopic material properties are themselves often distributed.

5.2.3 Microstructure modeling of cement paste systems

Models that lead to a relationship between the resistor and capacitor parameters and porosity, mean pore size, ion concentration of pore solution, and degree of hydration of the cement paste have been widely studied (Gu et al., 1993, 1995; Xie et al., 1993). Hydrated cement paste is described by a circuit consisting of N electrical elements connected in series (Xie et al., 1993). All the elements are the same physically and consist of three subelements: solid, pore (liquid), and a solid-liquid interface normal to the electrical field. It is emphasized that in any solid-electrolyte system there is a specific liquid region in contact with the solid surface, referred to as the solid-liquid double layer or diffuse layer. The double layer has different ionic composition and microstructure than the bulk liquid due to surface adsorption on the solid. It contains opposite charges to that on the solid surface. It is suggested that under an AC signal the separation of opposite charges in the solid and double layer results in capacitance behavior and the specific ionic composition and microstructure of the double layer results in a different electrical resistance than the bulk liquid (see Figure 5.3). The HFA diameter is proportional to the number of solid-liquid interfaces in the tested specimen. If the specimen thickness is smaller than its critical thickness, then the HFA will not be detected due to an insufficient number of solid-liquid interfaces. The subelement can therefore, be modeled by an equivalent circuit (Figure 5.1 b). The equivalent circuit for the whole specimen is a summation of the subcircuits.

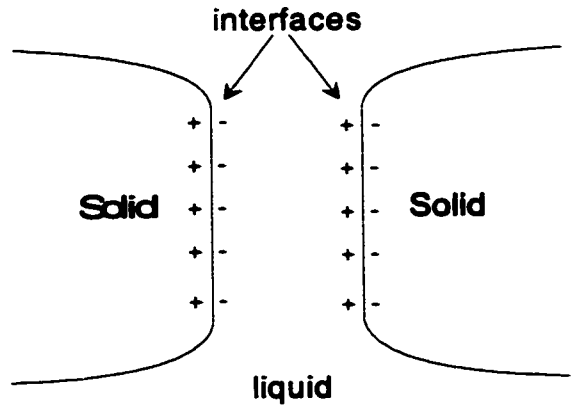

Figure 5.3 : A schematic representation of the "solid-liquid interface unit cell" model (After Gu et al., 1995)

The total impedance, Z, of the specimen can be calculated as follows:

$$Z = Z_1 + Z_2 \tag{5.3}$$

where, according to Xie et al. (1993), Z_1 and Z_2 can be expressed as:

$$Z_1 = \frac{L}{S} \bullet \frac{1}{(1-\Psi_s)} \bullet \frac{1}{\sigma_1} \tag{5.4}$$

$$Z_2 = \frac{NR_f}{1+(\omega C_f R_f)^2} - j\frac{N\omega C_f R_f^2}{1+(\omega C_f R_f)^2} \tag{5.5}$$

where L is the thickness of the specimen in the direction of the electrical field and S is its area normal to the electrical field. Ψ_s is the area fraction of solid phase, σ_1 is the electrical conductivity of liquid phase, and R_f and C_f are the electrical resistance and capacitance of the solid-liquid interfacial zone, respectively. N is the total number of solid-liquid interfaces within the specimen in the direction of the electrical field.

Substituting equations 5.4 and 5.5 into equation 5.3 yields:

$$Z = R_1 + \frac{R_2}{1+(\omega C_d R_2)^2} - j\frac{\omega C_d R_2^2}{1+(\omega C_d R_2)^2} \tag{5.6}$$

where

$$R_1 = \frac{L}{S} \bullet \frac{1}{(1-\Psi_s)} \bullet \frac{1}{\sigma_1}\ , \tag{5.6'}$$

$$R_2 = NR_f \quad \text{and} \quad C_d = C_f / N \tag{5.6''}$$

The corresponding high-frequency arc is presented in figure 5.1(a) and the figure 5.1(b) is the corresponding electrical circuit.

Relationship between High-Frequency Resistance (HFR) and Porosity

Equation 5.6' indicates that the value of HFR, R_1, is a function of both microstructure of the solid phase and the ion concentration of the pore solution. A theoretical foundation for quantitative analysis of ACIS is also provided by the relationship.

Part 3: Experimental Design and Methodology

CHAPTER 6

DESCRIPTION OF APPARATUS, SPECIMEN DESIGN AND EXPERIMENTAL PLAN

6.1 Introduction

One of the objectives of this thesis was to obtain real-time descriptions of microstructural change during creep and shrinkage of cement paste through the coupling of time-dependent deformation and impedance measurements. In addition the use of the solvent exchange process as a microstructural probe was investigated in order to provide additional insight into creep behavior. The experiments were designed to further understanding of creep mechanisms in cement-based materials.

Cement paste is believed to be the most important constituent influencing creep and shrinkage of mortar and/or concrete. Therefore, the choice of studying the behavior of hardened cement paste (hcp) and/or its constituents (CH and C_3S) rather than mortar or concrete has been adopted.

Experimentally, this is of advantageous, given the fact that cement paste is a homogeneous material in which the size of the coarser heterogeneity is that of non-hydrated cement particles. According to that, it is possible to considerably reduce the size of the specimen to be tested as well as the weight of the creep and shrinkage material and equipment. To have an idea of the differences, creep and shrinkage of concrete are usually tested on specimen 200-mm height by 100-mm diameter. The hardened cement paste tests will consist of "T-shaped" specimens having 25.4-mm height, 5-mm flange and ~ 1-mm web.

Given the role which water movement plays on creep and shrinkage mechanisms, the choice of using very thin specimens was made to minimize the moisture gradients within the specimens during the drying process. This specimen enables moisture equilibrium (relative humidity) to be rapidly attained in a very short period of time (less than 24 hours). The replacement of water within such specimens by an organic solvent (used as a microstructural probe) can also be obtained after a few hours.

Finally, given the fact that there is no restraint due to aggregate, the magnitude of the deformations will be greater than that of concrete and therefore, easier to measure with better precision.

6.2 Materials

For the present study, Portland cement was a normal type 10 with Blaine surface area of 332 m^2/kg provided by Lafarge Inc. Reagent grade powder $Ca(OH)_2$ with a surface area of 12000 m^2/kg was used to fabricate specimens formed by powder compaction for these studies. The ground tricalcium silicate (triclinic C_3S) used was supplied by Construction Technology Laboratory, USA. Blaine surface area was 433 m^2/kg. C-S-H was prepared and supplied by Lafarge Coppée Recherche. The C/S ratio varied from 0.68 to 1.49. Porous 96% silica glass (Vycor glass) was obtained from Corning glass in the form of 1-mm thick sheets. The glass had a nitrogen surface area of 175 m^2/g. The molecular sieves used were aluminosilicate based (potassium cations). The 0.4-nm and 0.5-nm material was supplied by Union Carbide USA.
The characteristics of Portland cement, triclinic C_3S and $Ca(OH)_2$ powder are described in Table 6.1. The mixing water used was distilled and de-aired.

Table 6.1: Material characteristics

Material	SiO_2	Al_2O_3	Fe_2O_3	CH	MgO	CaO	SO_3	$CaSO_4$	$CaCO_3$
$Ca(OH)_2$	0.38	0.05	0.05	97.7	0.49	-	0.035	0.15	0.58
C_3S	26.2	0.08	-	-	-	0.46	-	-	-
Cement	20.72	5.87	3.07	0.24	3.46	62.66	2.18	-	-
Bogue Composition of Cement			C_3S(46.5)		C_2S(24.6)		C_3A(10.4)		C_4AF(9.3)

6.2.1 Mixing and storage

C_3S paste (w/s=0.40) and cement pastes (w/c=0.50, 0.80 and 1.00) were prepared by vacuum mixing de-aired distilled water with triclinic C_3S and normal type 10 Portland cement respectively. The vacuum mixing consists of introducing a quantity of solid material (C_3S or cement) in to a 31.75-mm internal diameter by 80-mm long Perspex cylindrical tube with one end closed with a rubber plug. After that, a small magnetic stirrer was placed inside the cylinder and the other end was then closed with a rubber having two holes. From one hole, 10-mm diameter

pipette with an inlet valve was connected to the water system once the other was connected to a vacuum system.

Before introducing de-aired distilled water in order to achieve the targeted water-cement ratio, the cylinder containing the solid material was vacuumed through the end connected to the vacuum system for one hour. After the completion of vacuum, the associated hole was closed; the water was then introduced from the other hole, which was closed thereafter. Using the stirrer previously introduced into the cylindrical tube, the assembly was shaken between two large magnets to ensured homogeneity of the mix. The cylinders were slowly rotated while the paste hardened in order to avoid bleeding and produce a homogeneous product. Samples were removed from the cylinders with a hydraulic press after at least 24 hours, sealed and continuously stored in a rubber membrane containing a small excess of saturated lime water. They were then placed in a container with water at 22±2°C for up to the testing day.

Given the constant volume of the Perspex cylindrical tube, particular attention was paid to the proportions of solid material and de-aired distilled water to be used in order to achieve a given water-cement ratio. The experimental conditions were always chosen to minimize bleeding and local segregation, avoid drying or water penetration as well as to reduce the risk of premature cracking of the specimens.

6.2.2 Specimen preparation

6.2.2.1 Compact samples

Specimens were prepared by compacting $Ca(OH)_2$ and C-S-H powders (1.36 to 1360 MPa) in a mold 31.75-mm (1.25-in.) in diameter, care being taken to ensure that the material was evenly distributed so that the load could be evenly applied. Sufficient material was compacted to give a final thickness of 1-mm (0.04-in.) and a specimen of rectangular shape, approximately 25.4-mm (1-in.) by 6.35-mm (0.25-in.), was cut from it. The sample normally weighed less than one gram. Compacts of CH were vacuum dried at 60°C for 24 h to provide the dry condition. Pre-treatment beyond the dry state was achieved by exposure of compacts (for periods varying from a few days to several weeks) to various humidities in equilibrium with saturated salt solutions. The humidity was varied from 0% to 85% relative humidity. The range of water contents of the CH compacts is summarized in Table 6.2.

A mixture of 75% molecular sieve material and 25% calcium carbonate was compacted at a pressure of 340 MPa in the form of discs, 1-mm thick by 31.7-mm in diameter. Calcium carbonate diluents were used to reduce the very large expansion on wetting and to facilitate compaction.

Table 6.2 Ranges of water content for pre-conditioned CH compacts

Solvent	Water Content (mass %)
Water	0; 0.5; 0.7; 1.9-2.5; 5.2-9.6
Isopropanol	0; 0.5; 0.7; 1.4-1.5; 1.9-2.5; 4.8-6.9
Methanol	0; 0.5-0.7; 1.4-1.5; 1.9-2.5; 5.0-6.8
Benzene	0; 0.5-0.7; 1.4-1.5; 1.9-2.5; 5.1-10.5
Acetone	0; 0.5-0.7; 0.7-1.0; 1.4-1.5; 1.9-2.5; 4.8-6.9

6.2.2.2 Sliced samples

Specimens were made with triclinic C_3S paste (w/s=0.40) hydrated for 28 and 56 days, normal type 10 Portland cement paste (w/c=0.50, 0.80 and 1.00) hydrated for 2 and/or 30 years. These were used for all the experiment. Specimens were sliced in the form of discs, 1-mm thick by 31.75-mm in diameter. The specimens were thereafter cut to form a rectangular shape, approximately 25.4-mm by 6.35-mm sample to be set on the holder and held against the knife-edges of the extensometer by a light spring.

6.2.2.3 T-shaped samples

Specimens were made with CH compacts, C_3S paste (w/s=0.40) hydrated for 28 and 56 days, normal type 10 Portland cement paste (w/c=0.35 and 0.50) hydrated for 2 and/or 30 years. Some "T-shaped" specimens were also made on normal type 10 Portland cement paste (w/c=0.35 and 0.50) at early age (18 h, 24 h and 30 h).

The "T-shaped" specimens had a cross-section 7.00-mm deep with a flange width of 12.70-mm and flange and web thickness of 1.27-mm. The specimens were 25.4-mm long and were made from cylindrical samples cut from 31.75-mm diameter by 80-mm long sample cylinders prepared by vacuum mixing as described in Section 6.2.1. Once cut, the cylindrical sample was glued to a

jig specially constructed to facilitate the cutting of the "T-shaped" specimens with a precision saw (see Figure 6.1).

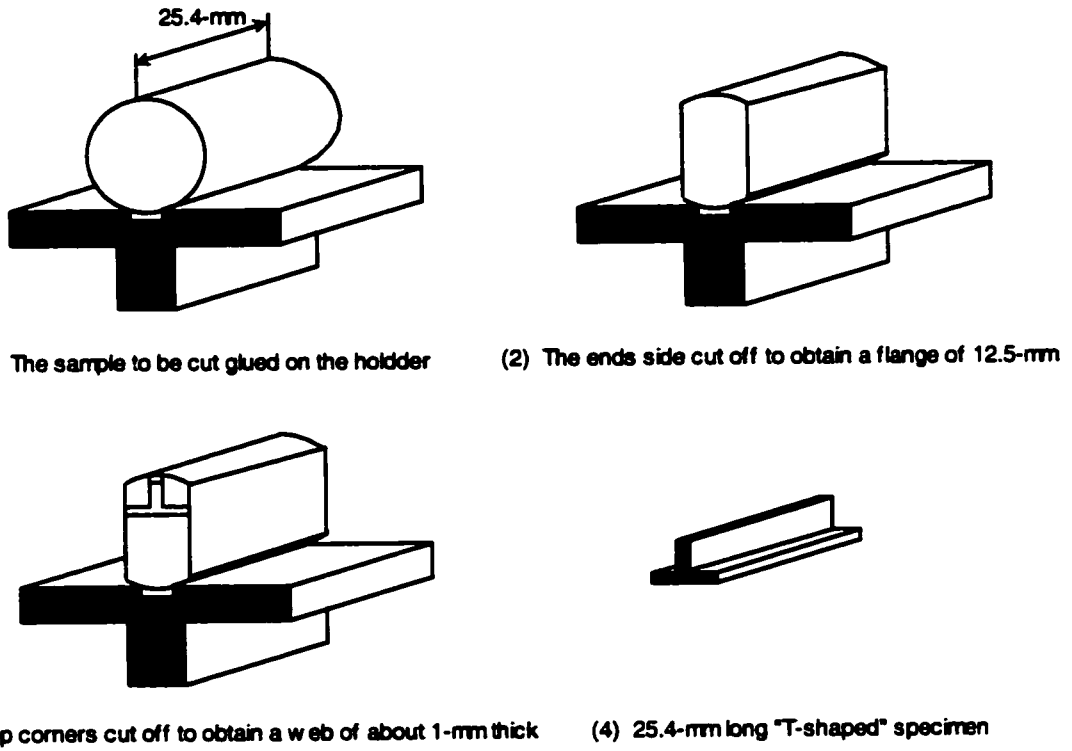

Figure 6.1: Cutting procedure of "T-shaped" specimens

6.3 Solvents

Analytical reagent grade anhydrous methanol, isopropanol, acetone, benzene, dimethyl sulfoxide (DMSO), and diallyldimethylammonium chloride (DDAL) were used. The solvent exchange experiments with DMSO are believed to be the first reported for this solvent. This solvent has been used in studies of layered silicates such as natural montmorillonite (Garwood and Condrate, 1978). Physi- and chemisorbed DMSO complexes can form in their interlamellar spacing. Co-ordination of DMSO molecules with exchangeable cations can also occur through their oxygen atoms. DMSO can also bond via its oxygen atom to clay hydroxyl surfaces. For these reasons, DMSO was considered for the present studies.

6.4 Apparatus

6.4.1 Vacuum apparatus

The vacuum system consists of a pump having an ultimate vacuum of 1×10^{-4} mm Hg and a free air displacement of 195 l/min. The vacuum system was used to avoid carbonation of the samples during the treatment period and to dry samples and/or remove physically adsorbed solvent from them. It was also used for vacuum re-saturation of the specimens with a synthetic pore solution prepared using saturated lime water to which potassium chloride was added to obtain the same resistivity as that of the pore solution of the cement paste.

6.4.2 Loading apparatus

The loading mechanism consists of a two stages miniature fixed frames on which is mounted a load cell with a maximum capacity of 250 lbs. (1112.4N) through a spring connected by a small steel bar to the upper end of the specimens holder. The constant stiffness of the spring was 450 lbs./in (78.8 N/mm) and was determined from calibration test with the MTS system used for compressive strength.

The load can be adjusted through a screw linking the spring to the fixed frame. The lower end of the spring transmits the load to two "T-shaped" specimens through the movable specimen holder. The modified Tuckerman optical extensometers used for length change measurements, were then mounted on the flanges of each of the two "T-shaped" specimens and coupled at their sides with appropriate springs. The assembly was then placed in cells or vacuum dessicators containing a drying agent and equipped with optical flat lids and for some experiments, in an environmentally controlled glove box equipped with a fan system. The deformations could be determined with a sensitivity of $1\text{x}10^{-6}$ mm/mm. Duplicate specimens were used for each test condition. Careful precautions to minimize carbonation were taken in all phases of the experiments including the use of glove boxes flushed with nitrogen when appropriate. Further details of the conditioning system are provided in Section 5.4.5. This was considered extremely important, as appreciable carbonation can significantly affect deformations and microstructure. The detail of the schematic diagram of the controlled environment for measuring deformations of "T-shaped" specimens is presented in Figure 6.2.

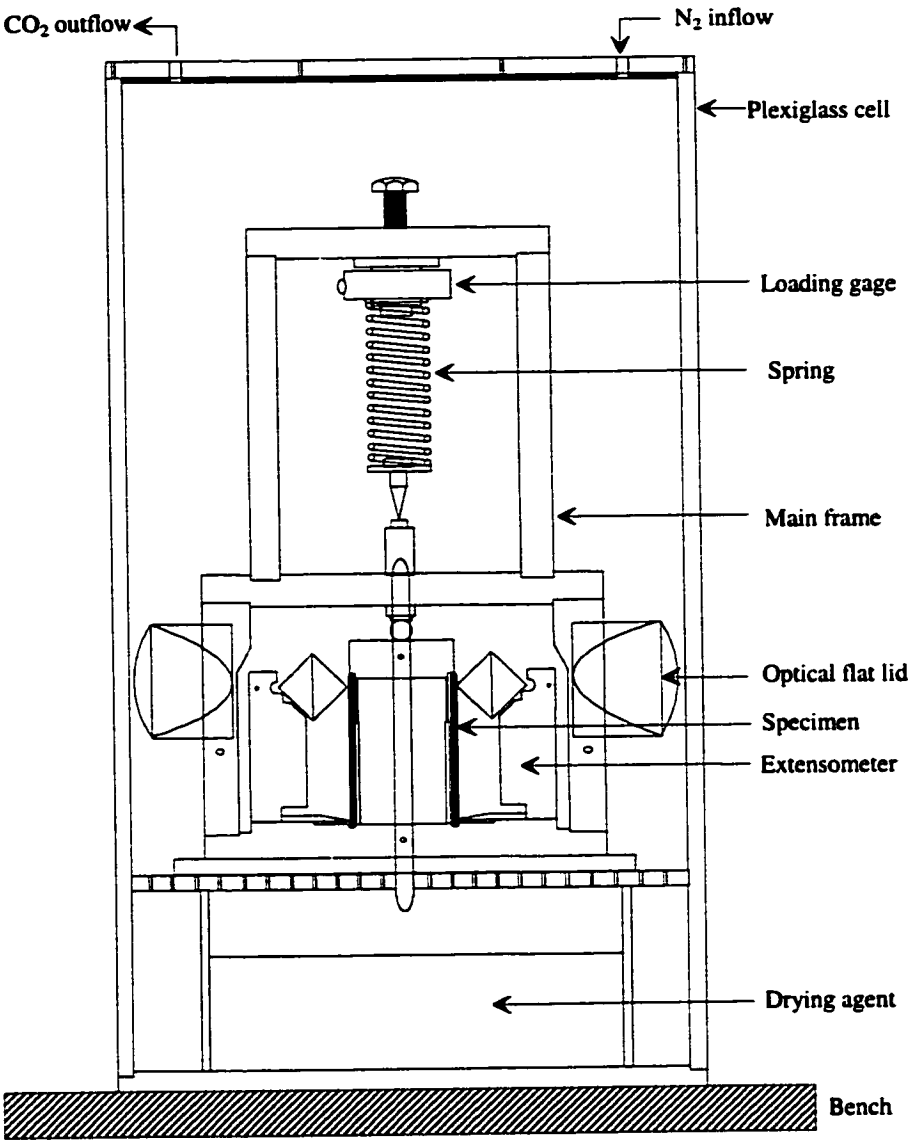

Figure 6.2: Loading mechanism and environment for creep measurement system

6.4.3 Extensometer (strain gage)

The gage used for the present study is a modified Tuckerman optical strain gage allowing to determine the length changes with a sensitivity of 1×10^{-6} mm/mm. The operation of this instrument is dependent upon the principle of reflected light. The extensometer (gage) is unique in that it incorporates two mirrors, oriented at right angles to each other, one of which is fixed in space (90°-roof prism) and the other rotating (lozenge). Using this arrangement, errors that are

inherent in other systems are eliminated. Used in conjunction with the extensometer, the Tuckerman Autocollimator is a reading autocollimating telescope whose sensitivity is dependent of its distance from the gage. The reflection of light by the two mirrors causes an image to appear in the autocollimator field of view. The position of the image on the reticule scale is a function of lozenge rotation caused by specimen deformation. The simplified optical diagram showing how light emanating from the autocollimator is reflected by the lozenge to the fixed mirror and back to the autocollimator to form an image is presented in Figure 6.3. All the deformations were measured with this Tuckerman gage.

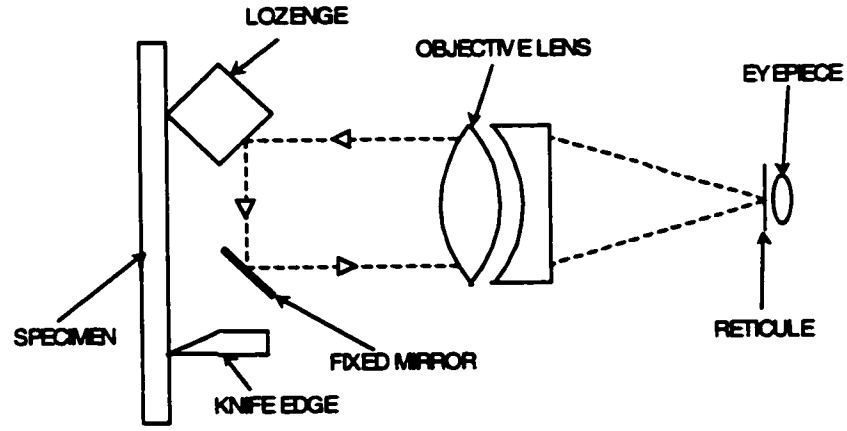

Figure 6.3: Simplified optical diagram

6.4.4 Hydraulic systems and compaction tool

Hydraulic press was used to compact some specimens while MTS system coupled to a personal computer (386DX33) was used to calibrate the loading apparatus and to determine the compressive strength of miniature cylindrical specimens of hardened paste systems 12.7-mm diameter by 25.4-mm in height. This length to diameter ratio of 2 was realized in order to minimize the end effects occurring due to shear in the compression test.

The hydraulic press consisted of 556.2 KN (125,000-lbs) capacity single-acting hollow hydraulic cylinder allowing the top head piston to move downward to compress material held in stainless steel mold 31.75-mm (1.25-in.) in diameter. Careful precautions were taken to ensure that the material was evenly distributed so that the load could be evenly applied. This hydraulic press was also used to extract pore fluid from the cement paste and to collect it in a syringe. The initial pore solution conductivity was thus determined.

The control of the MTS system used to calibrate the loading test apparatus and to determine the compressive strength of hardened pastes is provided by a "loop" of electronic and servo-hydraulic components. As shown in figure 6.4, these components include the programmer, the 458 Micro-Console and it's associated transducers (a LVDT and a load cell). The configuration of these devices provides means of comparing a command (programmer output) signal with a feedback (transducer output) signal to generate a signal that controls the servo-valve. The servo-valve controls hydraulic flow to the actuator, which moves the actuator piston rod. The actuator piston rod applies the force required to load or displace the specimen and/or structure being tested. The calibration and the paste cylinder compressive strength were performed with 10 KN load cell at 0.5 mm/min.

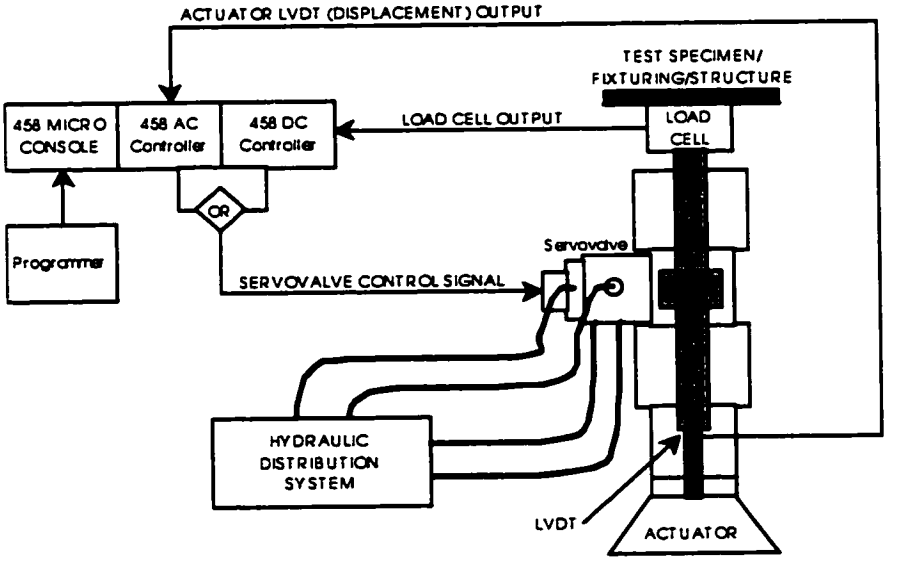

Figure 6.4: Typical closed-loop system

6.4.5 Environmentally controlled cells and cabinet

Conditioning was carried out in special cells as well as desiccators fitted with flat Lucite tops to permit reading of the extensometers (see Figure 6.5). Extreme precautions were taken to prevent any traces of carbonation during preparation of the samples in dry boxes and during conditioning over salt solutions, made with boiled distilled water, used for controlled relative humidities. Periodic, magnetic stirring was employed. The air in the conditioning glove boxes, cells or desiccators was evacuated by nitrogen gas before the conditioning process starts. The Figure 6.2

illustrated previously shows a typical conditioning cell in which the loading system was installed for monitoring the delayed deformations. The conditioning glove box system presented in the Figure 6.6 was designed to carry a thermal balance coupled to a personal computer and a desiccator containing specimens at a given relative humidity. The specimens in the desiccator were removed for test only when the relative humidity in the glove box at equilibrium was the same as that in the desiccator. The glove box was also used for measuring the mass change of damped wet specimens during the drying process. For this purpose, a very fine hole was made on the top of the box, and a digital balance with a sensitivity of ±0.0001 g coupled to a laptop was installed above.

Loading systems and in particular a loading system specially design for AC impedance experiment have also been directly installed in the glove box in order to simultaneously monitoring real time impedance spectra and deformations taking place as the material is drying and/or under sustained load. The details of the electrode interface of the specially designed loading system, which is only a modification of the original system, are described in the following section.

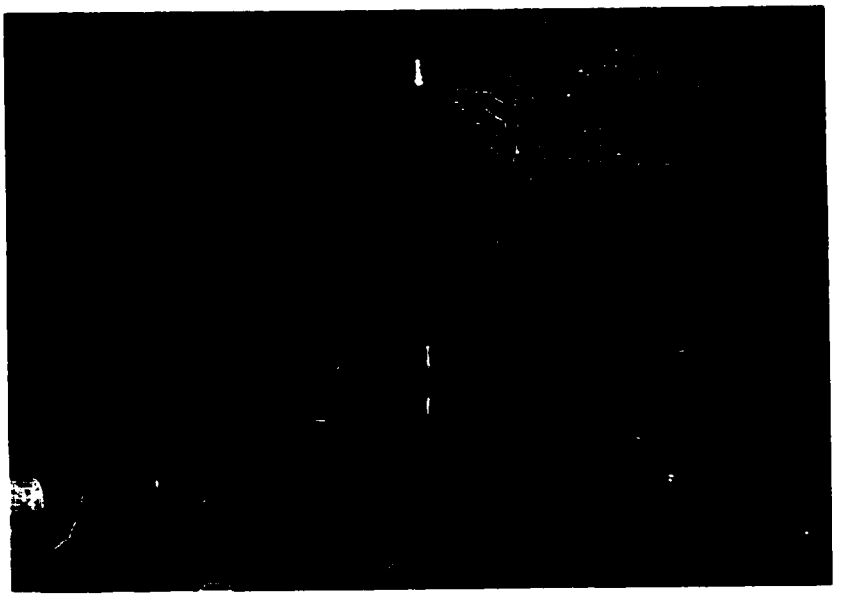

Figure 6.5: Conditioning desiccator fitted with flat lucite top

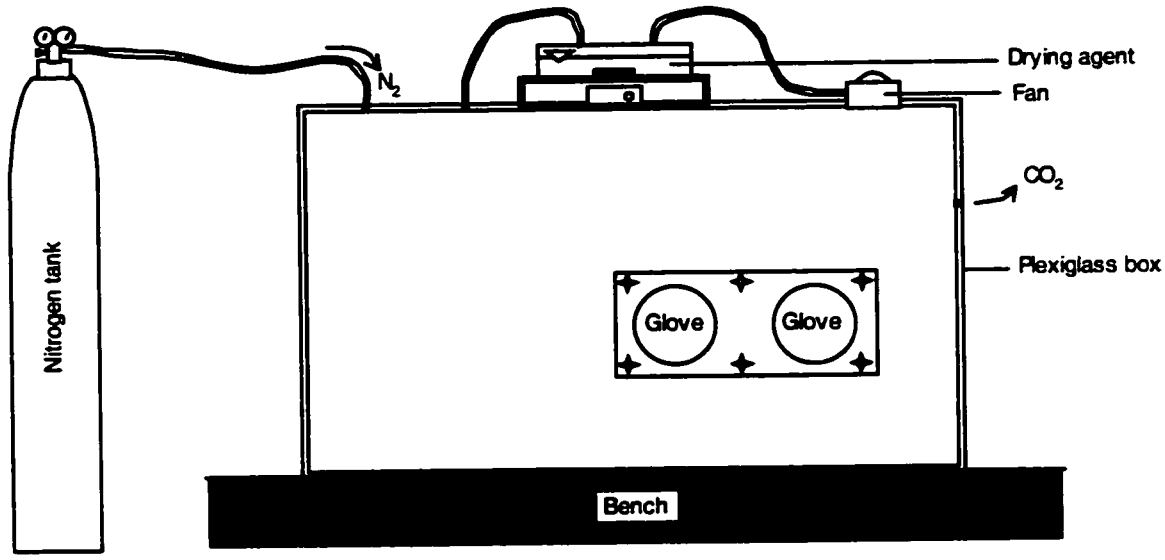

Figure 6.6: Detail of the conditioning glove box

6.4.6 Specially designed loading system

The specially designed miniature loading system utilizing the modified Tuckerman extensometers and stainless steel parallel plate electrodes were used to obtain real-time spectra from the coupled AC impedance spectroscopy and creep and shrinkage experiments. The detail of the "T-shaped" specimen-electrode connection interface is presented in Figure 6.7. It should be noted that the lower end of the specimens is also subjected to the same connection interface. Flat gold sheets were also used as electrodes. To avoid formation of inductance resistance, which may bias the results, very short wires were used between the special loading system (in the glove box) and the frequency response analyzer (placed beside the glove box). The photograph of the entire system showing the coupled loading frame and the AC impedance machine is illustrated in Figure 6.8.

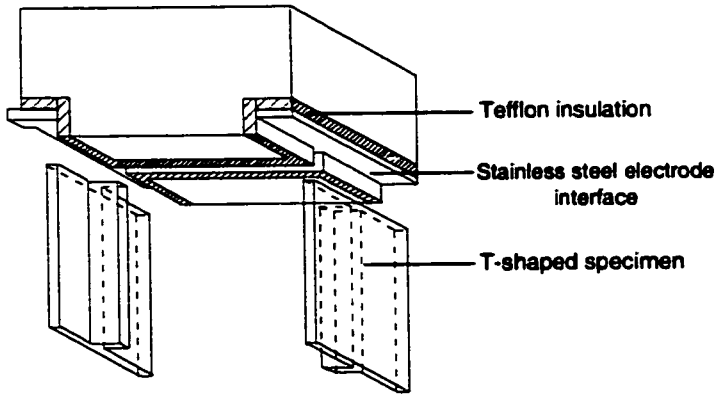

Figure 6.7: Detail of "T-shaped" specimen-electrode connection interface

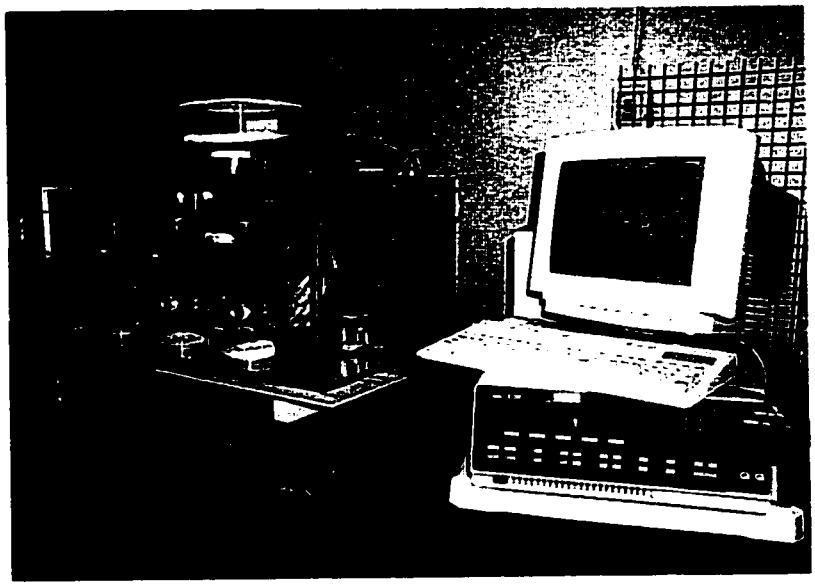

Figure 6.8: Photograph of coupled loading frame and AC impedance machine

6.4.7 Data acquisition systems

6.4.7.1 Humidity and temperature meter

For relative humidity and temperature measurements, a digital humidity meter model RH30-C was used and it is commercially available from Omega Engineering Inc.

6.4.7.2 Digital balance coupled with a laptop

The balance used was a top loading balance and was coupled to a laptop for a dynamic measurement of the mass change of the material while drying and/or during immersion in a organic solvent. The RS 232 data acquisition software "SARTO WEDGE" version 1.01 for data operating system (DOS) from T.A.L Enterprises was used for the present study.

6.4.7.3 Frequency response analyzer

The most common AC impedance spectroscopy procedure consists of measuring impedance directly in the frequency domain by applying a single-frequency voltage to the testing system and to measure the phase shift and amplitude, or the real and imaginary parts, of the resulting current at that frequency. Commercial instruments are available, and that used for this study is the Solartron 1260-frequency response analyzer, allowing measuring the impedance as a function of frequency automatically. The analyzer was interfaced to a personal computer (386 DX33) with real-time plotting capability. Signal amplitude of less than 0.5 V is used throughout the sweep. The advantages of this technique include operationally simple instrumentation and the capability and the possibility of controlling the frequency in the range of most interest. The range of frequencies of the impedance spectra recorded was wide varying from 15 MHz to 1 Hz.

6.5 Experimental program

Historically several practical difficulties have hindered the investigation of the central role which water plays in the creep and shrinkage of cement pastes. A primary difficulty rests with the detection of the small volume and weight changes involved in specimens at equilibrium with the surrounding environment. The thermodynamically irreversible character of the hydrating Portland cement paste and the unstable nature of the hydration products (C-S-H) are believed to

constantly change the chemical and physical properties of the material. In the proposed experiment particular attention was given to the relationship between the creep of hydrated cement paste and the length change generally observed in microporous materials as well as the water content of the paste determined from differential thermogravimetric analysis in controlled environment. To evaluate the microstructural changes taking place during the shrinkage and/or creep process, a coupled AC impedance spectroscopy spectra were monitored simultaneously with shrinkage, creep and creep recovery. The coupled AC impedance spectroscopy experiments involved fitting the "miniature" creep frames with appropriately shielded electrodes. Such tests were utilized to establish relationships between pore structure, pore solution, electrical resistivity and strain due to short-term creep and shrinkage.

The experimental program was subdivided in order to review the different contribution of hardened cement paste constituents to creep and volume variation after several pre-treatments.

6.5.1 Length change in microporous systems

This study was designed to determine the role of $Ca(OH)_2$ and C_3S in hydrated cement systems concerning the processes involved in the removal of water by solvent replacement methods. The length change characteristics of $Ca(OH)_2$ compacts containing varying amounts of water and immersed in large volumes of organic liquids (methanol, isopropanol, benzene, and acetone) were monitored for the ranges of water content presented in Table 6.2. Those of C_3S paste were monitored at two different curing periods (28 and 56 days).

The volume stability of partially saturated and saturated microporous systems subjected to the solvent exchange process was also studied. Several microporous systems were therefore considered (hydrated Portland cement, calcium silicate hydrate (C-S-H), calcium hydroxide (CH), Vycor glass and molecular sieves). Single and double exchanges were performed to assess the effects of the initial exchange on the reversibility of the length changes observed. The experimental scheme associated to the length change following immersion of specimens in organic solvents is presented in Figure 6.9.

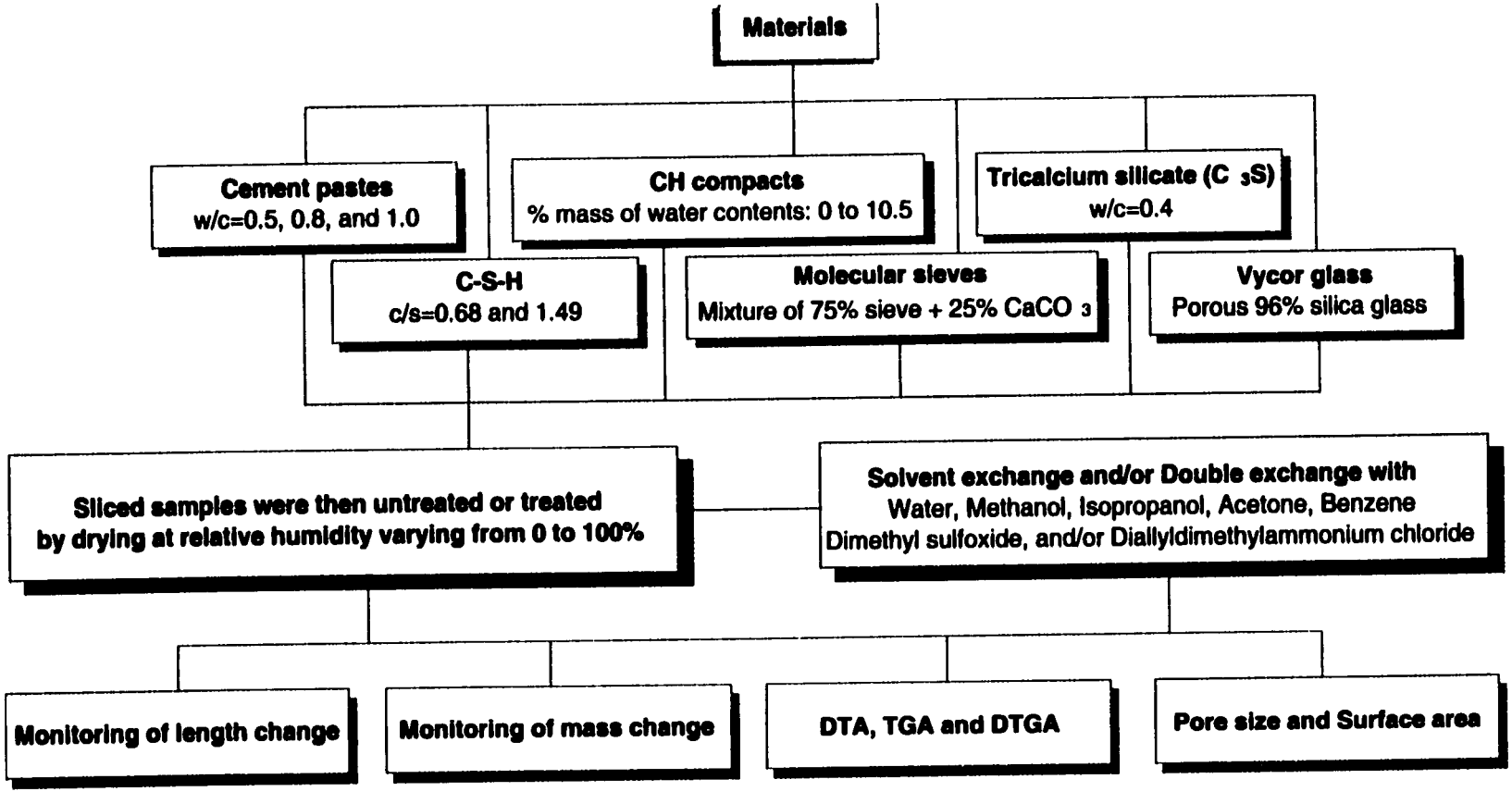

Figure 6.9: Experimental scheme for volume instability and length change study of Portland cement systems

6.5.2 Shrinkage and creep of Portland cement systems

The creep and shrinkage behaviors of specimens pre-treated by the organic solvent exchange procedure were investigated. Calcium hydroxide (CH), tricalcium silicate (C_3S) and Portland cement were used in the present study. Generally, most of the creep tests were performed at a constant relative humidity, meaning there was no moisture exchange between the specimens and the surrounding environment. Relative humidity varied from 0 to about 0.96. The stress-strength ratio used was 0.3 and the corresponding stress was computed according to the cross section area of the "T-shaped" specimens. The experimental scheme associated to the shrinkage and creep of Portland cement systems is presented in Figure 6.10.

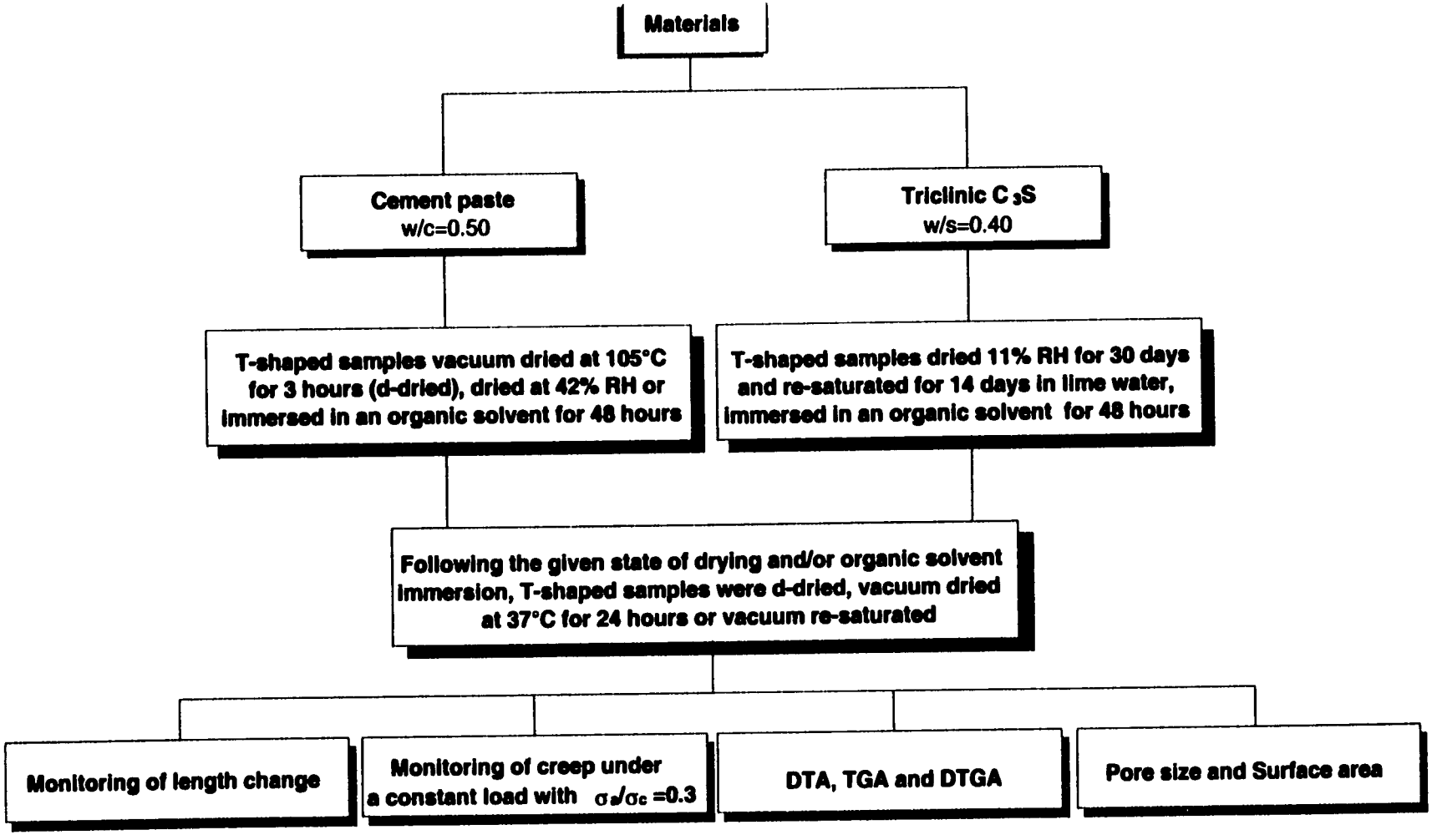

Figure 6.10: Experimental scheme for creep and shrinkage study of Portland cement systems

6.5.3 Coupled AC impedance - creep and shrinkage

The effect on creep and shrinkage in hardened cement paste observed through real-time measurements of the quantitative changes to the high frequency arc (HFA) under various loading and drying pre-treatments and environmental changes was investigated.

As mentioned previously in Chapter 5, the layer structure of hydrated cement paste can generally be described by a typical element consisting of the poorly crystallized material (solid), the pore solution (liquid), and a solid-liquid interface. It is emphasized that in any solid-electrolyte system there is a specific liquid region in contact with the solid surface, referred to as the solid-liquid double layer or diffuse layer. The double layer has a different ionic composition and microstructure than the bulk liquid due to surface adsorption on the solid. It contains opposite charges to that on the solid surface. It is suggested that under an AC signal the separation of opposite charges in the solid and double layer results in capacitance behavior and the specific ionic composition and microstructure of the double layer results in a different electrical resistance than the bulk liquid (Figure 5.3). The size of the high frequency arc (Figure 5.1) diameter is proportional to the number of solid-liquid interfaces in the tested specimen. If the specimen thickness is smaller than its critical thickness, then the HFA will not be detected due to an insufficient number of solid-liquid interfaces. Most materials exhibit an inclined semicircle with the center depressed below the real axis by an angle θ_d (Figure 5.2). The angle depression is the most common phenomenon in a. c. impedance studies and the HFA diameter is then equal to $R_2/\cos(\theta_d)$.

Coupled ACIS and creep and shrinkage was performed on 2 year old hydrated cement paste with water-cement ratio of 0.50. It was also performed on very young cement pastes (w/c=0.35 and 0.50) hydrated for 18, 24 and 30 hours. In all cases, the elapsed time under load was 3 days, and the recovery after the removal of the load was monitored for 2 days. The experimental scheme design for this particular study is presented in Figure 6.11.

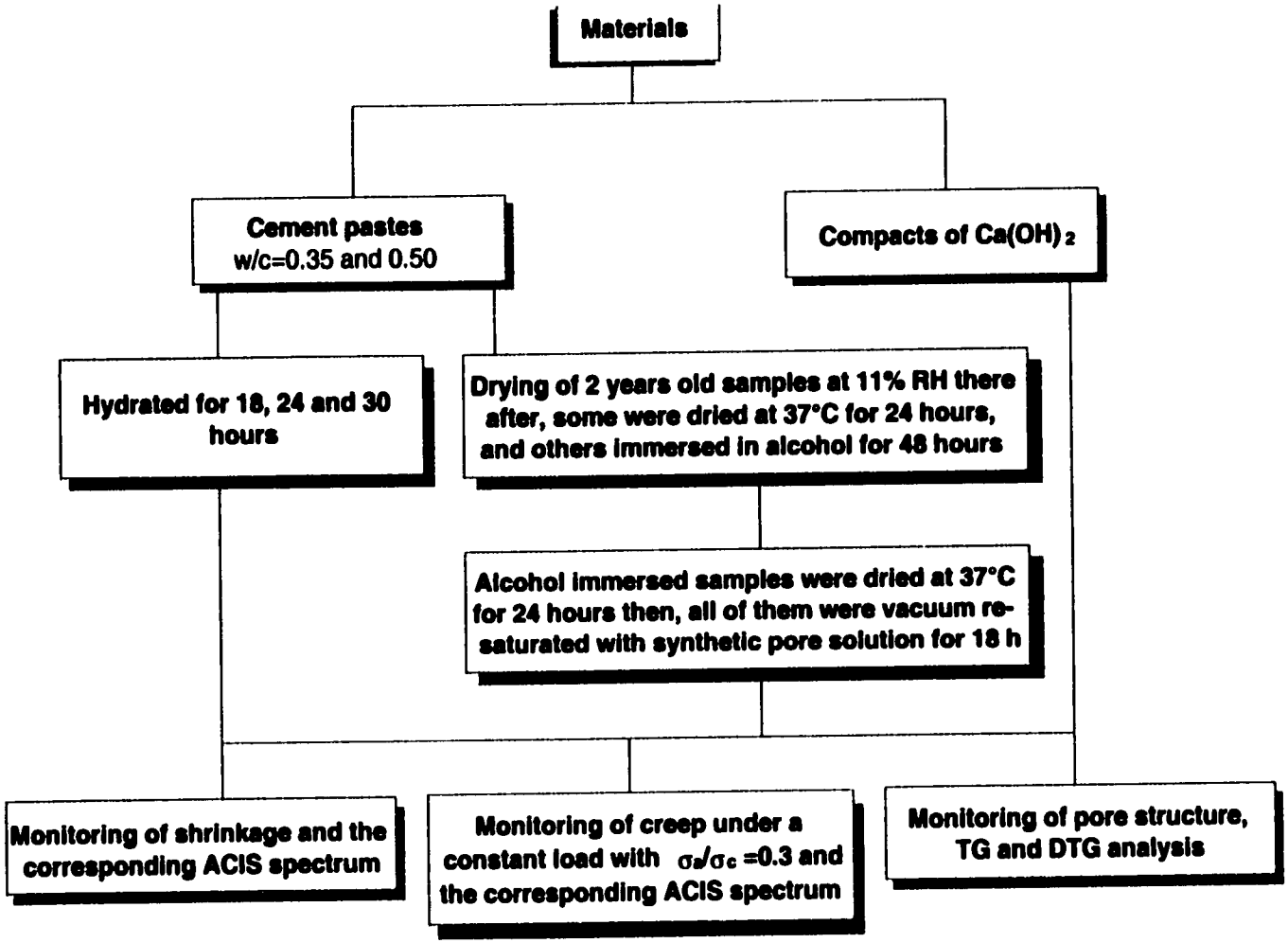

Figure 6.11: Experimental scheme for the coupled ACIS and creep and shrinkage study

CHAPTER 7

EXPERIMENTAL METHODOLOGY

7.1 Introduction

The normal drying process is believed to considerably affect the hardened cement paste microstructure or particularly the C-S-H layered structure. The surface area measured by water adsorption is strongly affected by drying; it is several times greater than that measured by the adsorption of nitrogen. The solvent replacement technique which, in effect, is a counter diffusion process consisting of the removal of water with a solvent has been used in order to minimize and possibly "preserve" the original microstructure of the hydrated cement paste. The application of this technique depends mainly on the fact that any interaction between the solid and organic solvent should not produce an artifact detectable with the microstructural method to be used. In such case, the use of different organic solvents will lead to different microstructures of cement paste or the C-S-H layered structure. Pre-treatment of cement paste with organic solvents should be of value in a creep and shrinkage investigation in providing a fundamental understanding of the role of C-S-H.

The solvent exchange of water in porous materials is usually accompanied by mass and length changes. The role of Portlandite or calcium hydroxide in the solvent replacement process as applied to hydrated cement systems should be determined to more fully understand the solvent interactions.

The creep and shrinkage behavior of specimens pre-treated by organic solvent exchange procedure is to be investigated. The hypothesis that no creep takes place in cement paste specimens from which evaporable water has been completely removed will be re-examined. The re-saturation of Portland cement paste systems with synthetic pore solution after several drying pre-treatments has been adopted as a method to investigate the shrinkage, creep, and creep recovery behavior. The analysis of the hardened cement paste using coupled (real-time) ACIS and creep and shrinkage measurements has also established ACIS as an effective method for evaluating pore structure modification as well as the nature of changes to the pore network of cement paste during creep and shrinkage experiments. The pastes samples in this study will all be well-characterized using mercury intrusion porosimetry, nitrogen adsorption surface area and thermogravimetric methods.

7.2 Drying of the pastes

The drying of hydrated Portland cement paste was the subject of considerable debate in the 1960's and 1970's due to its relevance to the development of models for the structure of C-S-H (Feldman, 1971). A primary issue was whether or not water was capable of re-entering the layered structure subsequent to drying. This had not only structural implications but also relevance to the validity of applying classical sorption theory to the cement paste - water system.

The concept of D-drying was first introduced by Copeland and Hayes (1953). It referred to drying of cement paste by outgassing to the vapor pressure of dry ice at -79 °C (0.5×10^{-3} mm Hg). They stated that it took from 4 to 7 days for equilibrium to be reached. This involves drying from fairly wet conditions to the removal of both the tightly held first layer and the even more tightly held interlayer water from the very narrow spaces. The slower than normal times required for equilibrium of water during the adsorption stage is probably due to the lengthy process of re-opening the layers.

The 11% RH condition corresponds to approximately a monolayer of coverage (Feldman, 1980). Other drying conditions described in this thesis are intermediate between the D-dry state and the equilibrium position at 11%RH. Feldman established an equivalent to D-dry method using a vacuum electrobalance and thermal balance techniques (Feldman, 1968). It was determined that vacuum degassing at 105°C for 3 hours was equivalent to D-drying. This corresponds to a mass loss of 8 to 9 % based on the D-dry state.

The drying pre-treatments described in this thesis are as follows:

(1) D-dry - this stage was attained using the equivalent drying method described above.

(2) Vacuum drying at 37°C for 24 hours - this "soft drying" procedure is equivalent to P-drying (Rayment and Majumdar, 1982). P-drying refers to drying to the vapor pressure of $Mg(ClO_4)_2.2H_2O$ or $Mg(ClO_4)_2.4H_2O$ i.e. 8×10^{-3} mm Hg. At this vapor pressure there is about 14% more water retained by the paste than by D-drying.

(3) Solvent exchange using methanol or isopropanol followed by vacuum drying at 37°C. The solvent replacement is effective in removing the bulk of the evaporable water. Subsequent vacuum drying provides a state intermediate between D-drying and P-drying.

The relevance of the different pre-treatments lies in the degree to which water is removed below the monolayer level and to its implication for volume change. The relevance of the solvent exchange process for creep is given in Section 7.3.

Drying to 96% RH

A characteristic of the water sorption isotherm for cement paste is that the desorption branch (in the high humidity region) is less steep than the adsorption branch as a result of the large secondary hysteresis (Feldman, 1968). The amount of water desorbed at 96% RH is only about six per cent of the D-dried mass of the cement pastes. Most of the capillary pores continue to contain some bulk water. Those pores that empty would still have adsorbed films on their surfaces.

AC impedance spectra are readily obtained when equilibrium is attained at 96% RH as the system is still effectively percolated. The objective of choosing a test humidity of 96% RH was to provide a test environment for both creep and shrinkage measurements (shrinkage, although small, will occur due to meniscus effects) while minimizing any significant decrease in percolation. Changes in the spectra are readily detected during the equilibrium process. It is well known that the menisci do not completely rupture until about 45% RH where there is a marked effect in the length change desorption isotherm due to elastic rebound (Ramachandran et al., 1981).

7.3 The Relevance of Solvent Exchange Techniques for Creep Investigations

Several studies of the microstructure of cement paste describe solvent exchange with methanol as a technique that "preserve" the wet-state structure of the material (Litvan, 1976; Parrott. 1983). For example, large decreases in surface area do not result subsequent to the removal of methanol. An implicit assumption in these studies is that the solvent does not interact with C-S-H. This may not be correct (Beaudoin, 1987). The "preservation" capacity of the solvent exchange process is relevant to creep investigations as the "in-situ" microstructure may be more closely approximated. Complete drying does not occur in practice. The accompanying collapse of the C-S-H structure due to water removal is therefore more moderate.

The "preservation" of C-S-H structure on drying is also influenced by the solvent exchange process. Powers reported that even a slow drying of a cement paste to 79% relative humidity

increases its water permeability 70 times suggesting the effect would be even greater if drying to equilibrium at a lower humidity had occurred (Powers et al., 1954). Studies by Parrott on the effect of drying history upon the exchange of pore-water with methanol corroborates Powers observations and suggests that drying even to intermediate humidities causes a partial collapse in the smaller pores and a corresponding increase in the volume of the largest pores (Parrott, 1981). This supports the assumption that the total porosity is relatively constant and that only the pore size distribution is altered.

AC impedance studies have also demonstrated a pore coarsening effect on drying (Beaudoin et al., 1998). The impedance spectra for cement paste (w/c=0.30) re-saturated with synthetic pore solution subsequent to cycles of wetting and drying undergo a systematic decrease in the size of the high frequency arc to lower resistance values (Figure 7.1) suggesting an increase in the mean pore size. The pore coarsening effect was confirmed by mercury intrusion data.

The microstructural "preservation" effect (including pore coarsening phenomena) of the solvent exchange process is useful for studying the varying degrees of microstructural collapse on the creep process. In addition the exchange process affords the opportunity of examining the "dry-state" (obtained through different procedures) and its effect on creep.

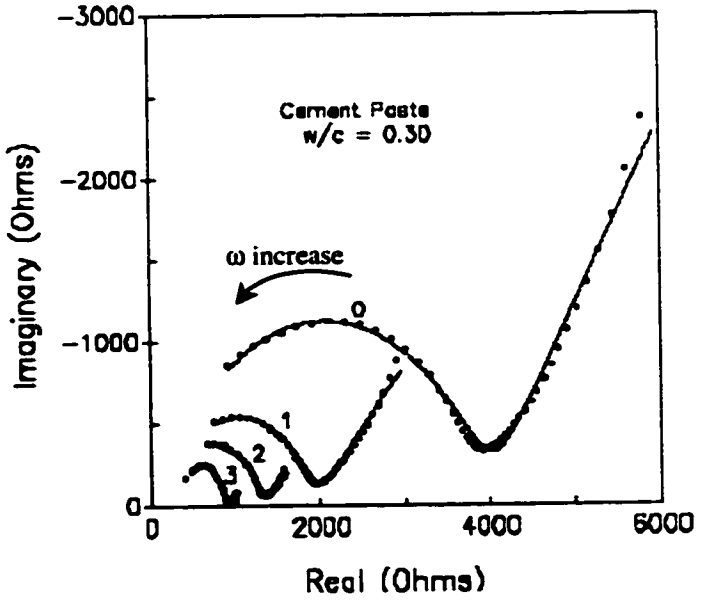

Figure 7.1: AC impedance spectra for cement paste (w/c=0.30) subjected to cycles of wetting/drying subsequent to re-saturation with synthetic pore solution. Numbers indicate the conditioning sequence. Data points are experimental; solid lines are obtained from computer simulation (Beaudoin et al., 1998).

7.4 Thermal analysis

Thermal analysis consisting of differential thermal analysis (DTA), thermogravimetric and differential thermogravimetric analysis (TGA and DTGA) was carried out using a 1090 DuPont thermal analyzer containing a 951 TGA accessory. Generally, in TGA experiment a 50-mg sample was heated at 5°C/min up to 200°C then heated at 10°C/min in a continuous flow of nitrogen up to the ignition state. For DTA test, a 25-mg sample was heated at 20°C/min. The DTA cell could be used up to 1200°C. These methods provided estimations of C_3S, CH, and ignition loss.

7.5 Mercury intrusion porosimetry

The determination of porosity and pore size distribution was made on selected samples using an American Instrument Company porosimeter capable of applying intrusion pressure up to 410 MPa. About 0.6-g of sample was intruded by mercury into the penetrometer. Prior to the test, samples were subject to different drying pre-treatment regimes.

7.6 Surface area

Nitrogen surface area measurements were obtained with a quantasorb surface area analyzer. A 0.5-g of pulverized sample was introduced into the holder and the adsorption was monitored with sample-holder cooled with liquid nitrogen.

7.7 Compressive strength and Young modulus

The compressive strength was performed using an Instron machine having a static load cell of 10 kN. The tests were performed on cylindrical specimens with 12.7-mm diameter by 25.4-mm in height. The crosshead speed was 0.5 mm/min, the room temperature was 21°C and the relative humidity was 50%.

The calibration of the pressure gauges for the load cell of the miniature loading system was performed using an Instron machine having a reversible load cell of 4.9 kN. The crosshead speed was set at 0.2 mm/min. Following the calibration, the miniature loading system was used to determine the modulus of elasticity and to monitor the creep of "T-shaped" specimens.

7.7.1 Calibration of the pressure gage

Six gauges with 2.5 lbs. per division were used for the present experiment consisting of gauge numbered 1481, 1984, 1992, 1993, 1994, and 1995. Average of two readings was considered and was plotted in order to compute the actual force corresponding to each division of the pressure gauge. The calibration results are presented in Figure 7.2.

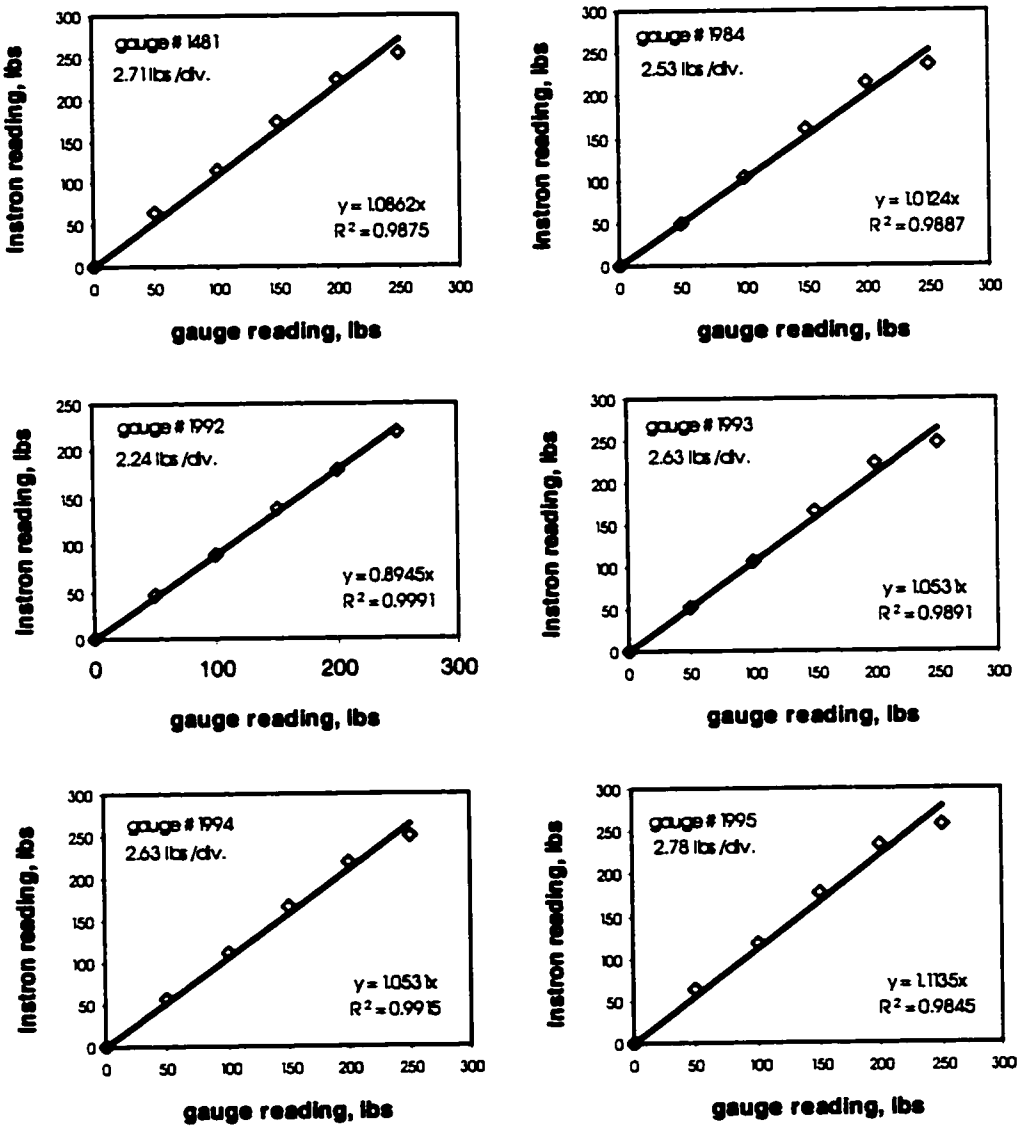

Figure 7.2: Calibration curves of pressure gauges for the miniature loading system

7.7.2 Calculation of the modulus of elasticity

The Young modulus of elasticity was determined by mounting the "T-shaped" specimens on miniature loading system and applying incrementally a load up to a level that results in a stress of 2 MPa (289.9 psi). This corresponded to 30% of the compressive strength of the material. During the loading process, the readings from an autocollimator were monitored in order to obtain the length change (Δl) of the specimens. This is equal to the change in the reading, times 0.0004-in.

The applied force or load divided by the cross section area of the "T-shaped" specimens (F/A) is then plotted against the deformation ($\Delta l/l$). The slope of the curve corresponds to the Young modulus of elasticity of the material (E).

7.8 AC impedance spectroscopy

The analysis of the hardened cement paste using coupled ACIS and creep and shrinkage measurements was used as an attempt establishing ACIS as an effective method for evaluating pore structure modification as well as the nature of changes to the pore network of cement paste during creep and shrinkage experiments.

As mentioned previously in Section 5.2.1, the methods are characterized by the application of a small-amplitude sinusoidal potential perturbation to the working electrode at a number of discrete frequencies. At each frequency, the resulting current waveform will exhibit a sinusoidal response that is out of phase with the applied potential signal by a certain amount. Impedance spectra recorded over a wide range of frequencies (from 15 MHz to 1 Hz) have provided new information and insight on cement paste microstructure and hydration.

Part 4: Analysis of results

CHAPTER 8

RESULTS-INTERPRETATION AND DISCUSSION

8.1 Introduction

The normal drying process is believed to greatly affect the hardened cement paste microstructure or particularly the C-S-H layered structure. The surface area measured by water adsorption is strongly affected by drying; it is several times greater than that measured by the adsorption of nitrogen. The solvent replacement technique which, in effect, is a counter diffusion process consisting of the removal of water with a solvent has been used in order to minimize and possibly "preserve" the original microstructure of the hydrated cement paste. The application of this technique depends mainly on the fact that any interaction between the solid and organic solvent should not produce an artifact detectable with the microstructural method to be used. If that is the case, the use of different organic solvents will lead to different microstructures of cement paste or the C-S-H layered structure. Pre-treatment of cement paste with organic solvents should be of value in a creep and shrinkage investigation in providing a fundamental understanding of the role of C-S-H.

The solvent exchange of water in porous materials is usually accompanied by mass and length changes. The role of Portlandite or calcium hydroxide in the solvent replacement process as applied to hydrated cement systems should be determined to more fully understand the solvent interactions. This aspect is included in the thesis and results indicate calcium hydroxide too has an active role in volume change phenomena. Length change of calcium hydroxide compacts pre-conditioned to various water contents was therefore monitored following immersion in various liquids in a strategy designed to separate out Bangham length change effects from those due to chemical interactions with solid surfaces. Mass change versus time measurements during exchange were carried out to support the interpretation of the length change behavior. Similar studies were conducted on Portland cement and tri-calcium silicate pastes.

Length change was monitored with the modified Tuckerman optical extensometers with an accuracy of one micro-strain. Drying of the test specimens was conducted under a vacuum at 37 °C for 24 hours. This gentle drying procedure was chosen to avoid or minimize any micro

cracking that may take place in the paste. On re-wetting, the specimens were vacuum saturated for 18 hours. The solutions used for re-wetting included saturated lime solution and synthetic pore solution (made with saturated lime solution and the required amount of a potassium salt to match the resistivity of the natural pore solution). The natural pore solution was expressed and collected for electrical measurements.

The results are presented and discussed in three separate sections. In Section 8.2, the volume instability of microporous systems is described analyzed while in Sections 8.3 and 8.4, creep and shrinkage of Portland cement systems are analyzed through strain and/or impedance spectra. Deformations or impedance spectra were obtained from a specially designed miniature creep frame utilizing the modified Tuckerman extensometers and stainless steel parallel plate electrodes.

8.2 Volume instability in microporous systems

8.2.1 Thermal analysis

8.2.1.1 Drying pre-conditioning

The general characteristics of a differential thermogravimetric analysis (DTGA) curve for cement pastes obtained under equilibrium condition are presented in Figure 8.1. The first endothermic peak is attributed to bulk water (this includes capillary and micropore) and the second peak to interlayer water (Feldman and Ramachandran, 1971). The results of TGA carried out on re-saturated specimens following pre-conditioning up to equilibrium at various relative humidities are presented in terms of the derivative of the mass loss versus time (expressed in %/minute) plotted against temperature. It was generally observed that the differential TGA curves are clustered into two groups. The first comprises those for specimens conditioned to humidities ranging from 11% to 42% RH. It is apparent that the specimens in this group contain predominately interlayer water. Figure 8.2 indicates that at these humidities, only the peak at 110°C is present in the differential TGA spectra obtained under controlled humidity conditions. Above 42% RH, there are two low temperature peaks, the lowest temperature peak being attributed to adsorbed and bulk pore water. The second group represents specimens equilibrated at humidities varying from 57% to 85% RH. The results can be grouped in a similar manner for all the test water cement ratios.

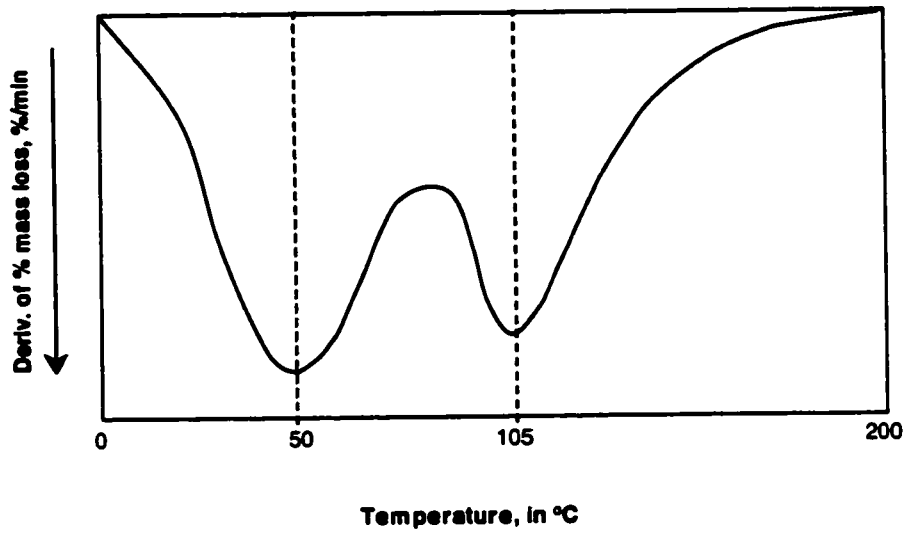

Figure 8.1: Ideal curve of derivative mass change of saturated hydrated cement paste

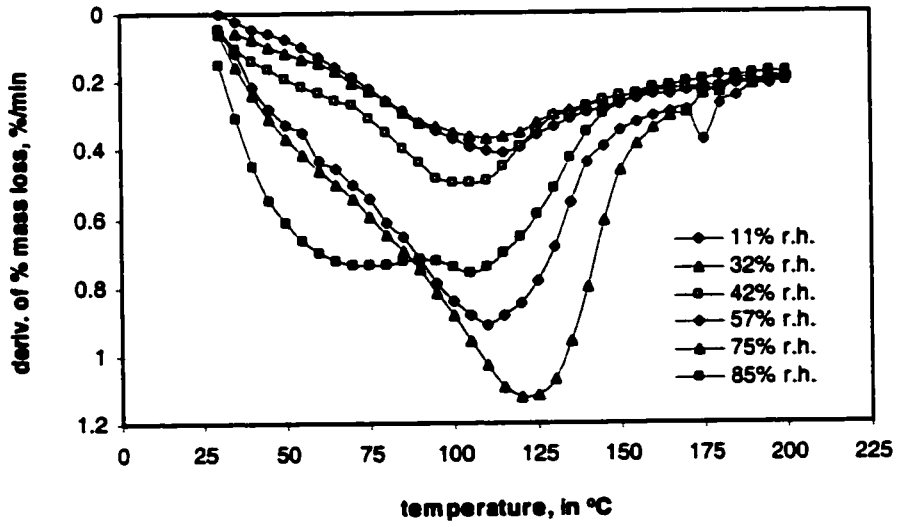

Figure 8.2(a): Differential TGA curves for cement paste (w/c=0.5) conditioned at various RH

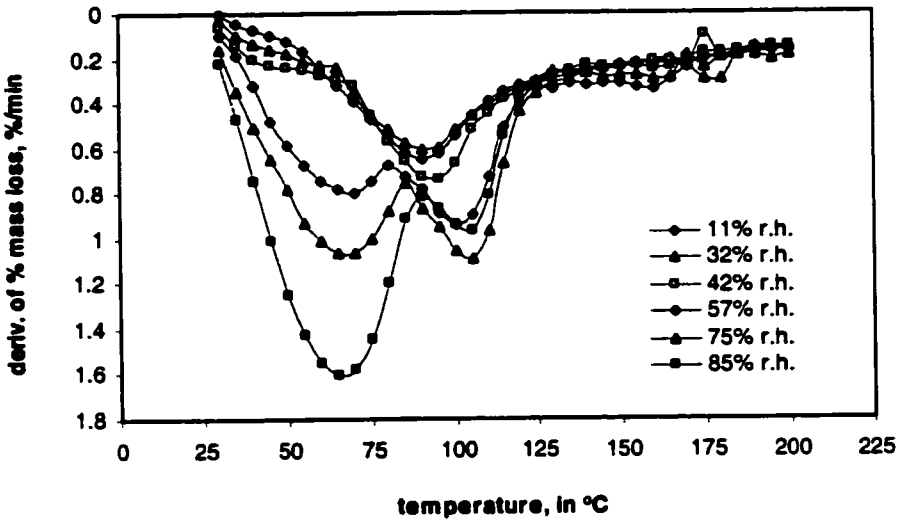

Figure 8.2(b): Differential TGA curves for cement paste (w/c=1.0) conditioned at various RH

Capillary water appears to be the more predominant type of water for w/c=1.0 cement paste only at 85% RH. Conversely, for w/c=0.5 cement paste, the interlayer water predominates at all conditioned humidities with the capillary water disappearing below 57% RH. It is also important to notice that at low water cement ratio, the removal of interlayer water requires a much higher temperature than that suggested by (Feldman and Ramachandran, 1971). This might be explained by the more refined pore network in such paste compared to w/c=1.0 cement paste. This refinement will then isolate some interlayer water, which might be reached only by increasing the necessary energy required for their removal. It is however difficult to explain why for this paste the 85% RH spectrum shows wide first and second peaks. Minimum drying to 85% RH however, appears to open up the C-S-H structure (facilitating intercalation) prior to collapse of further drying.

The 100% RH condition (Figure 8.3) yields results that are similar in character and magnitude to those for specimens conditioned at 11% and 32% RH. The 100% RH spectra show that while the first peak of the w/c=0.5 cement paste appears around 50°C, it takes much more time and thus higher temperature for the appearance of the same peak in case of the pastes with w/c=0.8 and 1.0. However, the capillary water in the latter's is very important and tend to overlap the second peak appearing at about 105°C. This second peak can be well observed in the w/c=0.5 spectrum and indicates that a much higher temperature is need to remove the interlayer water associated. It

is noted that a shoulder in the curve occurs at about the same temperature for the w/c=0.8 and 1.0 specimens. This peak is real as it can be reproduced and does not appear in the baseline curve for the reference material.

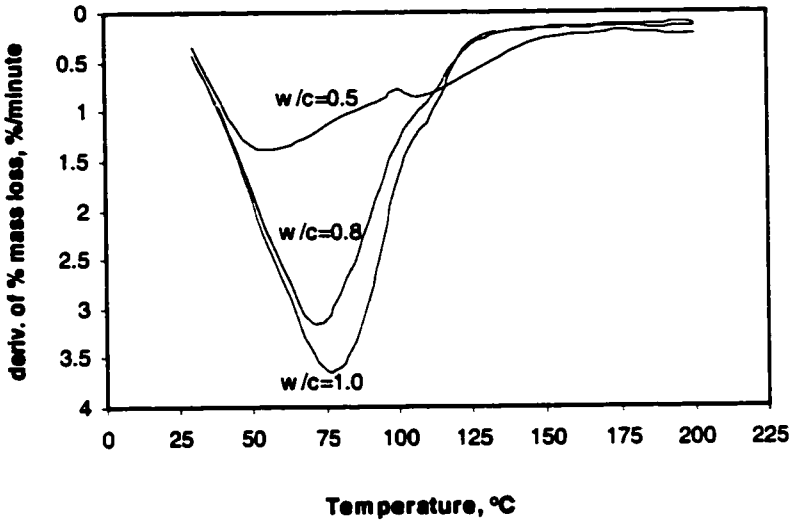

Figure 8.3: Differential TGA curves for cement paste (w/c=0.5, 0.8, and 1.0) conditioned at 100% RH

8.2.1.2 Organic solvent immersion

a) Hydrated tricalcium silicate paste

The saturated samples of hydrated C_3S paste were all dried at 11% relative humidity for 30 days in a desiccator and then re-saturated in lime saturated de-aired distilled water for 14 days. This is referred to as the second-saturation state. The desiccator was placed under vacuum to prevent carbonation. Before drying to 11% RH followed by re-saturation, the degrees of hydration were determined at 28 and 56 days using the DTA and TGA results. The 28 days sample was found to be 74% hydrated while that of 56 days was 85% hydrated. The effect of methanol and isopropanol immersion upon the mass change characteristics of hardened C_3S paste from the second saturation state is discussed in Section 8.2.4.5.

The differential of the percentage mass change versus time was determined from the TG analysis at different degrees of hydration to assist in understanding the microstructural changes caused by the solvent treatment. Specimens were heated isothermally at 100°C prior to the analysis. Mass losses up to 400°C are associated with the C-S-H phase. It appears that at 28 days, methanol removes some of hydrate water associated with the C-S-H (Figure 8.4). The curve for the specimens hydrated for 28 days is substantially below that for the control specimen and the peak has shifted to about 250°C. Isopropanol exchange had only a slight effect on the C-S-H at both 28 days and 56 days (Figure 8.5) and support the observation drawn from length change that this solvent appears to have a minimum net effect on volume stability. Therefore, isopropanol appears to be appropriate for specimen preparation following with 24 hours vacuum drying prior to porosimetry measurements. Specimens immersed in alcohol at any degree of hydration contained a significant amount of CO_2. There was a 1.1% CO_2 content in both treated specimens at 28 days, and 3.4% and 2.4% CO_2 in methanol and isopropanol exchanged specimens respectively at 56 days. Almost no CO_2 was found in the untreated specimens. Taylor & Turner (1987) also reported that solvent treatment increased the CO_2 content of the tricalcium silicate paste.

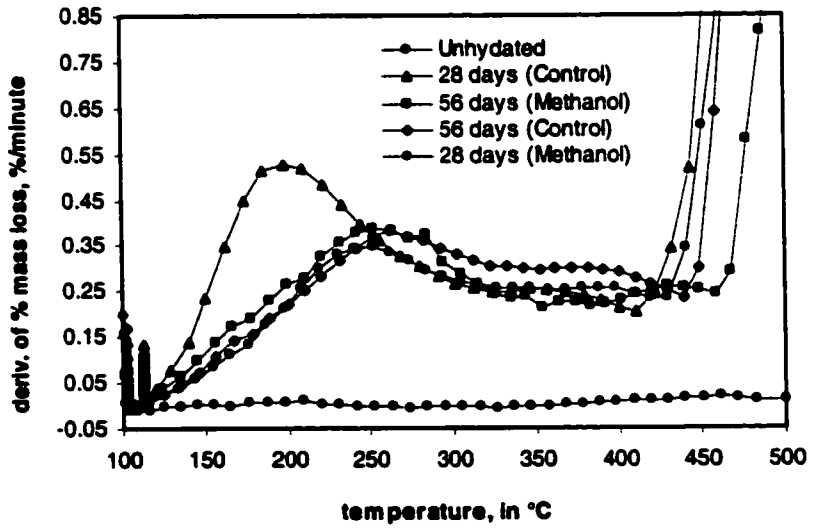

Figure 8.4: Effect of methanol treatment on the dehydration of C_3S paste (w/s=0.4)

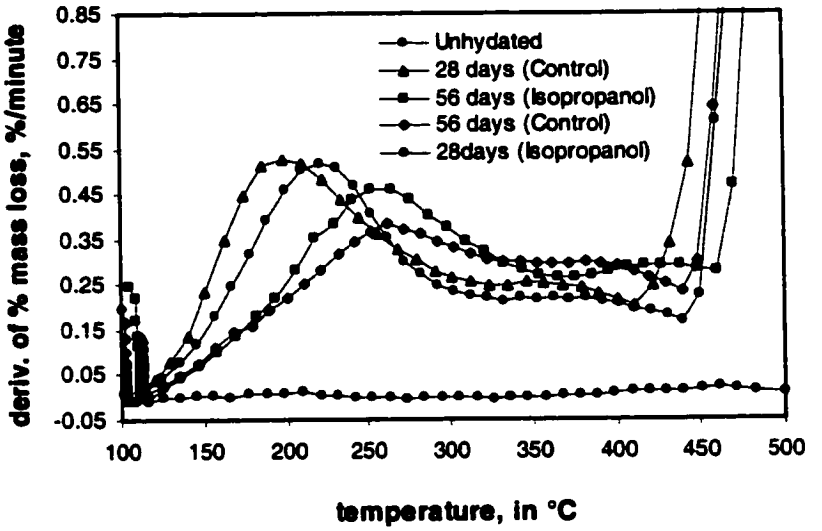

Figure 8.5: Effect of isopropanol treatment on the dehydration of C_3S paste (w/s=0.4)

b) Hydrated cement paste

The general characteristics of a differential thermogravimetric analysis (DTGA) curve for cement pastes obtained under equilibrium conditions were previously presented in Figure 8.1. The first endothermic peak is attributed to bulk water (this includes capillary and micropore) and the second peak to interlayer water (Feldman and Ramachandran, 1971). The results of TGA carried out on re-saturated specimens (in addition to reference specimens, saturated or equilibrated to 42% RH) after the treatment regimes describe in Table 8.1 are presented in Figure 8.6 in terms of the derivative of the mass loss versus time (expressed in %/minute) plotted against temperature. The methanol exchange curve is similar to the water saturated case in the temperature region above 75°C suggesting that after re-saturation water enters both the pores and interlayer space. Capillary water appears to be the more predominant type of water with methanol treatment. The reference curve for paste dried at 42% RH has a more pronounced peak at 105°C suggesting that it contains a large amount of interlayer water. The water saturated reference has both peaks. The other re-saturation curves all have (on close examination) evidence of more than one peak and exhibit a broad continuous response over entire temperature range. The second peak is

significantly broader and occurs at a much lower temperature suggesting that the structure has been altered and it is a much slower process to remove the interlayer water even though the removal starts at a lower temperature.

Table 8.1: Summary of the sample pre-treatment regimes

Initial State	Final Test State
Reference	Saturated (first state)
D-dried	Re-saturated (second state)
Vacuum dried at 37°C	Re-saturated
Dried at 42% RH.	Re-saturated
Saturated	D-dried
Saturated	Vacuum-dried at 37°C for 24 h
Methanol immersion	Vacuum-dried at 37°C for 24 h
Isopropanol immersion	Vacuum-dried at 37°C for 24 h

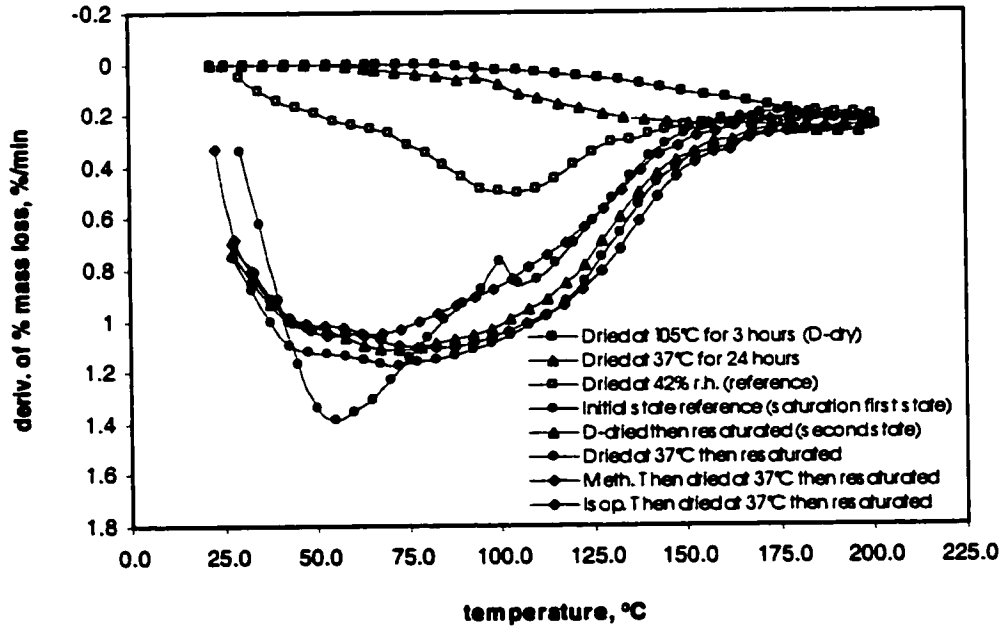

Figure 8.6: Derivative mass change of hydrated cement paste (w/c=0.5) from drying or re-saturation with pore solution subsequent to different drying pre-treatments

It is suggested that during the drying to 42% RH, part of interlayer water diffuses from small to coarser space within the specimen. This view is supported by the fact that the second peak of the

saturated (first state) sample which is at about 105°C significantly decreases during the drying process and does not reappear after re-saturation with pore solution. This suggests that micropores cannot be totally refilled after re-saturation under vacuum. D-drying, drying at 37°C under vacuum for 24 hours or drying at 37°C after isopropanol exchange all followed by re-saturation with pore solution appear to affect considerably the microstructure of the specimen by increasing the temperature required for the removal of water in the micro-spaces. An exception appears to be drying at 37°C after methanol exchange followed by re-saturation with pore solution which results in a slight modification of the micropore system, as the corresponding DTGA curve around 105°C has a shape similar to that of the original specimen (saturated). The use of organic solvents to remove water from the specimen results in a slight reduction of the total porosity as will be shown in the next section. The methanol exchange prior to drying produces a larger percentage of micropores than does the isopropanol exchange.

The effect of solvent exchange of hardened cement paste (w/c=0.5 and 1.0) conditioned up to the equilibrium at 42% relative humidity was also investigated. During the whole TGA monitoring process, the humidity chamber was kept at 42% RH. The derivative mass change versus time plotted against the temperature illustrates that for each solvent tested the general trend does not depend on the water cement ratio (Figure 8.7). The curves except that of DMSO exchange, present two peaks at lower temperature, one at 35-40°C and the other at 105°C. The first peak might be associated to the dynamic removal of solvent in capillary pores while the second might be associated to the dynamic removal of water and/or solvent entering the interlayer space during the exchange process. It can be observed, however, that the peak which constitutes the interlayer water mostly present in hydrated cement paste conditioned at 42% RH, disappears after methanol exchange process at all water cement ratios. Either the isopropanol or acetone exchange process seem to reduce the halo with isopropanol reducing it much more than acetone. The small size of methanol molecules may explain its total exchange with interlayer water and its polar nature may explain why acetone even with the same density (0.791) will not diffuse through the interlayer space. At high water cement ratio (w/c=1.0), isopropanol having a density less than that of methanol (0.785) seems to diffuse through the interlayer space given the fact that after the exchange is completed the second peak disappeared.

The DMSO has a density 1.101. The second peak associated with the interlayer space remains. Therefore, the removal of DMSO during thermogravimetric experiment is delayed. This may explain the gradual removal of both entrapped interlayer water and the DMSO as seen in Figure 8.7(a) with the first peak taking place at 90°C and the second at 110°C. These peaks merge to form a single peak at water cement ratio of 1.0 and its characteristic temperature shift to 105°C as

shown in Figure 8.7(b). The curve of samples conditioned up to the equilibrium at 42% RH is also presented in the figure for clarification.

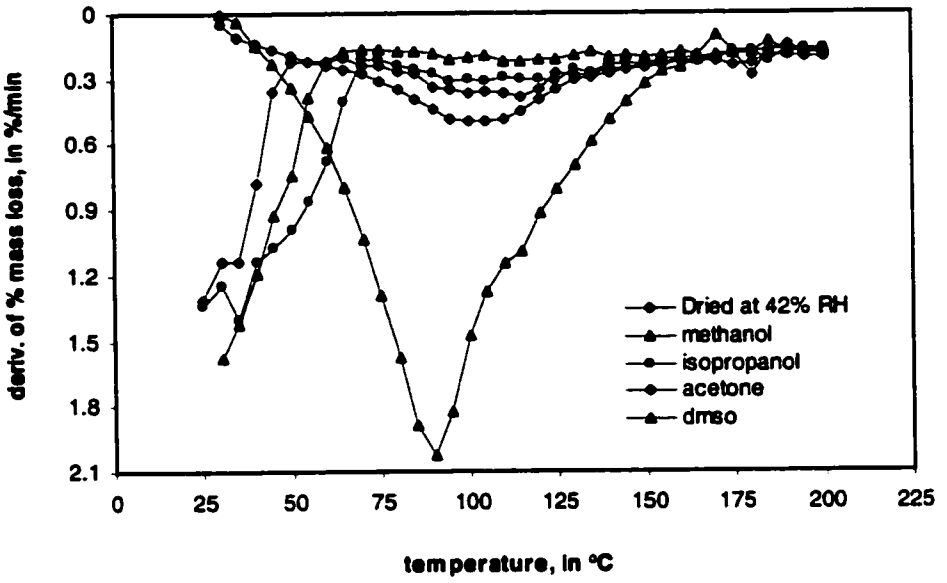

Figure 8.7(a): Solvent exchange of hydrated cement paste (w/c=0.5) following conditioning at 42% relative humidity

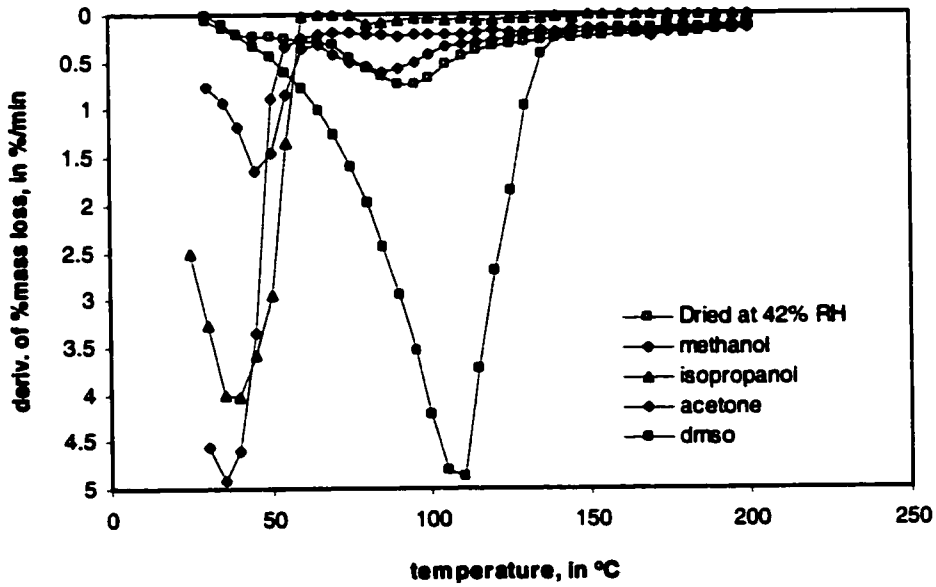

Figure 8.7(b): Solvent exchange of hydrated cement paste (w/c=1.0) following conditioning at 42% relative humidity

As already shown in the case of samples conditioned at 42% RH prior to solvent exchange, the 75% RH conditioned samples (w/c=1.0) present a decreasing of the peaks location. At 75% RH, the first peak is at about 60°C and the second peak appears at 105°C. It can be observed from Figure 8.8 that after the methanol exchange process, the methanol in capillary pores and interlayer spaces can be removed after heating to about 60°C. After isopropanol or acetone exchange process, higher temperature (~110°C) is needed to remove solvent and/or water remaining in the interlayer space. The DMSO exchange will in contrast merge the first and second peaks in order to form a single one at about 105°C. It is very important to note that the diffusion of isopropanol into the interlayer space seems to be confirmed at 75% RH given the reduction of the temperature necessary to removed the solvent and/or the remaining interlayer water.

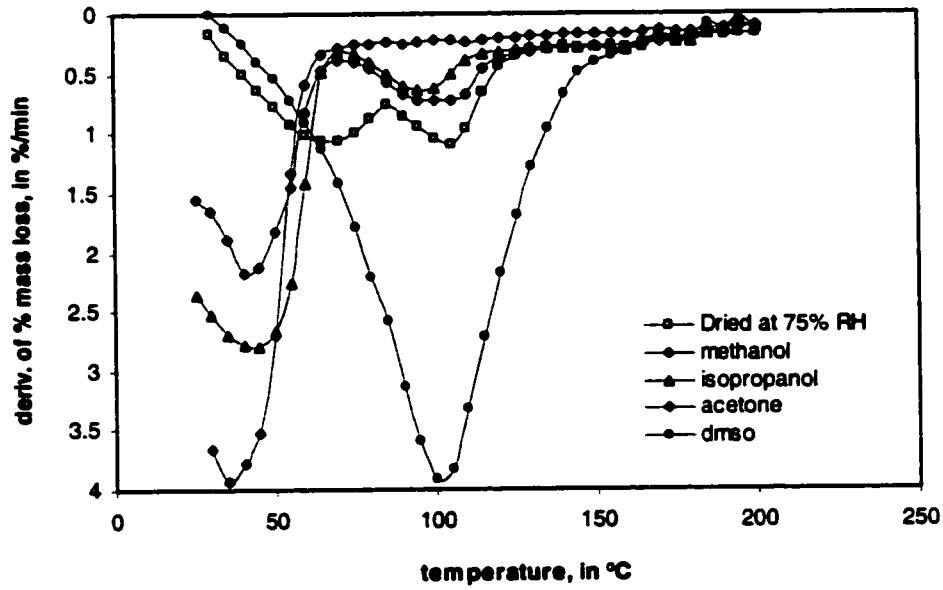

Figure 8.8: Solvent exchange of hydrated cement paste (w/c=1.0) following conditioning at 75% relative humidity

After vacuum drying of all the sampies previously mentioned at 37°C for 24 hours only the w/c=1.0 immersed in DMSO show a relatively large derivative curves shift from the others at about 130°C.

8.2.2 *Pore size distribution*

The pore size distribution of CH compacts following compaction pressures varying from 136 to 1360 MPa, hydrated triclinic calcium silicate (w/s=0.4) and hydrated cement paste (w/c=0.35, 0.5 and 1.0) was performed using a Quantachrome Autoscan-33 instrument mercury porosimetry at pressures up to 212 MPa.

8.2.2.1 CH compacts

The pore size distribution curves for CH compacts are presented in Figure 8.9. Pore size ranges vary from 0.200 to 0.005 μm and 0.020 to 0.005 μm for compacts prepared at 136 MPa and 1360 MPa, respectively. Total porosity ranges from about 31% to 7.5% decreasing with the increase of the compaction pressure.

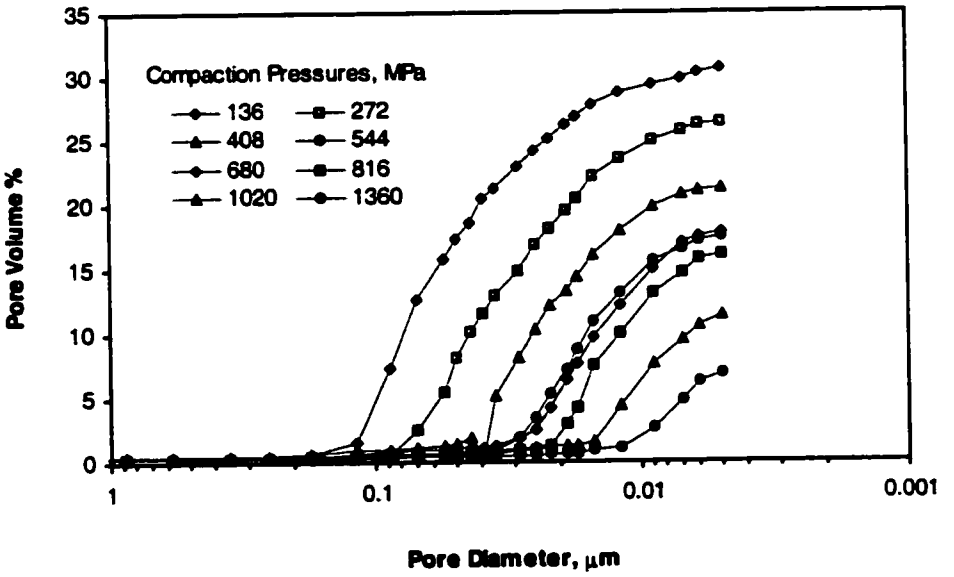

Figure 8.9: Pore size distribution curves of $Ca(OH)_2$ specimens compacted at different pressures

8.2.2.2 Hydrated triclinic calcium silicate (C_3S)

The pore size distribution performed on D-dried untreated and D-dried treated specimens is presented in Figure 8.10. Despite the alcohol treatment, the total porosity of the hydrated C_3S paste almost remains the same. However, depending on the pore ranges, alcohol exchange may or may not affect the pore structure. The untreated specimens gave the greatest volume of pores in the large pore regions, 0.3 to 1μm. Methanol treatment resulted in a reduction of pore volume for almost all size ranges except 0.1 to 0.3μm.

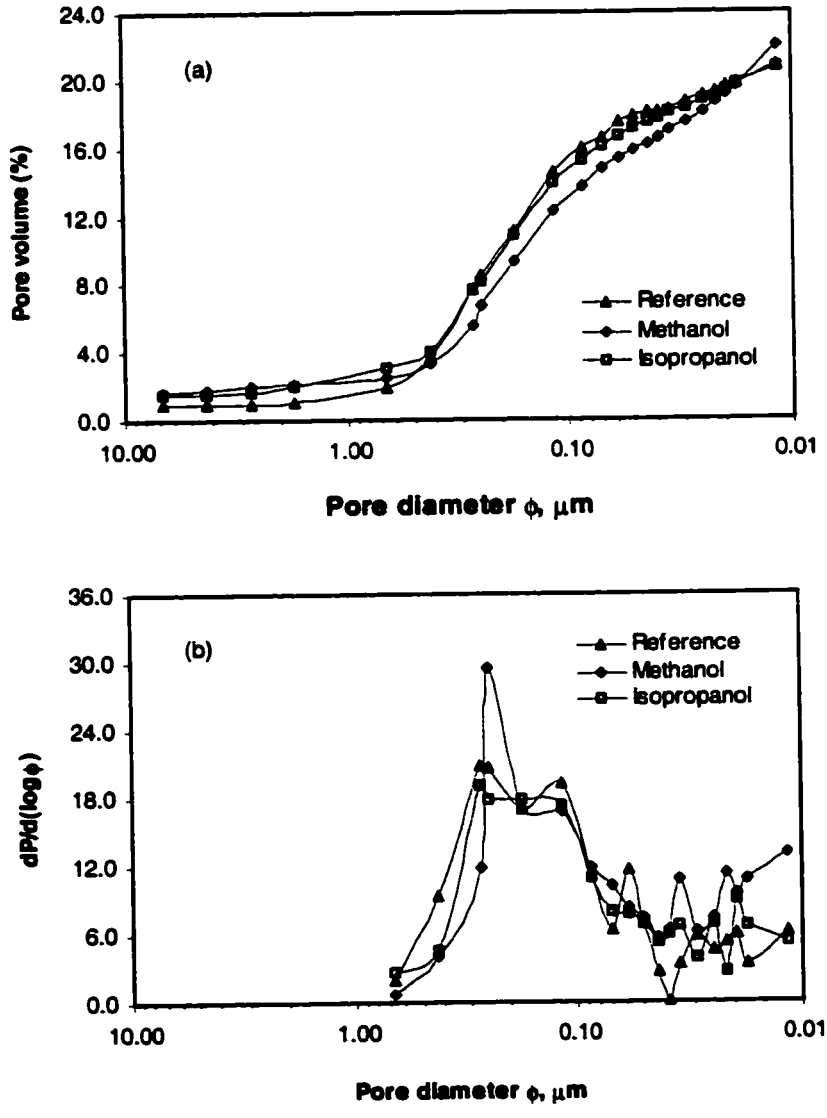

Figure 8.10: Cumulative (a) and differential (b) pore size distributions of D-dried C_3S paste 74% hydrated after solvent exchange

8.2.2.3 Hydrated cement pastes

The pore size distribution curves of hydrated cement pastes (w/c=0.35, 0.5, and 1.0) are presented in Figure 8.11. The pore size ranges vary from 0.003 to 0.1 μm, 0.003 to 8 μm, and 0.003 to 12 μm for water cement ratios of 0.35, 0.5, and 1.0 respectively. The total porosity ranges from 20% to 58% with the w/c=0.35 cement paste having the lowest and that of w/c=1.0 paste the greatest and almost the double of the w/c=0.5 paste.

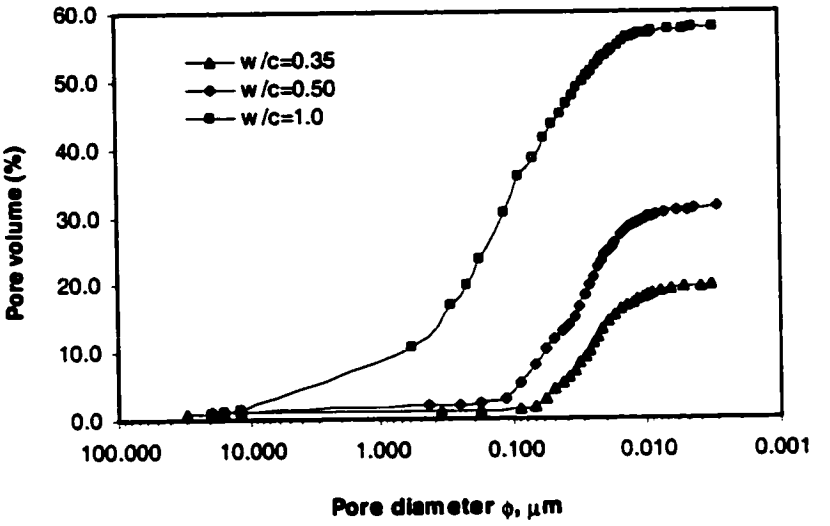

Figure 8.11: Pore size distribution of hydrated cement paste at different water cement ratios

The mercury intrusion measurements of hydrated cement paste (w/c=0.5) subjected to different drying pre-treatment regimes have also been performed. Figure 8.12 shows that the use of organic solvents to remove water from the specimen results in a slight reduction of the total porosity. The methanol exchange prior to drying produces a larger percentage of micropores than does the isopropanol exchange. Vacuum drying at 37°C for 24 hours on close examination seems to affect the hardened structure of cement paste at a lesser extend than those drying at 105°C for 3 hours (D-drying) given its smaller cumulative porosity. It can also be noticed the important amount of pore size between 0.02 μm and 0.09 μm. At all pre-treatment conditions, the pore size ranges from 0.003 to 8 μm.

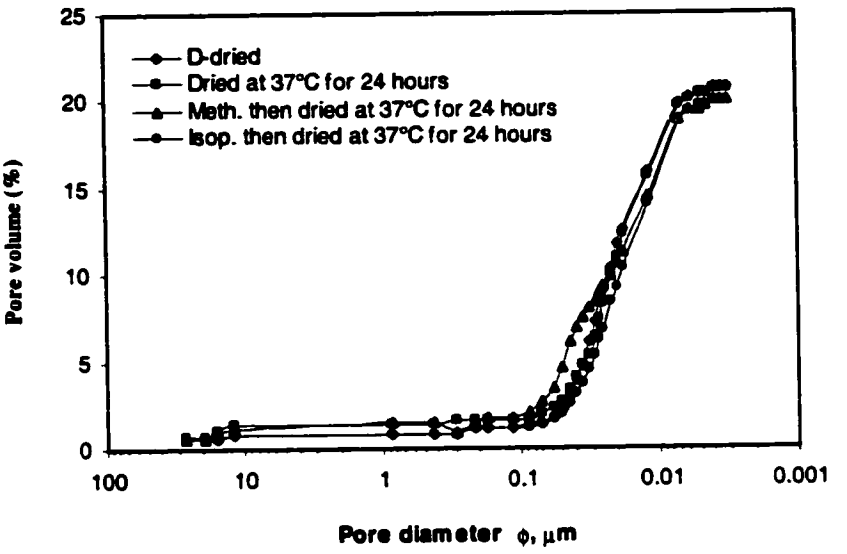

Figure 8.12: Pore size distribution of hydrated cement paste (w/c=0.5) after different drying pre-treatment regimes

8.2.3 Surface area

8.2.3.1 Hydrated triclinic calcium silicate (C_3S)

Surface area measurements were performed on hydrated triclinic silicate (w/s=0.4) at 74% degree of hydration D-dried from 5% RH, 42% RH, 75% RH, and saturated surface dried conditions. From the previously mentioned drying conditions, some specimens were immersed in methanol and isopropanol then D-dried prior to surface area measurements. The results are presented in Figure 8.13 as a function of drying condition and solvent immersion.

The drying at 5% RH up to the equilibrium condition may happen at a very high rate that severely damage the microstructure of the C_3S paste specimen and leading to the low values of the surface area observed at all drying and pre-treatment conditions. At 42% RH, methanol and isopropanol will reduce the surface area compared to that of the untreated samples with methanol treatment effect being less significant. For the relative humidities greater than 75% RH, the methanol treatment prior to D-drying seems to preserve the microstructure of the hydrated C_3S paste as it

can be explained by the higher values of surface area observed at 75% and 100% RH compared to that of the control samples. Even at 75% RH, isopropanol treatment may slightly affect the microstructure of the C_3S paste while preserving it to a lesser extend than methanol at 100% RH.

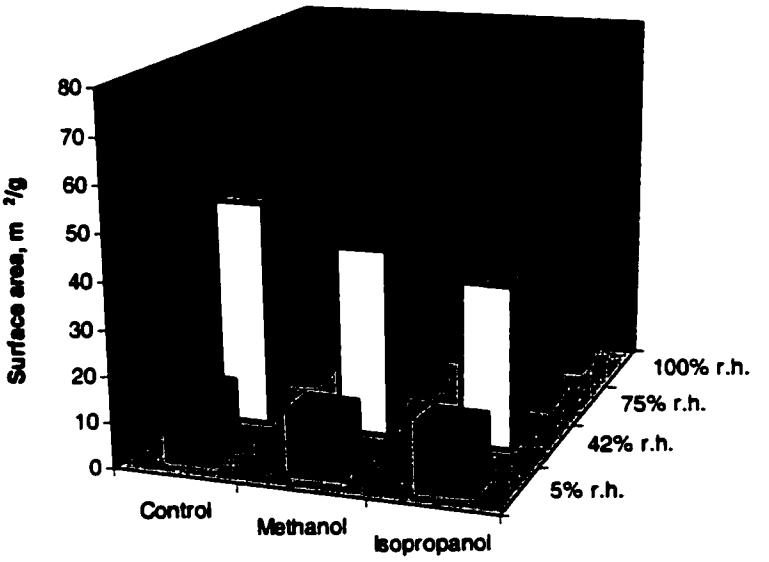

Figure 8.13: Surface area of 74% hydrated C_3S D-dried after immersion in solvent following different drying conditions

8.2.3.2 Hydrated cement pastes

Hydrated cement pastes (w/c=0.5, 0.8, and 1.0) were also subjected to surface area measurements after D-drying (Figure 8.14). The results show that when D-dried from 75% RH or saturated surface dried, the surface area of hydrated cement paste increased with an increase of water cement ratio. However, at 100% RH, the relation seems totally different from water cement ratio of 0.8. For hydrated cement paste having a water cement ratio of 0.5, re-saturation with synthetic pore solution following a second drying negatively affects the surface area at all pre-treatment conditions as can be seen in Figure 8.15. The figure shows that D-dried (untreated) paste as opposed to drying at 37°C for 24 hours (control) significantly affects the microstructure of hardened cement paste as the change in the value of surface area can increase by about 20 m^2/g. As shown previously on hydrated C_3S, methanol pre-treatment preserves the microstructure of the cement paste as to a lesser extend does the isopropanol pre-treatment.

The reduction in surface area observed after re-saturation of D-dried hydrated cement paste with synthetic pore solution may be explained by the collapse of some capillary pores which on second drying will create a network with coarser pores than that observed in first drying.

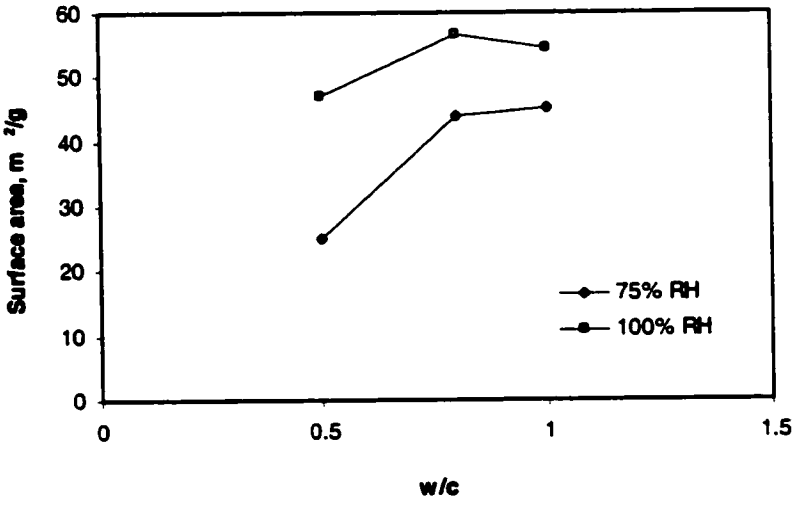

Figure 8.14: Surface area of hydrated cement paste (w/c=0.5, 0.8, and 1.0) D-dried following conditioning at 75% and 100% RH

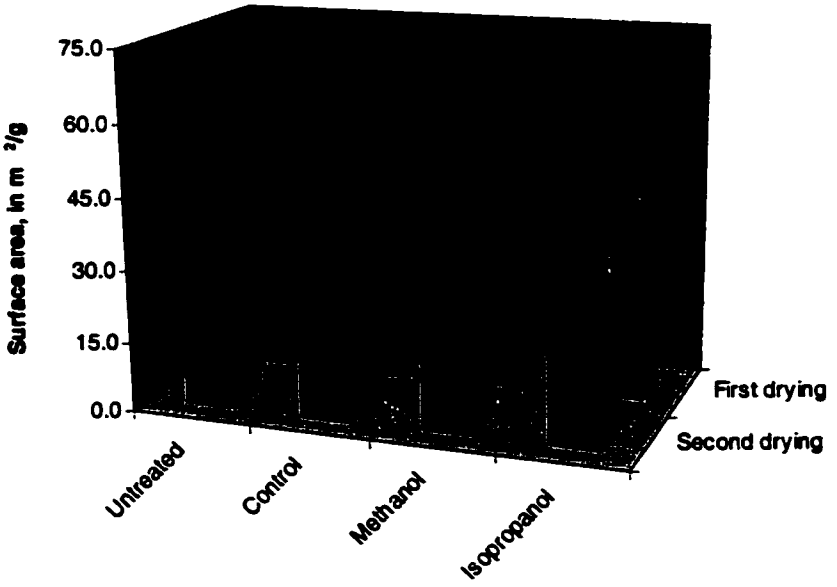

Figure 8.15: Surface area of hydrated cement paste (w/c=0.5) after several drying and pre-treatment regimes

8.2.4 Length and mass changes

8.2.4.1 CH compacts

The weight change versus time measurement of the CH compacts was obtained to facilitate interpretation of the length change information. Given the greater attention that methanol and isopropanol exchanges have received in the literature, results for partially saturated CH compacts pre-conditioned from 0% to 85% RH are presented. The weight change versus time curves all had the following general characteristics. The weight increased to a maximum within the first few minutes and then steadily decreased to a constant value after 2 hours. The initial increase in weight is due to the rapid ingress of solvent into empty pore space. The process of counter-diffusion is considered to begin at the time the maximum increase in weight is reached. Calculations to determine the relative amount of the solvent taken up by diffusion utilize the time at maximum weight increase as the starting point or zero.

At relatively low RH, the water into the CH compacts is not enough to assure a gradual diffusion of solvent. Therefore, from the starting point, which is the time at maximum weight increase, the curves are scattered. The ratio w_t/w_∞ defined the amount of solvent diffused at time t or w_t to the amount when the weight reaches a constant value w_∞. Figure 8.16 is a plot of the ratio w_t/w_∞ versus the square root of time for CH compacts pre-conditioned at 85% RH and immersed in isopropanol (I85) and methanol (M85). Compacts designated CH20, CH60, and CH100 were prepared at 20, 60, and 100 kilo-lbs., corresponding to pressures of 136, 272, and 408 MPa respectively. The curves have similar shape to that of carbon spectra of ethanol in the cement paste pore system (Hansen and Gran, 1996). It is apparent that methanol diffuses much more rapidly than isopropanol into the compacts during the exchange process. The rate of exchange is dependent on compaction pressure and is in the following order for both solvents: CH20 > CH60 > CH100. Maximum rates of exchange for methanol were determined to 0.192, 0.180, and 0.090 g/h and for isopropanol, 0.072, 0.042, and 0.018 g/h. Methanol, in general, has a significantly greater exchange rate than all the solvents studied.

The length change results for the compacted CH systems prepared at the dry condition and immersed in various solvents are presented in Figures 8.17 to 8.21. The length change results for the compacted CH systems pre-conditioned at various moisture contents are presented for each adsorbate separately in Figures 8.22 to 8.26.

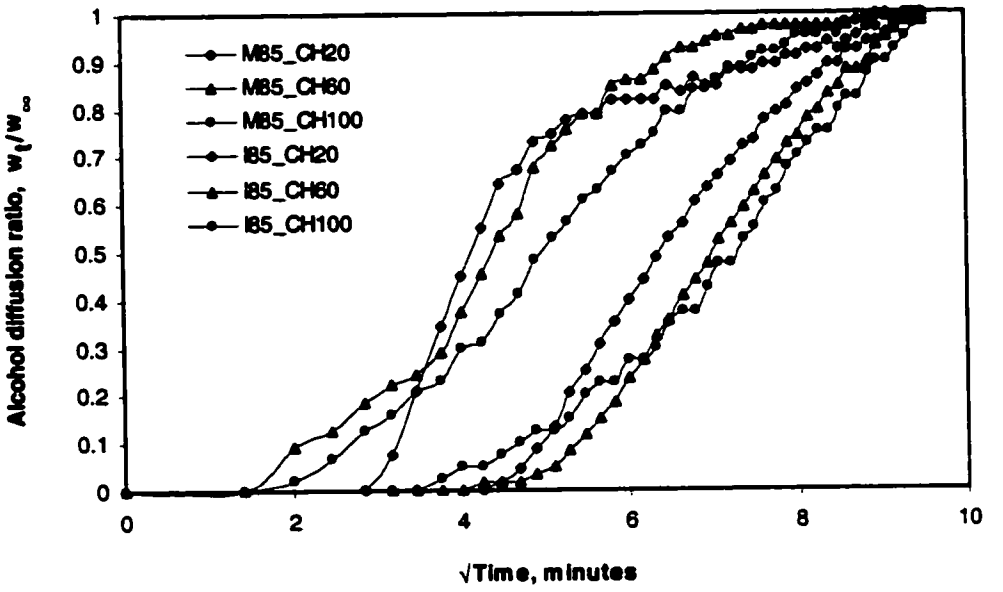

Figure 8.16: Ratio w_t/w_∞ versus square root time after isopropanol (I85) and methanol (M85) exchanges of CH samples pre-conditioned at 85% RH.

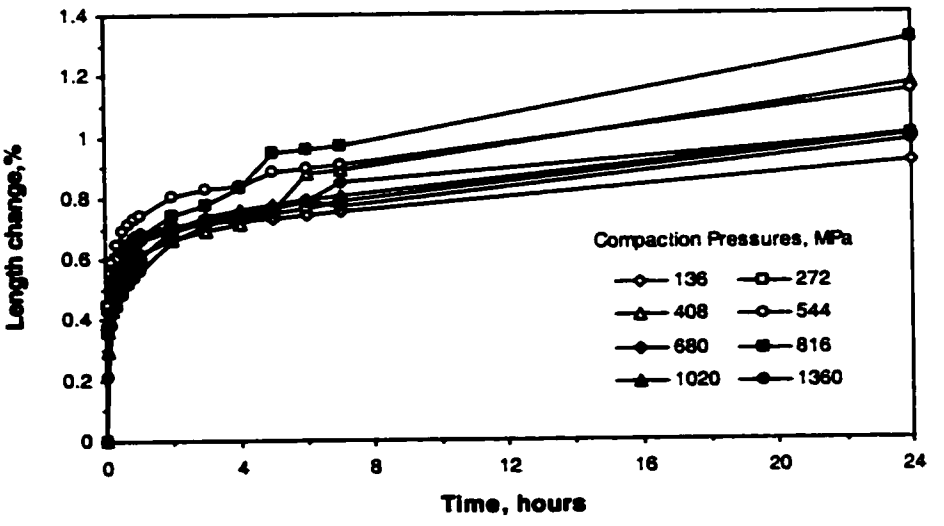

Figure 8.17: Length change of CH compacts pre-conditioned to 0% RH and immersed in water

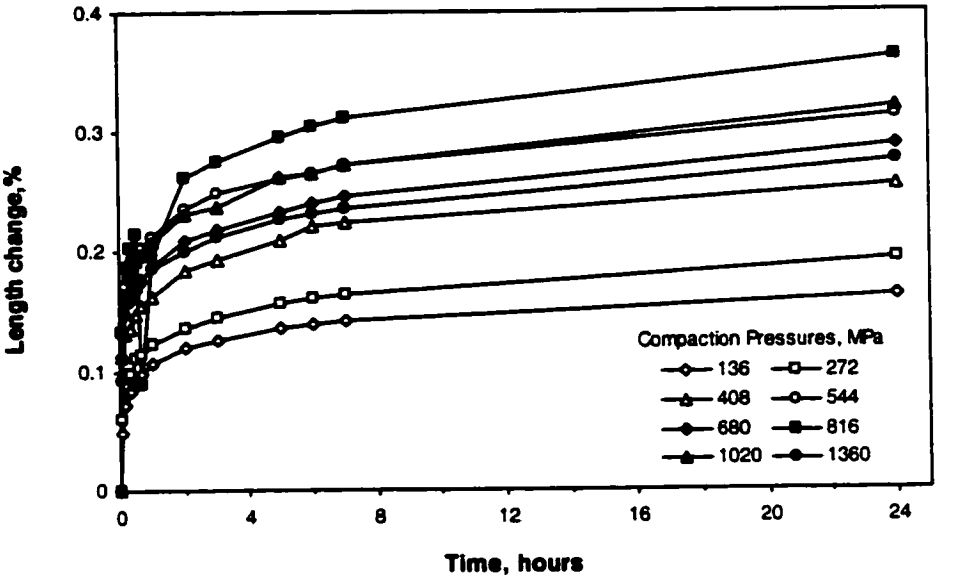

Figure 8.18: Length change of CH compacts pre-conditioned to 0% RH and immersed in methanol

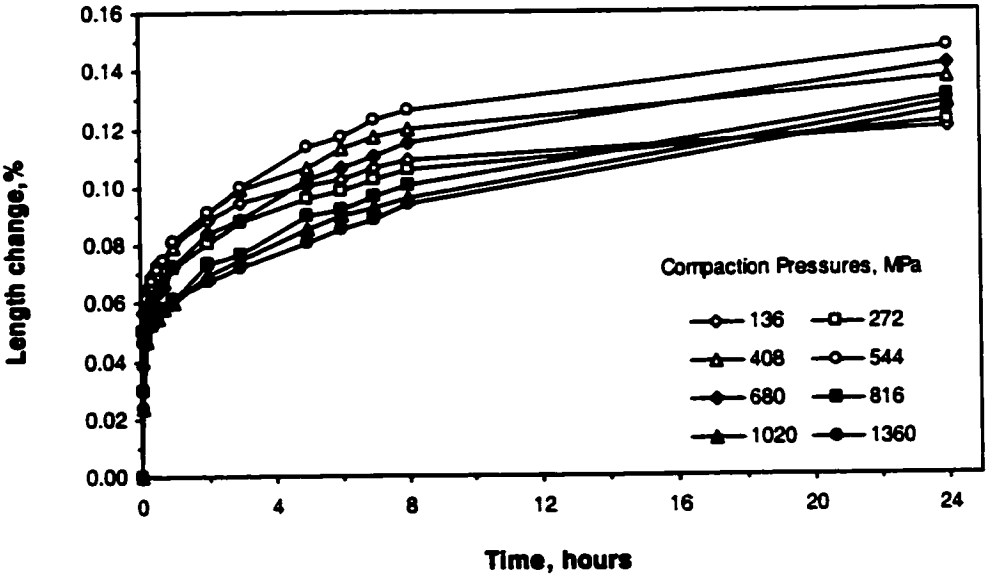

Figure 8.19: Length change of CH compacts pre-conditioned to 0% RH and immersed in isopropanol

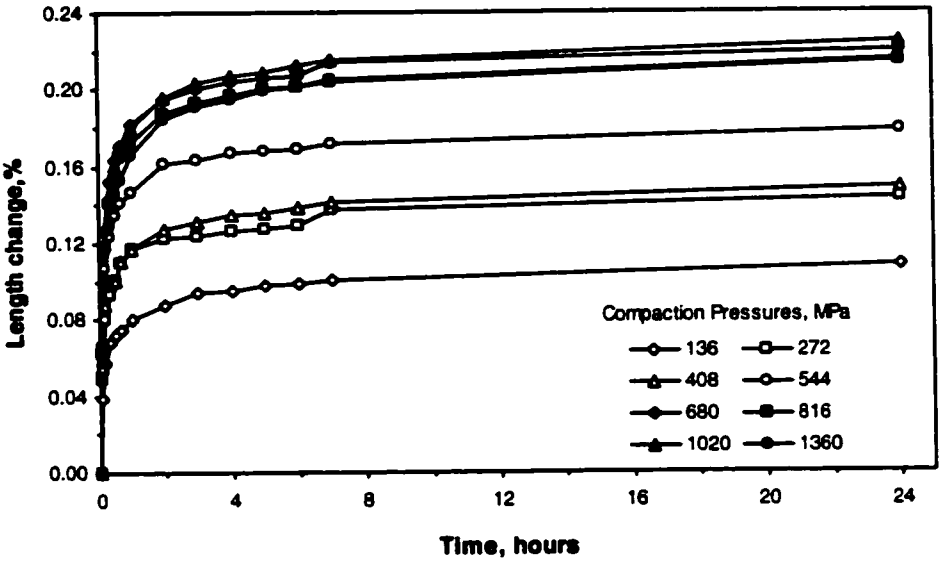

Figure 8.20: Length change of CH compacts pre-conditioned to 0% RH and immersed in acetone

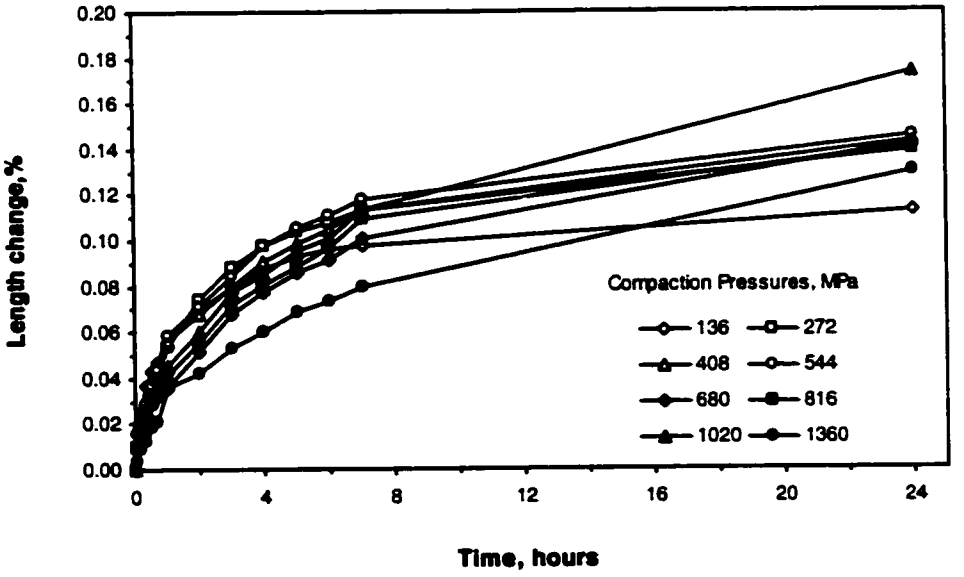

Figure 8.21: Length change of CH compacts pre-conditioned to 0% RH and immersed in benzene

a) Dry CH Compacts

All compacts pre-conditioned at 0% RH expanded when immersed in any of the test solvents (Figures 8.17 to 8.21). Total expansion was generally in the following order: water > methanol > acetone > benzene > isopropanol. Compacts prepared at the lowest pressure (136 MPa) expanded the least in all solvents. Compacts prepared at the highest pressure (1360 MPa) did not give maximum expansion. The mechanisms of expansion are discussed in detail in the following sections for each solvent.

b) Water

The CH compacts prepared at pressures ranging from 136 to 1360 MPa were pre-conditioned at water contents ranging from 0% to 9.6%. Expansion subsequent to immersion increased with time at all levels of moisture content and compaction pressure (Figure 8.22). There was no clear dependence of total expansion on compaction pressure.

Expansion is attributed to the Bangham effect (at least up to a weight change of 0.70%) and solution/precipitation at points of contact involving diffusion and re-crystallization to other sites. A dual mechanism is consistent with the observations of Feldman (1968) and Litvan (1980, 1984). The Bangham effect is likely operative at least up to a weight change of 0.70% and can account for length change up to 0.10%. Ramachandran and Feldman (1967) demonstrated this for CH compacts. They obtained a linear Bangham relation for length change on adsorption in accordance with equation 4.6. Larger total expansion at higher pressures is likely due to greater strain energy release on dissolution in spite of the lower surface area available to the adsorbate. The possible existence of holes in the structure at higher water content may account for reduced expansion due to the counter-effect of van der Waals forces or bridging of molecules across micro-spaces. There would also be a dilution effect as the amount of bulk water (per unit mass of solid) would be greater in compacts prepared at high pressure for the same percentage of adsorbate.

c) Methanol

The CH compacts undergo expansion (at all water contents and compaction pressures) during solvent replacement with methanol (Figure 8.23). Unlike the case for isopropanol, there is no contraction observed with time. It is noted that water-saturated paste specimens expand on

solvent exchange with methanol up to about 0.035%, whereas isopropanol solvent replaces pastes shrink by up to 0.08%. The expansion isotherm for a methanol adsorbate/cement paste adsorbent system will be presented in Section 8.2.4.6, showing that length change due to adsorption of degassed cement paste systems can alone account for expansions of up to 0.10% at saturation (Feldman, 1968). The total expansion of the CH compact in the dry state ranges from 0.12% to 0.36% (Figure 8.23A). It is suggested that this is due to a combination of the Bangham effect and some type of chemical interaction. Several authors have presented evidence that some form of chemical interaction occurs between methanol and the constituents of hydrated cement systems.

The compacted CH systems pre-conditioned at various water contents all exhibit reduced expansion (i.e., about 50% of that in the dry state) (Figures 8.23B and 8.23C). It would appear that the expansion nature of the chemical interaction (as proposed by the Litvan) dominates any tendency for contraction due to solvent replacement action or changes in surface free energy due to replacement of water with solvent molecules at the solid surface.

Low-pressure compacts exhibit the least expansion in the dry state and up to water content of about 1.52%. At higher water contents the high-pressure compacts have the least expansion. It is possible that the solvation effects at high water contents are more pronounced in compacts prepared at low pressures accelerating and increasing interaction with methanol. Strain energy release due to chemical interaction with methanol may be the dominant mechanism at lower water contents. This can account for higher expansion at higher compaction pressures.

d) Isopropanol

The expansion of the CH compacts vacuum dried prior to exposure to isopropanol increases with time up to about 0.15% (Figure 8.24A). The lowest expansion generally occurs at lowest pressures, i.e., 136 and 272 MPa. Most of the expansion is probably due to the Bangham effect, as a value of about 0.12% would be expected. Calcium hydroxide is insoluble in isopropanol and a dissolution/precipitation mechanism for length change is not considered likely.

The length change behavior for CH compacts pre-conditioned to various water contents prior to immersion in isopropanol is markedly different (Figures 8.24B and 8.24C). In general, there is an immediate expansion (up to 0.04%) followed by a rapid progressive contraction. The immediate expansion may be due to some surface interaction between isopropanol and CH, as water at the solid surfaces is replaced with the solvent. This cannot be explained by the Bangham effect, for an immediate net shrinkage would be expected as the surface free energy balance (Bangham effect) would favor a reduced length change for the reduced molar surface coverage when water

is replaced by isopropanol where the rate of removal exceeds the rate of replacement. These observations are consistent with the results of Litvan (1980) for cement paste immersed in ethylene glycol and those of Hughes (1988) for paste samples immersed in isopropanol and ethanol. This was also observed in hydrated cement paste where water is removed from the interlayer regions/micro-pores and not replaced by solvent (Feldman, 1987). The cement paste system undergoes continuous contraction on exposure to isopropanol solvent consistent with the results of Feldman. No initial expansion, however, was observed. Any initial expansion of CH contained in the paste may be compensated by a net shrinkage of the paste.

The initial expansion is greater for the systems compacted at high pressure irrespective of the water content due to the pre-treatment. For high-pressure compacts there is significantly less surface water to be replaced by solvent; however, the strain energy release may exceed that of CH compacts prepared at low pressure.

e) Acetone

Acetone is highly soluble in water and reported to interact with the constituents of cement paste (Taylor and Turner, 1987). Expansion of CH compacts prepared in the dry state and immersed in acetone ranges from 0.08% to 0.20% (Figure 8.25A). It is likely due to a combination of the Bangham effect and chemical interaction with the surface. It is noted that there was a color change exhibited by the compacts (light to medium brown). The high-pressure compacts expanded the most, suggesting the interaction effects were sufficient to produce a larger strain energy release.

A significantly reduced expansion (by factor of 10) occurred at all pressures when the water content of the samples was about 0.50% (Figure 8.25B). This suggests that chemical interaction at the surface remains the dominant mechanism for expansion.

At higher water contents (Figure 8.25C), there is an initial immediate expansion followed by a progressive contraction similar to that observed for isopropanol and benzene exchange. The explanation of the length change behavior is also similar. The compaction pressure effects also have similarities to those observed for the isopropanol experiments.

f) Benzene

The behavior of the CH compacts immersed in benzene (a solvent only slightly soluble in water) exhibited some similarities and some differences to that observed in isopropanol. The general

character of the length change curves was either continuous expansion or immediate expansion followed by progressive contraction (Figure 8.26). The compacts that were vacuum dried expanded up to 0.12% when immersed in benzene. The length change is attributed primarily to the Bangham effect and is consistent with observations for the other solvents.

Compacts at a water content of about 0.5% also expanded continuously, unlike those immersed in methanol. The expansion was relatively small, ranging from 0.008% to 0.02%. The expansion suggests there may be some chemical interaction between benzene and the CH surface. The surface interaction would appear to continue at higher water contents as manifested by the immediate expansion in all cases. The contraction at higher water contents is possibly due to an increase in the rate of solvent replacement becoming a dominant influence. Unlike compacts immersed in isopropanol, the net length change is always positive.

The effect of compaction pressure is described as follows. There is generally less expansion at high pressures for CH compacts that were vacuum dried. There is less surface for the realization of the Bangham effect. In the presence of 0.50% water, the high pressures for CH compacts expand the most. This suggests that there is a larger release of strain energy due to CH solid/benzene interaction at higher pressures.

The initial expansions of the compacts observed at the highest water contents (5.1% to 10.5%) are followed by progressive contractions. The initial expansions and the subsequent contractions are greater at higher pressures. The greater contraction may be due to generation of van der Waals forces resulting from surface perturbation effects on the rapid removal of a smaller amount of adsorbate from a larger number of fine pores.

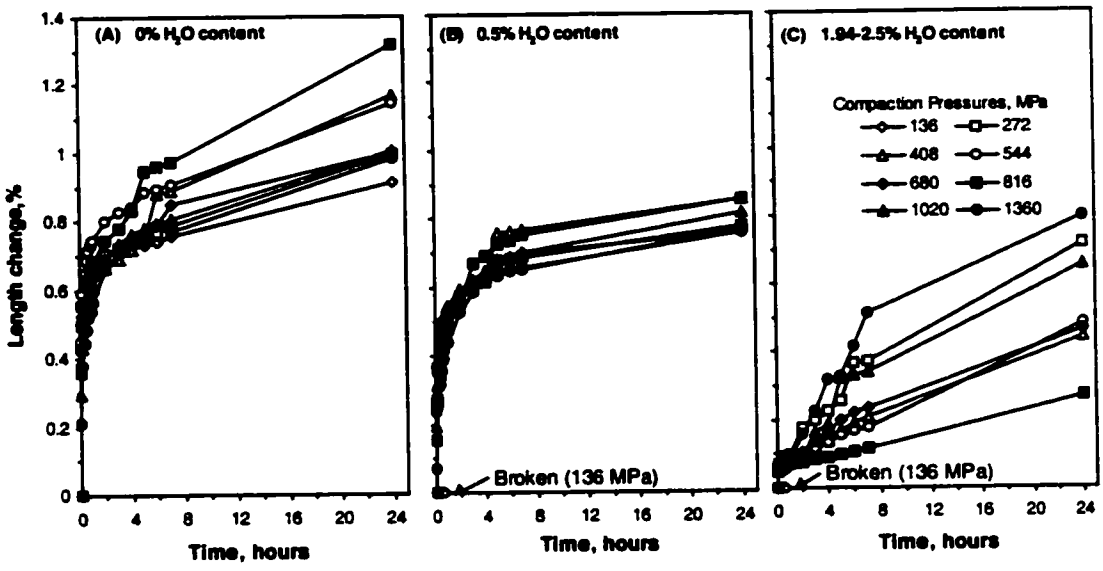

Figure 8.22: Length change of $Ca(OH)_2$ compacts of varying water content immersed in water

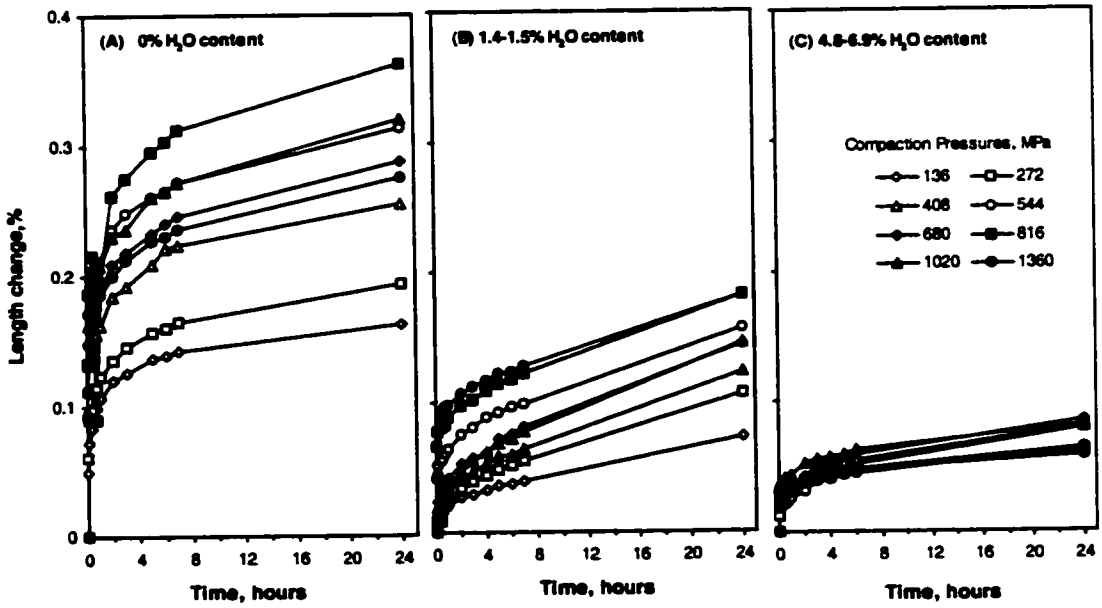

Figure 8.23: Length change of $Ca(OH)_2$ compacts of varying water content immersed in methanol

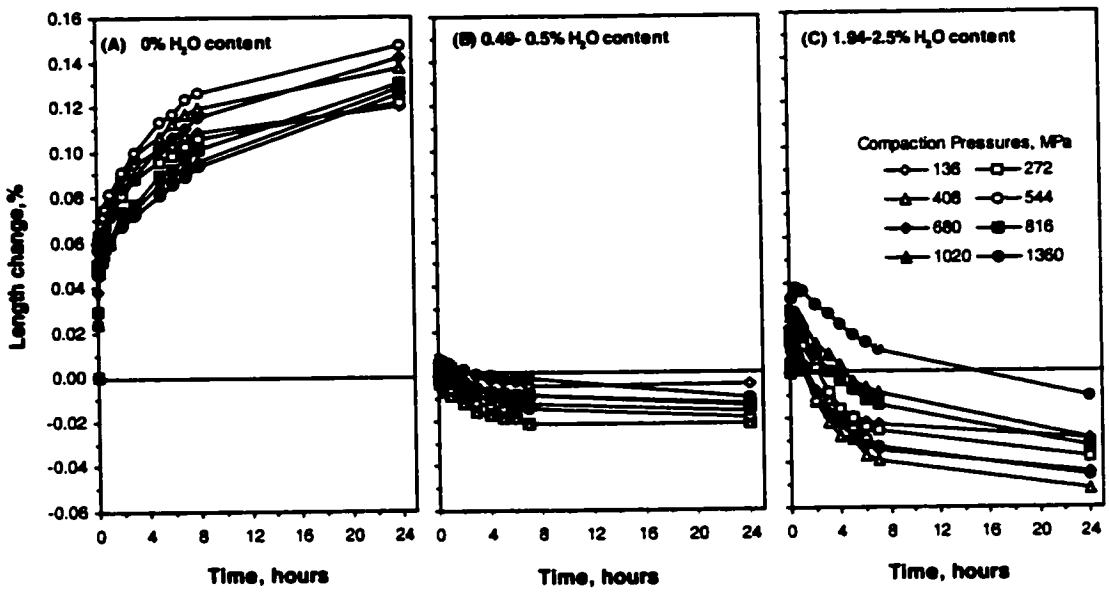

Figure 8.24: Length change of $Ca(OH)_2$ compacts of varying water content immersed in isopropanol

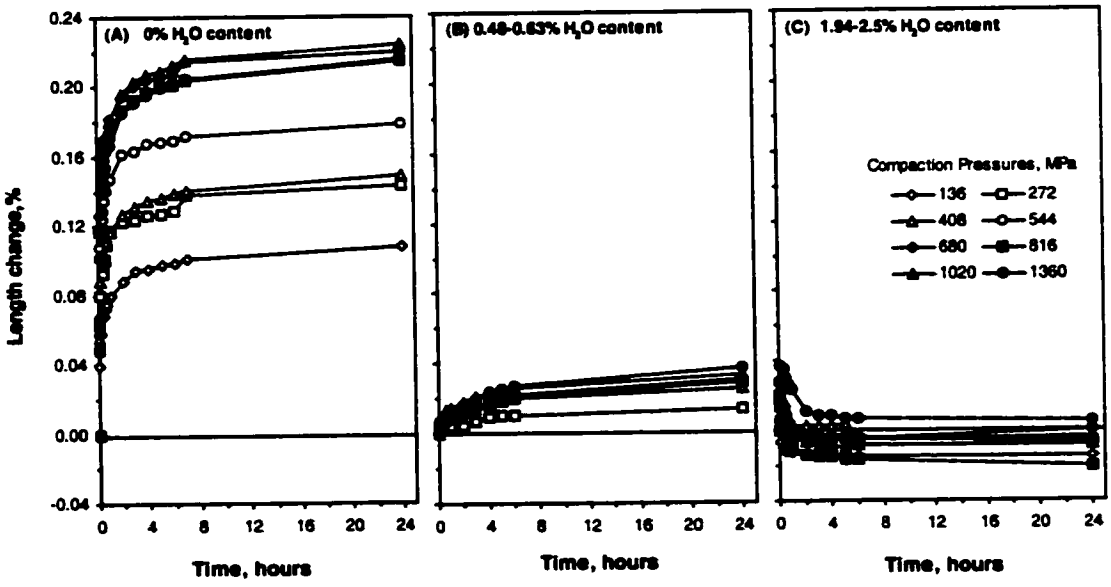

Figure 8.25: Length change of $Ca(OH)_2$ compacts of varying water content immersed in acetone

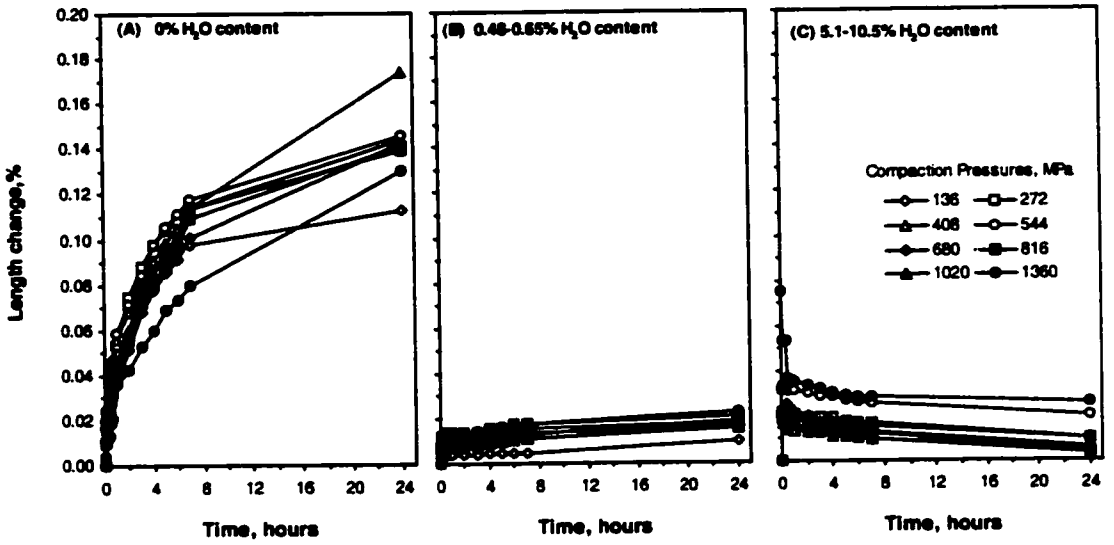

Figure 8.26: Length change of $Ca(OH)_2$ compacts of varying water content immersed in benzene

8.2.4.2 C-S-H

a) D-dry condition

Length change versus time curves for D-dried C-S-H (C/S=0.68, 0.87) immersed in the test solvents and lime-saturated water are presented in Figure 8.27. Large expansions (0.09% to 0.14%) were observed during the first hour of wetting with methanol and water. Expansion for the C/S=0.68 preparation exceeded the expansion for the C/S=0.87 preparation. It is suggested that intercalation of water and methanol is a primary cause of expansion. A secondary cause could be chemical interaction between the solvent and the C-S-H. Small expansions in the first few minutes were observed during the isopropanol exchange experiments followed by continuous contractions. Contractions were greater for the C/S=0.68 specimens reaching -0.15% at 24 hours. Continuous small contractions or expansions were also observed for the DMSO exchange. Contractions during either isopropanol or DMSO exchange could be due to adsorption of reaction products (assuming chemical interaction between the solvent and C-S-H) on unreacted C-S-H (Hughes, 1994).

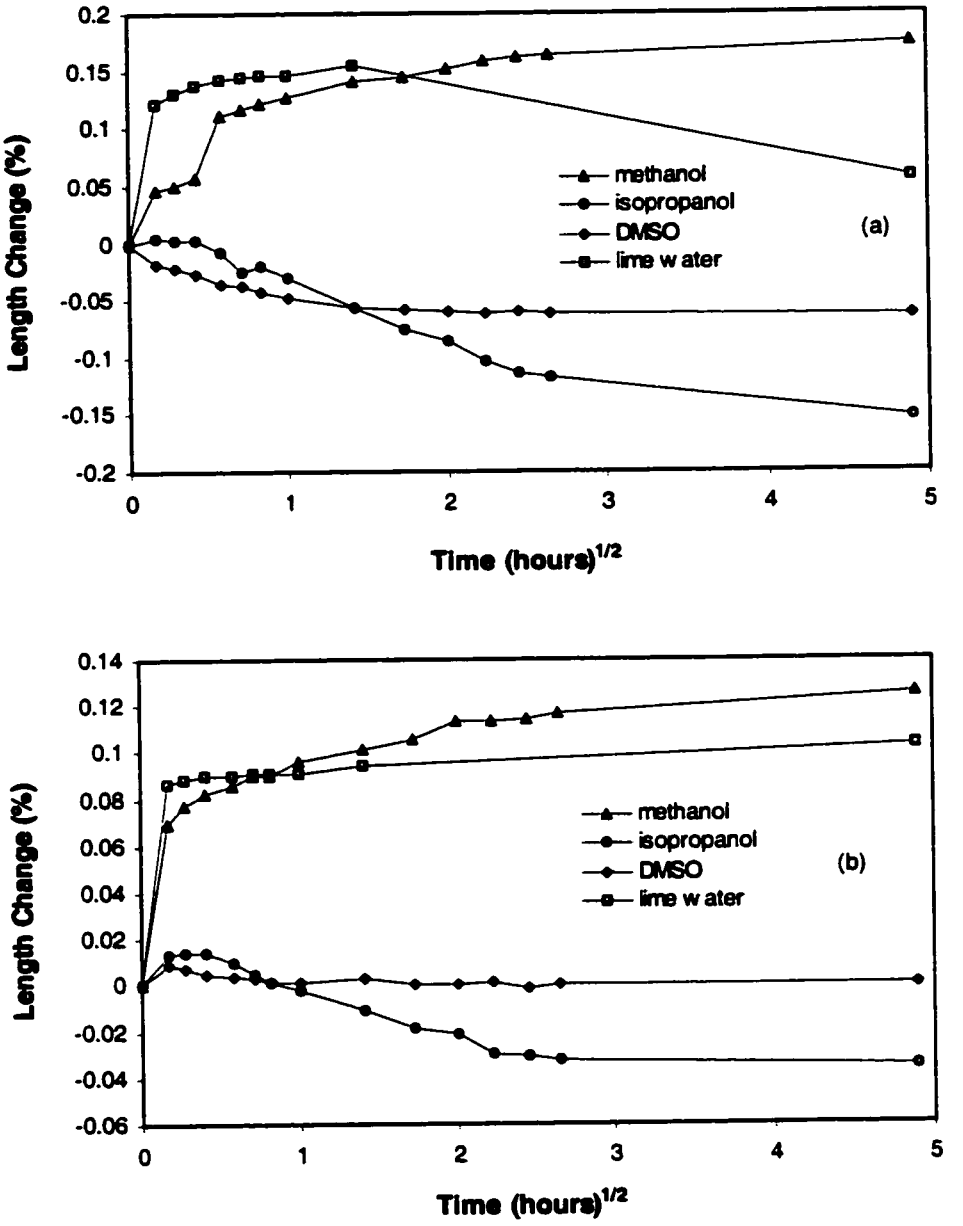

Figure 8.27: Length change of D-dried C-S-H (a) C/S=0.68 and (b) C/S=0.87 immersed in solvent

b) Water-saturated condition

The length change versus time curves for water-saturated C-S-H (C/S=0.68, 0.87, 1.26, and 1.49) immersed in the test solvents are characteristically different from those for the D-dried C-S-H

specimens (Figure 8.28). In methanol, the specimens either slightly contract or expand during the first 4 hours. Length change at 24 hours is -0.01%, 0.02%, 0.06% and 0.04%, respectively for the four C-S-H preparations. In isopropanol, large contractions occur at 24 hours (-0.24%, -0.13%, and -0.17%) for C/S=0.68, 0.87, and 1.49, respectively. For the C/S=1.26 preparation, there is an expansion of 0.05%. Intercalation may occur to a larger extent for this particular C/S ratio. The large contractions may be due to both changes in surface-free energy of the C-S-H on exchange with water and possible deposition of reaction products if any chemical interaction has taken place.

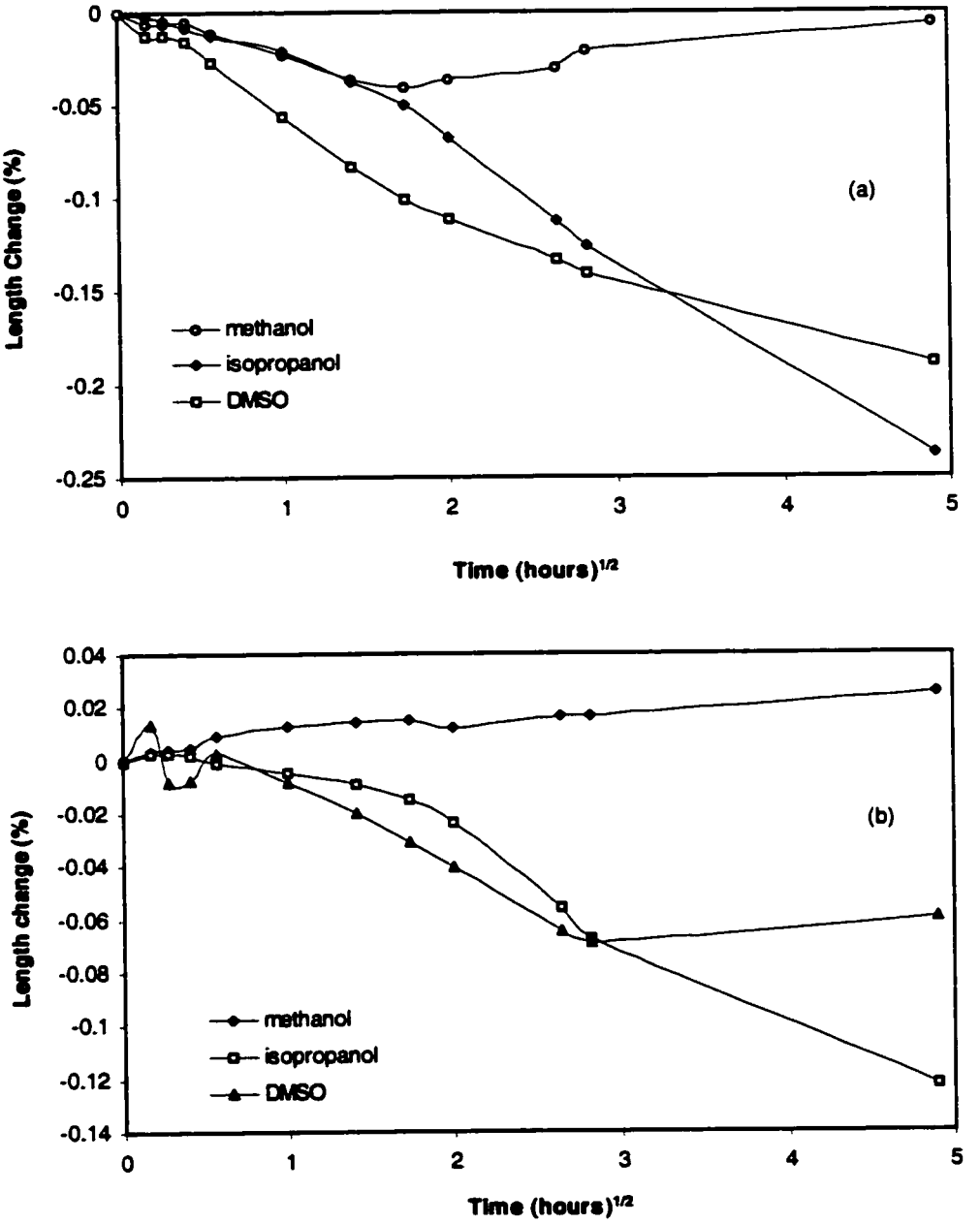

Figure 8.28: Length change of C-S-H (a) C/S=0.68 and (b) C/S=0.8 conditioned at 100% RH then immersed in solvent

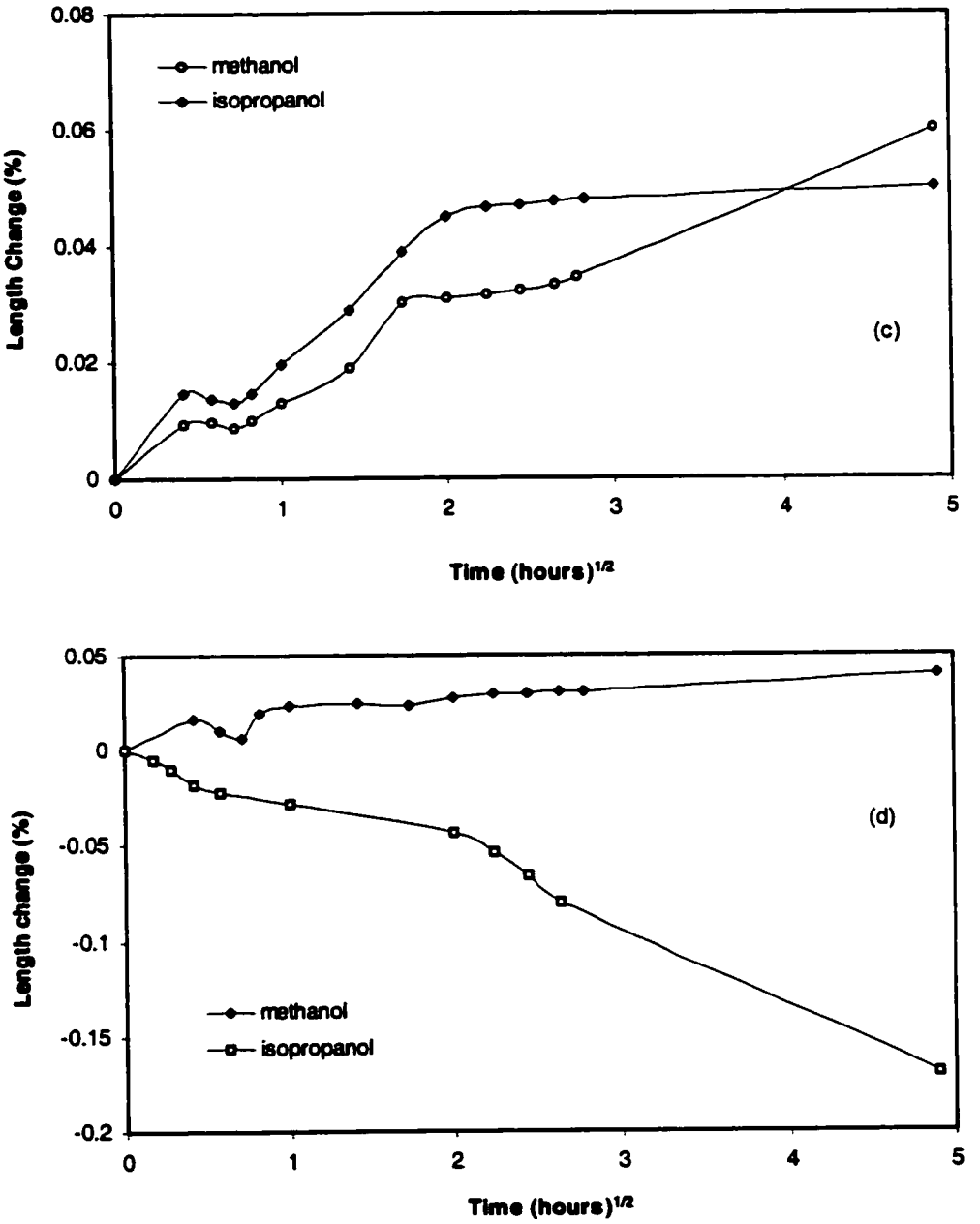

Figure 8.28: Length change of C-S-H (c) C/S=1.26 and (d) C/S=1.49 conditioned at 100% RH then immersed in solvent

8.2.4.3 Molecular sieves

The 0.3, 0.4, and 0.5 nm molecular sieves were saturated with water and immersed in the test solutions. The 0.3 nm sieve material expanded in methanol (0.15%) at 24 hours and contracted the same amount in DMSO (Figure 8.29). Isopropanol had very little effect on length change. The 0.4 nm sieve material immersed in methanol expanded slightly in the first few minutes and then contracted, reaching a value of about 0.14% at 24 hours. Isopropanol and DMSO exchange resulted in continuous contractions reaching values of 0.37% and 0.39%, respectively. The 0.5 nm sieve material expanded rapidly in methanol reaching 0.22% at 24 hours. Isopropanol exchange resulted in contractions of the system reaching a value of 0.12% at 24 hours. Exchange with DMSO resulted in an initial contraction to -0.07% at 1 hour followed by a slow recovery to -0.055% at 24 hours.

Comparison of the length change behavior of the molecular sieve systems with the hcp systems reveals similar behavior in most cases with some significant differences. Both systems experienced expansions with methanol exchange and contractions with isopropanol and DMSO exchanges. The slight expansion of the 0.3 nm molecular sieve resulting from isopropanol exchange and the continuous contractions (after the first few minutes) of the 0.4 nm sieves during methanol exchange are exceptions. The 0.5 nm molecular sieve has similar behavior to the cement in all test solvents. The expansion at 24 hours after methanol exchange was considerably larger for the molecular sieve material than the corresponding value for cement paste (0.21% and 0.03%, respectively).

A summary of the length change data for single and double exchange of water-saturated molecular sieves is given in Table 8.2. Examination of the data in the table would indicate that initial exchanges with any of the test solvents do not irreversibly affect the volume stability of the material, e.g., the exchange sequence 100% RH $\rightarrow$ I $\rightarrow$ M has a net length change of 0.165% compared to 0.150% for an initial exchange with methanol. The molecular sieves consist of a network of cage-like structure with entrances having dimensions indicated. Expansions and contractions occur on adsorption of water due to both surface energy changes and molecular bridging (Lankhanpal and Flood, 1957). In a solvent exchange experiment, the solvent may be excluded from or enter the cage structure depending on the size of the solvent molecule or the cage opening. The solvent exchange data for the 0.3 nm system would suggest that the expansion occurring on immersion of the specimens in methanol might occur as a result of a "disjoining pressure" effect due to surface double layers at cage entrances. If the electric fields of two

surfaces overlap, a repulsive force is created. It is unlikely that any of the solvents would penetrate into the cages with entrances smaller than the molecular diameter of the solvent.

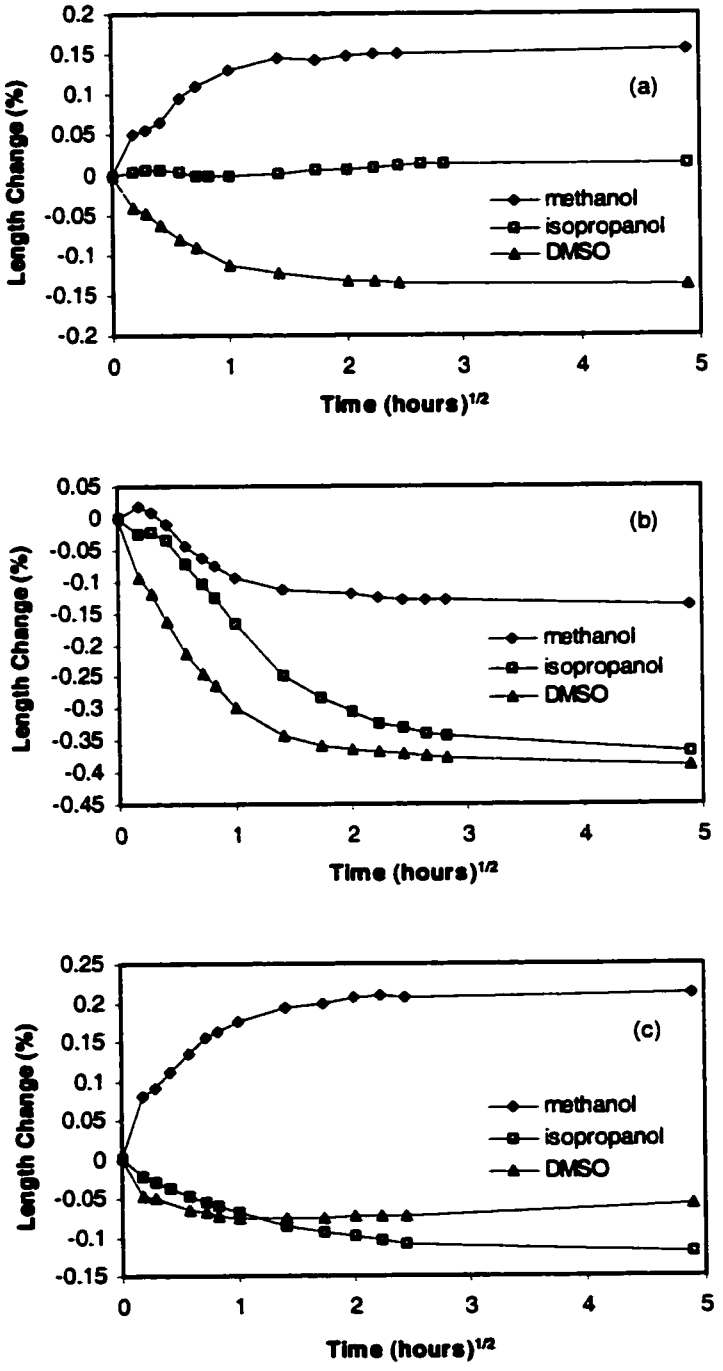

Figure 8.29: Length change of compacts (75% molecular sieve + 25% CaCO3) (a) 0.3 nm, (b) 0.4 nm, and (c) 0.5 nm immersed in solvent

Table 8.2: Solvent exchange length-change data of water-saturated molecular sieves

Length change (Δl/l, %) at 24 hours					
Sieve (nm)	Starting condition	Methanol (M)	Isopropanol (I)	DMSO (D)	Net length change
0.3	100% RH	+0.150	+0.010	-0.140	-
	100% RH → I	+0.155			+0.165
	100% RH → DMSO	+0.310			+0.170
0.4	100% RH	-0.140	-0.360	-0.390	-
	100% RH → M		-0.160		-0.300
	100% RH → I	+0.180			-0.180
	100% RH → DMSO	+0.280			-0.110

Chemical interaction of the solvents with the molecular sieves is ruled out as the double exchange data (Table 8.2) indicate length change is not irreversibly affected by the solvent. Changes in surface energy (in addition to the disjoining pressure described above) can account for the length change behavior with isopropanol and DMSO. It is suggested that the balance between disjoining pressure and the surface energy changes results in small expansion (0.01%) at 24 hours for the isopropanol exchanged specimens. The change in surface-free energy change appears to be the predominant length change mechanism during exchange with DMSO.

Contractions for the 0.4 nm molecular sieves at 24 hours are very large being 0.14%, 0.36%, and 0.39% for exchange with methanol, isopropanol, and DMSO, respectively. It is suggested that in addition to surface energy changes, some penetration of the solvents into the cage structure may produce contractions due to molecular bridging.

The cause of expansion for the 0.5 nm sieves material exchanged with methanol is not clear. Large contractions resulting from exchange with isopropanol and DMSO can be explained by a combination of surface energy changes and molecular bridging.

8.2.4.4 Vycor glass

Water-saturated vycor glass samples were immersed in the test solvents (Figure 8.30a). The specimens expanded during the first 15 minutes and then contracted. Expansion was less and contraction more when the exchange took place in isopropanol. The contraction at 24 hours was -

0.05%. The general behavior was similar to that of partially saturated cement paste (from 11 to 85% RH) immersed in isopropanol. Volume stability studies of vycor glass in sodium hydroxide have led to the suggestion that dissolution of glass leads to expansion and that surface reaction and chemisorption lead to contraction. In the present experiments, the surface energy of the glass may change as a result of (a) elimination of surface irregularities; (b) changed composition of the surface as water molecules are replaced by solvent molecules; and (c) adsorption of the reaction products on the interior surfaces of the solid.

Length change versus time curves for double exchange experiments are also given in Figure 8.30b. A summary of the length change data for the single and double exchange of the test solvents with water-saturated vycor glass is given in Table 8.3.

Examination of the data indicates that a first exchange with methanol or isopropanol produces highly irreversible effects with respect to the volume stability of water-saturated vycor glass. A first exchange with DMSO leads only to a small irreversible effect.

Table 8.3: Solvent exchange length-change data of water-saturated vycor glass

Length change (Δl/l, %) at 24 hours				
Starting condition	Methanol (M)	Isopropanol (I)	DMSO (D)	Net length change
100% RH	+0.015	-0.055	0.000	-
100% RH → M		+0.080		+0.095
100% RH → I	-0.065			-0.110
100% RH → DMSO	+0.030			+0.030

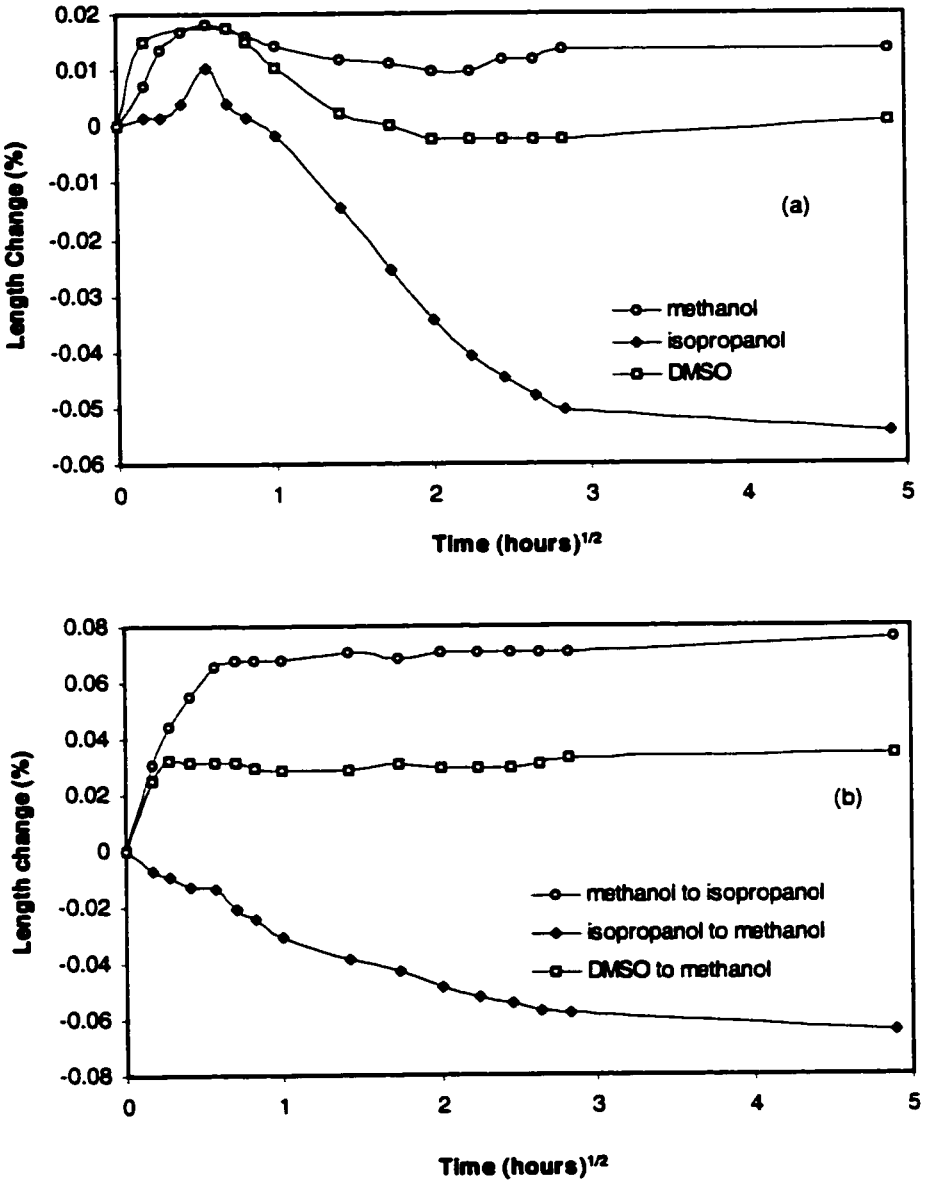

Figure 8.30: Length change of vycor glass immersed in solvent (a) after conditioning to 100% RH and (b) after 14 days initial immersion and re-immersion in another solvent.

8.2.4.5 Tricalcium silicate (C_3S)

The effect of methanol and isopropanol immersion upon the mass change characteristics of hardened C_3S paste from the second saturation state (defined previously) is shown in Figure 8.31. It appears that up to 10 hours after immersion, the rate of water removal was greater in methanol than in isopropanol. After that time, specimens immersed in isopropanol continue to lose mass at a very low rate reaching equilibrium at a mass loss of about 9%. Those immersed in methanol continuously gain mass at a slow but constant rate. The mass loss observed in the first stage is predominately due to the displacement of the denser water by the solvents. The mass gained by specimens when immersed in methanol may be due to the formation of a new complex as suggested by Day (1981) and Beaudoin (1987). Evidence suggests that this occur when either C-S-H or CH is immersed in methanol. These results do not negate the use of methanol to preserve the structure, as they do not appear to affect the collapse of structure as observed by nitrogen surface area measurements.

The shrinkage of sliced C_3S paste specimens was recorded while drying at 11% relative humidity under vacuum. There were no significant variations within the readings for the three companion specimens used. It was observed that about 80% of the total shrinkage (0.425%) took place within the first 6 hours. After 30 days, there was almost no further shrinkage observed on the specimens; it was assumed that the hygral equilibrium in the desiccator was achieved (Figure 8.32). Some specimens of 85% hydrated C_3S paste dried at 42% RH for 14 days was immersed in solvent immediately after drying. It was found that the specimens initially swell, and after a few minutes of readjustment, those in isopropanol shrink while those in methanol undergo continuous swelling. This expansion may be due to the smaller molecular size of methanol and the corresponding intercalation in C-S-H. The methanol molecule is closer to the water molecule size than isopropanol. Drying to 11% RH results in significantly greater shrinkage than drying to 42% RH.

The results for the specimens dried at 5%, 11% and 22% relative humidity under vacuum from the second saturation state prior to solvent immersion are shown in Figures 8.33 and 8.34. It can be observed that, at any given RH, immersion in methanol leads to a rapid swelling following by a further small length change. Specimens immersed in isopropanol continuously shrink, with a little swelling at the beginning for the 5% RH specimens. Swelling or shrinkage taking place in methanol and isopropanol exchanged specimens respectively are related to the humidity level. The specimens dried at 11% and 22% RH may contain a quantity of inter-crystalline adsorbed water (two molecules thick) and intra-crystalline zeolitic water (one molecule thick) embedded

between C-S-H crystallite layers. The latter may be the only type present in specimens dried at 5% RH. It is believed to be strongly bound and accounts for the slight change in length observed. The tendency of swelling or shrinkage is still observable at that very low relative humidity. Intercalation particularly of methanol appears to be enhanced at the higher humidities.

At zero humidity, corresponding to the D-dry state, specimens immersed in methanol and/or isopropanol show the same trend starting with a swelling in the first stage, followed by a small amount of shrinkage and then continuous swelling (Figures 8.35 and 8.36). For both specimens, the length changes that take place are probably due to the changes in the surface free energy of C-S-H sheets and intercalation effects. Swelling is likely associated with the latter phenomena.

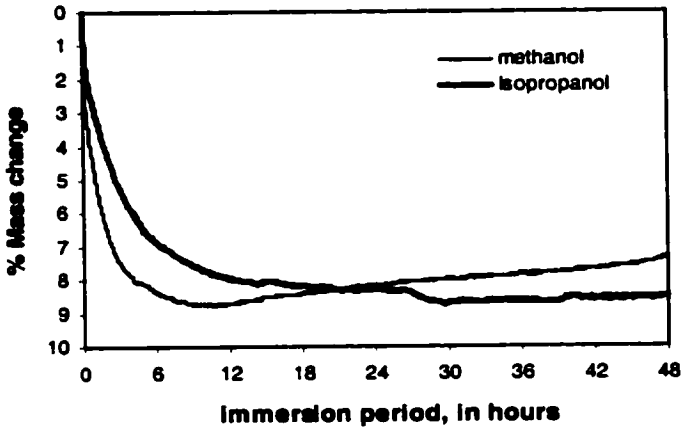

Figure 8.31: Mass change of C_3S blend (w/s=0.4) immersed in alcohol from saturated state

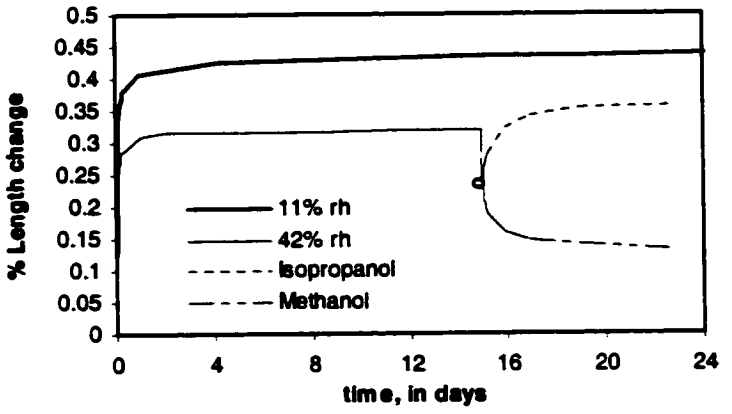

Figure 8.32: Effect of solvent immersion upon 85% hydrated C_3S dried at 11% and 42% RH

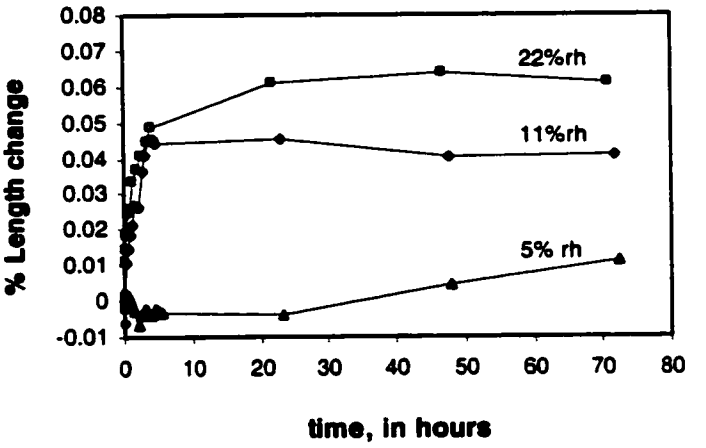

Figure 8.33: Length change of 74% hydrated C_3S immersed in methanol from different relative humidity

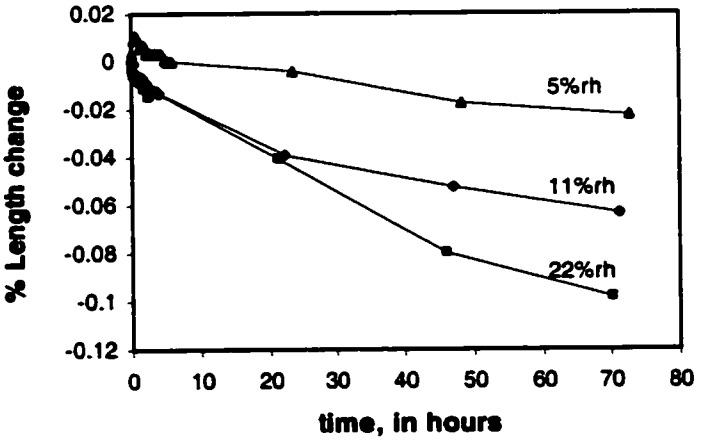

Figure 8.34: Length change of 74% hydrated C_3S immersed in isopropanol from different relative humidity

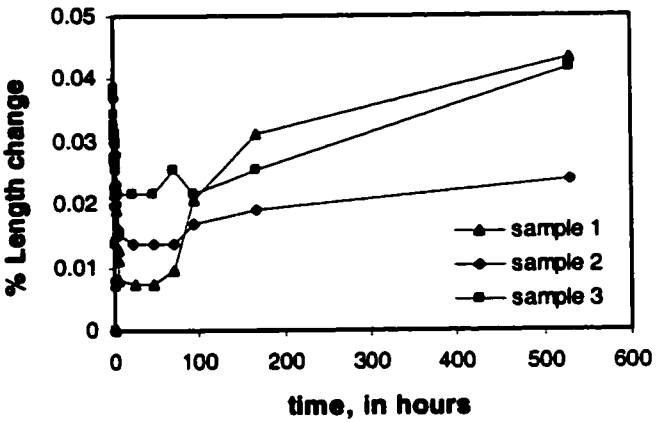

Figure 8.35: Effect of methanol immersion on length change of D-dried 74% hydrated C_3S paste

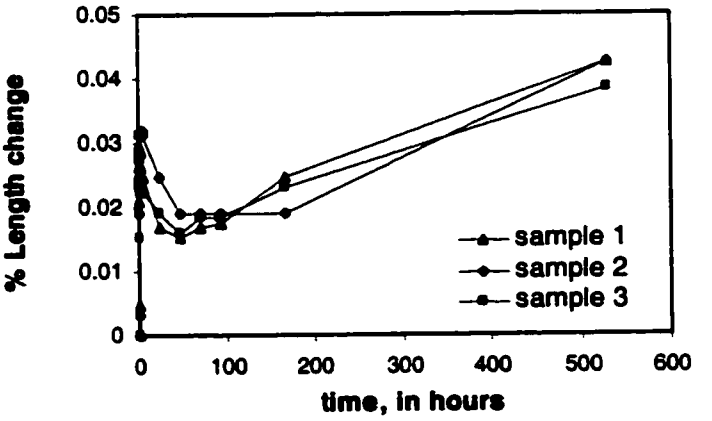

Figure 8.36: Effect of isopropanol immersion on length change of D-dried 74% hydrated C_3S paste

8.2.4.6 Cement pastes

a) Adsorption from the D-dry state

The cement paste samples (w/c=0.5 and 1.0) that had been D-dried (drying to the vapor pressure of dry ice at -79°C) and subsequently immersed in solvents (methanol, isopropanol, DMSO) all exhibited an immediate (within the first 2 minutes after immersion) expansion followed by a slight contraction (except for the specimens immersed in DMSO) over the next few hours and eventual slow expansion (Figure 8.37). In each case, the slight contractions were observed for each of the duplicate samples. Initial expansions are due primarily to the free energy change due to surface adsorption effects, some intercalation into the C-S-H structure (with particular reference to methanol) and chemical interaction with the solid hydrated phases (Feldman, 1968; Litvan, 1984). The slow expansion (after 4 hours) may be due to intercalation effects. The observation that DMSO does not have the same effect may be an indication that intercalation is less pronounced with this solvent.

Chemical interaction of solvents with solids usually produces significant immediate expansions (Prins, 1967). These have been attributed to surface-free energy changes, osmotic pressure, disjoining pressure and strain energy considerations due to pre-treatment conditions.

Contractions following expansions during dissolution experiments are known to occur (e.g., porous silica glass in $NaNO_3$ solution) and are attributed to the adsorption of reaction products on the undissolved solid. The slight contractions observed (for each of the duplicate cement paste specimens) may have a similar origin as surface interactions with methanol, for example, are known to occur.

b) Solvent exchange of water-saturated hardened cement paste

The paste samples (w/c=0.5 and 1.0) underwent an initial contraction during the first hour in all the test solvents (Figure 8.38). The methanol-exchanged samples began to expand after 2.25 hours and continued expanding to the end of the test at 24 hours. Expansion is greatest at 24 hours for the water/cement ratio of 1.0 preparation. The samples exchanged with isopropanol and DMSO contracted continuously over the 24 hours period. In isopropanol there is a contraction over the first 24 hours (0.08% to about 0.09%) for all pastes.

The changes in free energy of the adsorbent due to exchange of solvents (water for methanol, isopropanol or DMSO) can result in contraction if the surface-free energy increases. The

expansion observed during methanol exchange could be the result of intercalation into the layer C-S-H structure, surface interaction between the solvent and the C-S-H and adsorption effects on the portlandite surfaces (Feldman, 1987; Beaudoin et al., 1983). It is important to note that it is not only the C-S-H phase in hydrated cement systems that is affected by the solvent exchange process. Parallel behavior (i.e., observations of expansions or contraction specific to methanol and isopropanol exchange) was observed for C-S-H and CH specimens.

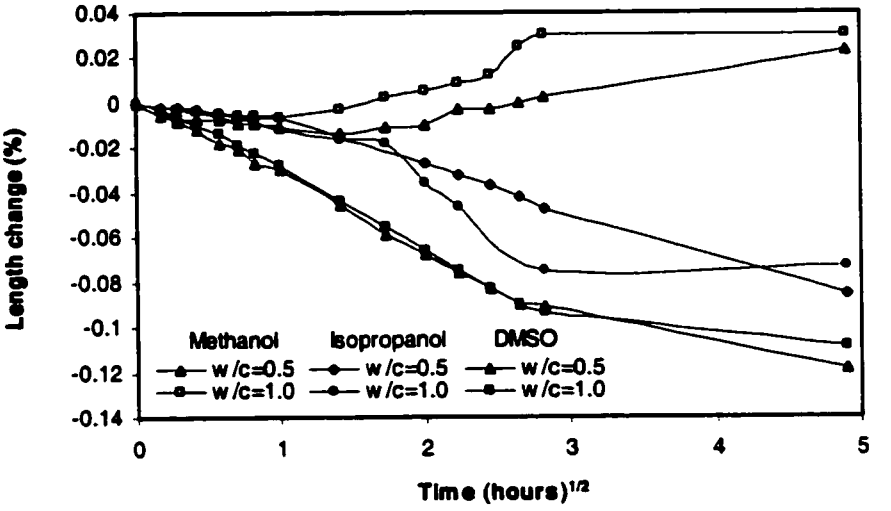

Figure 8.37: Length change of cement paste (w/c=0.5 and 1.0) D-dried and immersed in solvent

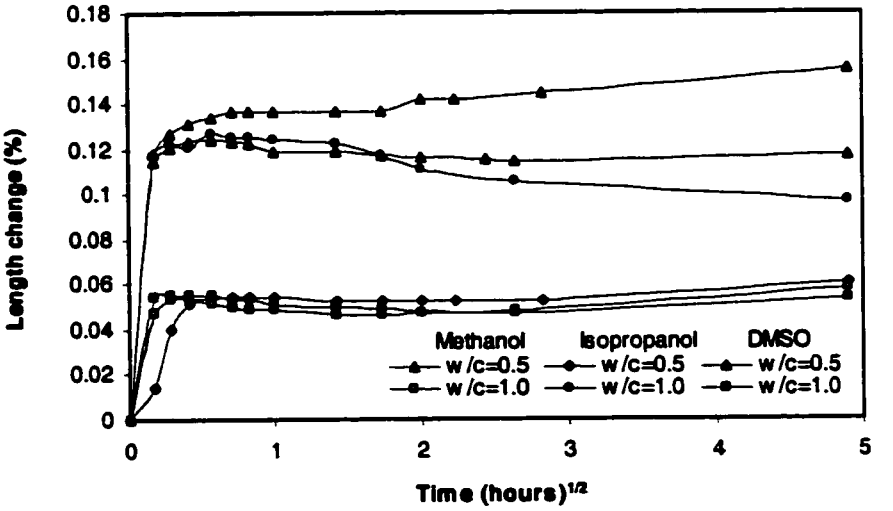

Figure 8.38: Length change of saturated cement paste (w/c=0.5 and 1.0) immersed in solvent

c) *Double exchange of solvents*

The irreversible effects of solvent exchange on solid phases in cement paste can be assessed through a double exchange process. Solvent exchange experiments were carried out where the starting condition was either the D-dried state and subsequent saturation with solvent or the water-saturated state and subsequent saturated with solvent. Specimens prepared with these pre-treatments as the starting condition were subjected to a second exchange (see length change data, Figures 8.39, 8.40). Table 8.4 provides the data representing the net length change after the second solvent exchange process. The length of the sample at the starting condition is taken as the reference length. The net length change is referred to this length. Data for the initial reference starting conditions, i.e., D-dry and 100% RH are also included in the table.

The double exchange for initial saturated samples (methanol to DMSO) would indicate that a first exchange with methanol has an irreversible effect on length change (the net length change of the sample being -0.050% compared to -0.110%). However, the double exchange (isopropanol to DMSO) would appear to have a reversible effect on length change, the net length change being similar to that observed for a direct exchange with DSMO. When the starting condition is the D-dry state saturation with isopropanol or DMSO prior to exchange with methanol appears to have an irreversible effect for the former and a reversible one for the latter saturant. Saturation of specimens with methanol prior to exchange with isopropanol also has irreversible effects on sample length.

It is apparent that the starting condition (D-dry or water-saturated), selection of solvent, and sequence of exchange have an effect on the stability of the solid. Solvent exchange of water-saturated samples would appear to best be carried out using isopropanol. D-dry samples would appear to be least affected by saturation with DMSO compared to methanol or isopropanol.

c) *Equilibrium drying - single and double exchange*

Cement paste specimens were equilibrated at various positions along the desorption branch of water isotherm (85% to 11% RH). The strains that were observed during the first equilibrium drying are presented in Table 8.5. The paste specimens were then immersed in the test solvents and length change was monitored.

Length change results (normalized to zero strain after equilibrium has been established) for both the w/c=0.5 and 1.0 paste specimens were obtained and plotted in Figures 8.41 and 42 respectively. For the w/c=1.0 paste, the length change at 48 hours generally increases with

equilibrium humidity for the entire test solvents. The length change versus time curves is clustered into two groups. The first comprises those for specimens pre-conditioned to humidities ranging from 11% to 42% RH. It is apparent that the specimens in this group contain predominately interlayer water, as it has been shown in the Section 8.2.1. The second group represents specimens equilibrated at humidities ranging from 57 to 85% RH.

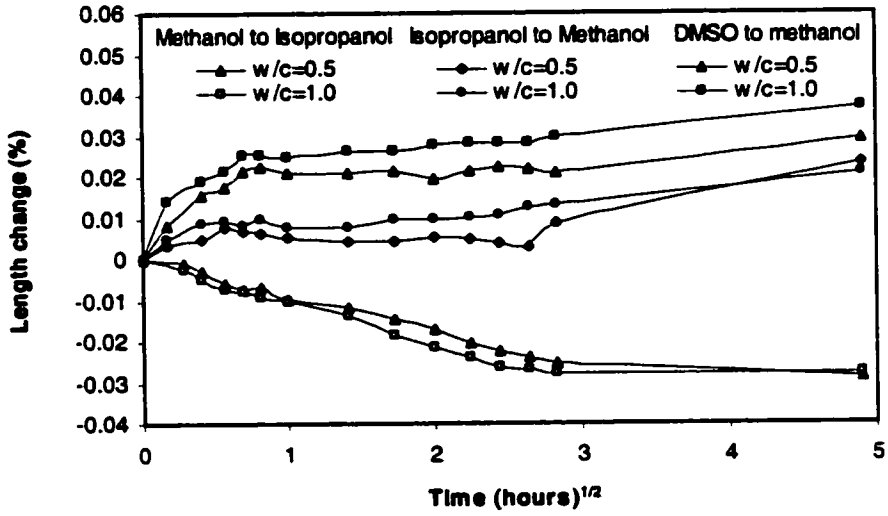

Figure 8.39: Length change of cement paste (w/c=0.5 and 1.0) D-dried, saturated in solvent, and immersed in an alternate solvent

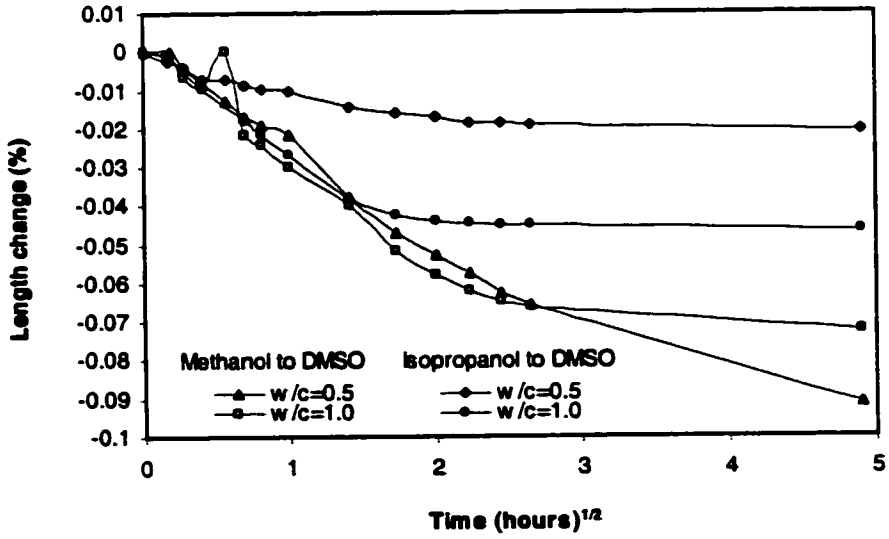

Figure 8.40: Length change of cement paste (w/c=0.5 and 1.0) conditioned at 100% RH, exchange with methanol or isopropanol and re-exchange with DMSO

Table 8.4: Single and double exchange length change data for D-dried or water saturated cement paste

Length change (Δl/l, %) at 24 hours [a]				
Starting condition	Methanol (M)	Isopropanol (I)	DMSO (D)	Net length change
D-dry	+(0.12-0.15)	+(0.050-0.080)	+(0.12-0.14)	-
100% RH	+(0.025-0.030)	-(0.080-0.090)	-(0.11-0.12)	-
100% RH → M			-0.08	-(0.050-0.055)
100% RH → I			-(0.02-0.045)	-(0.10-0.135)
D-dry → M		-(0.028-0.030)		+(0.090-0.132)
D-dry → I	+(0.020-0.027)			+(0.070-0.107)
D-dry → DMSO	+(0.280-0.030)			+(0.148-0.170)

[a] Zero length change is referred as the D-dry or 100% RH condition.

Table 8.5: Length change on first drying of cement paste to various equilibrium relative humidities

Length change (Δl/l, %) at equilibrium		
RH, %	w/c	
	0.5	1.0
85	0.06	0.08
75	0.14	0.14
57	0.25	0.22
42	0.28	0.31
32	0.31	0.32
11	0.39	0.34

For the methanol exchange experiments, group two specimens expanded significantly in the first few minutes and continued to expand over the test period. The expansion was greater than 0.20% at the 85% RH condition. It is suggested that partial drying of the layered silicates (at higher humidities, e.g., 85% RH) facilitates the intercalation process and resultant expansion due to penetration of methanol. This would appear to be the predominant mechanism of expansion for this condition and solvent. The first group of specimens either slowly expand over the entire test period (42% RH) or slightly contract (up to about 4 hours) and then slowly expand.

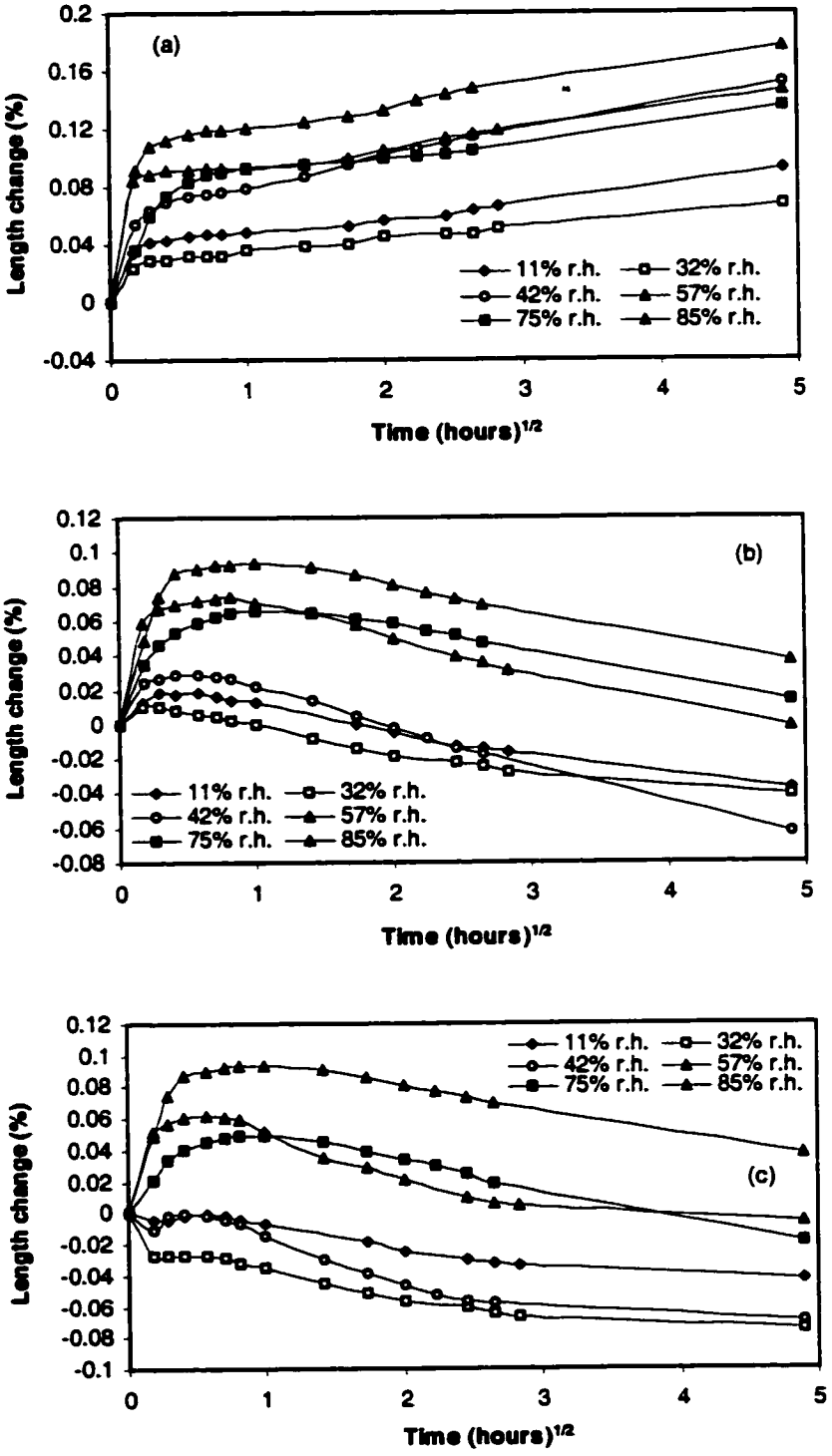

Figure 8.41: Length change of cement paste (w/c=0.5) conditioned at different humidities and immersed (a) in methanol, (b) in isopropanol, and (c) in dimethylsulfoxide

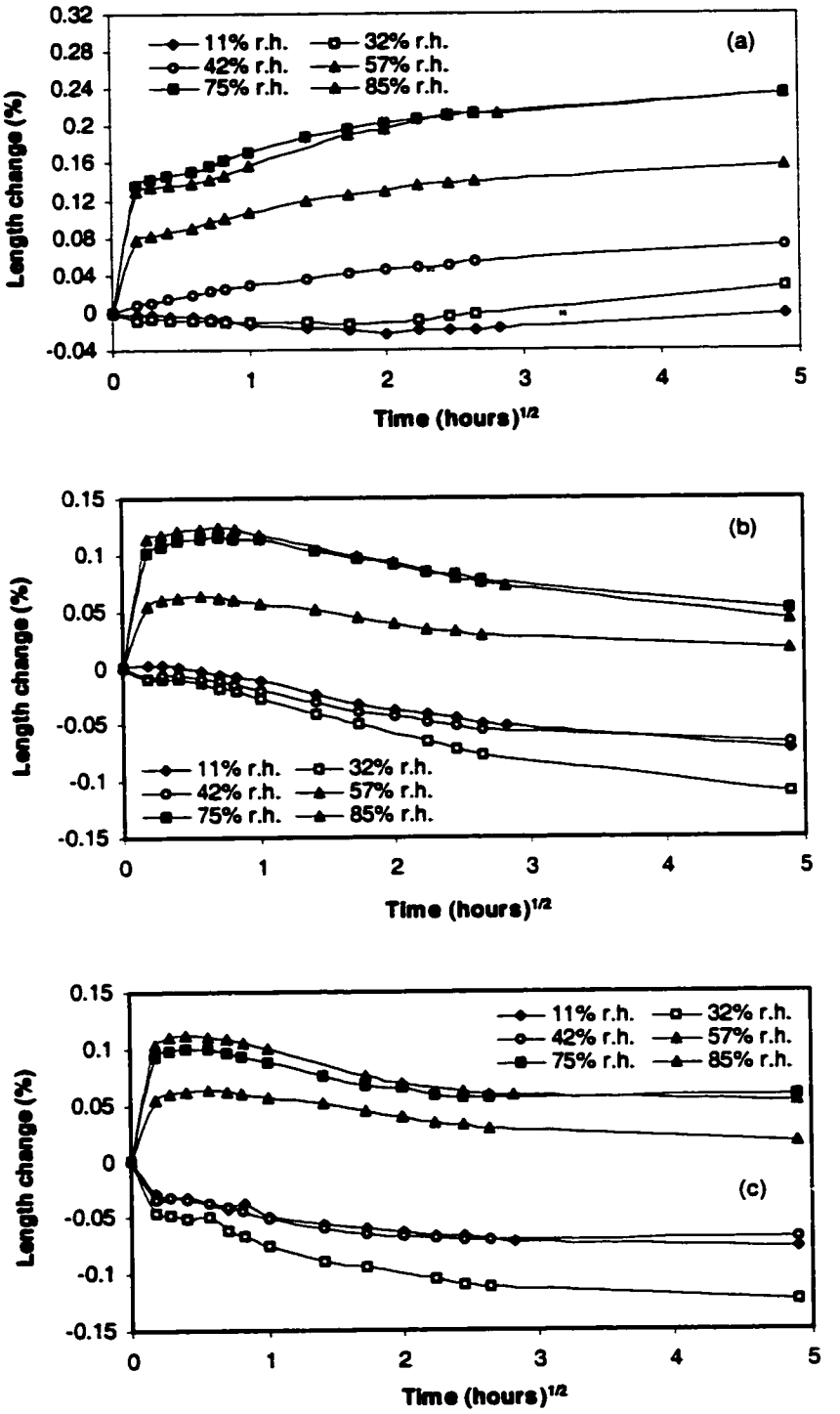

Figure 8.42: Length change of cement paste (w/c=1.0) conditioned at different humidities and immersed (a) in methanol, (b) in isopropanol, and (c) in dimethylsulfoxide

The isopropanol exchange experiments were characteristically different from those for methanol exchange. Specimens in both groups expanded during the first 15 minutes and then contracted. Expansion reached 0.12% for specimens conditioned at 75% and 85% RH. Some intercalation into the C-S-H structure may be possible at high humidities as spaces at layer entrances may be more readily accessible. Contractions for group one specimens were as high as 0.10%.

Group one specimens exchange with DMSO continuously contract and a value of 0.12% was reached on the specimen conditioned at 32% RH. Group two specimens behaved similarly to those exchanged with isopropanol.

The 100% RH condition yield results that are similar in character and magnitude to those for specimens conditioned at 11% and 32% RH. Minimum drying to 85% RH however, appears to open up the C-S-H structure (facilitating intercalation) prior to collapse with further drying.

Any significant intercalation of solvent into the C-S-H structure is unlikely at low humidities. Contraction is possibly due to changes in surface-free energy resulting from the solvent exchange.

Double exchange experiments were conducted on specimens pre-conditioned to 11%, 32%, and 85% RH. The results are summarized in Table 8.6. The data for net length change (with respect to the original starting condition at 11%, 32%, or 85% RH) clearly indicate that a first exchange (on specimens pre-conditioned to equilibrium at 11%, 32%, or 85% RH) with any of the test solvents has irreversible length change effects on samples that have been partially dried. This is an important consideration when preparing samples for tests that involve the use of mercury porosimetry (Feldman and Beaudoin, 1991; Mikhail and Selini, 1966).

Preparation of cement paste specimens for mercury intrusion involves drying to completely remove the water. The drying process changes the system resulting in a coarser pore structure. The argument for replacing the water with a solvent is that removal of a liquid with a lower surface tension result in a lower applied stress on the solid matrix. The resulting pore structure is less disturbed. It would appear that replacement of water with methanol is highly expansive indicating the possibility of intercalation effects and chemical interaction with solid phase (Beaudoin, 1987). Replacement of water with other solvents is not a net expansive process. Isopropanol appears to have the minimum net effect on dimensional stability (Feldman, 1987; Beaudoin et al., 1998). It appears to be an appropriate solvent for specimen preparation. Vacuum drying for 24 hours to remove the isopropanol is recommended prior to porosimetry measurements.

Table 8.6: Single and double exchange length change data for cement paste (w/c=0.5) conditioned to various equilibrium humidities

Length change (Δl/l, %) at 24 hours				
Starting condition	Methanol (M)	Isopropanol (I)	DMSO (D)	Net length change
11% RH	0.000	-0.060	-0.080	-
11% RH → M		-0.030		-0.030
11% RH → I	+0.030			-0.030
11% RH → DMSO	+0.030			-0.050
32% RH	+0.020	-0.100	-0.120	-
32% RH → M		-0.070		-0.050
32% RH → I	+0.035			-0.060
32% RH → DMSO	+0.035			-0.090
85% RH	+0.240	+0.050	+0.060	-
85% RH → M		-0.080		+0.160
85% RH → I	+0.090			+0.140
32% RH → DMSO	+0.090			+0.150

8.3 Shrinkage and creep of Portland cement systems

8.3.1 Microstructure variation

From the results discussed in Section 8.2 after performing thermal analysis, pore structure and surface area, it follows that; Portland cement systems can be subjected to various microstructure modifications depending up on the drying pre-treatment regimes.

Normal drying and vacuum drying at 37°C for 24 hours following solvent immersion were found to reduce the microstrutural changes taking place when saturated surface dried specimen was directly normally dried (dried at 105°C for 3 hours). Organic solvents, particularly methanol, were found to penetrate the interlayer space after a counter diffusion process bringing the C-S-H sheets on close proximity one another after drying. This microstructure preservation can be explained by the surface area measurements showing the higher value when saturated surface dried specimen of C_3S and/or cement pastes were immersed for 48 hours in either isopropanol or methanol.

In a strategy to understand the behavior of the microstructural changes taking place in hardened cement paste, several microporous systems including some cement paste constituents were studied. This was done in order to establish more clearly the mechanisms responsible for the observed volume changes, which indirectly may help in further understanding the shrinkage and creep behavior.

The application of solvent exchange technique depends mainly on the fact that any interaction between the solid and organic solvent should not produce an artifact detectable with the microstructural method to be used. As shown previously, the use of different organic solvents led to different microstructures of cement paste or C-S-H layered structure. Pre-treatment of cement systems with organic solvents should then be of value in a shrinkage and creep investigation in providing a fundamental understanding of the role of C-S-H and CH.

8.3.2 Shrinkage of cement systems

8.3.2.1 C_3S paste

The creep and shrinkage of hydrated C_3S paste was investigated in the dry state in cells environmentally controlled (see Figure 6.2). The cells were maintained dried with magnesium perclorate reagent grade removing moisture from the cells in order to provide a 0% RH condition. For the specimens kept in the cells without loading, no significant swelling or shrinkage was observed following the treatment regimes described in Section 8.2.2.2.

8.3.2.2 Cement pastes

The hardened cement paste "T-shaped" specimens were pre-conditioned as described in table 8.1 then re-saturated with lime water prior to loading. Given the 0 and 100% relative humidity achieved in the environmentally controlled cells, no variation in length was observed on companion "T-shaped" specimens placed in parallel cells.

8.3.3 Creep of cement systems

For all the results presented, the initial strain was determined indirectly by measuring the modulus of elasticity (Young's modulus) of companion specimens. Given that no swelling or shrinkage takes place while the "T-shaped" specimens are under load, the creep results presented in this section are the basic creep only expressed in terms of compliance which is the strain per unit applied stress.

8.3.3.1 C_3S paste

The Young's modulus values obtained for the hydrated C_3S paste tested were 40.7 GPa for the reference D-dried specimens, and 27.0 GPa and 27.3 GPa for specimens immersed in methanol and isopropanol respectively then D-dried. For the stress/strength ratio of 0.3, the corresponding applied stress was 15.3 MPa. From modulus of elasticity and the applied stress, the initial elastic strains are therefore 376, 567 and 560 μm/m respectively.

The creep results are presented in Figure 8.43 in terms of basic compliance i.e. micro-strain per unit stress. The results indicate that without considering the initial elastic strain presented above, solvent treatment especially immersion in methanol before drying reduces creep. Methanol treated samples exhibit less specific basic creep than isopropanol treated samples.

Plots of the compliance (total deformation per unit stress) vs. time (log-log scale) are linear. The parameters obtained from regression analysis depend on the water content of the sample and/or the pretreatment history. The curves describing the compliance rate are power functions and can be expressed as follows:

$$\frac{dJ(t,t_o)}{dt} = \alpha(t-t_o)^{\beta} \qquad (8.1)$$

where, $J(t,t_o)$ is the compliance of hcp at age t loaded at t_o, α and β are constants, and $(t - t_o)$ is the time elapsed under loading. The constant β is dimensionless whereas the constant α has units of $\mu\epsilon$/MPa/day$^{1+\beta}$.

The basic creep rate is more pronounced in isopropanol treated specimens at early times after loading. Methanol treated specimens have a smaller basic creep rate than the untreated

specimens (see Figure 8.44). The compliance rates are all close one another as the power functions, which defined them show similar parameter values.

It is especially important to note that reference samples that are D-dried exhibit significant creep. This suggests that the presence of water is not an 'a priori' condition for creep to occur. Slipping and sliding of C-S-H layers may be an operative mechanism (Ishai, 1968).

The removal of water by a solvent prior to D-drying may reduce the microstructural changes taking place in normal drying and therefore reduce the creep capacity of the hydrated C_3S paste.

The TGA results discussed above in Section 8.2.1 indicate that immersion in either methanol or isopropanol may remove water from C-S-H and therefore, bring the sheets in closer proximity once dried under vacuum. This may explain the smaller magnitude of creep in such specimens particularly those immersed in methanol.

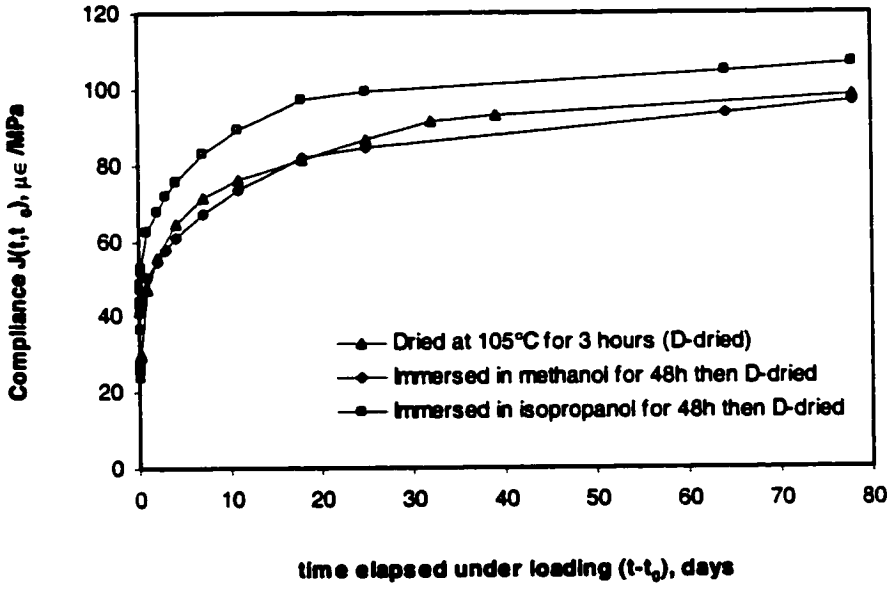

Figure 8.43: Basic compliance of D-dried 74% hydrated C_3S paste after organic solvent exchange

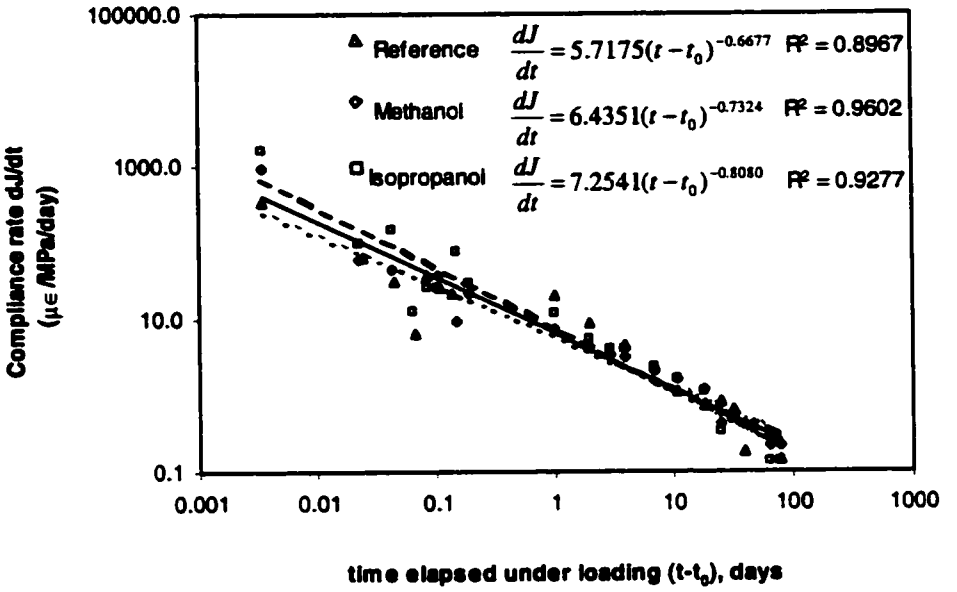

Figure 8.44: Basic compliance rate of D-dried 74% hydrated C_3S paste after organic solvent exchange

8.3.3.2 Cement pastes

The results presented are those of 30 years old hydrated cement paste (w/c=0.5). The Young's modulus of "T-shaped" specimens pre-treated as described previously in Table 8.1 is presented in Table 8.7. The constant stress/strength ratio used was 0.3 corresponding to an applied stress of 11.5 MPa.

Table 8.7: Modulus of elasticity of hardened cement paste (w/c=0.5) re-saturated following several pre-treatment regimes

Final pre-treatment condition	Young modulus (GPa)	Initial strain (μm/m)
Saturated (1st state)	18.4	625
D-dried then re-saturated (2nd state)	14.7	782
Dried at 37°C then re-saturated	16.8	685
Dried at 42% RH then re-saturated	15.1	762
D-dried (dried at 105°C for 3 h)	16.7	689
Dried at 37°C for 24 h	14.3	804
Meth. then dried at 37°C for 24 h	10.2	1127
Isop. then dried at 37°C for 24 h	11.6	991

As already mentioned in Section 8.2.2.3, the use of organic solvents to remove water from the specimen results in a slight reduction of the total porosity as shown on Figure 8.12. The magnitude of the basic compliance of "T-shaped" samples kept moist while under load (Figure 8.45) is dependent on drying history. Samples dried at 42% RH or D-dried and then re-saturated have significantly greater creep at 25 days than the saturated reference specimen. These compliance values are smaller than or even similar to that of D-dried samples (Figure 8.46) for which the corresponding magnitude is significant and about 180 με/MPa at 30 days. These results confirm some previous findings relating the basic creep to the water content of hardened cement paste specimens prior to loading (Neville, 1957; Ruetz, 1968; Wittmann, 1970). However, contrary to the hypothesis that no creep results from fully dried hcp specimen (Wittmann, 1971), the D-dried sample exhibits a significant amount of basic creep. The amount of creep of the dry specimens can be very large if the specimens are immersed in isopropanol or methanol prior to the drying process (Figure 8.46). This suggests that the hydroxylic water molecules remaining on the crystallite after D-drying as well as their orientation may contribute to the creep. The creep taking place in hcp is believed to be mainly due to microsliding between adjacent sheets of C-S-H (Figure 8.47) and/or due to a change in orientation of hydroxylic water strongly held on the crystallite surfaces of D-dried paste.

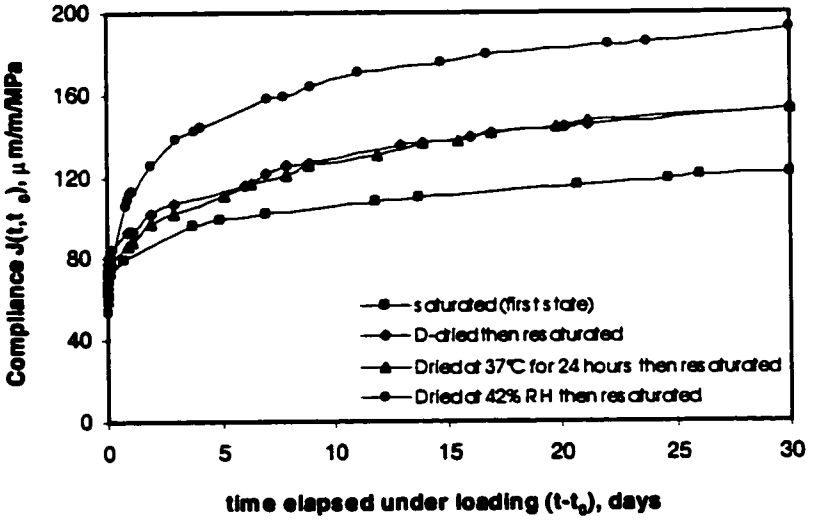

Figure 8.45: Basic compliance of hardened cement paste (w/c=0.50) after re-saturation from Different drying pre-treatments

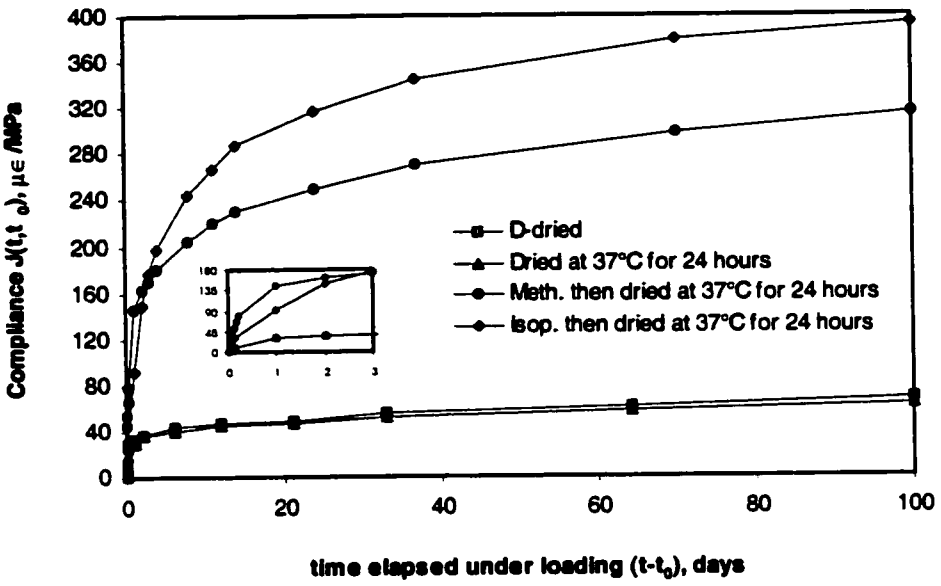

Figure 8.46: Basic compliance of hardened cement paste (w/c=0.50) after different drying pre-treatments

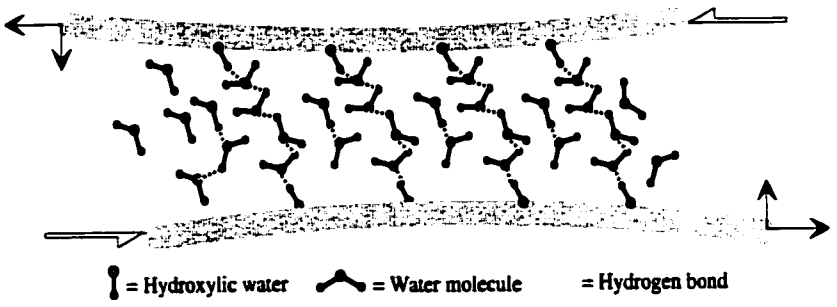

Figure 8.47: Sliding between C-S-H sheets resulting in breaking and reconstitution of hydrogen bonds

The removal of water by a solvent prior to vacuum-drying may reduce the microstructural changes taking place in normal drying and therefore, increase the creep capacity of hcp as indicated by the results in Figures 8.45 and 8.46 and the corresponding high surface area as shown in Section 8.2.3 and previously reported by Taylor and Turner (1987). The available creep

sites (due to the reduced amount of structural collapse) may then be greater in number resulting in an increase in the magnitude of basic creep.

The diffusion process may possibly be responsible for drying shrinkage or swelling of cement paste. The analogy suggesting a microdiffusion process in hcp under applied stresses as responsible for the early age creep is however questionable particularly in case of basic creep. Such microdiffusion if any would support the seepage theory. This has been seriously questioned by Young (1974) because of the fact that creep can occur in sealed or immersed hcp specimens where water will not diffuse out of the loaded sample. The water of type (3) and/or (4) described previously (Ishai) may facilitate sliding of C-S-H sheets one over the other by acting as lubricant (Ruetz, 1968; Ali and Kesler, 1964). The sliding taking place may be followed by the changing orientation of intra- and intercrystallite water as the surface of the C-S-H sheets approach each other resulting in further layering or aging as suggested by Feldman (1972).

The results indicate that organic solvents used to remove water from the cement paste sample result in significant basic creep after vacuum drying at 37°C. The methanol-exchanged specimens exhibit less specific basic creep than isopropanol-replaced specimens. This may be explained by the fact that after the water exchange process, some of the organic solvent remains physically adsorbed on the surface of the C-S-H sheets and is not totally removed after 24 h of vacuum-drying at 37°C or by other procedures based on evacuation or heating at temperatures below those at which reactions yielding carbonate begin to occur (Taylor and Turner, 1987). The creep results can also be explained by the formation of a new complex from the reaction between the solvent and cement paste. Methanol has been shown to react with CH and C-S-H (Beaudoin, 1987; Day, 1981). Such physically adsorbed films and/or complexes may weaken the C-S-H surface resulting in an increase in the sliding capacity between the sheets.

It is apparent from Figures 8.48 to 8.55 and the parameters α and β obtained from regression analysis (see Table 8.8) that the rate of change of the total deformation per unit stress (compliance) obtained by experiment follows the trend expressed by equation (8.1). In each case, the power function parameters were determined with a correlation coefficient greater than 0.90. This has implications for models of long-term creep developed from early age data. The basic compliance equation can be obtained by simple integration of equation (8.1).

$$J(t,t_o)=\frac{\alpha}{1+\beta}(t-t_o)^{1+\beta} \qquad (8.2)$$

Table 8.8: Parameters α and β obtained from regression analysis

Pre-treatment regimes	α	β	Correlation coefficient
Saturated (first state)	10.10	-0.77	0.94
Re-saturated from D-dried state	11.41	-0.72	0.97
Re-saturated from drying at 37°C	12.45	-0.72	0.97
Re-saturated from 42% RH	14.32	-0.66	0.90
D-dried	7.96	-0.89	0.94
Vacuum-dried at 37°C for 24 hours	6.96	-0.86	0.93
Methanol vacuum-dried at 37°C	42.00	-0.94	0.98
Isopropanol vacuum-dried at 37°C	43.96	-0.80	0.95

Experiments by Ulm et al. (1999) on concrete showed the same trend of compliance rate with time except that, in equation (8.1), the parameter β was chosen to be equal to -1 and the parameter α was the only variable. The range of variation for the β parameter in this study is small i.e. 0.66-0.94. The assumption that α is the only variable seems reasonable. The variation in α (Table 8.8) indicates that methanol and isopropanol exchanged specimens behave quite differently from the others. Ulm's results showed that the specific creep rate was independent of loading age and degree of hydration. An important observation supporting this was the co-linearity of the log creep rate-log time curves. It was also demonstrated that the long-term aging effect was characterized by a decrease of the creep rate that was proportional to the inverse of the material age. This would seem to suggest that the rate determining mechanism is associated with the behavior of C-S-H sheets themselves; perhaps involving a slipping and sliding process (see Figure 8.47). Despite the similarity between the compliance rates of both cement paste and concrete samples, more experimental data are needed in order to consider modeling the long-term creep of concrete specimens from early creep data collected on hcp samples.

The creep rate is more pronounced for the methanol-treated specimens at early ages after loading. Isopropanol-treated specimens creep more than methanol treated specimens but have a similar creep rate after a few weeks. Both these solvents appear to alter the structure of cement paste.

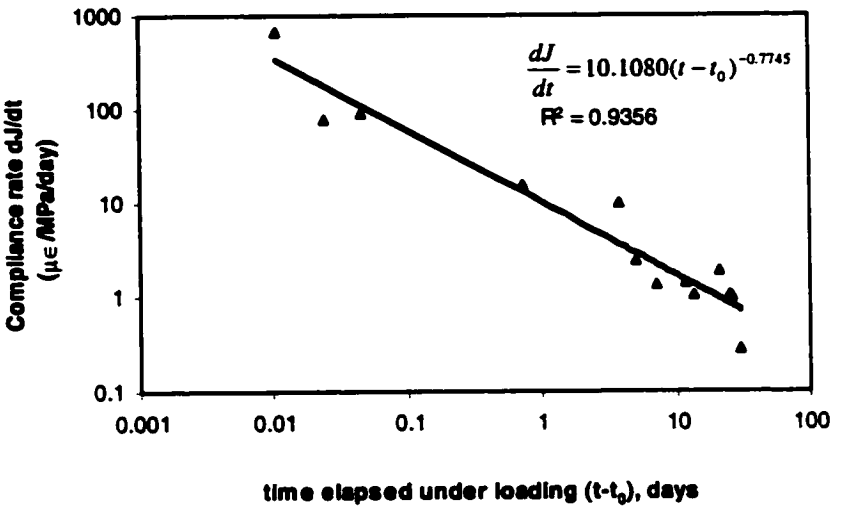

Figure 8.48: Basic compliance rate of untreated hardened cement paste (w/c=0.50)

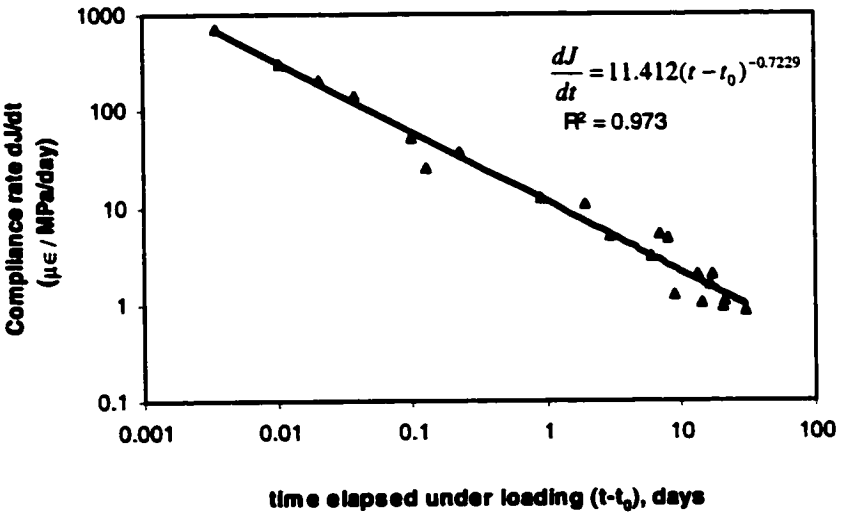

Figure 8.49: Basic compliance rate of hardened cement paste (w/c=0.50) D-dried then re-saturated

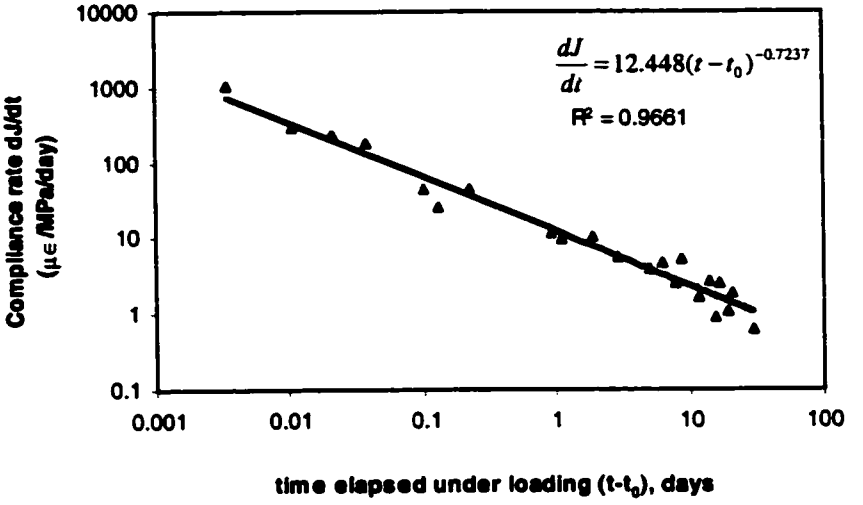

Figure 8.50: Basic compliance rate of hardened cement paste (w/c=0.50) vacuum dried at 37°C for 24 hours then re-saturated

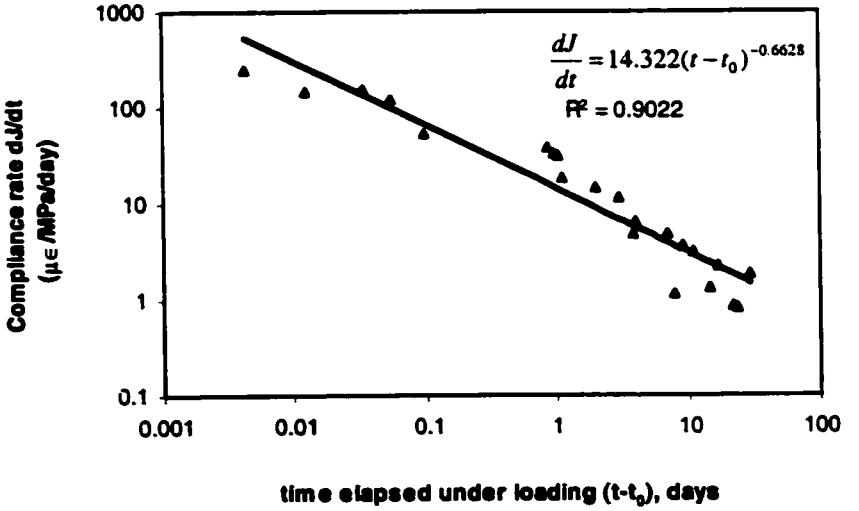

Figure 8.51: Basic compliance rate of hardened cement paste (w/c=0.50) conditioned at 42% relative humidity then re-saturated

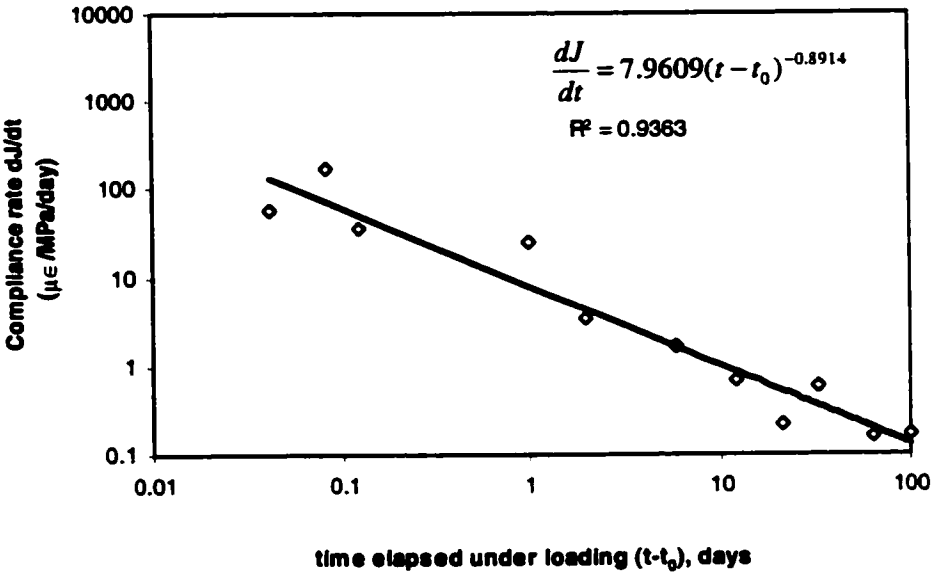

Figure 8.52: Basic compliance rate of hardened cement paste (w/c=0.50) vacuum dried at 105°C for 3 hours (D-dried)

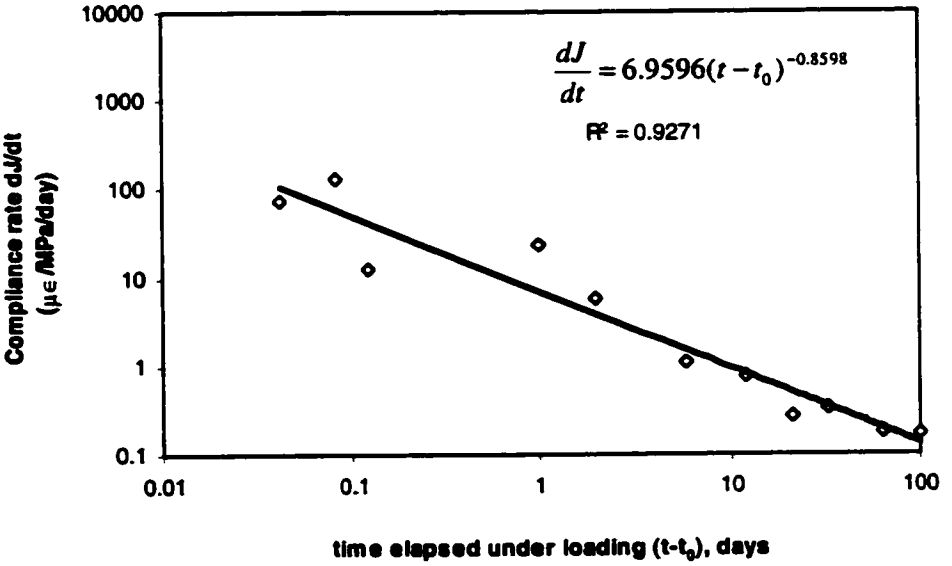

Figure 8.53: Basic compliance rate of hardened cement paste (w/c=0.50) vacuum dried at 37°C for 24 hours

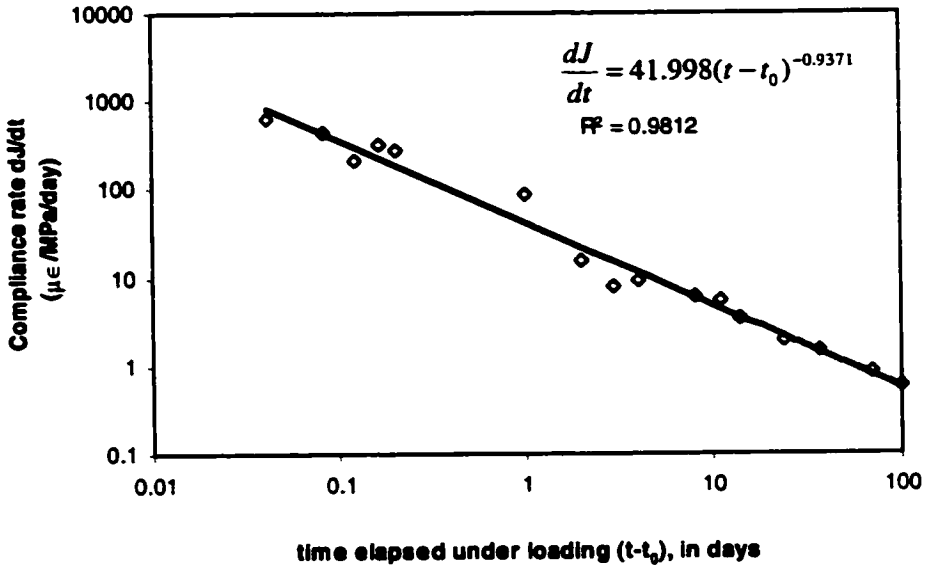

Figure 8.54: Basic compliance rate of hardened cement paste (w/c=0.50) vacuum dried at 37°C for 24 hours after immersion in methanol for 48 hours

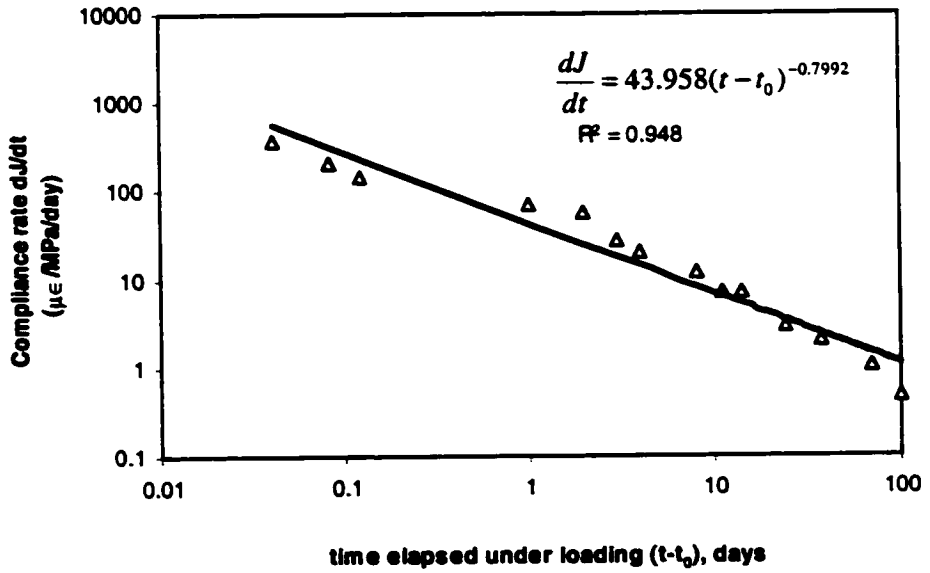

Figure 8.55: Basic compliance rate of hardened cement paste (w/c=0.50) vacuum dried at 37°C for 24 hours after immersion in isopropanol for 48 hours

8.4 Coupled AC impedance - creep and shrinkage

Coupled AC impedance - creep and shrinkage experiments were performed on very young specimens of hardened cement paste (18, 24 and 30 hours old) as well as mature specimens (2 years old). The investigations of young specimens were made on cement paste having 0.35 and 0.50 water cement ratios while those of mature specimens were made on paste with 0.50 water cement ratio.

For the mature paste, samples were re-saturated with synthetic pore solution having the same resistivity as that of the natural pore solution. In all cases, the elapsed time under load was 3 days and the recovery period after the removal of the load was 2 days in an environmentally controlled cabinet at (96 ± 2)% relative humidity. This relative humidity range was the maximum achievable with the controlled environmental set-up design for these coupling experiments.

8.4.1 Pre-drying

The initial pore solution conductivity was determined by extracting pore fluid from the cement paste using a hydraulic press and collecting it in a syringe. Measurements were taken using a conductivity probe. A synthetic pore solution was prepared using saturated lime water to which potassium chloride was added to obtain the same resistivity as that of the pore solution of the cement paste. Only the untreated and three pre-treated specimens from those presented in Table 8.1 were used for the present investigation. The pre-treatment of the specimens is described as follows:

Treatment 1 (Drying at 37°C): Samples were initially saturated surface dried, vacuum dried at 37°C for 24 hours and then re-saturated under vacuum for 18 hours. Prior to the re-saturation process, the samples were vacuum dried for 3 hours in a desiccator at $1x10^{-4}$ mm Hg.

Treatment 2 (Methanol Exchange): Water saturated samples were soaked in methanol for 48 hours, vacuum dried at 37°C for 24 hours, then re-saturated under vacuum for 18 hours. Prior to the re-saturation process, the samples were vacuum dried for 3 hours in a desiccator at $1x10^{-4}$ mm Hg.

Treatment 3 (Isopropanol Exchange): Water saturated samples were soaked in isopropanol for 48 hours, vacuum dried at 37°C for 24 hours, then re-saturated under vacuum for 18 hours. Prior to

the re-saturation process, the samples were vacuum dried for 3 hours in a desiccator at $1x10^{-4}$ mm Hg.

8.4.2 Thermal analysis

The derivative thermogravimetric analysis (DTGA) curves performed on mature specimens were all presented previously in Figure 8.6 following the pre-treatment regimes just mentioned. These curves provide an appreciation of the initial moisture state of the specimen prior to loading. As already observed in Section 8.2.1.2, pre-treatment (heat or solvent exchange) appears to perturb the C-S-H structure.

From thermogravimetric analysis data the degree of hydration of Portland cement paste while hardening was determined for loaded and unloaded very young samples. Powers and Brownyard (1948), define the degree of hydration as the ratio of non-evaporable water content of the cement paste at time t and the non-evaporable water content at the complete hydration of the cement paste (at $t=\infty$). For a typical Portland cement paste, the latter is generally about 25% by mass of the cement content while bound water at time t is determined by the mass loss of the paste heated between 105°C and 1050°C. The degrees of hydration as well as CH content are presented in Tables 8.9 and 8.10 for 0.35 and 0.50 water-cement ratio hardening cement pastes respectively.

Other definitions of bound water have been proposed by Danielsson (1966) giving slightly different results. In the present study small variations in the degree of hydration are not significant, as it is the time dependent changes that are of interest.

It appears from Table 8.10 that the loading of samples at very early age, 18 hours or less can increase the hydration (compared to that of unloaded samples) of ordinary hardening cement paste (w/c=0.50). After 24 hours of hydration or greater, the loading shows a negative effect on the degree of hydration for 0.35 and 0.50 water-cement ratio pastes at various hardening times.

Table 8.9: Degree of hydration and $Ca(OH)_2$ content of hardening cement paste (w/c=0.35) loaded at 18, 24 and 30 hours at stress/strength ratio of 0.3.

Age	Unloaded sample		Loaded sample	
	Degree of hydration	$Ca(OH)_2$ content	Degree of hydration	$Ca(OH)_2$ content
18h	0.54	0.068	0.54	0.068
24h	0.64	0.073	0.57	0.072
30h	0.65	0.079	0.62	0.078
42h	0.74	0.080	0.66	0.080
24h	0.65	0.078	0.65	0.078
36h	0.71	0.080	0.67	0.083
48h	0.77	0.084	0.70	0.087
72h	0.84	0.091	0.78	0.089
30h	0.67	0.081	0.67	0.081
54h	0.79	0.086	0.77	0.088
78h	0.82	0.089	0.79	0.088
102h	0.88	0.088	0.81	0.090

Table 8.10: Degree of hydration and $Ca(OH)_2$ content of hardening cement paste (w/c=0.50) loaded at 18, 24 and 30 hours at stress/strength ratio of 0.3.

Age	Unloaded sample		Loaded sample	
	Degree of hydration	$Ca(OH)_2$ content	Degree of hydration	$Ca(OH)_2$ content
18h	0.50	0.064	0.50	0.064
24h	0.55	0.068	0.79	0.076
30h	0.63	0.075	0.86	0.077
42h	0.73	0.079	0.88	0.083
24h	0.60	0.075	0.60	0.075
36h	0.70	0.079	0.69	0.078
48h	0.72	0.086	0.71	0.084
72h	0.81	0.093	0.78	0.089
30h	0.61	0.080	0.61	0.080
54h	0.80	0.087	0.73	0.085
78h	0.78	0.090	0.79	0.088
102h	0.80	0.092	0.77	0.093

8.4.3 Strains and impedance spectra

8.4.3.1 Mature cement pastes

The total strain-time curves for the cement paste specimens (w/c=0.50, stress-strength ratio=0.30) under sustained load at 96% RH are presented in Figure 8.56. The rate of change of total strain in the first 20 hours is lower for the saturated control specimens than the rates for specimens dried by heating or solvent exchange plus heating. The total strain at 72 hours is 320, 450, 515 and 600 $\mu\epsilon$ for the control specimens and those dried at 37°C, solvent exchanged with isopropanol and solvent exchanged with methanol respectively prior to re-saturation with pore solution. Strain recovery for the control specimens and those dried at 37°C or exchanged with isopropanol prior to re-saturation with pore solution is about 100 $\mu\epsilon$. The value of strain recovery for the methanol exchanged specimen is about 200 $\mu\epsilon$. The increase in total deformation of the dried (37°C) or solvent exchanged specimens may be partly due to the pore coarsening effect. However, substantial evidence has been presented that indicates methanol perturbates (interacts with) the solid (Beaudoin, 1987). Nevertheless the collapse of the C-S-H structure on drying prior to re-saturation may occur to a lesser extent for pastes that have undergone solvent exchange. This may be a reason for the higher strain values observed.

The shrinkage behavior of the re-saturated cement paste in the first few hours is similar for all drying pre-treatments (Figure 8.57). The isopropanol exchanged specimens re-saturated with pore solution and the control specimen shrink about 150-160 $\mu\epsilon$ after 120 hours. The re-saturated methanol exchanged specimens and those dried to 37°C before re-saturation shrink about 300 and 275 $\mu\epsilon$ at 120 hours respectively. The bulk of the shrinkage takes place in the first 20 hours for all specimens. Methanol exchanged results in both the largest total strain and shrinkage for these specimens.

The drying creep curves (total strain - shrinkage strain) are plotted in Figure 8.58. Solvent exchange and drying at 37°C prior to re-saturation results in significantly larger creep (e.g. at 72 hours). Isopropanol and methanol exchanges result in creep of 325 and 280 $\mu\epsilon$ respectively. The specimens dried at 37°C have creep values of about 265 $\mu\epsilon$. The control saturated specimens have a creep value of about 160 $\mu\epsilon$, considerably less than the treated specimens.

Creep recovery at 120 days is 110, 170, 230, 125 $\mu\epsilon$ for control specimens and those treated by 37°C drying, methanol and isopropanol exchanges. Methanol exchange results in the largest total strain, the largest shrinkage and the largest creep recovery. Creep of methanol exchanged specimens is also large and approaches that of the isopropanol exchanged specimens.

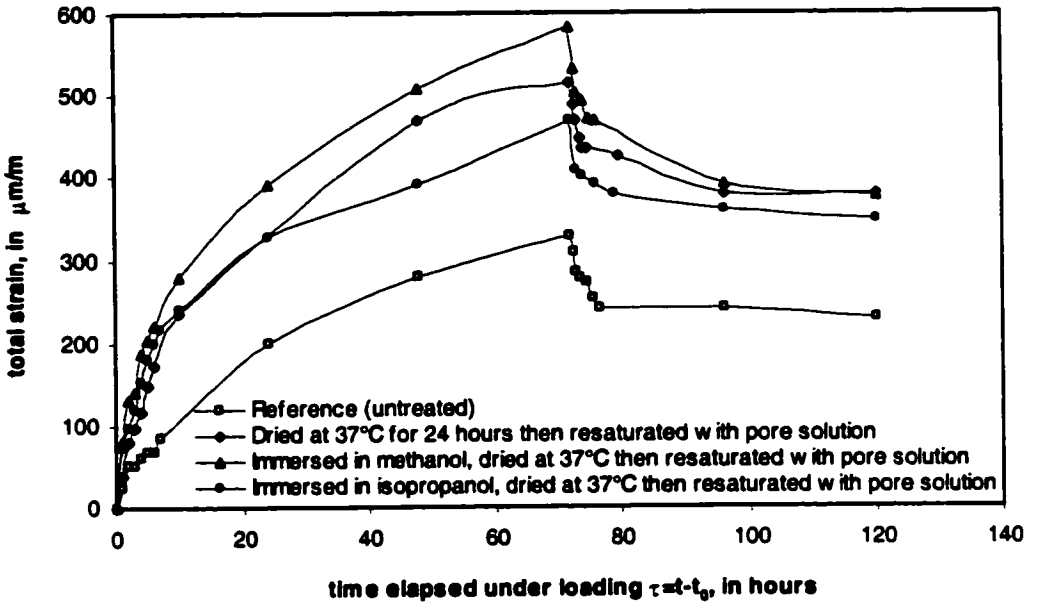

Figure 8.56: Total strain (creep + shrinkage) and strain recovery of hardened cement paste (w/c=0.50) conditioned at about 96% RH after re-saturation with synthetic pore solution following different drying pre-treatments

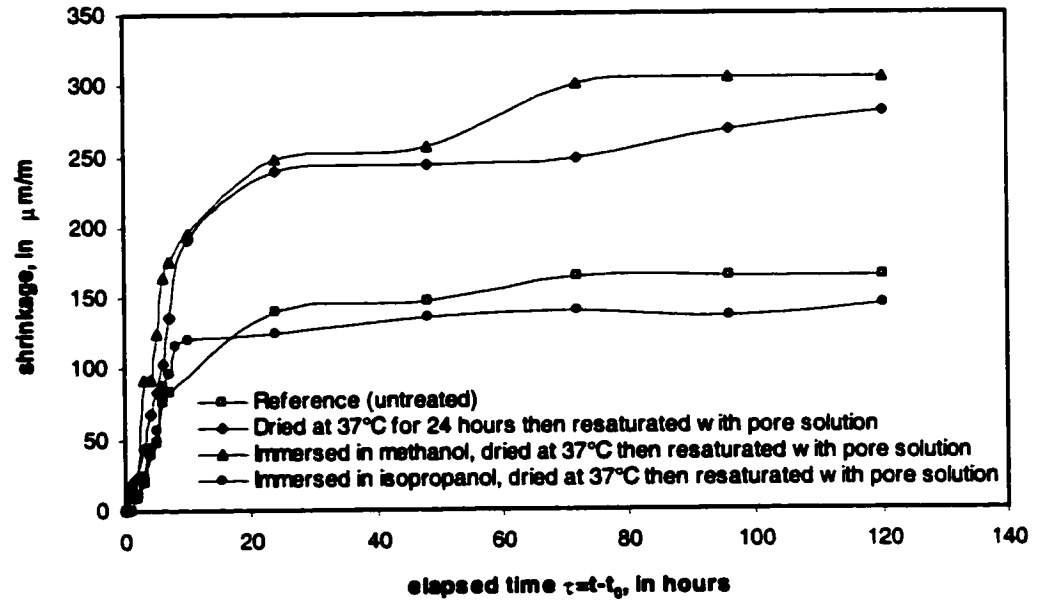

Figure 8.57: Shrinkage of hardened cement paste (w/c=0.50) conditioned at about 96% RH after re-saturation with synthetic pore solution following different drying pre-treatments

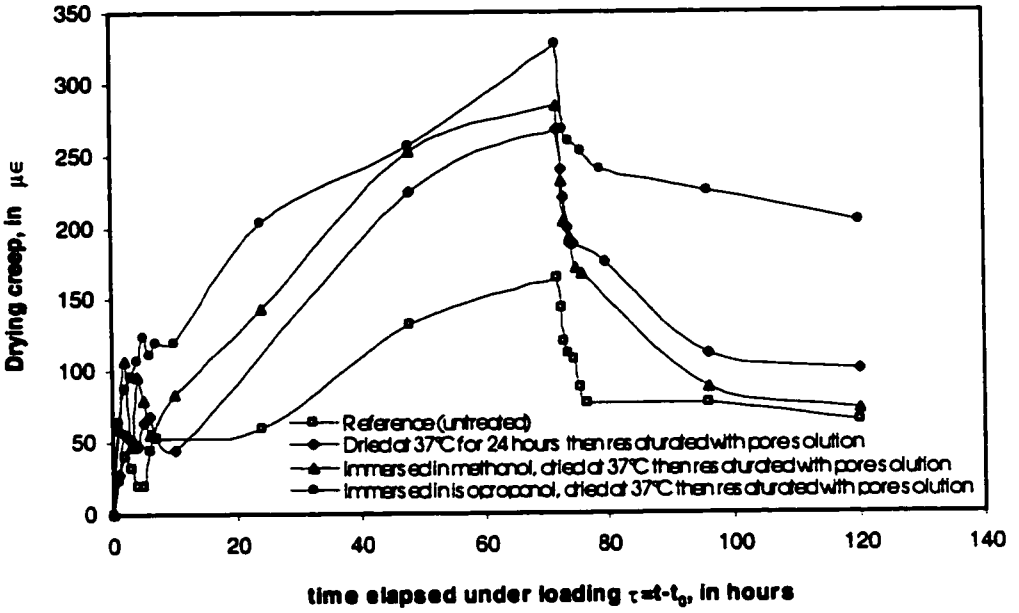

Figure 8.58: Drying creep of hardened cement paste (w/c=0.50) conditioned at about 96% RH after re-saturation with synthetic pore solution following different drying pre-treatments

A.C. Impedance spectra (real-time) were obtained at 96% RH for unloaded and loaded cement paste specimens for all four pre-treatment conditions. The magnitude of the high frequency resistance (HFR) and the size of the high frequency arc diameter (HFA) have been attributed to the properties of the pore solution, pore size and pore network (McCarter and Curran, 1984; Xu et al., 1993; Gu et al., 1993). Only the information provided by HFA will be presented and discussed in this paper. Figures 8.59 and 8.60 are Nyquist plots for shrinkage and total strain of untreated saturated specimens. The shift observed at the beginning of the plot is not related to the material structure but instead to the acquisition system. The shrinkage of the untreated specimens however show two stages of high frequency arc diameter which may be explained by the fact that the non altered paste structure may have discontinuous pore network acting as two different capacitors while drying. The second arc stage disappear with the loading of the specimens. Re-saturation with synthetic pore solution following pre-treatments prevent the second arc stage to form. Plots for all the three pre-treatments are similar in character and are shown in Figures 8.61 to 8.66. The size of the high-frequency arc increases with time (up to 72 hours) in both cases for all pre-treatments. The growth of the high-frequency arc is also consistent with loss of moisture

accompanying shrinkage. About six percent (by mass of D-dried paste) capillary water is lost at 96% RH. The size of the high-frequency arcs for the unloaded specimens is significantly greater than the corresponding arcs (at each specific time) for the loaded specimens.

The growth of the high-frequency arc diameter (total strain conditions) for all the specimens subjected to the four pre-treatments is plotted in Figure 8.67. The size of the arc at 72 hours is in the following order: Untreated > isopropanol exchanged > methanol exchanged > drying at 37°C. The total strain (Figure 8.56) was in the following order: methanol exchanged > drying at 37°C > isopropanol exchanged > untreated. These results are consistent with the relative pore coarsening effects (described earlier) due to the pre-drying treatments. The fact that the methanol exchanged specimens and those pre-dried at 37°C exhibited the smallest arcs and largest total strains suggests that pore coarsening affects these samples to a greater extent. Pore coarsening and subsequent re-saturation reduces overall resistivity relative to the untreated specimen (Beaudoin et al., 1998).

It is suggested that the smaller arc sizes for the total strain sequences (compared to shrinkage) are indicative of processes involving displacement (slipping and sliding) of C-S-H sheets induced by the applied load. This suggestion is supported by the observation that creep of cement paste occurs even in the dry state as already demonstrated in the previous section (Figure 8.46). Previous work has shown that loading cement paste up to about 50 percent of the maximum load did not significantly affect the size of the high frequency arc (Gu et al., 1993). This suggests that microcracking process had little effect on the a. c. impedance response (stress/strength ratio ≈ 0.30) obtained in these experiments.

Figure 8.68 is a plot of the difference in high-frequency arc diameter between the shrinkage and the total strain impedance spectra at corresponding times. The differences reflect the effect of the applied load on creep. There is generally an increase in the difference with time (except at early times (up to 4 hours) for the isopropanol exchanged specimens). At 24 hours the differences are in the following order: methanol exchanged > isopropanol exchanged > untreated > pre-drying at 37°C. The large differences for the methanol and isopropanol exchanged samples are consistent with the large relative creep observed for these specimens. There may be an enhanced tendency for the relative displacement of the C-S-H sheets at the microstructural level. The early decrease in arc diameter difference with time for the isopropanol exchanged specimens suggests that sliding-slipping processes affecting displacement of the C-S-H sheets may be delayed. In this case it would appear that some pore compression (pore size reduction) may occur in the early stages.

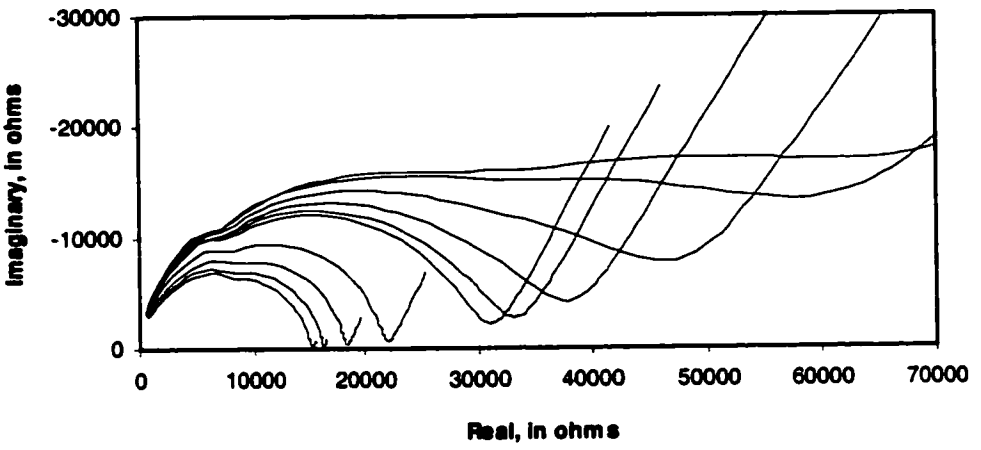

Figure 8.59:AC impedance spectra: shrinkage of untreated hcp (w/c=0.50) specimens conditioned at about 96% RH for 0, 1, 2, 3.7, 6.5, 9, 12.7, 24, 48 and 72 hours

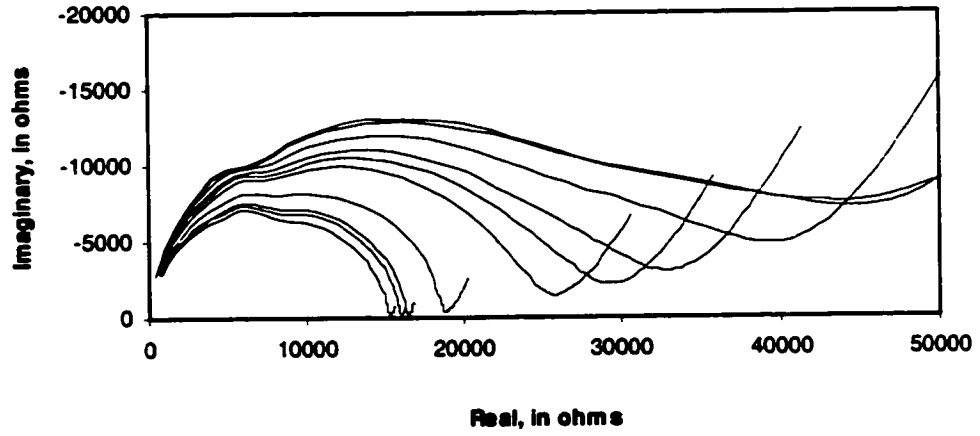

Figure 8.60:AC impedance spectra: total strain of untreated hcp (w/c=0.50) specimens conditioned at about 96% RH for 0, 1, 2, 3.7, 6.5, 9, 12.7, 24, 48 and 72 hours

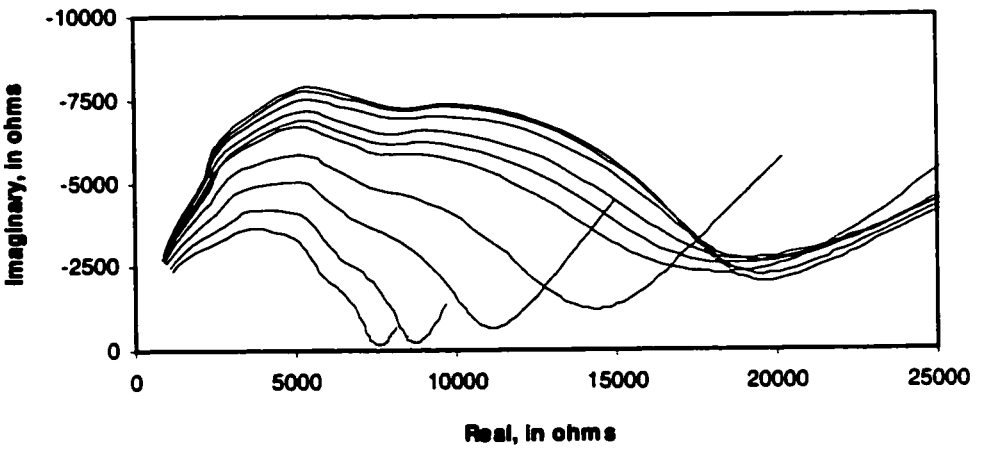

Figure 8.61:AC impedance spectra: shrinkage of hcp (w/c=0.50) dried at 37°C and re-saturated with synthetic pore solution; specimens conditioned at about 96% RH for 0, 1, 2, 3.7, 6.5, 9, 12.7, 24, 48 and 72 hours

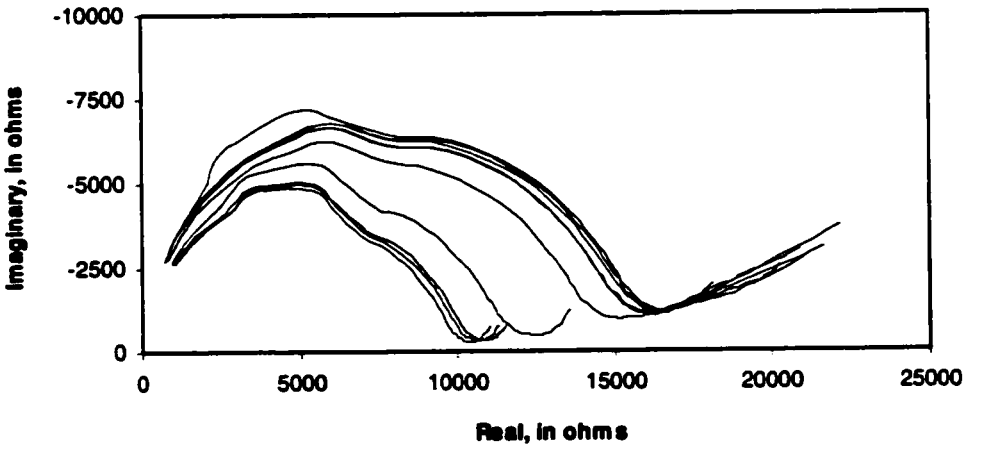

Figure 8.62:AC impedance spectra: total strain of hcp (w/c=0.50) dried at 37°C and re-saturated with synthetic pore solution; specimens conditioned at about 96% RH for 0, 1, 2, 3.7, 6.5, 9, 12.7, 24, 48 and 72 hours

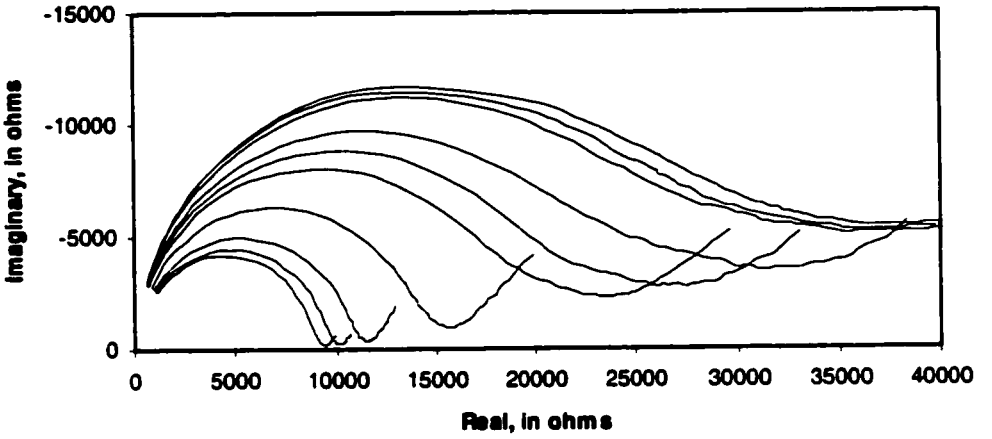

Figure 8.63:AC impedance spectra: shrinkage of hcp (w/c=0.50) methanol soaked vacuum dried at 37°C and re-saturated with synthetic pore solution; specimens conditioned at about 96% RH for 0, 1, 2, 3.7, 6.5, 9, 12.7, 24, 48 and 72 hours

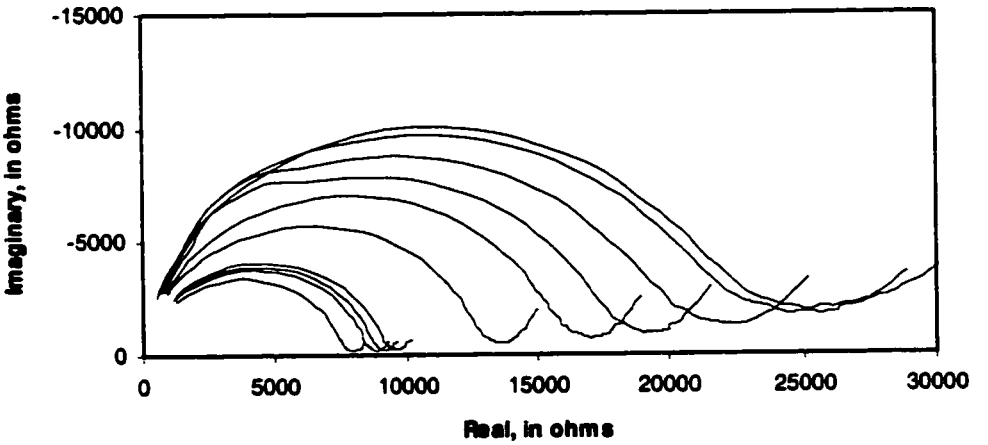

Figure 8.64:AC impedance spectra: total strain of hcp (w/c=0.50) methanol soaked vacuum dried at 37°C and re-saturated with synthetic pore solution; specimens conditioned at about 96% RH for 0, 1, 2, 3.7, 6.5, 9, 12.7, 24, 48 and 72 hours

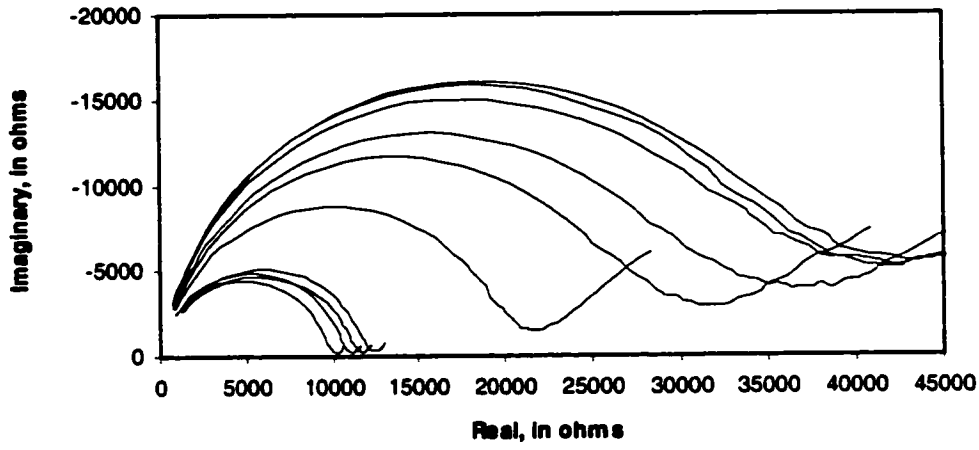

Figure 8.65:AC impedance spectra: shrinkage of hcp (w/c=0.50) isopropanol soaked vacuum dried at 37°C and re-saturated with synthetic pore solution; specimens conditioned at about 96% RH for 0, 1, 2, 3.7, 6.5, 9, 12.7, 24, 48 and 72 hours

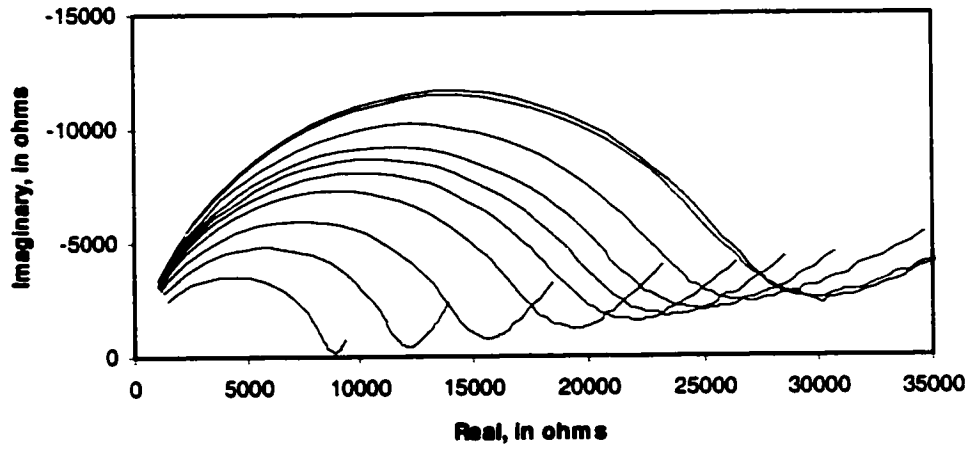

Figure 8.66:AC impedance spectra: total strain of hcp (w/c=0.50) isopropanol soaked vacuum dried at 37°C and re-saturated with synthetic pore solution; specimens conditioned at about 96% RH for 0, 1, 2, 3.7, 6.5, 9, 12.7, 24, 48 and 72 hours

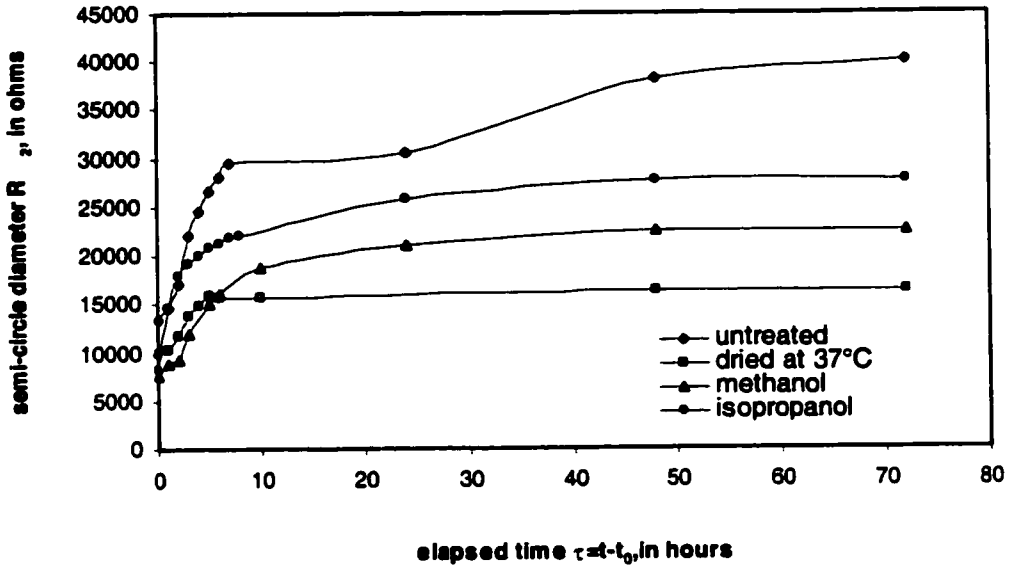

Figure 8.67: High frequency-arc diameter R_2 following re-saturation of several pre-treated cement pastes during a total strain (creep + shrinkage) test at about 96% RH

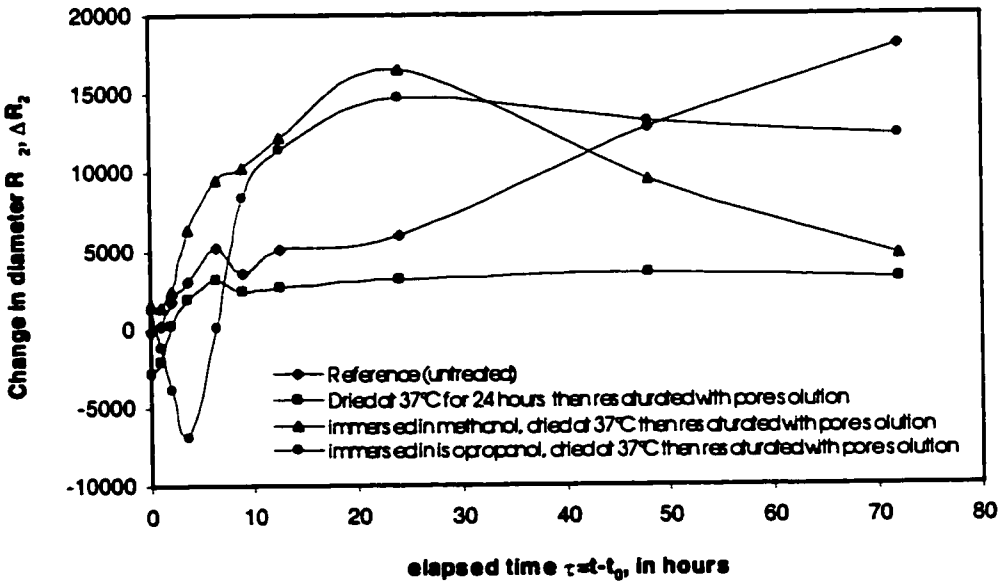

Figure 8.68: Difference between shrinkage and total strain (creep + shrinkage) high-frequency arc diameter R_2 following re-saturation of several pre-treated cement pastes conditioned at about 96% RH

The depression angle parameter n=1-θ_d is plotted against time for the cement paste specimens in Figure 8.69. The initial value of n is in the following order: untreated > methanol exchanged > isopropanol exchanged > pre-drying at 37°C. The order remains the same after the first few hours with the exception of n for the untreated specimen which decreases rapidly between 2 and 6 hours reaching a value significantly lower than for the treated specimens. This suggests that initially the drying treatments perturbate (increase the roughness) the surface. It has been suggested that grain boundary effects in polycrystalline materials contribute to the arc depression (Mulder and Sluyters, 1988). The dependence of the arc depression has also been linked to fractal characteristics of the surfaces (Pajkassis and Nyikos, 1986; Brug et al., 1984). The low values of drying creep for the untreated specimens may be related to the low values of the depression angle parameter. As previously stated a broader pore size distribution would result in a wide spread of relaxation times corresponding to a larger depression angle. The low value of creep for the untreated specimen is consistent with a broader pore size distribution (no pore coarsening) and hence larger depression angle (smaller values of n). The fractal nature of the surface may affect the slipping-sliding behavior of the C-S-H sheets in cement paste under load. The relative magnitude of the creep of methanol and isopropanol exchanged specimens corresponds to a higher value of the depression angle parameter, n. This is consistent with smaller depression angles and a narrower pore size distribution (pre-treatment leads to significant pore coarsening).

The specific total strain rate versus time is plotted as a log-log relation in Figure 8.70. As previously defined by the equation (8.1), two straight lines describe the data. The line for the untreated control specimens lies below a line representative of the other specimens. Ulm et al. (1999) had demonstrated that the specific creep rate is independent of loading time and degree of hydration. An important observation supporting this was the co-linearity of the log creep rate-log time curves. It was also demonstrated that the long-term aging effect was characterized by a decrease of the creep rate that was proportional to the inverse of the material age. This would appear to suggest that the rate determining mechanism is associated with the behavior of the C-S-H sheets themselves, perhaps involving a slipping and sliding process. This is supported by the previous observation that D-dry cement paste specimens were found to exhibit significant creep.

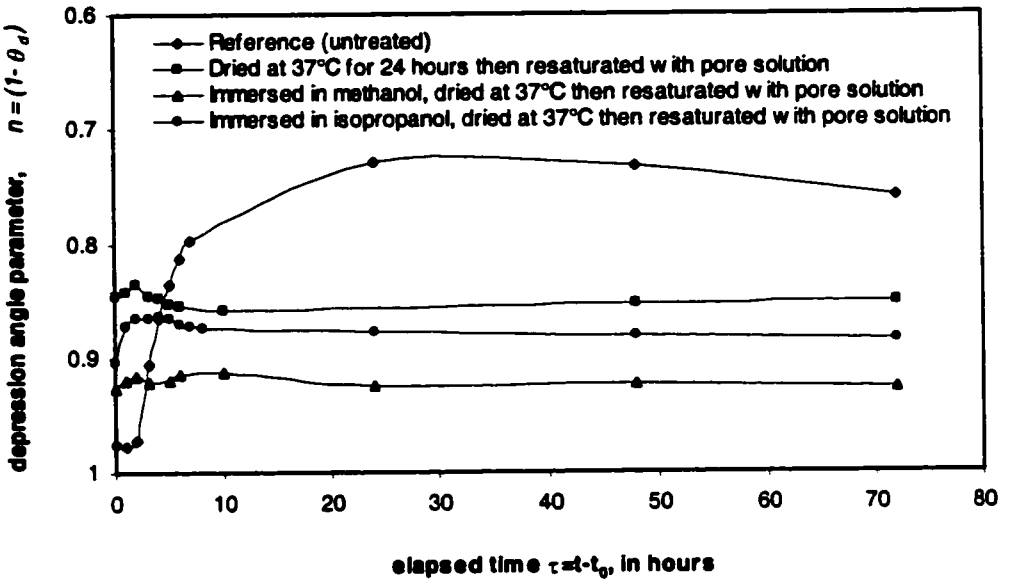

Figure 8.69: Depression angle parameter of high-frequency arc following re-saturation of hardened cement paste (w/c=0.50) after several drying conditions during total strain (creep + shrinkage) test at about 96% RH

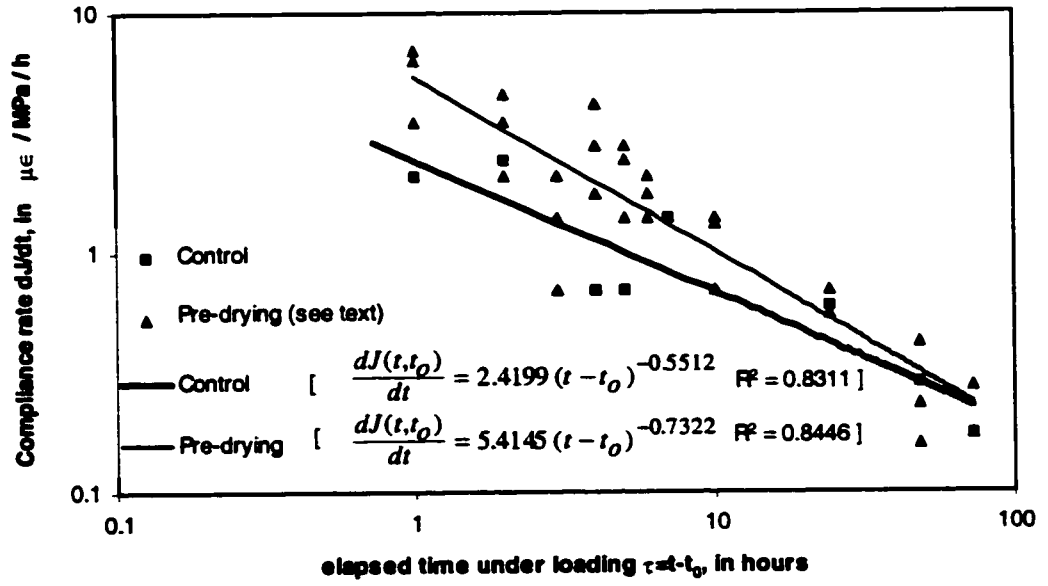

Figure 8.70: Compliance rate of hardened cement paste (w/c=0.50) conditioned at about 96% relative humidity after re-saturation from different drying pre-treatments

8.4.3.2 Very young cement pastes

The total strain-time curves for the very young cement paste specimens (w/c=0.35 and 0.50, stress-strength ratio=0.30) under sustained load at 96 ± 2% RH are presented in Figures 8.71 and 8.72. The rate of change of total strain in the first 18 hours seems to be similar for the ordinary cement paste (w/c=0.50) loaded at 18, 24 and 30 hours old. The high strength cement paste (w/c=0.35) shows the rate of change of total strain increasing with the age of the paste at loading. The total strain after 3 days of loading at age of 18, 24 and 30 hours is 811, 1153, 2248 $\mu\epsilon$ for high strength specimens and 1646, 1614, 1297 $\mu\epsilon$ for normal strength specimens respectively. Strain recovery for the high strength cement paste specimens loaded at 18, 24 and 30 hours old is 384, 356 and 1080 $\mu\epsilon$ respectively while that of normal strength specimens is 484, 416 and 380 $\mu\epsilon$ respectively. The increase in total deformation of the high strength cement paste (particularly the 30 hours old specimens) may be partly due to the larger volume fraction of the hydrated product leading to an increase in creep sites as the hydration progress.

The relatively high shrinkage rate and magnitude of the 30 hours old high strength specimens (see Figure 8.73) may also contribute to the high value of the total strain. This may be due to "Pickett effect", which is defined as the induced creep rate caused by the tensile stresses due to shrinkage. It particularly takes place if an abnormal variation in the environmental conditions (temperature and/or humidity) occurs. The swelling has also been observed by Vernet and Cadoret (1991) between 4 to 20 hours. It has been attributed to the precipitation of some coarse crystals during the setting period (Vernet et al., 1991). This behavior was observed for the w/c=0.50 specimens particularly for the 18 hours old paste as shown in Figure 8.74.

Both high and normal strength pastes exhibit at very early ages an increase in shrinkage strain values with an increase in the age of the specimens. After three days the shrinkage strain for the high strength cement paste specimens loaded at 18, 24 and 30 hours old is 152, 176 and 248 $\mu\epsilon$ respectively while that of normal strength specimens is 20, 80 and 260 $\mu\epsilon$ respectively. Substantial evidence has been presented that indicates that the shrinkage of young concrete is higher as the water/cement ratio is lower (de Larrard and Acker, 1990). The high strength 18 hours old specimens do not show any swelling indicating that it either takes place earlier or it may be less of a factor in the behavior of high strength paste than in normal strength paste.

The creep strain per unit stress or compliance J of the high strength cement paste is lower at any age of loading compared to that of normal strength specimens (see Figures 8.75 and 8.76). For high strength paste (w/c=0.35) the specimens loaded at 30 hours old show a significant compliance rate and magnitude with a behavior totally different from the normal strength paste

(w/c=0.50) in which the magnitude of creep or compliance decreases with the increase of the age at loading.

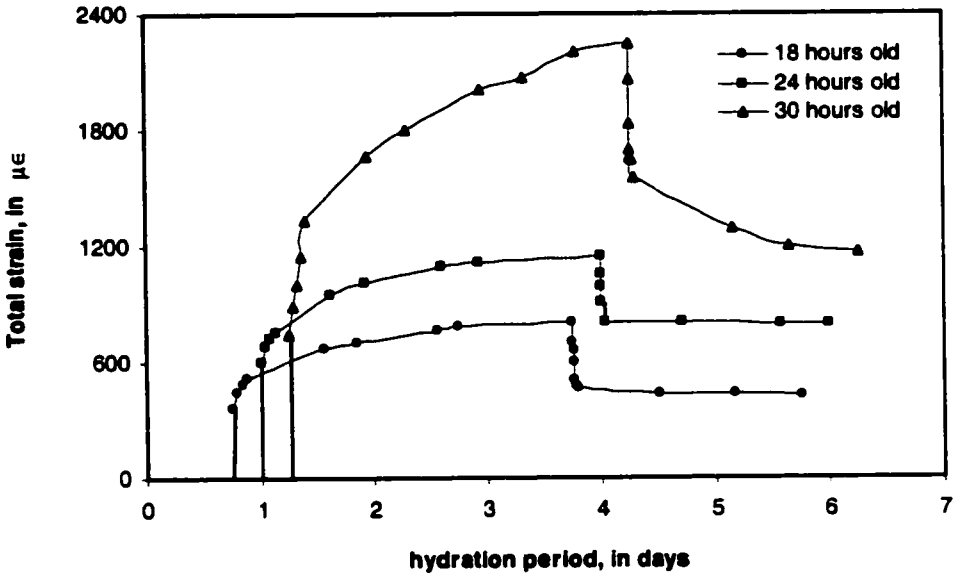

Figure 8.71: Total strain (creep+shrinkage) of hardened cement paste (w/c=0.35) while conditioning at 96% RH and loaded at different ages of hydration

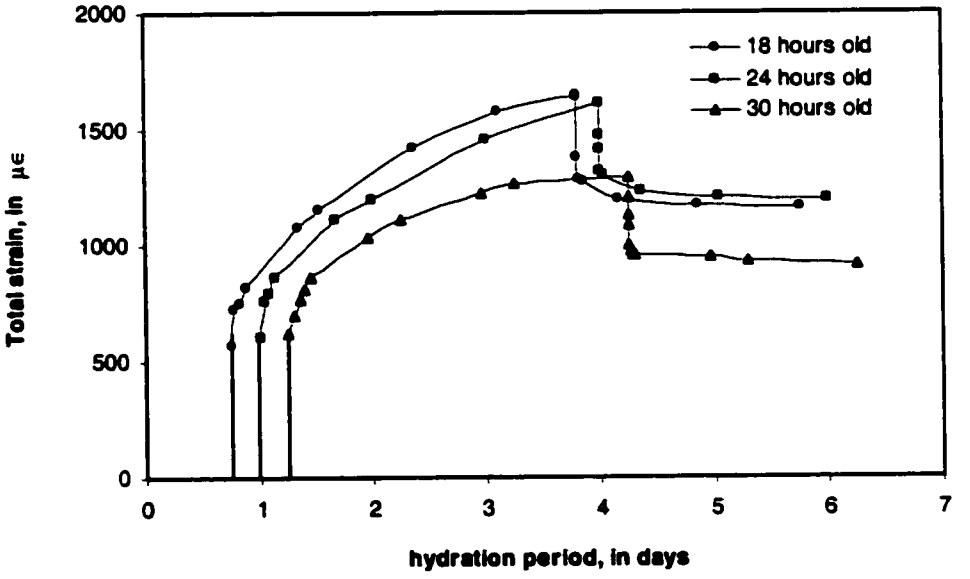

Figure 8.72: Total strain (creep+shrinkage) of hardened cement paste (w/c=0.50) while conditioning at 96% RH and loaded at different ages of hydration

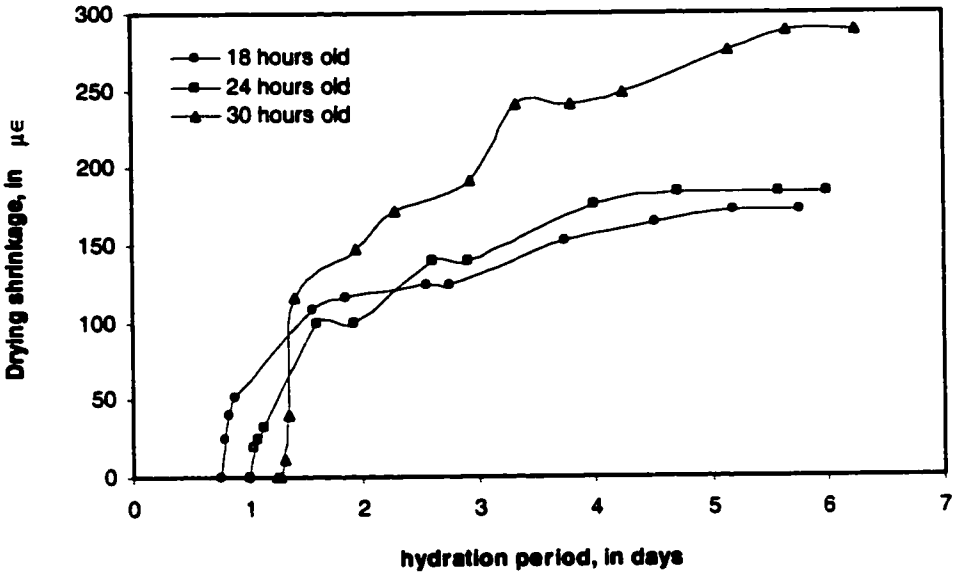

Figure 8.73: Shrinkage of hardened cement paste (w/c=0.35) while conditioning at 96% RH at different ages of hydration

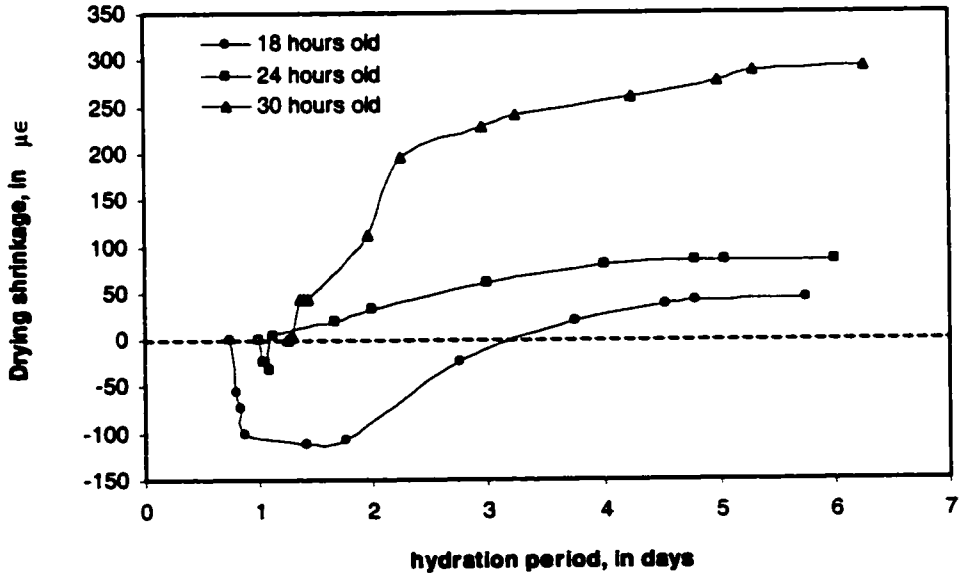

Figure 8.74: Shrinkage of hardened cement paste (w/c=0.50) while conditioning at 96% RH at different ages of hydration

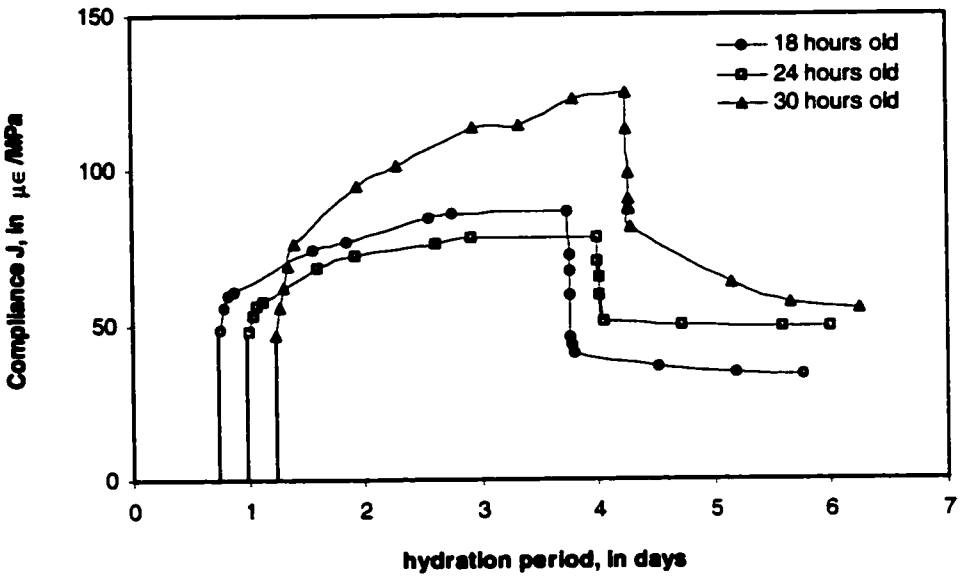

Figure 8.75: Compliance J of hardened cement paste (w/c=0.35) while conditioning at 96% RH and loaded at different ages of hydration

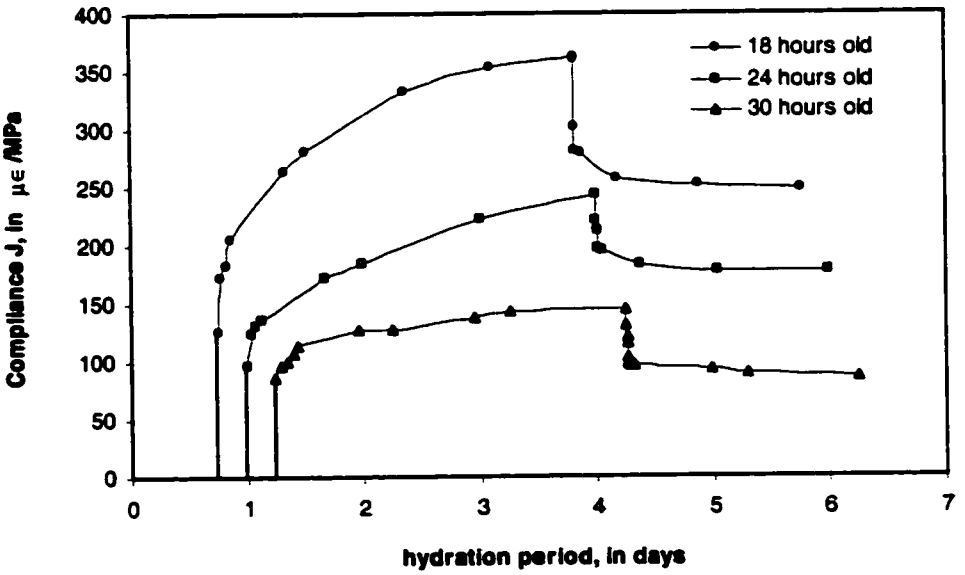

Figure 8.76: Compliance J of hardened cement paste (w/c=0.50) while conditioning at 96% RH and loaded at different ages of hydration

The compliance recovery of the normal strength paste (w/c=0.50) also decreases with the age at loading (see Figure 8.76).

There may be two factors governing the magnitude of compliance: degree of hydration and porosity. These factors are controlled by the water-cement ratio. The creep process may have a greater dependence on the state of hydration (reflecting the contribution of the solid phase) of the hardening Portland cement paste in the case of the w/c=0.35 specimens. The increase of creep magnitude at early age seems to be related to the amount of C-S-H. The 18 hours old specimens of normal strength paste (w/c=0.50) and 30 hours old specimens of high strength paste (w/c=0.35) both undergo a considerable increase in the degree of hydration while under load (Tables 8.9 and 8.10). In such specimens, the large amounts of C-S-H (with respect to the loaded samples) signify the presence of a significant number of creep centers and consequently the development of a significant creep magnitude. The difference is that this is a less important effect at higher water-cement ratio as porosity is a dominant factor.

The compliance rate data of very young normal and high strengths specimens loaded at 18, 24 and 30 hours plotted against the elapsed time under loading is presented in Figures 8.77 and 8.78 respectively. The log-log scale curves obtained indicate a linear trend of the compliance rate similar to that previously presented in Figure 8.48 (see Section 8.3.3.2) for normal strength and mature hardened cement paste. The parameter α, which is the coefficient of the power function fitted to the curves in the figures decreases with the increase of the degree of hydration of the normal strength paste. The high strength paste does not show the same relation. This may be due to the high value of the magnitude of shrinkage and the corresponding total creep for the 30 hours old specimens.

During the first few days following loading of hardening Portland cement paste, creep may be largely dependent on the capillary porosity. There may also be space for load-induced hydration products to form especially at higher water-cement ratios. This may explain the high magnitude of compliance observed in normal strength paste compared to that of high strength specimens (see Figures 8.75 and 8.76 and earlier discussion). Further, the fact that both compliance magnitude and rate of the specimens are influenced by the degree of hydration while under load suggests that the rate-determining mechanism proposed by Wittmann (1982), may be effective i.e. the volume growth of C-S-H in the capillaries is related to an increase of creep centers. The water diffusion, which may occur after loading, may then have a significant effect on very young hardening cement paste and a lesser effect on more mature cement paste.

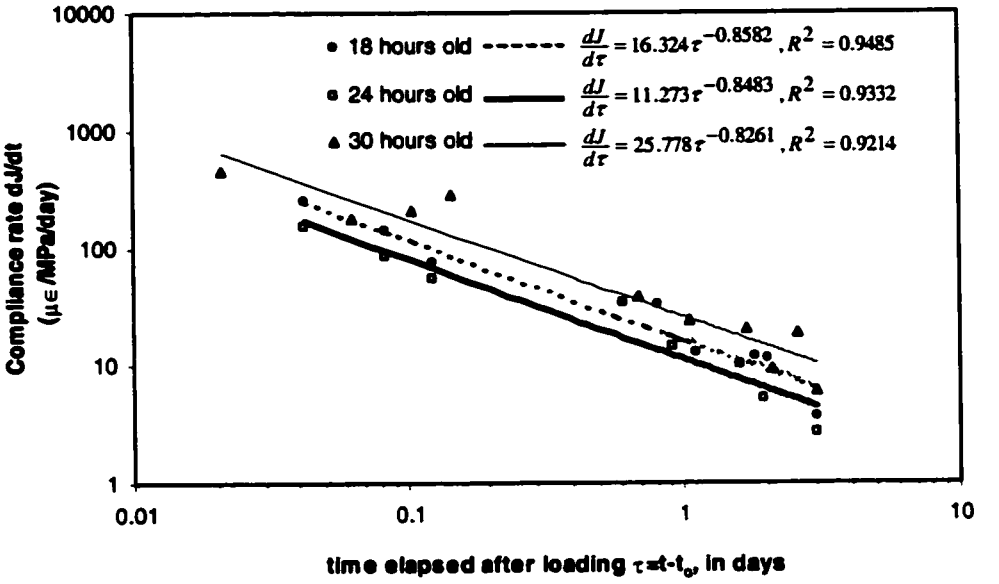

Figure 8.77: Compliance rate dJ/dt of hardened cement paste (w/c=0.35) while conditioning at 96% RH and loaded at 18, 24 and 30 hours of hydration

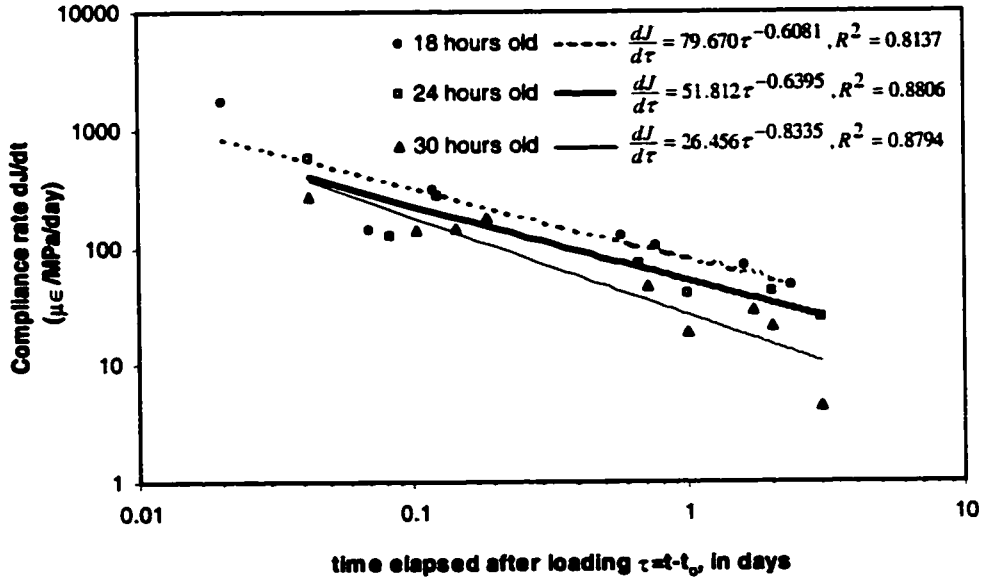

Figure 8.78: Compliance rate dJ/dt of hardened cement paste (w/c=0.50) while conditioning at 96% RH and loaded at 18, 24 and 30 hours of hydration

Analysis of the compliance rate curves obtained for very young and more mature cement pastes suggests that several factors may contribute to the magnitude of short-term creep. These include the water content of the paste or relative humidity and the quantity of C-S-H formed while under load. The sliding of C-S-H sheets may start at very early ages and may significantly contribute to the magnitude of short-term creep. It is therefore very important to determine the degree of hydration from loaded specimens, as hydration can be induced by the loading itself particularly in a very young normal strength cement paste.

The compliance rates of very young specimens (18, 24 and 30 hours old) and that of a mature 30 years old normal Portland cement paste are plotting in Figure 8.79. It can be seen that the overall rate (at early ages of loading) may become coincident with the fitted curve. The first segment can not considered to be due to the diffusion within the hardening matrix (Ulm et al., 1999) due to the coincidence of the data within 5 to 10 days. Water diffusion alone is not sufficient to explain the large and significant magnitude of creep observed on very young cement paste specimens (Bazant et al., 1997). Both the material age (t) and the elapsed time ($\tau=t-t_o$) under loading seem to be of importance with respect to the compliance rate of hardening cement paste.

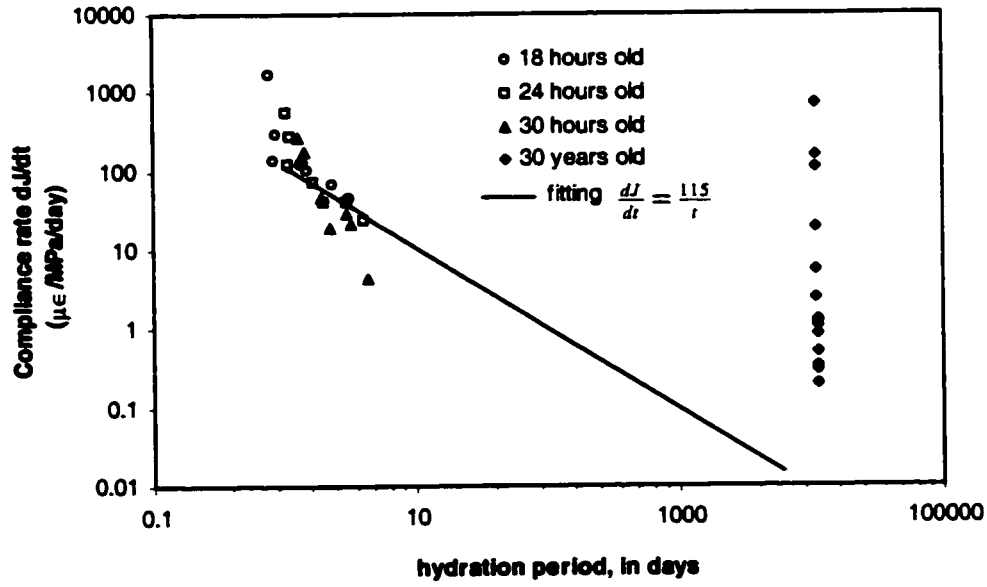

Figure 8.79: Compliance rate dJ/dt of hardened cement paste (w/c=0.50) while conditioning at 96% RH and loaded at 18, 24, 30 hours and 30 years of hydration

As schematically presented in Section 4.4, the creep strain is generally defined as the difference between the total strain and shrinkage. It can be expressed as follows in terms of the corresponding experimental compliance.

$$\varepsilon_c = \varepsilon - \varepsilon_{sh} = J(t,t_o).\sigma \qquad (8.3)$$

The stress σ is the applied compressive stress at the age $t=t_o$. At any given age of loading in the present study, σ corresponds to 30% of the compressive strength of the material at age of loading. Part of the creep strain (ε_c) represents the elastic strain (ε_{co}) and the other represents the time dependent induced strain (ε_{cc}) caused by sustained load σ. The equation (8.3) can then be rewritten as follows:

$$\varepsilon_c = \varepsilon_{co} + \varepsilon_{cc} = J(t,t_o).\sigma \qquad (8.4)$$

By dividing the equation (8.4) by σ and re-arranging terms, the compliance can be expressed as follows.

$$J(t,t_o) = J_o(t_o,t_o)[1+\Phi(t,t_o)] \qquad (8.5)$$

J_o is the compliance at the age of loading t_o, and represents the inverse of the modulus of elasticity at t_o. $\Phi(t,t_o)$, defined as the creep coefficient, represents at any time, the constant by which the elastic strain should be multiplied in order to obtain the corresponding creep strain.

In order to avoid taking into account both t and $\tau=t-t_0$ while formulating models for creep strain of cement paste and/or concrete, it seems advantageous to consider the degree of hydration (α_d) of loaded specimens as the main variable. Neville et al. (1959, 1960) have reported a relation between the strength and stress/strength ratio of concrete at the time of application of load and the creep strain following a given elapsed time under loading. Further Ross (1959) noted that the properties of concrete are profoundly affected not only by age of the material but also by temperature during the curing period. It is apparent that time alone is not sufficient for comparison of creep properties.

Mills (1969) stated that water penetrating into areas of restricted adsorption in the gel is capable of bearing load and contributing to stiffness of the concrete. He therefore assumed that strongly

adsorbed water is capable of resisting shear stress while that condensed in comparatively coarse capillaries is incapable of making this contribution. The relative humidity and the corresponding state of water of the cement paste are thus of great importance for creep properties. Feldman and Sereda (1970b) modeled the layer structure of the gel particles by two parallel surfaces (C-S-H sheets) and described the effect of moisture content on the modulus of elasticity of cement paste as shown previously in Figure 4.3.

On the basis of the literature review and the results obtained on partially saturated and totally dried mature specimens as well as those obtained on wet mature and very young specimens it seems reasonable to conclude that at a given stress/strength level, the compliance will mainly depend on the degree of hydration (α_d), the degree of hydration at loading (α_{do}) and the relative humidity (rh) in the hardening cement paste and/or concrete. The proposed mathematical formulation corresponding to these observations is as follows:

$$J(\alpha_d, \alpha_{do}, rh) = J_o(\alpha_{do}, rh)[1+\Phi(\alpha_d, \alpha_{do}, rh)] \tag{8.6}$$

$$\Phi(\alpha_d, \alpha_{do}, rh) = k_1(\alpha_{do}, rh)\left[f_{\alpha_d} \right]^{k_2(\alpha_{do}, rh)} \tag{8.6a}$$

$$f_{\alpha_d} = \frac{\alpha_d - \alpha_{do}}{\alpha_{do}} \tag{8.6b}$$

$f_{\alpha d}$ is the fractional increase in degree of hydration while under loading and k_1 and k_2 are experimental parameters depending both on degree of hydration at loading (α_{do}) and relative humidity (rh) provided that the experiments are all conducted at the same initial stress-strength level.

For the present study, the relative humidity was kept constant at (96 ± 2)%. The temperature was also maintained at 22 ± 2 °C as any significant change of these parameters was considered to affect the degree of hydration. Special precautions were therefore taken by continuously monitor the humidity and temperature in order to avoid any abrupt changing during the creep test. From the results presented in the first part of the section, experimental creep coefficients were obtained

both for normal and high strength paste and plotted against those obtained using the mathematical model previously described. The Figure 8.80 shows a good correlation between model creep coefficient and experimental creep coefficient either for normal strength paste or for high strength paste. The parameters k_1 and k_2 are presented in Table 8.11.

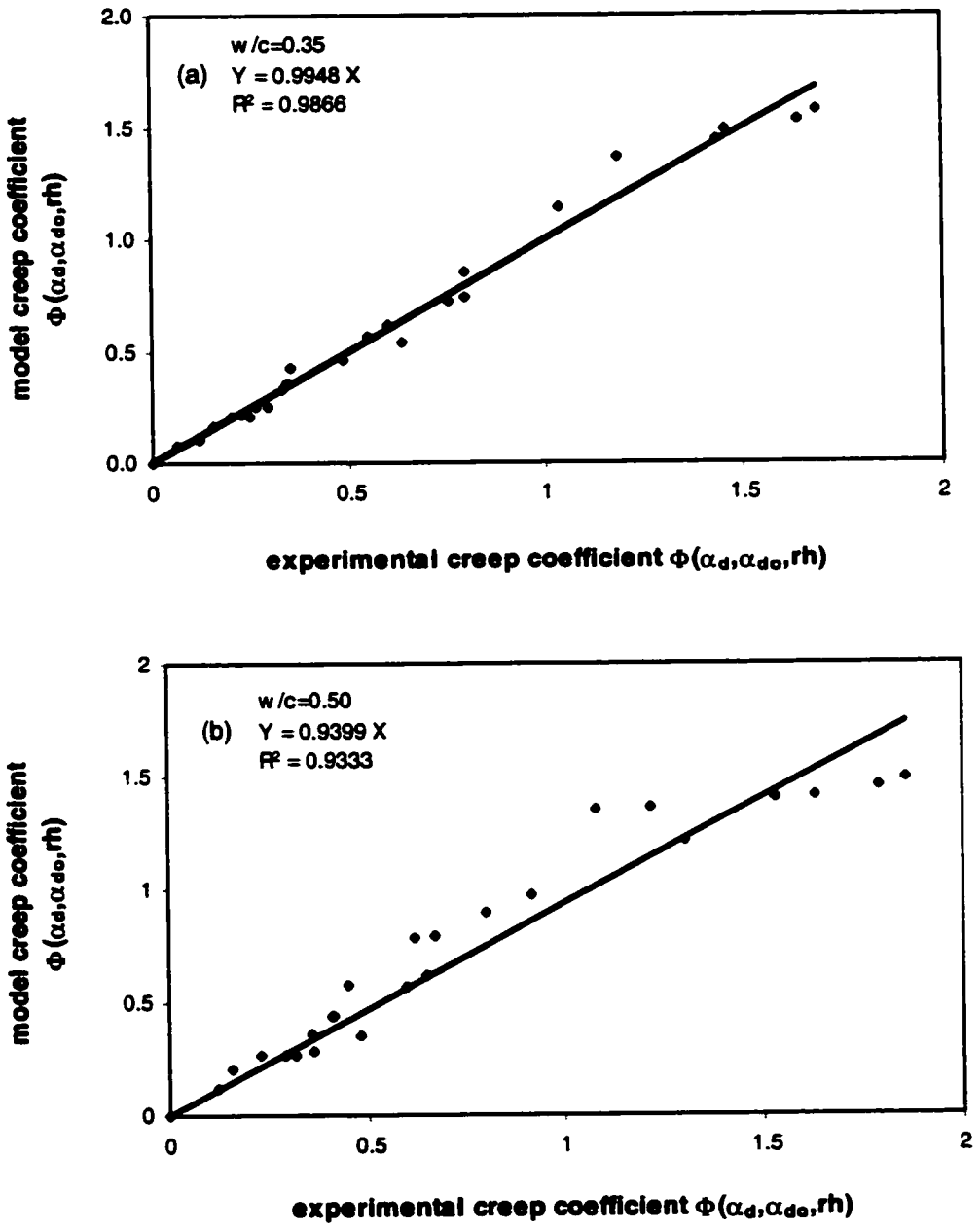

Figure 8.80: Comparison of model and experimental creep coefficients for high strength (a) and normal strength (b) hardening cement pastes while conditioning at 96% RH

Table 8.11: Mechanical model parameters

	w/c=0.35			w/c=0.50		
parameters	18h old	24h old	30h old	18h old	24h old	30h old
$J_o(\alpha_{do}, \alpha_{do})$	48.31	48.08	46.51	126.58	96.15	86.21
α_{do}	0.5454	0.6480	0.6766	0.5048	0.5992	0.6066
k_o	52.49	30.24	160.77	207.13	205.07	153.27
k_2	0.3863	0.3443	0.4820	0.5621	0.4770	0.8648
$k_1 = k_o / J_o$	1.0865	0.6290	3.4567	1.6364	2.1328	1.7779
$k_1 \times k_2$	0.4197	0.2166	1.6661	0.9198	1.0174	1.5375
R^2	0.9914	0.9421	0.9851	0.8777	0.9831	0.9217

In the first order of approximation the parameters k_1 and k_2 can be expressed by the following linear equations. However, it is strongly recommended to determine these parameters form a set of short-term creep experiment given the fact that huge amount of experimental data is required for more accurate expressions of the parameters k_1 and k_2.

For high strength paste: $k_1 = 12.0770\ \alpha_{do} - 5.8038$ (8.7a)

$k_1 \times k_2 = 6.4479\ \alpha_{do} - 3.2517$ (8.7b)

For normal strength paste: $k_1 = 3.0340\ \alpha_{do} + 0.1190$ (8.7c)

$k_1 \times k_2 = 3.9288\ \alpha_{do} - 1.0820$ (8.7d)

Impedance spectra (real-time) were simultaneously monitored during the shrinkage and creep experiments of hardening normal and high strength cement pastes and is presented in Figures 8.81 to 8.86. The size of the high frequency arc diameter (HFA) has been widely investigated and attributed to the intrinsic properties of the hardening cement paste which are pore solution conductivity, pore diameter and pore size distribution (McCarter and Curran, 1984; Xu et al.,

1993; Gu et al., 1993). As stated earlier in Section 8.4.3.1, only the information provided by HFA will be presented and discussed in this thesis.

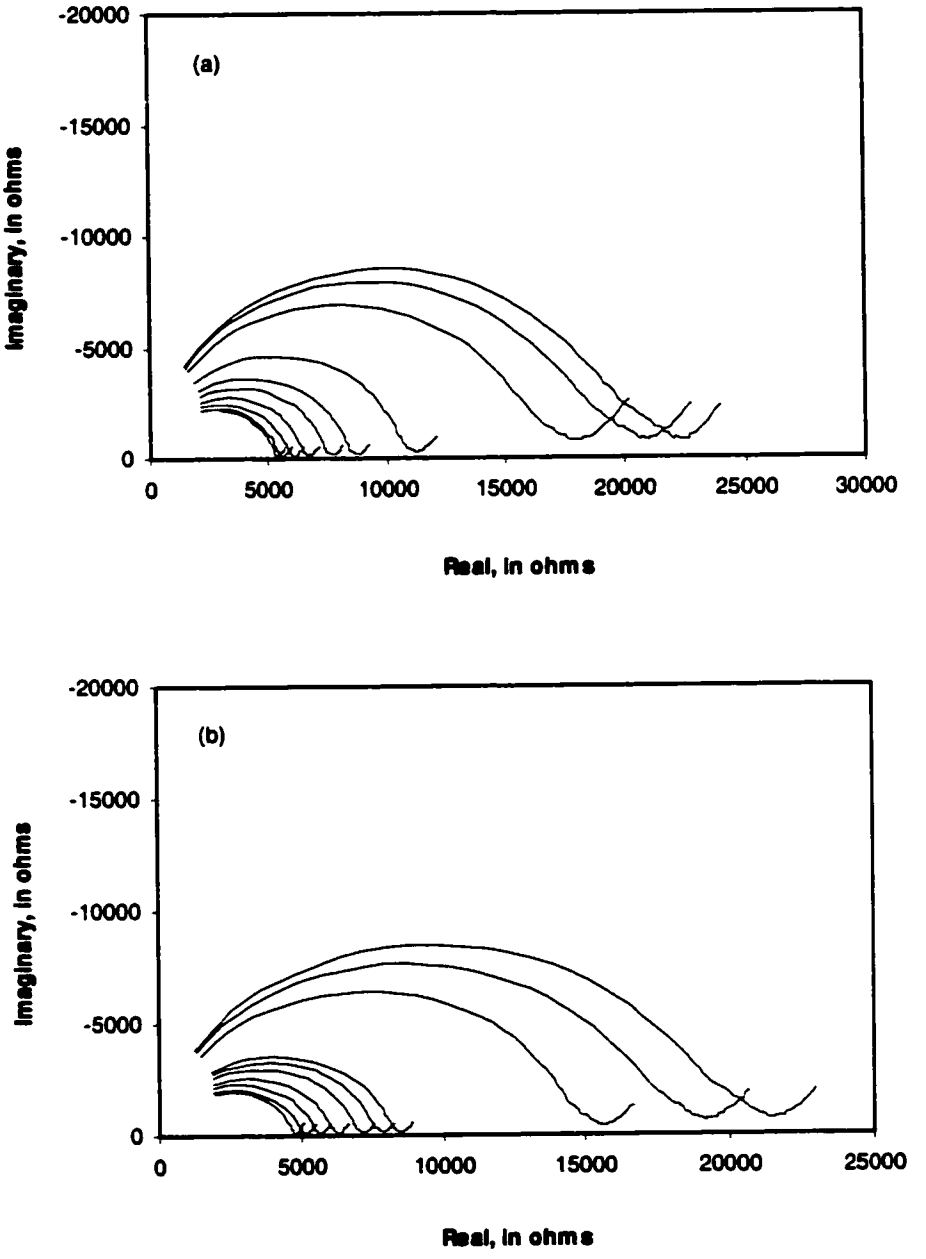

Figure 8.81:AC impedance spectra: (a) shrinkage and (b) total strain of 18 hours old hardening cement paste (w/c=0.35); specimens conditioned at about 96% RH for 0, 1, 2, 3.7, 6.5, 9, 12.7, 24, 48 and 72 hours

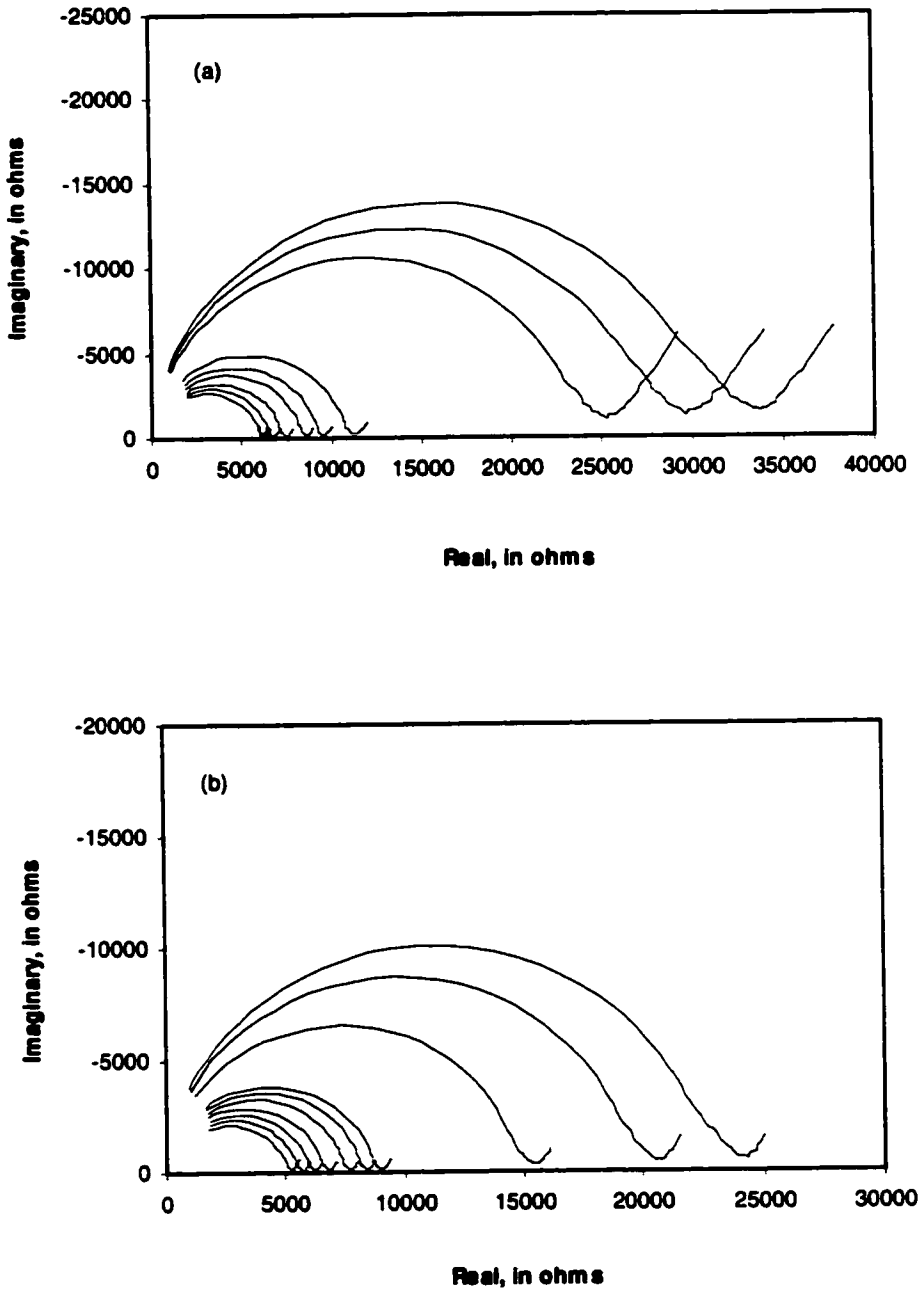

Figure 8.82:AC impedance spectra: (a) shrinkage and (b) total strain of 24 hours old hardening cement paste (w/c=0.35); specimens conditioned at about 96% RH for 0, 1, 2, 3.7, 6.5, 9, 12.7, 24, 48 and 72 hours

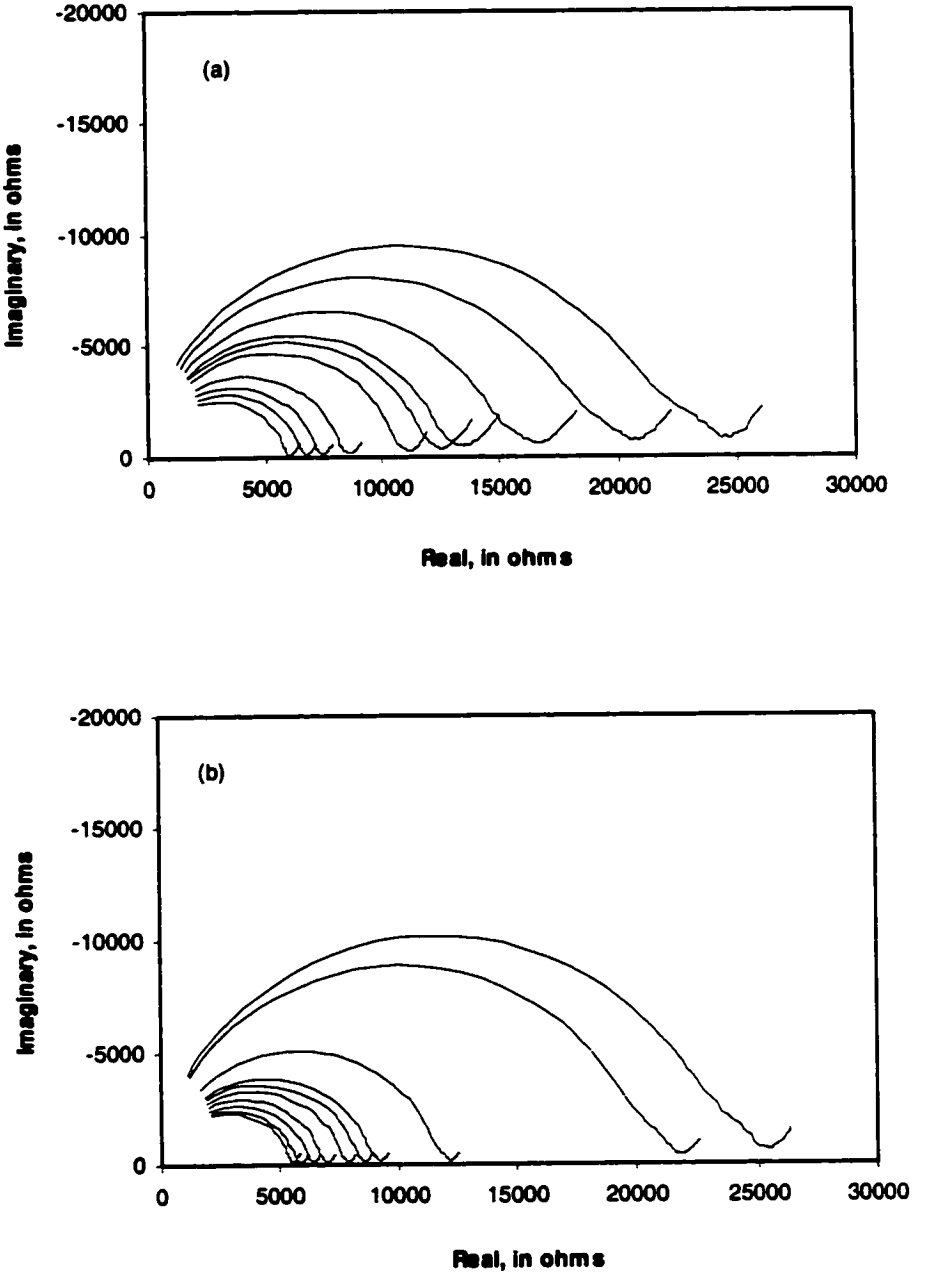

Figure 8.83:AC impedance spectra: (a) shrinkage and (b) total strain of 30 hours old hardening cement paste (w/c=0.35); specimens conditioned at about 96% RH for 0, 1, 2, 3.7, 6.5, 9, 12.7, 24, 48 and 72 hours

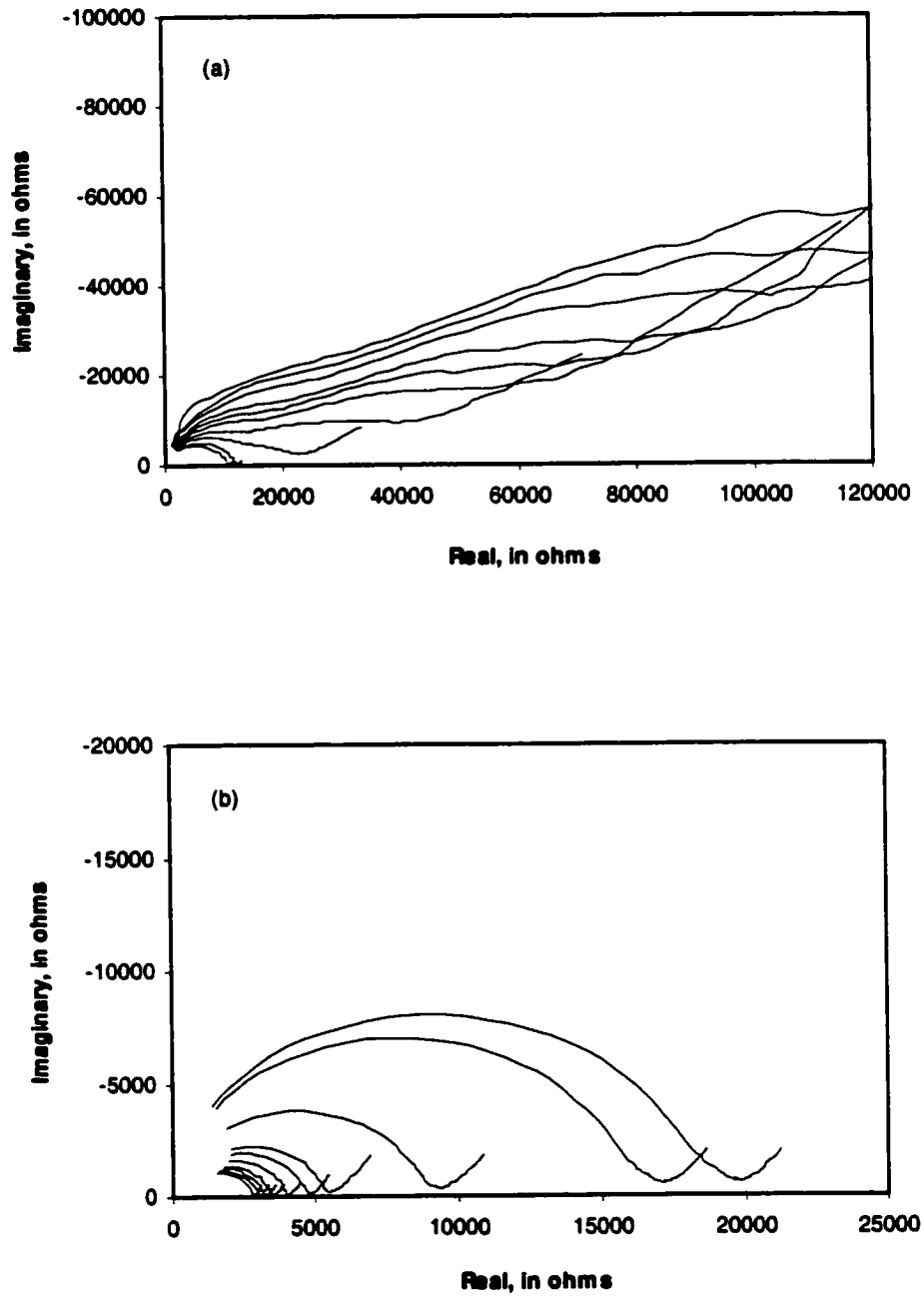

Figure 8.84:AC impedance spectra: (a) shrinkage and (b) total strain of 18 hours old hardening cement paste (w/c=0.50); specimens conditioned at about 96% RH for 0, 1, 2, 3.7, 6.5, 9, 12.7, 24, 48 and 72 hours

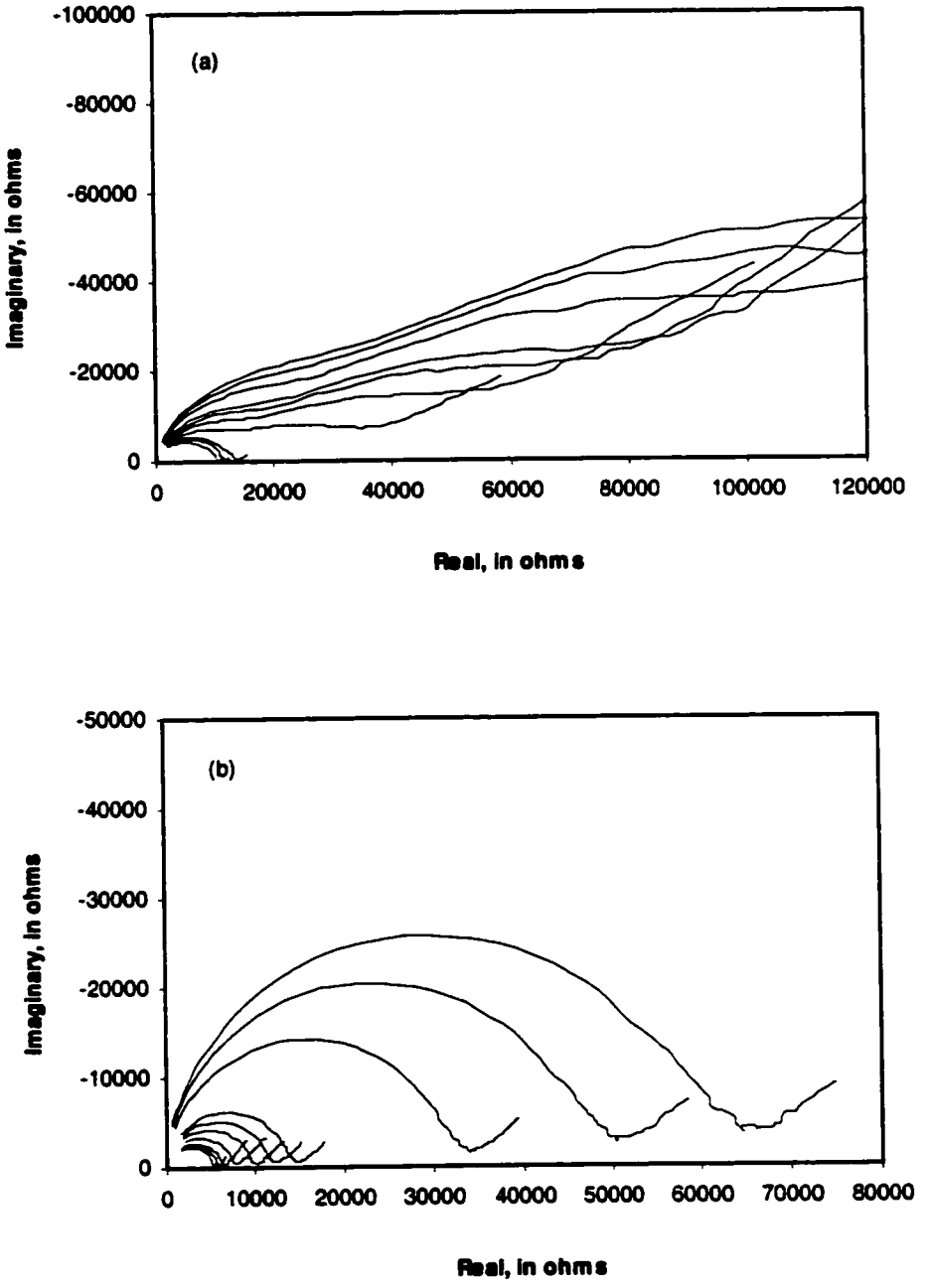

Figure 8.85:AC impedance spectra: (a) shrinkage and (b) total strain of 24 hours old hardening cement paste (w/c=0.50); specimens conditioned at about 96% RH for 0, 1, 2, 3.7, 6.5, 9, 12.7, 24, 48 and 72 hours

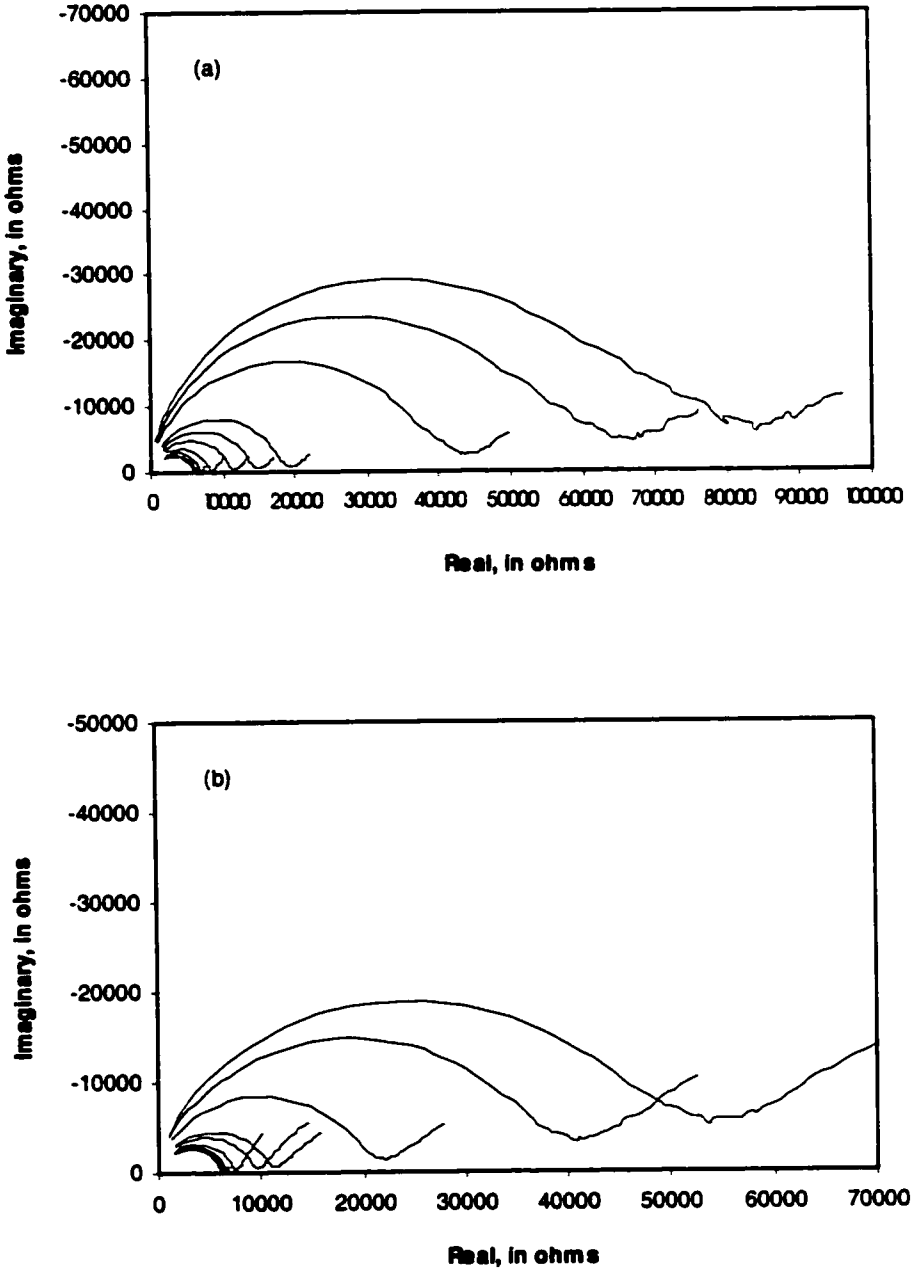

Figure 8.86:AC impedance spectra: (a) shrinkage and (b) total strain of 30 hours old hardening cement paste (w/c=0.50); specimens conditioned at about 96% RH for 0, 1, 2, 3.7, 6.5, 9, 12.7, 24, 48 and 72 hours

The Figures 8.81 to 8.83 illustrate the high frequency arc of unloaded and loaded specimens of high strength cement paste maintained in the same environmentally controlled cabinet. It can be observed that at any period of time following conditioning, the spectra of unloaded specimens are greater than those of loaded specimens. They also increase with hydration and/or loaded period. The difference between unloaded and loaded spectra can be defined as the HFA diameter induced by the loading of cement paste specimens.

The shrinkage of the normal strength 18 and 24 hours old specimens however, shows (Figures 8.84 and 8.85) unusual behavior exhibiting two high frequency arcs. This may be explained by the fact that the unloaded paste structure may have a largely discontinuous pore network that can be modeled as two different capacitors while drying. The second arc disappears with the loading of these specimens implying that the load may contribute to establishing continuity of the pore network during hardening of the paste. Companion specimens of normal and high strength cement pastes kept continuously wet indicate that the HFA diameter increase with the hydration as already reported by several researchers (Gu et al., 1992; McCarter et al., 1988; Scuderi et al., 1991). It has been well demonstrated that during the hydration period, the bulk resistance steadily increases with time, as does the depression of the arc below the real axis. This was attributed to "a spread of relaxation of times" of the ions adsorbed on the solid-liquid interface as hydration proceeds. The drying even at very high relative humidity (96% in the present study) and/or the loading of the specimen during hydration may perturb the ions movement and therefore slightly affect the relative changes of the associated depression angle.

McCarter and Garvin (1989) have shown that the absolute values of resistance and reactance increase dramatically as a high proportion of the free capillary water evaporates from the matrix. Such evaporation of capillary water even at (96 ± 2)% RH may explain the high value of HFA observed on Nyquist plots of shrinking cement paste during hydration. At this humidity level, even though part of the free capillary water is removed, adsorbed water would require a higher energy input or lower humidity to be removed from the gel surface. The load may redistribute the water within the matrix, contributing to the continuity of water through the capillary and interlayer pores. During the subsequent hydration increased layering and sliding of C-S-H sheets of the loaded specimens may decrease the pore network connectivity resulting in a substantial increase of HFA diameter. The results of HFA diameter, determined from the electrical model described previously in Chapter 5, are presented in Figures 8.87 to 8.92. The figures also illustrate the growth of HFA diameter of continuously wet normal and high strength pastes corroborating the observations just mentioned. It can also be observed from the figures that on the removal of the sustained load, the HFA diameter shows an abrupt increase followed by a very

slight change during the recovery period. The HFA diameter values following the removal of the sustained load, however, do not necessary reach those of the shrinkage specimens (Figures 8.90, 8.91, 8.92) for normal strength (w/c=0.50) cement paste (18 and 24 hours old). This may be due to the large amount of water in such paste, which leads to a very broadly distributed range of pore size network at setting. On loading, the matrix may alter the characteristics of the pore network during the subsequent hydration, which in turn may decrease the connectivity and the water available to assure the continuity.

As already mentioned the 18 and 24 hours old normal strength specimens were found to have two high frequency arc diameters (see Figures 8.84a and 8.85a) during the monitoring of impedance spectra for the shrinkage test. The HFA diameters presented in previous figures were obtained from an electrical circuit capable of fitting both arcs except that only the higher values were used given the difficulty of determining the single equivalent HFA diameter associated to the electrical model chosen. Difficulty in obtaining an equivalent value of HFA diameter for the 18 and 24 hours normal strength spectra may lead to an inaccurate expression of mathematical model relating all of them.

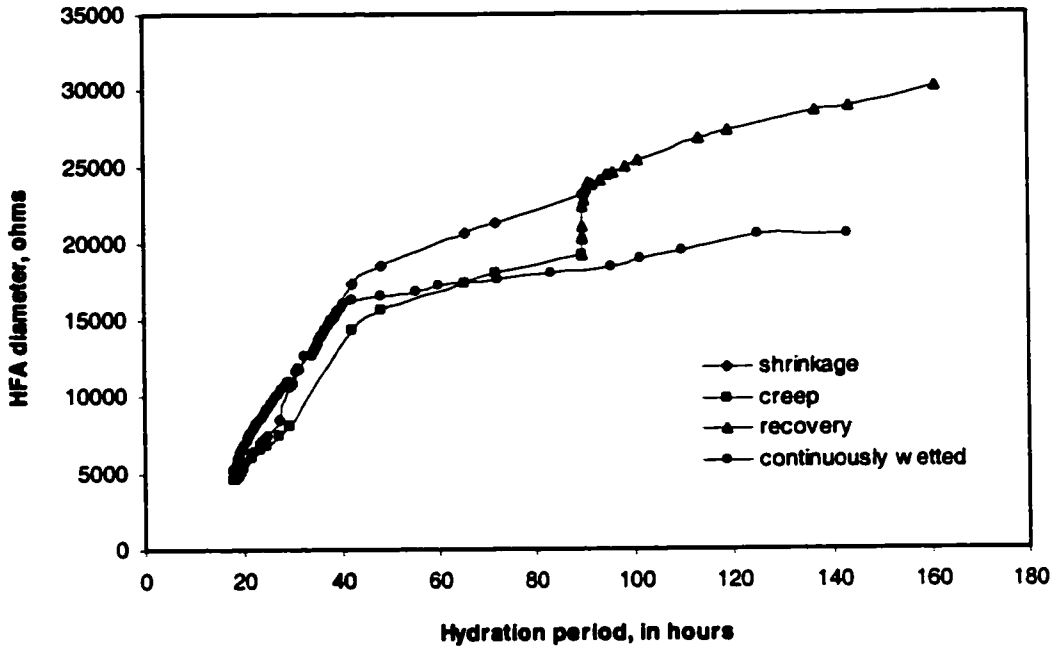

Figure 8.87: High frequency-arc diameter (ϕ) variation of unloaded and loaded 18 hours old hardening cement paste (w/c=0.35) specimens tested at about 96% RH

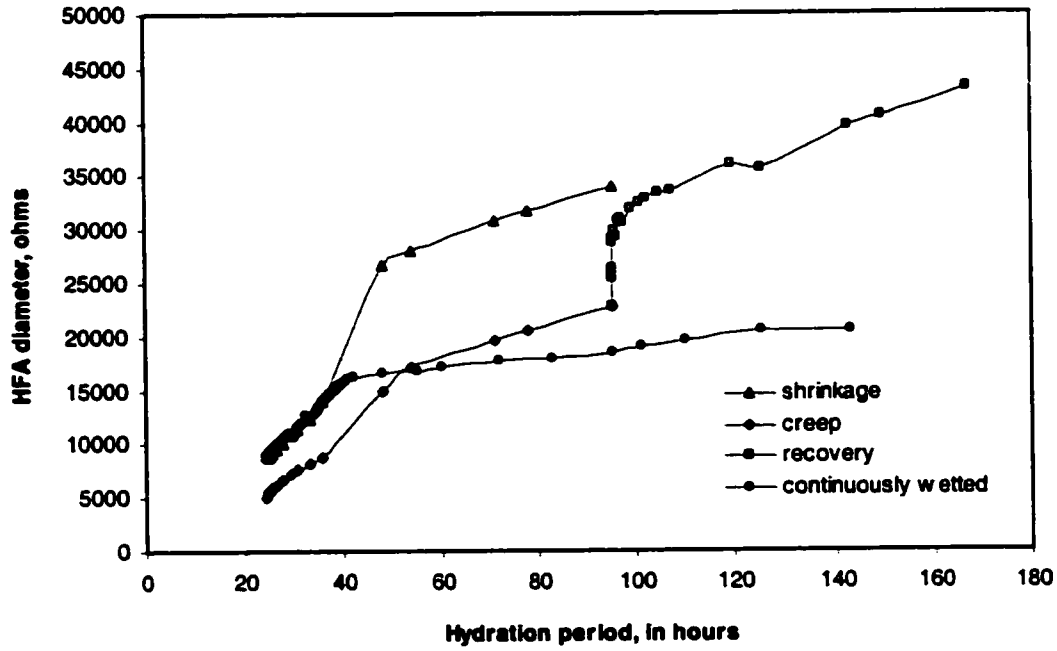

Figure 8.88: High frequency-arc diameter (ϕ) variation of unloaded and loaded 24 hours old hardening cement paste (w/c=0.35) specimens tested at about 96% RH

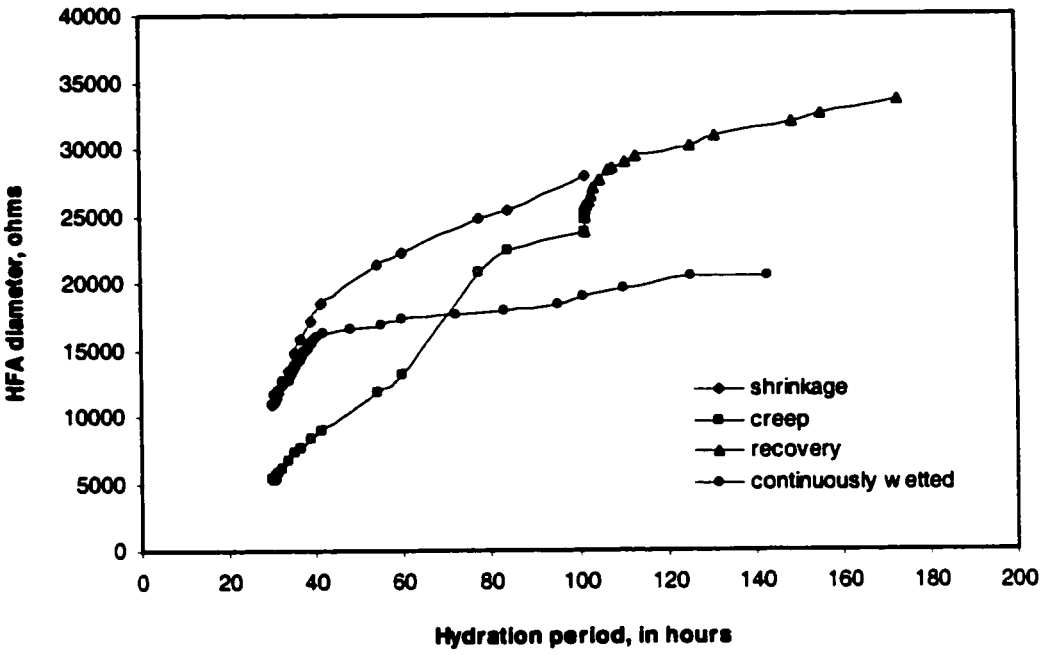

Figure 8.89: High frequency-arc diameter (ϕ) variation of unloaded and loaded 30 hours old hardening cement paste (w/c=0.35) specimens tested at about 96% RH

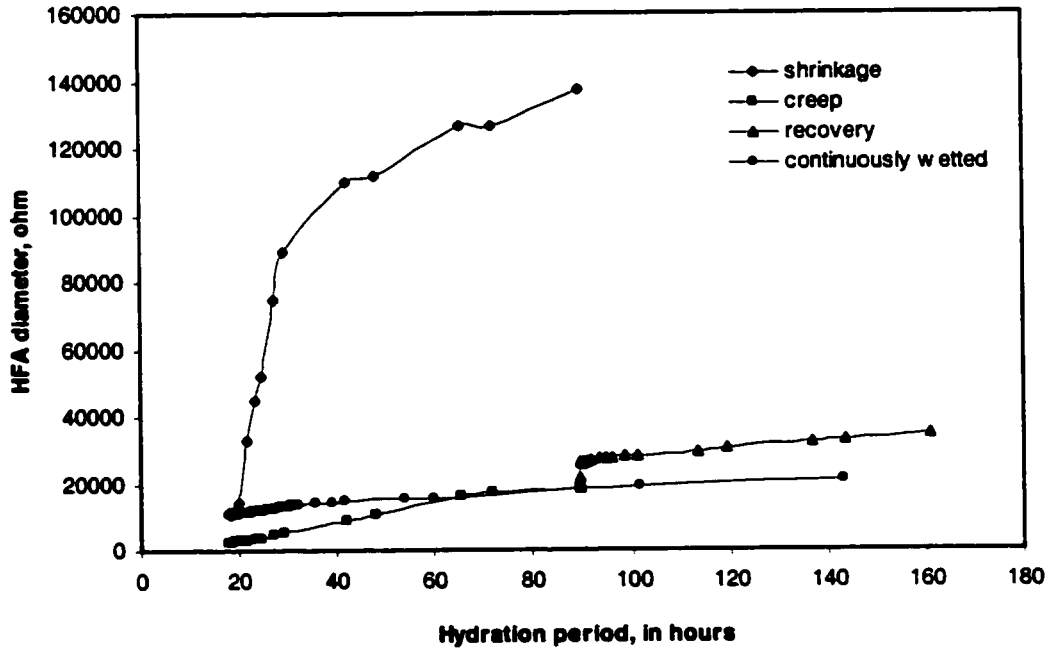

Figure 8.90: High frequency-arc diameter (ϕ) variation of unloaded and loaded 18 hours old hardening cement paste (w/c=0.50) specimens tested at about 96% RH

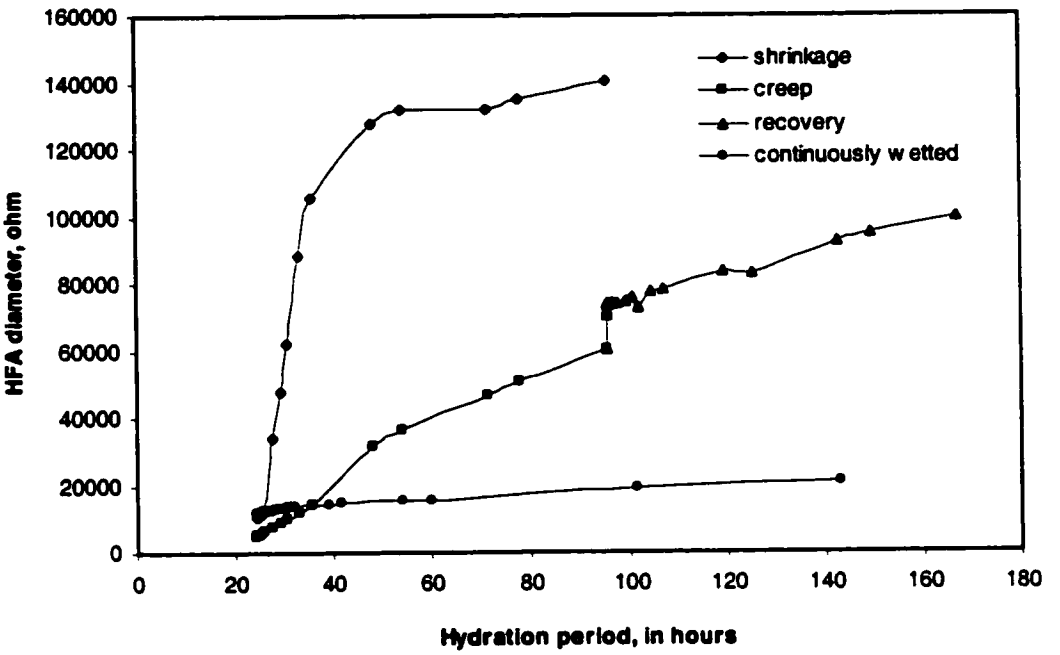

Figure 8.91: High frequency-arc diameter (ϕ) variation of unloaded and loaded 24 hours old hardening cement paste (w/c=0.50) specimens tested at about 96% RH

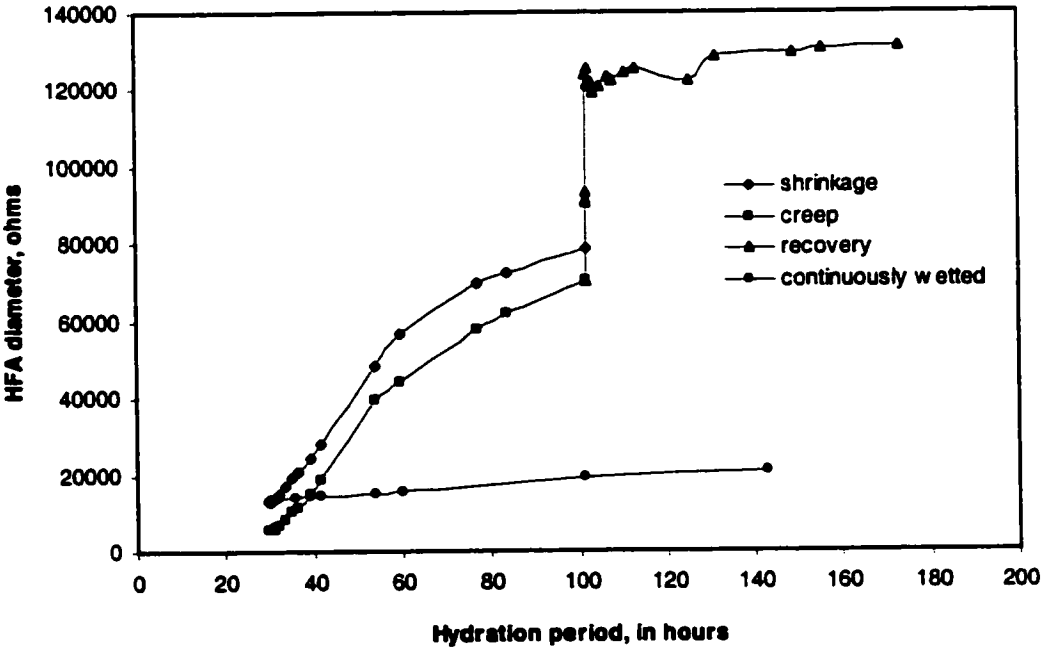

Figure 8.92: High frequency-arc diameter (ϕ) variation of unloaded and loaded 30 hours old hardening cement paste (w/c=0.50) specimens tested at about 96% RH

It is apparent from the figures described above that the size of the high frequency arc diameter (ϕ) is not dependent only on the pore solution conductivity, pore size and pore network characteristics. The relative humidity (rh) is also an important variable. The pore solution conductivity, pore size and pore network characteristics which are the intrinsic properties of hardening cement paste can collectively be associated with the degree of hydration of the matrix (α_d). By introducing the degree of hydration at loading (α_{do}) as another variable, the part of the HFA diameter which is associated with the loading of the specimens ($\Delta\phi$) can be said to depend on variables α_d, α_{do} and rh provided that all the tests are performed at the same stress-strength level. From previous figures, the HFA diameter (ϕ) of hardening cement paste during shrinkage and total strain experiment can qualitatively be related to the hydration period as illustrated in Figure 8.93. ($\phi_{shrinkage}$) and ($\phi_{total\ strain}$) of the Figure 8.93 are respectively the HFA diameter plots of unloaded and loaded specimens of hardening cement paste. The difference between them can be associated to creep with its initial value ($\Delta\phi_0$) being considered as the instantaneous change in HFA diameter following loading of the cement paste specimens.

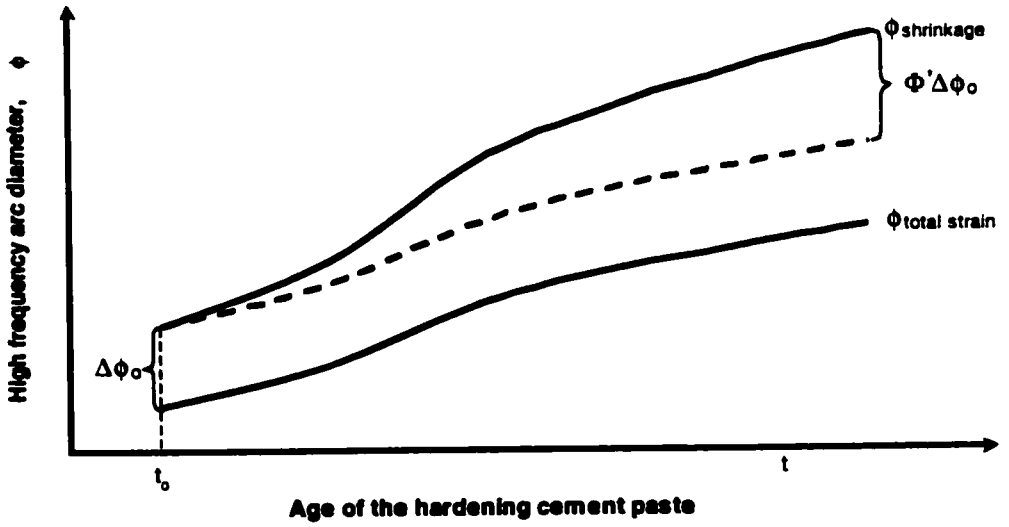

Figure 8.93: Schematic variation of high frequency-arc diameter (ϕ) during total strain and shrinkage experiment of hardening cement paste specimens tested at about 96% RH

Using a similar approach to that adopted for the modeling of the compliance J, the changes in high frequency arc diameter ($\Delta\phi$) observed can be formulated as follows:

$$\Delta\phi\,(\alpha_d, \alpha_{do}, rh) = \Delta\phi_o\,(\alpha_{do}, rh)\,[1 + \Phi'\,(\alpha_d, \alpha_{do}, rh)] \qquad (8.8)$$

$$\Phi'(\alpha_d,\alpha_{do},rh) = k_1'(\alpha_{do},rh)\left[f\alpha_d\right]^{k_2'(\alpha_{do},rh)} \qquad (8.8a)$$

$$f\alpha_d = \frac{\alpha_d - \alpha_{do}}{\alpha_{do}} \qquad (8.8b)$$

As stated previously, $f_{\alpha d}$ is the fractional increase in degree of hydration while under load and k'_1 and k'_2 are experimental parameters depending both on degree of hydration (α_{do}) at loading and relative humidity (rh) provided that the experiments are all conducted at the same stress-strength level. For the present study, the relative humidity is assumed to be constant at (96 ± 2)%; the temperature was also maintained at 22 ± 2 °C. From the results presented above, experimental creep coefficients were obtained both for normal and high strength pastes and plotted against those obtained using the mathematical model previously described. Figure 8.94 shows a good correlation between model and experimental electrical creep coefficients particularly for high strength paste. The poor correlation coefficients obtained for the electrical model creep coefficient for the normal strength paste are believed to be due to the different type of impedance spectra for 18 and 24 hours old specimens, in contrast to those of 30 hours old specimens. The HFA diameter (ϕ) results show that the electrical model for creep may not only have the degree of hydration (α_d) as the main variable. The microstructural change associated with the change in HFA diameter (ϕ) may also significantly depend on the type of pore solution. It can be observed from previous figures that as hydration proceeds, the character of the electrolyte changes within the matrix. The electrolyte seems to be more stable in high strength paste than in normal strength paste. These observations are confirmed by the parameters k'_1 and k'_2 presented in Table 8.12 and obtained with a very low coefficient of correlation R^2.

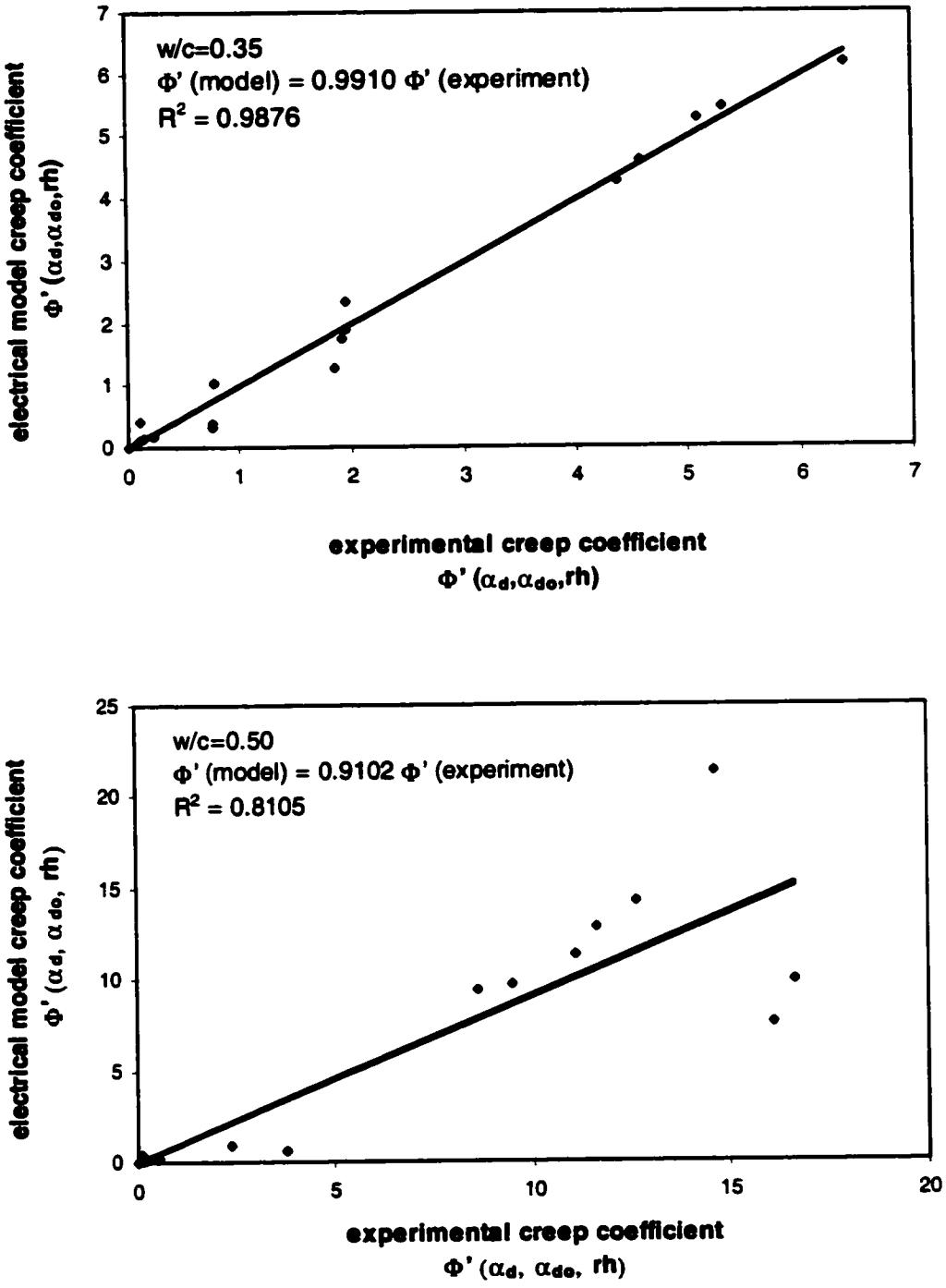

Figure 8.94: Comparison of electrical model and experimental creep coefficients for high strength (w/c=0.35) and normal strength (w/c=0.50) hardening cement pastes while conditioning at 96% RH

Table 8.12: Electrical model parameters

	w/c=0.35			w/c=0.50		
parameters	18h old	24h old	30h old	18h old	24h old	30h old
$\Delta\phi_o(\alpha_{do}, \alpha_{do})$	531	3786	5472	8675	5461	7742
α_{do}	0.5048	0.5992	0.6066	0.5454	0.6480	0.6766
k'_o	4082	13719	5083	186477	82631	9005
k'_2	0.3508	0.3872	0.4422	2.4462	1.6518	1.2021
$k'_1 = k'_o/\Delta\phi_o$	7.6881	3.6236	0.9289	21.4959	151.1868	1.1631
R^2	0.9544	0.6143	0.4708	0.9117	0.8244	0.5408

In the first order of approximation the parameters k'_1 and k'_2 can be expressed by the following linear equations. However, it is strongly recommended to determine these parameters form a set of short-term creep experiment given the fact that huge amount of experimental data is required for more accurate expressions of the parameters k'_1 and k'_2.

For high strength paste:

$$k'_1 = 34.2210 - 48.3540\ \alpha_{do} \qquad (8.9a)$$

$$k'_2 = 0.6058\ \alpha_{do} + 0.0158 \qquad (8.9b)$$

For normal strength paste:

$$k'_1 = 468.8600\ \alpha_{do} - 209.4 \qquad (8.9c)$$

$$k'_2 = 7.8132 - 10.6040\ \alpha_{do} \qquad (8.9d)$$

It is also apparent that the mathematical formulation developed for HFA diameter change taking place while hydrating cement paste is subjected to a sustained load requires further investigation. Nevertheless in order to consider the effect of the electrolyte, it can arguably be compared to the compliance formulation. The high frequency arc diameter as a response to the impedance signal applied to the specimens through the stainless steel electrodes is not generally ideal or perfect. However, as described previously in Section 5.2 most materials exhibit an inclined semicircle

with the center depressed below the real axis by an angle $\theta_d.\pi/2$ (Figure 5.2). The angle depression is a common phenomenon in a. c. impedance studies and the HFA diameter is then equal to $R_2/\cos(\theta_d.\pi/2)$. The depression angle parameter $n=1-\theta_d$ is commonly used and describes the degree of perfection of the semi-circle. There may be several causes of the inclined of semi-circle including factors associated with "a spread of relaxation times" of the ions adsorbed on the solid-liquid interface (McCarter and Curran, 1984; McCarter et al., 1988), surface roughness (De Levie, 1965; Iseki et al., 1972) and uneven current distribution at the interface.

During creep experiment, the depression angle parameter was found to be scattered particularly in the case of normal strength hydrating cement paste when compared to unloaded and continuously wet companion specimens (see Figure 8.95). From Figure 8.95, it can be observed for unloaded specimens that as the hydration proceeds, the degree of perfection of the semi-circle improves as n-values approach 1. The depression angle parameter appears to be affected by the loading and reaches a steady state with an increase of the fractional increase in degree of hydration for the hydrating high strength cement paste specimens.

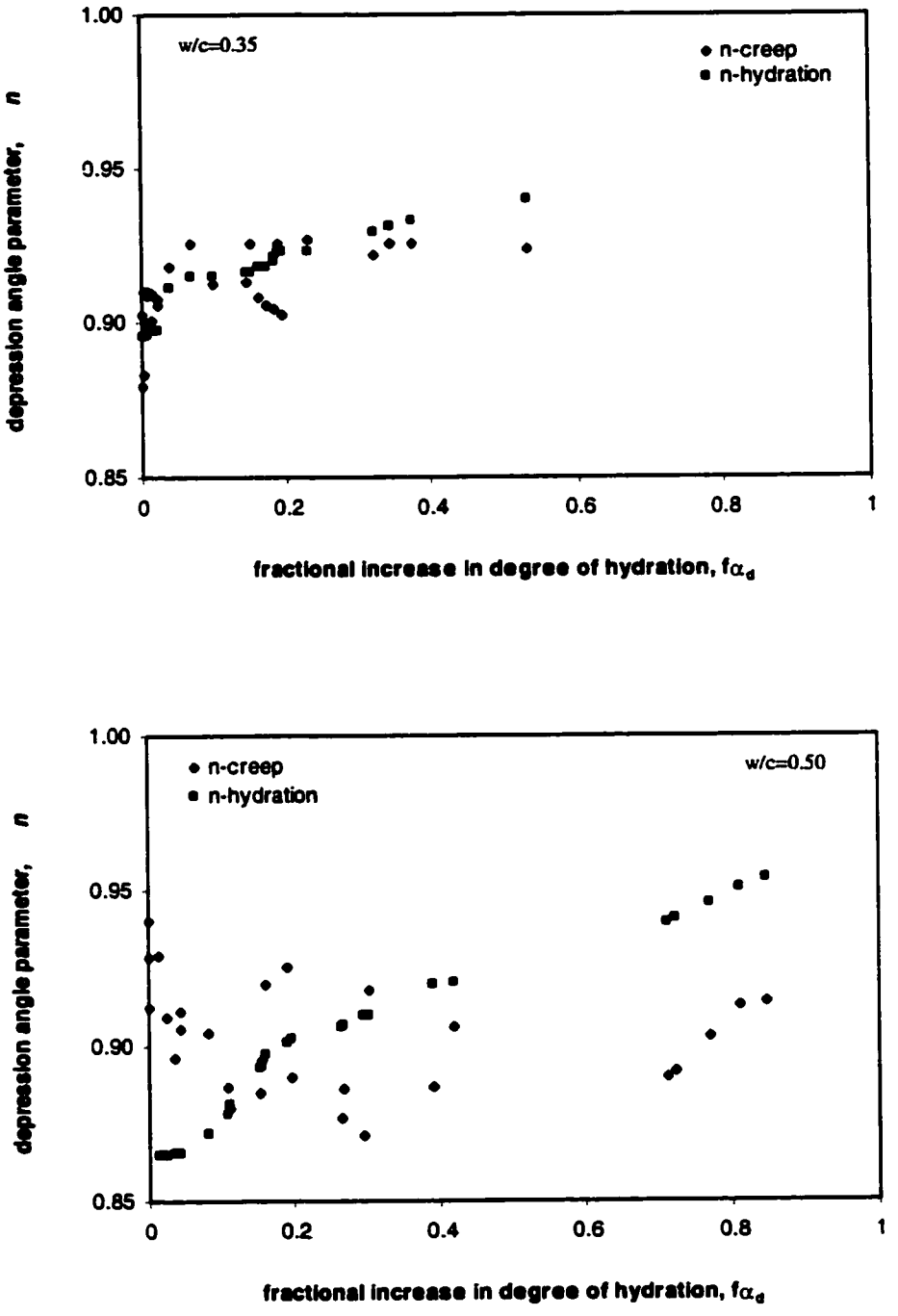

Figure 8.95: Depression angle parameter n of high strength (w/c=0.35) and normal strength (w/c=0.50) hardening cement pastes while conditioning at 96% RH

8.4.3.3 CH compacts

A special mould was made to fabricate compacts of calcium hydroxide having a thickness of about 6-mm and diameter of 38-mm. From such compacts, we were able to cut "T-shaped" specimens using isopropanol to lubricate the diamond saw given its low interaction with calcium hydroxide. The total porosity of such compacts was determined from the weight and volume of the compact samples, using the solid density of $Ca(OH)_2$ of 2.24 g/cm^3 and was found to be 19.7%. The modulus of elasticity of 17.2 GPa was obtained from "T-shaped" specimens loaded incrementally up to 19.3 MPa (applied load for creep test) which corresponds to 5% of the compaction pressure (386 MPa). The "T-shaped" specimens were D-dried (vacuum dried at 105°C for 3 hours) prior to creep measurement. The whole experiment was performed in an environmentally controlled chamber maintained dry (0% RH) at 22 ± 2°C with nitrogen. In the chamber, the creep frames were placed in the cells containing drying agent (magnesium perclorate). During the creep experiments, unloaded companion specimens were also placed in the cells in order to determine the environmental effect on the deformation of the "T-shaped" specimens. No variation in length was observed from the unloaded specimen meanings that the creep strains obtained from loaded specimens were the dry basic creep only. The compliance result is presented in Figure 8.96 for which the initial value J_o was obtained indirectly from elastic modulus (17.2 GPa) previously determined. It is important to note that the Young modulus obtained by the present approach lies between the values reported previously by Beaudoin (1983) and Wittmann (1986) for Calcium hydroxide compacts having similar total porosity.

From Figure 8.96 it can be observed that $Ca(OH)_2$-compacts creep and show at the very beginning, a creep trend similar to that observed in cement systems. However, during the first half-hour, the observed basic creep strain and/or compliance seem to be linear reaching a short steady state an hour following the loading. The creep observed at very early age may be due to the rearrangement of the $Ca(OH)_2$ crystals along their preferential plane of minimum energy which allows the specimens to become more stable. Even if the powder of $Ca(OH)_2$ used for the present study is well-crystallized and therefore, may leads to a rapid stability following loading of compacts, the nature of $Ca(OH)_2$ in cement paste may not be exactly similar. Amorphous $Ca(OH)_2$ is believed to be present in hydrated cement paste in different amounts (Ramachandran, 1979) and may thus lengthy the period of its contribution to creep strain of cement paste. The present result is very unique given the significant amount of this phase in cement paste (20 to 26% by weight) and the importance of understanding the role of $Ca(OH)_2$ in cement paste

systems. The random distribution of $Ca(OH)_2$ in cement pastes has led to evidence that some $Ca(OH)_2$ may be porous (Mills, 1981; Feldman et Ramachandran, 1982).

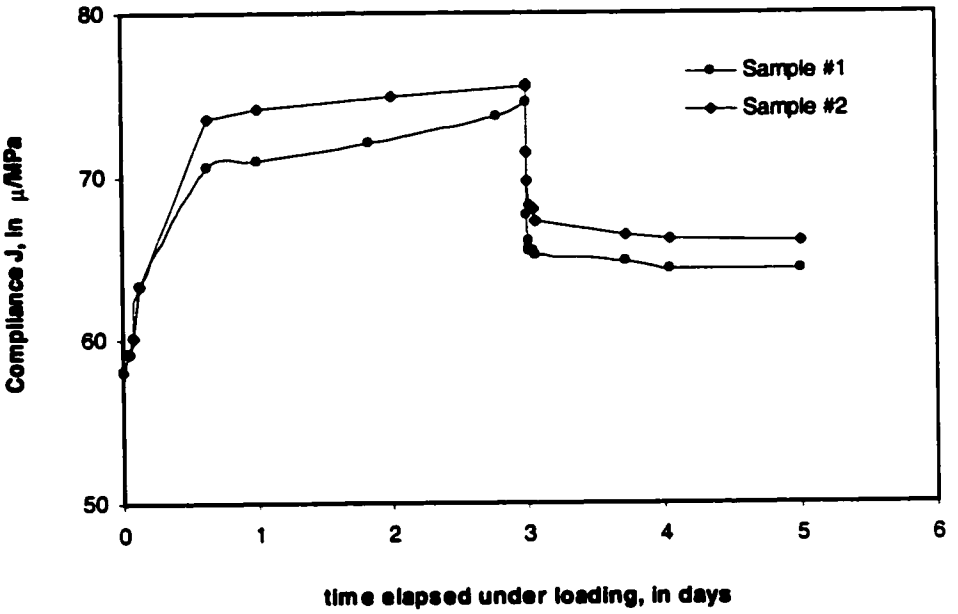

Figure 8.96: Compliance J of $Ca(OH)_2$-compacts while conditioning at 0% RH and loaded at a stress level corresponding to 5% of the compaction pressure (386 MPa)

The behavior of $Ca(OH)_2$ in cement pastes is believed to follow a similar pattern and may have a greater contribution to creep strain compared to the values observed on loaded $Ca(OH)_2$ compacts. The previous results on hydrating cement pastes presented in Section 8.4.3.2 have shown that creep can suitably be related to the state of hydration of the paste. However, as the cement paste is hydrating, the formation of C-S-H is followed by the precipitation of $Ca(OH)_2$ and by considering the C-S-H as creep center, the basic creep strain observed at macroscopic level may be caused by sliding of C-S-H sheets one another and to a lesser extend by amorphous and porous $Ca(OH)_2$ particles. The difficulty to determine the contribution of $Ca(OH)_2$ lies with the difficulty to determine the amount of amorphous and porous $Ca(OH)_2$ in hydrated cement pastes.

It is very important to take into account the fact that the $Ca(OH)_2$-compacts were loaded at a stress level corresponding only to 5% of the compaction pressure compared to 30% used for tests performed on cement pastes. However, it is important to note that such level of compaction

pressure corresponds to an applied stress of 19.3 MPa, which is almost twice the stress applied on well hydrated normal strength cement paste. The initial compliance and/or strain of $Ca(OH)_2$ compacts obtained experimentally was several times greater than the basic creep strain and/or compliance (see Figure 8.96). Even though $Ca(OH)_2$ in cement systems may contribute to their overall deformations, it may have a considerable contribution to the initial deformations and only a slight effect on long term deformations which, however, is not negligible. The creep recovery of $Ca(OH)_2$ compacts indicate that part of the deformation taking place after loading even at 0% relative humidity is irreversible as the creep recovery of cement paste systems.

The impedance spectra of loaded and unloaded $Ca(OH)_2$ compact specimens were also monitored and coupled to creep experiment. Given the dry state of the $Ca(OH)_2$ compacts, a conductive metal epoxy usually used for circuit works was spread at both ends of the specimens in order to improve conductivity at electrode interface during the impedance measurements. The spectra obtained from unloaded companion specimens were found to be almost similar after 0, 1, 2, 5, 12, 24, 48, and 72 hours following conditioning at 0% relative humidity with nitrogen. In contrast, the loaded specimens showed a slight but consistent changing of the spectra during the same period of time. A typical spectrum of unloaded specimens is presented in Figure 8.97. The variation of the change in high frequency resistance R_Ω with the time elapsed under loading is presented in Figure 8.98 illustrating the effect of load alone on R_Ω. The data presented correspond to frequencies ranging from 2 MHz to 70 kHz from which, the changing of the resistance R_Ω at high frequency (2 MHz) can be related to the change in deformation observed during creep experiments. The spectra obtained in the case where an electrode is in contact with an electrolyte solution were reported by Mulder and Sluyters (1987) to be represented by equivalent circuit made up of a resistance R_Ω in series either with a capacitor or with a constant phase element. Contrary to the reported straight line spectra, the spectra obtained in the present study are all in the form of an arch in the high frequency range and therefore can be represented by the equivalent circuit presented in Section 5.2.1. Its generally consist of a resistance R_Ω in series with a distributed element (DE) from which the high frequency arc diameter can be obtained as well as the corresponding depression angle parameter n. The arc diameters obtained from simulation are very high, varying between 3600 kΩ and 35000 kΩ. The effect of sustained load on depression angle parameter n is presented in Figure 8.99. The reason why the spectra obtained here do not show an appropriate semi-circle in the high frequencies range may be due partly to the lack of electrolyte in the specimens studied which are D-dried $Ca(OH)_2$ compacts. This behavior is generally observed in Portland cement systems for which semi-circle spectra disappears with the removal of evaporable water as showed by the results reported by Brantervik

and Niklasson (1991) after studying mortar samples from which evaporable water was partially or totally removed.

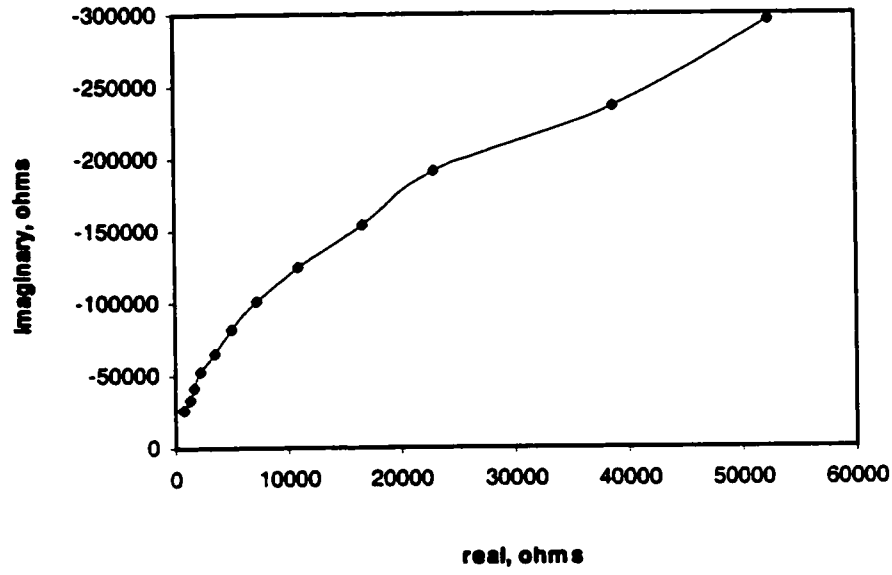

Figure 8.97: Complex impedance plot for unloaded $Ca(OH)_2$-compacts while conditioning at 0% RH

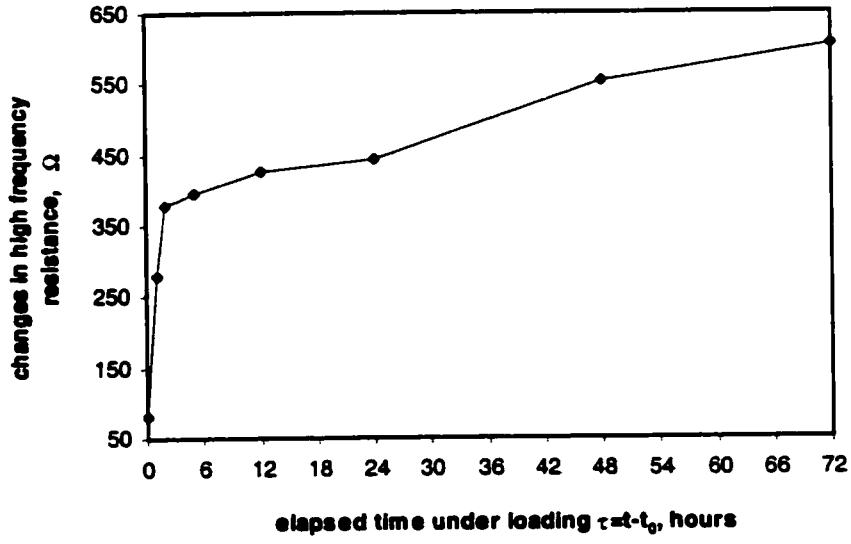

Figure 8.98: The variation of the change in high frequency resistance R_Ω for loaded $Ca(OH)_2$ compacts while conditioning at 0% RH at a stress level corresponding to 5% of the compaction pressure (386 MPa)

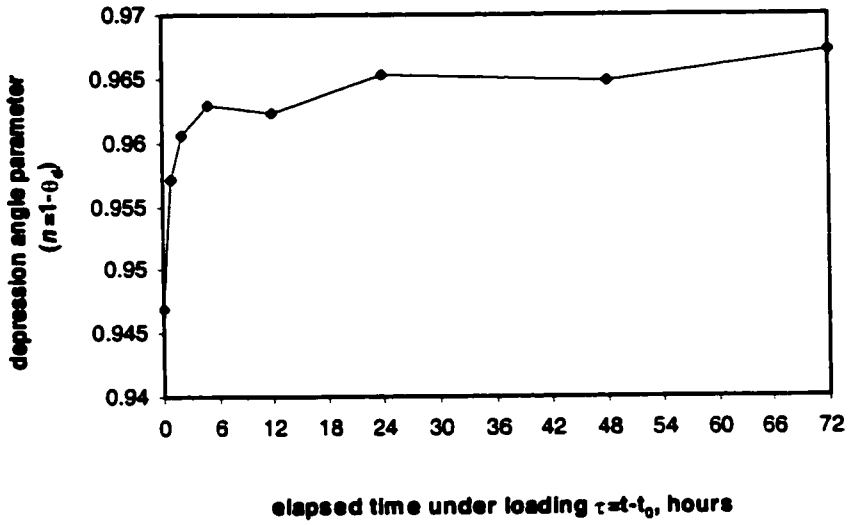

Figure 8.99: The variation of the depression angle parameter n for loaded $Ca(OH)_2$ compacts while conditioning at 0% RH at a stress level corresponding to 5% of the compaction pressure (386 MPa)

8.5 Proposed possible creep mechanism in cement paste systems

From the results discussed above in this chapter and from the review of the literature presented in Part 2, several parameters may have a considerable effect on creep of cement paste and/or concrete. However, in agreement with the Feldman-Sereda model of cement paste structure, the tentative mechanism of creep proposed here is believed to be caused by microsliding between adjacent C-S-H sheets. For a given stress level, the more is the presence of calcium silicate hydrates (C-S-H) in the paste, the more significant the magnitude of creep will be due to the action of C-S-H as creep centers. Layering or aggregation of C-S-H sheets may affect such microsliding. To a lesser extent, calcium hydroxide contributes to the magnitude of creep in cement paste systems. Figure 8.100 illustrates the suggested mechanism of creep in Portland cement paste. For the model proposed, it is assumed that collapse or rearrangement of unstable pores will only have very small contributions at room temperature.

In Figure 8.100, K_P represents the bulk stiffness of the hydrated cement paste and reflects the composite stiffness of the solid phase and the interlayer water contributing to the structure of the paste. This stiffness is associated to the instantaneous deformation observed when the cement

paste specimens is subjected to a stress field either by drying (shrinkage) or a sustained load (creep). $K_{C\text{-}S\text{-}H}$ represents the stiffness of the calcium silicate hydrates (C-S-H) solid phase, and K_{CH} is the stiffness of calcium hydroxide crystals, which are deformed by the stress relaxed from K_P. The parameters η_{CH} and $\eta_{C\text{-}S\text{-}H}$ represent the viscosity of the calcium hydroxide and calcium silicate hydrates respectively. At room temperature (22 ± 2°C), both parameters depend on the age of the material *t* and relative humidity *rh*. This rate determining approach is quite similar to that proposed by Powers (1965), with the addition that the magnitude of creep is a function of degree of hydration and that sliding is operative from creep centers at the very early age in saturated or dried hardened cement paste specimens. The description of the state of the water in layered structure of C-S-H and layering associated to sliding taking place during creep process was already illustrated in Figure 8.47.

During the initial period following the loading of the paste specimens, part of the adsorbed water at the entrance of C-S-H sheets will be entrapped as further layering is getting form. The density of the stressed interlayer water will therefore tend to increase with time as the same quantity of water is retained in a smaller space. The characteristics of the interlayer water can also being modified by the applied stress as the results of impedance analysis reveal considerable changes in HFA diameter of normal strength specimens loaded at very early age. The stress may increase the mobility of ions in hydrating cement paste and thus modify its resistivity.

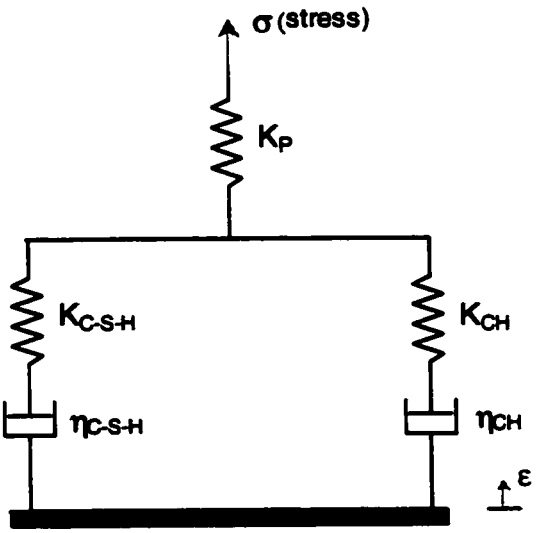

Figure 8.100: Suggested mechanical model for basic creep in cement paste

Part 5: Summary and recommendations

CHAPTER 9

CONCLUSIONS AND SUGGESTIONS FOR FUTURE RESEARCH

9.1 Introduction

The normal drying process consisting of vacuum drying at 105°C for 3 hours compared to vacuum drying at 37°C for 24 hours following solvent exchange or not was found to greatly affect the structure of either $Ca(OH)_2$ compacts, hydrated C_3S paste or hydrated cement paste. The solvent exchange technique, which in effect is a counter diffusion process, was shown to be influenced by calcium hydroxide, calcium silicate hydrates having different c/s ratios and hydrated C_3S paste. The role of either calcium hydroxide or calcium silicate hydrates in hydrated Portland cement systems was therefore clearly established through the inferences regarding the relevance of the Bangham effect and possible chemical interaction with the solid as to the mechanisms responsible for length and mass changes.

The volume instability of porous solids including cement systems in aqueous and non-aqueous media is believed to be complex and relevant to both microstructural and durability investigations. The effect of the presence or absence of solvent interactions in cement paste systems was established by studying the volume changes observed in partially saturated and saturated vycor glass and molecular sieves which are microporous systems different to hydrated cement systems. For the results presented, emphasis was given to reporting more extensively the length change and volume stability observations as opposed to mass change data due to the large number of results and the greater facility for meaningful interpretation of phenomena. Some anomalous volume changes observed from solvent exchange studies may partly explain the discrepancy of deformations during shrinkage and/or creep experiments. The effect of capillary and interlayer water on creep measurements was eliminated by performing some measurements at D-dry state which corresponds to 0% humidity in the cement systems. The effects of compressive stress on the density and porosity of hydrated C_3S and cement pastes have been isolated by introducing another fluid either methanol or isopropanol into the pore system. The contribution of calcium hydroxide to creep deformation was clearly established. Short-term deformations were found related to some electrical response parameters through a coupling with

AC impedance spectroscopy. All these approaches have produced results, which contribute to a significant advance in the understanding of the mechanisms of creep and shrinkage. The conclusions of experiments performed by solvent exchange of microporous systems, shrinkage and creep as well as coupling AC impedance - creep and shrinkage are presented in the following section.

9.2 Conclusions

1. The expansive character of the length change response of calcium hydroxide compacts when immersed in water, isopropanol, methanol, benzene, and acetone suggests that the length change is primarily due to both the Bangham effect and chemical interaction with the solid surfaces.

2. Expansion of calcium hydroxide compacts pre-conditioned to water contents in excess of that required for the full potential of Bangham expansion to be realized indicates that some form of chemical interaction mechanism between the adsorbate and the solid was likely operative.

3. Shrinkage (observed in certain cases), following the immediate expansion of calcium hydroxide compacts pre-conditioned to various water contents, was similar to that observed during isopropanol replacement of water in cement paste, suggesting that the length change on removal of water may be related to surface energy changes not always specific to the C-S-H phase alone.

4. Expansion of calcium hydroxide compacts (at all moisture contents), following immersion in methanol is similar to the length change response of cement paste immersed in methanol. This would appear to corroborate published evidence that methanol interacts with cement paste including the calcium hydroxide phase.

5. The similar pattern of length change behavior of calcium hydroxide compacts immersed in solvents with low affinity for water (benzene) and high affinity (acetone) suggests that length change mechanisms are similar.

6. The general transition of the length change dependency on compaction pressure (for CH compacts) from a direct to an inverse relationship during solvent replacement as a result of the pre-conditioning with water as an adsorbate suggests that the dissolution processes activated by

water are sufficient to further activate the release of strain energy during the solvent replacement process.

7. Length change of water-saturated hcp resulting from methanol exchange is different in character from that observed for methanol and DMSO exchange. Expansion as opposed to contraction (observed for other solvents) generally occurs. This is an indication that intercalation effects may be operative and supports expressed views that chemical interactions with the solid phase are possible in presence of methanol. It is not recommended for use in pre-treating specimens for mercury porosimetry tests.

8. Double exchange (i.e., with two different solvents) experiments with water-saturated cement paste provide evidence that initial exchange with methanol has an irreversible effect on length change. An initial exchange with isopropanol has a reversible effect on length change.

9. The starting conditions of hcp (D-dry or water-saturated), selection of solvent, and sequence of exchange have an effect on the volume stability of the hcp solids. Minimum effects on volume stability suitable for specimen preparation for porosimetry tests are desirable. Exchange of saturated specimens with isopropanol followed by vacuum drying for 24 hours is recommended.

10. Length change of hcp due to the solvent replacement process is dependent on drying history. This implies that if solvents are used as microstructural probes or as part of pre-treatment procedures for pore structure determination, the test results will be dependent on drying history. This applies to practical cases where cores from concrete structures are subject to examination.

11. Partial drying of hcp to equilibrium pressures near saturation (prior to solvent exchange) results in significantly larger expansion than is obtained for the water-saturated condition. This observation for exchange with all test solvents suggests that at higher equilibrium pressures, length change may be due to intercalation processes.

12. Solvent exchange of partially dried hcp with many of the test solvents has irreversible length change effects as indicated by the results of double exchange experiments.

13. There are similarities in the length change behavior of water-saturated C-S-H and hcp exchanged with the test solvents. The expansive nature of the methanol exchange process on both systems is similar.

14. Anomalous length change behavior (isopropanol exchange) occurs for C-S-H with C/S=1.6. It is the only C-S-H preparation for which isopropanol exchange results in expansion (similar to the methanol exchange). It is possible that isopropanol intercalation effects are similar to those of methanol at this C/S particular ratio.

15. Length change of CH due to solvent exchange is significant and similar in character to that of hcp. This is an indication that both C-S-H and CH contribute to the length change process.

16. Length changes of water-saturated vycor glass (resulting from the solvent exchange) have some similarities and some differences to those of hcp. A first exchange with methanol or isopropanol produces highly irreversible effects with respect to volume stability. Second exchanges of isopropanol for methanol and vice-versa result in increases in expansion or contraction trends associated with the first exchange. This suggests that the first exchange interactions are similar for cement paste and vycor glass and involve surface energy effects. The glass surfaces are perturbed to a greater extent and length change direction is not reversible on second exchange.

17. Length changes of water-saturated molecular sieves (resulting from the solvent exchange) also have similarities and differences to those of hcp. It is significant that initial exchanges with any of the test solvents do not irreversibly affect the volume stability of the material. It is suggested that the mechanisms responsible for length change in these materials are physical in nature.

18. Evidence based on thermogravimetric analysis suggests that methanol exchange and to a lesser extent isopropanol exchange removes water from the structure of C-S-H present in hydrated tricalcium silicate paste.

19. The state of stress of partially saturated tricalcium silicate paste exchanged with methanol is opposite to that obtained with isopropanol (tensile for the former and compressive for the latter).

20. Initial swelling of partially saturated tricalcium silicate paste exchanged with methanol or isopropanol is attributed to intercalation and possibly to Bangham effect. Continued swelling with methanol may be due to surface interaction with the C-S-H.

21. The D-dried tricalcium silicate reference paste (without exchange) exhibits a significant amount of creep (greater than 60 μstrain at 15 days) suggesting that creep mechanisms associated with water transport are not necessarily dominant.

22. Methanol and isopropanol exchanges prior to drying reduce the magnitude of creep in the dry state. This may be due to irreversible interactions of solvent with C-S-H.

23. Hardened cement paste specimens that have been fully dried (if there is no moisture exchange with the surrounding medium) creep as much or more than saturated reference specimens.

24. Cement paste dried to an intermediate humidity equal to 42% RH and re-saturated creeps significantly more than saturated cement paste that has not been dried. This is attributed to the pore coarsening effect due to drying and possible increase in creep sites due to increased layering of C-S-H.

25. The effect of D-drying and/or vacuum drying at 37°C on basic creep is similar and significant.

26. Exchanging water-saturated paste samples with methanol and isopropanol for 48 h followed by vacuum drying at 37°C will increase the basic creep of hardened cement paste relative to D-drying.

27. Re-saturation of D-dried cement paste specimens will increase the basic creep relative to the creep of initially water-saturated specimens.

28. Solvent exchange (methanol and isopropanol) for 48 h followed by vacuum-drying at 37°C has a smaller effect on the microstructure of cement paste than normal drying or vacuum-drying at 37°C for 24 h as indicated by their lower total porosity.

29. Specific basic creep can be expressed as a power function the parameters of which will depend on the water content of the samples and/or on the drying condition and pre-treatment history.

30. A re-examination of the role of water suggests that creep of hardened cement paste specimens is primarily due to microsliding between adjacent particles of C-S-H which additionally is affected by layering or aggregation of C-S-H sheets.

31. The pre-drying of cement paste prior to re-saturation with synthetic pore solution results in an increase in the total strain with time due to the application of a sustained load.

32. The increase in total deformation (under sustained load) of the vacuum dried (37°C) or solvent exchanged cement paste may be partly due to a pore coarsening effect.

33. Methanol exchange appears to perturb the solid phase of the cement paste to the extent that total strain, strain recovery and shrinkage have the largest values in this study.

34. Creep of cement paste subjected to drying is most affected by the solvent exchange pre-drying treatment. This also applies to the creep recovery.

35. AC Impedance spectroscopy can detect real-time microstructural changes in cement paste unloaded or subjected to a sustained load.

36. There is a systematic time-dependent growth in the size of the impedance high-frequency arc for unloaded or loaded cement paste.

37. The size of the high-frequency arc is consistent with a pore coarsening effect in the cement paste due to pre-drying treatment. Observation of the smallest arcs corresponds with the largest values for total strain.

38. Smaller high frequency arc sizes for total strain measurements relative to the arcs obtained for shrinkage measurements suggests that continuous processes involving slipping and sliding of the C-S-H sheets may be operative when cement paste is under sustained load.

39. The value of the high-frequency arc depression angle parameter (with time) appears to reflect the relative amount of creep that occurs. Low values of creep for the untreated specimens may be related to the low values of the depression angle parameter.

40. The compliance rate of hardening cement paste appears to depend on the state of hydration of the material and is a linear function (log-log plot) of time after loading, suggesting that the rate determining mechanism may be associated with slipping and sliding of the C-S-H sheets.

41. The creep process may partly depend on the state of hydration of the hardening Portland cement paste and not necessarily on period of loading. The presence of C-S-H at early age seems to induce an increasing of the amount of creep centers and consequently the development of a significant creep magnitude.

42. The sustained loading of normal strength cement paste (w/c=0.50) loaded after 18 hours hydration seems to increase the degree of hydration during early creep. The significant creep observed suggesting that initially, creep may depend on the capillary space as water in coarser pores may signify more room for load-induced hydration products.

43. The creep and shrinkage results obtained from impedance spectra indicate that the HFA diameter of cement paste specimens increases with hydration. It is suggested that this may be due to a loss of electrolyte accompanied by a decrease of pore connectivity and/or an increase in layering following sliding between C-S-H sheets.

44. The compliance or creep coefficient of hardening cement paste can be expressed as the function of the degree of hydration (α_d) at any time t, the degree of hydration at loading (α_{do}) and the relative humidity (rh) in the hardening cement paste and/or concrete.

45. The depression angle parameter n increases with the hydration of continuously wet unloaded hardening cement paste. However, sustained loading may contribute to the wide scatter observed for this parameter, particularly for normal strength paste.

46. The HFA diameter of unloaded specimens is greater than that of loaded one. This may be due to load induced redistribution of water within the matrix. The effect of electrolyte on the

impedance behavior in hydrating cement paste seems to be less pronounced in high strength paste than normal strength.

47. Calcium hydroxide undergoes basic creep at D-dry state and the observed magnitude at very early age may be due to the rearrangement of the $Ca(OH)_2$ crystals along their preferential planes of minimum energy which allows the specimens to become more stable. Such a rearrangement is believed to take place through a slipping and sliding process along these planes.

9.3 Suggestions for future research

Even though the data collected in the present study have brought a certain light for a better understanding of creep mechanism in hydrated cement paste, the following points, which remain uncertain, still need further investigation.

1. The influence of temperature, mineral and chemical admixtures and their corresponding change in the degree of hydration on shrinkage and on creep characteristics given the actual civil application of high strength concrete.

2. The improvement of coupling AC impedance - creep and shrinkage setup in order to establish a indirect method for determining deformation in cement paste and concrete through spectral response of a electrical signal.

3. The determination of lower (a_L) and upper (a_U) coefficients to establish an appropriate interval of confidence for the compliance rate dJ/dt, defined as an inverse function of the age of the material t (see Figure 9.1) from extensive experimental data collected from different laboratories.

4. The adequacy of the suggested mechanical model to the deformations of hardened cement paste and its application to shrinkage and creep of concrete.

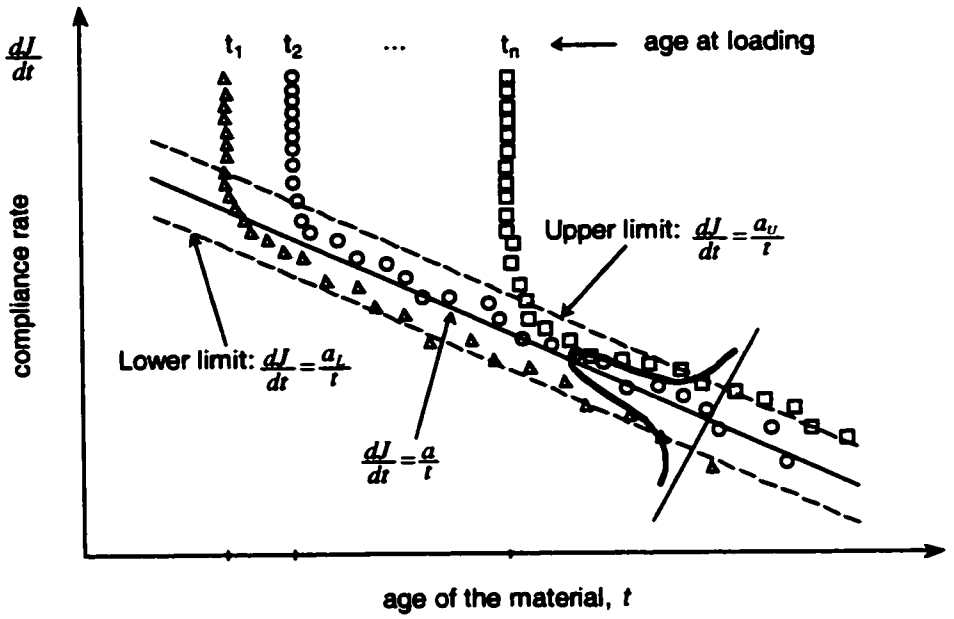

Figure 9.1: Sketch of the compliance rate obtained from extensive data collection to establish an interval of confidence in determining the inverse function parameter a

REFERENCES

Abdul-Maula S. and Odler I. (1981), *Hydration Reactions in Fly-ash-Portland Cements*, In: Malhotra, V Edition, Proceedings of Symposium N on Effects of Fly Ash Incorporation in Cement and Concrete, Boston, 16-18 November, Materials Research Society, pp. 102-111

Alexander K. M., Wardlaw J. and Ivanusec I. (1979), *The Influence of SO_3 Content of Portland Cement on the Creep and Other Physical Properties of Concrete*, Cement and Concrete Research, Vol. 9, No. 4, pp. 451-459.

Ali I and Kesler C. (1972), *Mechanism of Creep in Concrete*, Symposium on Creep of Concrete, Detroit, ACI Publication SP-9

Anson, M. (1964), *An Investigation Into a Hypothetical Deformation and Failure Mechanism for Concrete*, Magazine of Concrete Research, Vol. 47, No. 16, pp. 73-82

Asgeirsson H. and Gudmundsson G. (1979), *Pozzolanic Activity of Silica Dust*, Cement and Concrete Research, Vol. 9, pp. 249-252

Bazant Z. P. (1970), *Constitutive Equation for Concrete Creep and Shrinkage Based on Thermodynamics of Multiphase Systems*, Materials and Structures (RILEM), Vol. 3, No. 13, pp. 3-36

Bazant Z. P. (1971), *Thermodynamic Theory of Deformations of Concrete with Explanation of Drying Creep*, ACI Symposium on Designing for Effects of Creep, shrinkage and Temperature, SP 27, p. 411

Bazant Z. P. (1975), *Theory of Creep and Shrinkage in Concrete Structure: A Precis of Recent Developments*, Mechanics Today, Vol. 2, pp. 1-93

Bazant Z. P. and Moschovidis Z. (1973), *Surface-Diffusion Theory for Drying Creep Effect in Portland Cement Paste and Concrete*, Journal of American Ceramic Society, Vol. 56, No. 5, pp. 235-241

Bazant Z. P. and Najjar L. J. (1997), *Nonlinear Water Diffusion in Nonsaturated Concrete*, Fifty Years of Evolution of Science and Technology of Building Materials and Structures, Edited by F. H. Wittmann, pp. 435-452

Bazant Z. P. and Raftshiel W. J. (1982), *Effect of Cracking in drying and Shrinkage Specimens*, Cement and Concrete Research, Vol. 12, No. 2, pp. 209-226

Bazant Z. P., Asghari A. A. and Schmidt J. (1976), *Experimental Study of Creep of Hardened Portland Cement Paste at Variable Water Content*, Materials and Structure, Vol. 9, No. 52, pp. 279-290

Bazant Z. P., Hauggaard A. B., Baweja S. and, Ulm F. J. (1997), *Microprestress-Solidification Theory for Concrete Creep I: Aging and Drying Effects*, Journal of Engineering Mechanics, Vol. 123, No. 11, pp. 1188-1194

Beaudoin J. J. (1985), *Effect of Water and Other Dielectrics on Subcritical Crack Growth in Portland Cement Paste*, Cement and Concrete Research, Vol. 15, No. 6, pp. 988-994

Beaudoin J. J. (1987), *Validity of Using Methanol for Studying the Microstructure of Cement Paste*, Materials and Structure, Vol. 20, No. 115, pp. 27-31

Beaudoin J. J. (1987), *Validity of using methanol for studying the microstructure of cement paste*, Materials and Structures, Vol. 20, No.115, pp. 27-31

Beaudoin J. J. and Brown P. W. (1992), *The Structure of hardened cement paste*, in Proceedings of the 9th International Congress on the Chemistry of Cement, New Delhi, India, Part III, vol. 1, pp. 485-525.

Beaudoin J. J. and Ramachandran V. S. (1992), *A New Perspective on the Hydration Characteristics of Cement Phases*. Cement and Concrete Research, Vol. 22, No. 4, pp. 689-694.

Beaudoin J. J., Gu P., Tumidajski P. J., and Perron S. (1996), *Microstructural Changes on Drying and Rewetting of Hydrated Cement Paste – An A.C. Impedance Spectroscopy Study, Concrete: from Material to Structure*, Proceedings of the RILEM International Conference, Arles, France, September 11-12, pp. 32-42

Bentur A. (1980), *Effect of Curing Temperature on the Pore Structure of Tricalcium Silicate Paste*, Journal of Colloid and Interface Science, Vol. 74, No. 2, pp. 549-560.

Bentur A. (1980), *The Pore Structure of Hydrated Cementitious compounds of Different Chemical Composition*, Journal of The American Ceramic Society, Vol. 63, No. 7-8, pp. 381-356.

Bentur A. and Young J. F. (1981), *Simplified Method of Determining the Polysilicate Content in Cementitious Pastes Using Trimethylsilyl Derivatives*, Cement and Concrete Research, Vol. 11, No. 2, pp. 287-290

Bentur A., Berger R. L., Lawrence F. V., Milestone N. B., Mindess S. and Young J. F. (1979), *Creep and Drying Shrinkage of Calcium Silicate Pastes III. A Hypothesis of Irreversible Strains*, Cement and Concrete Research, Vol. 9, pp. 83-96.

Bentur A., Berger R. L., Lawrence F. V., Milestone N. B., Mindess S., and Young J. F. (1979), *A Reply to S. Chatterji's Discussion of Creep and Drying Shrinkage of Calcium Silicate Pastes. III. A Hypothesis of Irreversible Strains*, Cement and Concrete Research, Vol. 9, No. 5, p. 657

Bentur A., Kung J. H., Berger R. L., Young J. F., Milestone N. B. Mindess S. and Lawrence F. V. (1980), *Influence of Microstructure on the Creep and Drying Shrinkage of Calcium Silicate*

Pastes, Proceeding 7th International Congress on Chemical of Cement, Paris, Vol. III, Editions Septima, pp. VI.26-31

Bentur A., Milestone N. B. and Young J. F. (1978), *Creep and Shrinkage of Calcium Silicate Pastes II. Induced Microstructural and Chemical Changes*, Cement and Concrete Research, Vol. 8, pp. 721-732.

Berger R. L. (1972), Calcium Hydroxide: Its *Role in the Fracture of Tricalcium Silicate Paste*, Science, Vol. 175, pp. 626-629.

Berger R. L. and McGregor T. D. (1972), *Influence of admixture on the Morphology of Calcium Hydroxide Formed During Tricalcium Silicate Hydration*, Cement and Concrete Research, Vol. 2, No. 1, pp. 43-57.

Berger R. L. and McGregor T. D. (1973), *Effect of Temperature and Water-Solids Ratio on Growth of $Ca(OH)_2$ Crystals Formed During Hydration of Ca_3SiO_5*, Journal of The American Ceramic Society, Vol. 56, No. 2, pp. 73-79.

Berger R. L., Kung J. H. and Young J. F. (1976), *Influence of Calcium Chloride on Drying Shrinkage of Alite Paste*, Journal of Testing and Evaluation, Vol. 4, No. 1, pp. 85-93

Berjaguin B. V. and Churaev N. V. (1974), *Structural Component of Disjoining Pressure*, Journal of Colloid Interface Science, Vol. 49, No. 2, pp. 249-257

Brantervik Kjell and Niklasson G. A. (1991), *Circuit Models For Cement Based Materials Obtained From Impedance Spectroscopy*, Cement and Concrete Research, Vol. 21, No. 4, pp. 496-508

Bray W. H. and Sellevold E. J. (1973), *Water Sorption Properties of Hardened Cement Paste Cured or Stored at Elevated Temperatures*, Cement and Concrete Research, Vol. 3, No. 6, pp. 723-728

Brown N. H. and Hope B. B. (1976), *The Creep of Hydrated Cement Paste*, Cement and Concrete Research Vol. 6, No. 4, pp. 475-486

Chatterji S. (1976), *Drying Shrinkage of Cement Paste and Concrete: A Reappraisal of the Measurement Technique and its Significance*, Cement and Concrete Research, Vol. 6, No. 1, pp. 145-148

Chatterji S. (1979), *A Discussion on paper 'Creep and Shrinkage of Calcium Silicate Pastes III: A Hypothesis of Irreversible Strains' by A. Bentur et al.*, Cement and Concrete Research, Vol. 9, No. 5, pp. 655-656

Cole K. S. and Cole R. H. (1941), *Dispersion and Absorption in Dielectrics I. Alternating Current Characteristics*, J. Chem. Phys., Vol. 9, pp. 341-351

Collepardi M. and Marchese B. (1972), *Morphology and Surface Properties of Hydrated Tricalcium Silicate Paste*, Cement and Concrete Research, Vol. 2, No. 1, pp. 57-65

Daimon M., Abo-El-Enein S. A., Hosaka G., Goto S., and Kondo R. (1977), *Pore structure of calcium silicate hydrate in hydrated tricalcium silicate*, Journal of American Ceramic Society, vol. 60, pp. 110-114.

Daimond S. (1971), *A critical Comparison of Mercury Porosimetry and Capillary Condensation Pore Size Distributions of Portland Cement Pastes*, Cement and Concrete Research, Vol. 1, No. 5, pp. 531-545.

Danielsson, U. (1974), *An apparatus for easy determination of the amount of bound water in cement pastes yielding highly reproducible results*, Materials and Structures, RILEM, vol. 7, n° 40, pp. 231-246

Davis R. E. and Troxell G. E. (1954), *Properties of Concrete and their Influence on Prestress Design*, ACI journal, Proceeding 50, pp. 381-391

Day R. L. (1981), Reactions Between Methanol and Portland Cement Paste, Cement and Concrete Research, Vol. 11, No. 3, pp. 341-349

Day R. L. and Illston J. M. (1983), *The effect of Rate of Drying on the Drying/Wetting Behavior of Hardened Cement Paste*, Cement and Concrete Research, Vol. 13, No. 1, pp. 7-17

De Larrard, F. and Acker, P. (1990), *Un exemple d'ingénierie du matériau: Amélioration de l'étanchéité à l'air des enceintes internes de centrales nucléaires, intérêts de l'emploi d'un béton à hautes performances de formulation spéciale*, Rapports des Laboratoires édités par le LCPC, Série Ouvrages d'Art OA-7

De Levie R. (1965), Electrochemical Acta, Vol. 10, p. 113

Delvasto S. (1986), *Pozzolanic Activity and Characteristics of Colombian materials*, In: Malhotra, V Edition, Proceeding of the 2nd International Congress on Fly Ash, Silica Fume, Slag, and Natural Pozzolans in Concrete, Madrid, American Concrete Institute Special Publication 91, Vol. I, pp. 77-79

Dent Glasser L. S., Lachowski E. E., Qureshi M. Y., Calhoun H.P., Embree D.J., Jamiesan W.D. and Masson C.R. (1981), *Identification of Some of the Polysilicate Components of Trimethylsilylated Pastes*, Cement and Concrete Research, vol. 11, No. 5/6, pp. 775-780.

Diamond S. (1972), *Identification of Hydrated Cement Constituents Using a Scanning Electron Microscope-Energy Dispersive X-ray Spectrometer Combination*, Cement and Concrete Research, Vol. 2, pp. 617-632.

Diamond S. (1976), *Cement paste microstructure-an overview at several levels*, in Hydraulic Cement Pastes: Their Structure and Properties, Cement and Concrete Association, Wexham Springs, Slough, UK, pp. 2-30.

Dollimore D. (1981), *Thermal Analysis Studies on Cement Pastes Treated with Organic Solvents*, Proceeding 2nd European Symposium on Thermal Analysis, Heyden, London, p. 485

Domone P. L. J. (1994), *Hardened Properties of Portland Cement Grouts*, Structural grouts, Edited by Chapman & Hall, pp. 58-93

Feldman R. F. (1968), *Sorption and Length-Change Scanning Isotherms of Methanol and Water on Hydrated Portland Cement*, Proceeding Symposium on Chemistry of Cement, Tokyo, 3, pp. 53-66

Feldman R. F. (1968), *Sorption and Length-change Scanning Isotherms of Methanol and Water on Hydrated Portland Cement*, Proceeding, 5th International Symposium Of Chemistry of Cement, Tokyo, Part III, Vol. III, pp. 53-66

Feldman R. F. (1972), *Mechanism of Creep of Hydrated Portland Cement Paste*, Cement and Concrete Research, Vol. 2, No. 5, pp. 521-540

Feldman R. F. (1987), *Diffusion measurements in cement paste by water replacement using propano-2-ol*, Cement and Concrete Research, Vol. 17, No. 4, pp. 602-612

Feldman R. F. and Beaudoin J. J (1976), *Microstructure and Strength of Hydrated Cement*, Cement and Concrete Research, Vol. 6, pp. 389-400

Feldman R. F. and Beaudoin J. J. (1974), Microstructure and Strength of Hydrated Cement, Symposium on Chemistry of Cement, Moscow, pp.895-911

Feldman R. F. and Sereda P. J. (1970a), *A Model for Hydrated Portland Cement Paste and its Practical Implications*, Journal of Engineering, Vol. 53, No. 9, pp. 53-59.

Feldman R. F. and Sereda P. J. (1970b), *A New Model for Hydrated Portland Cement Paste as Deduced from Sorption Length Change and Mechanical Properties*, Materials and Structure, Paris, Vol. 1, No. 6, pp. 509-520.

Feldman R. F. and Swenson E. G. (1975), *Volume changes on First Drying of Hydrated Cement with and without Admixture*, Cement and Concrete Research, Vol. 5, No. 1, pp. 25-35.

Gamble B. R. and Illston J. M. (1976), *Rate of Deformation of Cement Paste and Concrete During Regimes of Variable Stress, Moisture Content and Temperature*, in Hardened Cement Paste: Its Structure and Properties, Cement and Concrete Assoc., Wexham Springs, Slough, UK, pp. 297-311

Gimblett II-225

Glucklich J. and Ishai O. (1962), *Creep Mechanism in Cement Mortar,* Journal of American Concrete Institute Vol. 59 No. 7 pp. 923-948

Gu P., Xie P., Fu Y. and Beaudoin J. J., *Microstructural Characterization of Cementitious materials: Conductivity and Impedance Methods*, Materials Science of Concrete IV, The American Ceramic Society, 1995, pp. 201-262

Gu P., Xie P., Fu Y., and Beaudoin J. J. (1998), *Microstructural Characterization of Cementitious Materials: Conductivity and Impedance Methods*, Materials Science of Concrete IV, American Ceramic Society, Westerville, Ohio, pp. 201-262

Gu P., Xu Z., Xie P. and Beaudoin J. J. (1993), *Application of A.C. Impedance Techniques in Studies of Porous Cementitious Materials (I). Influence of Solid Phase and Pore Solution on High Frequency Resistance*, Cement and Concrete Research, Vol. 23, No. 3, pp. 531-540

Gu P., Xu Z., Xie P. and Beaudoin J. J. (1993), *Application of AC Impedance Techniques in Studies of Porous Cementitious Materials, (I). Influence of Solid Phase and Pore Solution on High-Frequency Resistance*, Cement and Concrete Research, Vol. 23, No. 3, pp. 531-540

Gu, P.; Xie, P.; Beaudoin, J.J. and Brousseau, R. (1992), *AC Impedance Spectroscopy (I): A New Equivalent Circuit Model for Hydrated Portland Cement Paste*, Cem. Conc. Res., No. 22, Vol. 5, pp. 833-840

Haller P. (1940), *Shrinkage and Creep of Mortar and Concrete*, DisKussionbericht, No. 124, EMPA, Zurich, German.

Hannant D. J. (1968), Strain Behavior of Concrete up to 95°C Under Compressive Stresses, Proceeding Conference on Prestressed Concrete Pressure Vessels, London, The Institute of Civil Engineers

Hashin Z. (1962), *Elastic Moduli of Heterogeneous Materials*, Journal of Applied Mechanics, Vol. 29, No. 1, pp. 143-150

Helmuth R. A and Turk D. H. (1967), *The Reversible and Irreversible Drying Shrinkage of Hardened Cement and Tricalcium Silicate Pastes*, Journal of Research and Development Laboratory of Portland Cement Association, Vol. 9, No. 2, pp. 8-21

Helmuth R. A. and Turk D. H. (1966), *Elastic Moduli of Hardened Portland Cement and Tricalcium Silicate Pastes: Effect of Porosity*, Highway Research Bulletin, Special Report, No. 90, pp. 135-144

Hobbs D. W. (1978), *The Influence of SO_3 Content on the Behavior of Portland Cement Mortars*, World Cement Technology, Vol. 9, No. 3, pp. 211-222.

Hooton R. D. (1986), *Permeability and Pore Structure of Cement Pastes Containing Fly Ash, Slag, and Silica Fume*, In: Blended Cements, Denver 1984, American Society for Testing and Materials Special Technical Publication 897, pp. 128-143

Hughes D. C. (1988), *The Use of Solvent Exchange to Monitor Diffusion Characteristics of Cement Pastes Containing Silica Fume*, Cement and Concrete Research, Vol. 18, No. 2, pp. 321-324

Hunt C. M., Tomes L. A. and Blaine R. L. (1960), *Some Effects of Aging on the Surface Area of Portland Cement Paste*, Journal Research of National Bureau Standard, Vol. 64A, No. 2, pp. 163-169

Hwang C.L. (1983), *Drying Shrinkage and Microstructure of Hydrated Cement Pastes*, Ph.D. Thesis, University of Illinois.

Idorn M. (1968), Hydration of Portland Cement Paste at High Temperature Under Atmospheric Pressure, Proceeding Symposium on Chemistry of Cement, Tokyo, Vol. 3, pp. 411-435

Iseki S., Ohashi K. and Nagaura S. (1972), Electrochemistry Acta, Vol. 17, p. 2249

Iseki, S.; Ohashi, K. and Nagaura, S. (1972), Electrochemical Acta, Vol. 17, p. 2249

Ishai O. (1968), *The Time-Dependent Deformation Behavior of Cement Paste, Mortar and Concrete*, Proceeding of Conference of the Structure of Concrete and its Behavior Under load, London 1965, p. 345, Cement and Concrete Association, Slough, U. K.

IUPAC (1972), Manual of Symbols and Terminology, Appendix 2, Part 1, Colloid and Surface Chemistry, Pure Applied Chemistry, Vol. 31, p578.

Kalousek G. L. (1957), *Crystal chemistry of hydrous calcium silicates.* I. Substitution of aluminum in lattice of tobermorite, *J. Am. Ceram. Soc.*, vol. 40, pp. 74-80.

Kalousek G. L. (1957), *Discussion on Simplified Method for Determination of Apparent Surface Area of Concrete Products*, Journal of American Concrete Institute, vol. 51, No. 4, p. 448

Kawamura M. (1978), *Internal Stresses and Microcrack Formation Caused by Drying in Hardened Cement Pastes*, Journal of The American Ceramic Society, Vol. 61, No. 7/8, pp. 281-283

Kohno K., Aihara F. and Ohno K. (1989), *Relative Durability Properties and Strengths of Mortars Containing Finely Ground Silica and Silica Fume*, In: Malhotra, V Edition, Proceeding of the 3rd International Congress on Fly Ash, Silica Fume, Slag, and Natural Pozzolans in Concrete, Trondheim, American Concrete Institute Special Publication 114, Vol. I, pp. 815-826

Kondo R. and Daimon M. (1974), Phase composition of hardened cement paste, Proc. 5th Int. Congr. On the Chemistry of Cement, Moscow.

L'Hermite R. G. (1960), *Volume Change of Concrete*, Proceeding 4th International Symposium on the Chemistry of Cement, Washington D. C., pp. 659-694

Lachowski E. E. (1979), *Trimethylsilylation as a tool for the study of cement pastes.* II. *Quantitative analysis of the silicate fraction of Portland cement pastes*, *Cem. Concr. Res.*, vol. 9, No. 3, pp. 337-343.

Lachowski E. E. (1979), *Trimethylsilylation as a tool for the study of cement pastes.* I. *Comparison of methods of derivatization*, *Cem. Concr. Res.*, vol. 9, No. 1, pp. 111-114.

Lachowski E. E., Mohan K., Taylor H. F. W. and Moore A. E. (1980), *Analytical electron microscopy of cement pastes.* II. Pastes of Portland cement and clinkers, *J. Am. Ceram. Soc.*, vol. 63, pp. 447-452.

Lankard D. R. (1972), *A Low Temperature Sintering Phenomenon in Heated Portland Cement Pastes*, Cement and Concrete Research, Vol. 2, No. 2, pp. 195-200

Lawrence C. D. (1973), *Porosity/Strength Relationships for Portland Cement Pastes*, In: RILEM/IUPAC Symposium: Pore structure and properties of materials, Prague, Vol. V, pp. 167-176

Lentz C. W. (1966), *The Silicate Structure Analysis of Hydrated Portland Cement Paste*, Symposium on the Structure of Portland Cement Paste and Concrete, Highway Research Board Special Report, No. 90, pp. 269-283

Li J. F., Ai H. and Viehland D. J. (1995), American Ceramic Society, Vol. 78, pp. 416-420

Litvan G. G. (1976), *Variability of the Nitrogen Surface Area of Hydrated Cement Paste*, Cement and Concrete Research, Vol. 6, No. 1, pp. 139-144.

Lowell S. (1979), *Introduction to Powder Surface Area*, Published by John Wiley & Sons, New York, 199p.

Luikov A. V. (1997), *Heat and Moisture Transfer in Capillary Porous Media*, Proceeding Fifty Years of Evolution of Science and Technology of Building Materials and Structures, Edited by F. H. Wittmann, pp. 427-434

MacCarter, W.J. and Garvin, S. (1989), *Dependence of Electrical Impedance of Cement Based Materials on their Moisture Condition*, Journal of physics, D: Applied Physics, No. 22, Vol. 11, pp. 1773-1776

Marsh B. K. (1985), *The Effect of Solvent Replacement Upon the Pore Structure Characteristics of Portland Cement Paste*, Proceeding of RILEM/CNR Symposium on Principles and Applications of Pore Structural Characterizatio, Arrowsmith, Bristol, pp. 651-658

Massazza F. and Costa U. (1979), Aspetti dell 'attivita' pozzolanica e proprieta' dei cementi pozzolanici, Il Cemento, No. 1, pp. 3-18

Massazza F. and Daimon M. (1992), *Chemistry of hydration of cements and cementitious systems*, in Proceedings of the 9th International Congress on the Chemistry of Cement, New Delhi, India, Part III, vol. 1, pp. 383-429.

McCarter W. J. and Brousseau R. (1990), *The A.C. Response of Hardened Cement Paste*, Cement and Concrete Research, Vol. 20, No. 6, pp. 891-900

McCarter W. J. and Curran P. N. (1984), *The Electrical Response Characteristics of Setting Cement Paste*, Magazine of Concrete Research, Vol. 36, No. 126, pp. 42-49

McCarter W. J. and Curran P. N. (1984), *The Electrical Response Characteristics of Setting Cement Paste*, Magazine of Concrete Research, Vol. 36 No. 126, pp. 42-49

McCarter W. J., Garvin S. and Bouzid N. J. (1988), Jounnal of Materials Science Lettre, Vol. 7, No. 10, pp. 1056-1057

McCarter W. J., Garvin S., and Buzzed N. (1988), *Impedance Measurement on Cement Paste*, Journal of Material Science Letters, Vol. 7, No. 10, pp. 1056-1057

Metha P. K. (1981), Studies on Blended Portland cements Containing Santorin Earth, Cement and Concrete research, Vol. 11, pp. 507-518

Mikhail R. S. and Selim S. A. (1966), *Adsorption of Organic Vapors in Relation to the Pore Structure of Hardened Portland Cement Pastes*, Highway Research Board Special Report, No. 90, pp. 123-134

Mills R. H. (1960), RILEM International Symposium on Concrete and Reinforced Concrete in Hot Countries, Haifa

Mills R. H. (1969), *Supplementary Paper III-46: Molecular sieve Effect in Concrete*, Proceedings, Fifth International Symposium of Chemistry of Cement, Tokyo, Cement Association of Japan, Vol. III, pp. 74-85.

Mindess S. and Young J. F. (1981), *Concrete*, Prentice-Hall, Inc. Englewood Cliffs, New Jersey, 481-500.

Moore A. E. (1980), *Structure and Composition of Compounds in Some Fully Hydrated Cement Pastes*, Proceeding of the 7th International Congress on Chemistry of Cement, Paris, Vol. III, pp. VI.97-102.

Moore A. E. and Taylor H. F. W. (1970), *Crystal Structure of Ettringite*, Acta Crystal, Vol. B26, pp. 386-393.

Moranville-Regourd M. (1998), *Cement Made From Blastfurnace Slag*, In: Lea's Chemistry of Cement and Concrete, Fourth Edition, Edited by Peter C. Hewlett, pp. 633-674

Mullen W. G. and Dolch W. L. (1964), *Creep of Portland Cement Paste*, Proceeding of the American Society of Testing Materials, Vol. 64, pp. 1146-1171

Nasser K. W. and Neville A. M. (1965), *Creep of Concrete at Elevated Temperature*, Journal of the American Concrete Institute, Vol. 62, No. 12, pp. 1567-1574

Nelson J. A. and Young J. F. (1977), *Additions of Colloidal Silicas and Silicates to Portland Cement Pastes*, Cement and Concrete Research, Vol. 7, No. 3, pp. 277-282

Neville A. M. (1962), *Shrinkage and Creep in Concrete*, Structural Concrete, Vol. 1, No. 2, pp. 49-85

Neville A. M. (1970), *Creep of Concrete: Plain, Reinforced and Prestressed*, North-Holland, Amsterdam, 622p

Neville, A.M. (1959), *Role of Cement in the creep of Mortar*, Proc. Journal of American Concrete Institute, Vol. 65, pp. 963-984

Neville, A.M. (1960), *The Relation Between Creep of Concrete and the Stress-Strength Ratio*, Applied Scientific Research, Section A, Vol. 9, pp. 285-292

Norberg P. (1999), *Electrical Measurement of Moisture Content in Porous Building Materials*, Durability of Building Materials and Components, Edited by M.A. Lacasse and D. J. Vanier, pp. 1030-1039

Odler I. (1991), *Strength of Cement, Final report of RILEM-TC 68-MMH Mathematical Modeling of Cement Hydration Task Group 1*. Materials and Structure, Vol. 24, p143.

Odler I. and Rossler M. (1985), *Investigations on the Relationship Between Porosity, Structure and Strength of Hydrated Portland Cement Pastes*, Cement and Concrete Research, Vol. 15, No. 3, pp. 401-410

Ogawa K. and Roy D. M. (1982), *C_4A_3S Hydration, Ettringite Formation, and Its Expansion Mechanism: II. Microstructural Observation of Expansion*, Cement and Concrete Research, Vol. 12, No. 1, pp. 101-109.

Orr C. and Dalla Valla J. M. (1959), *Fine Particle Measurement*, Macmillan, New York, 175p.

Parrott L. J. (1977a), *Recoverable and Irrecoverable Deformation of Heat-Cured Cement Paste*, Magazine of Concrete Research, vol. 29, No. 98, pp. 26-30

Parrott L. J. (1977b), *Basic Creep, Drying Creep and Shrinkage of a Mature cement Paste After a Heat Cycle*, Cement and Concrete Research, vol. 7, No. 5, pp. 597-604

Parrott L. J. (1978), *A Study of Basic Creep in Relation to Phase Changes in Cement Paste*, RILEM Int. Colloq. Adv. Theory, Mechanism and Phenomenology of Creep

Parrott L. J. (1979), *Change in Saturated Cement Paste Due to Heating*, Cement and Concrete Association, Technical Report 528.

Parrott L. J. (1980), *Effect of the First Drying Upon the Pore Structure of Hydrated Alite Paste*, Cement and Concrete Research, Vol. 10, No. 5, pp. 647-655

Parrott L. J. (1981), *Effect of Drying History Upon the Exchange of Pore Water with Methanol and Upon Subsequent Methanol Sorption Behavior in Hydrated Alite Paste*, Cement and Concrete Research, Vol. 11, No. 5, pp. 651-658

Parrott L. J. (1983), *Thermogravimetric and Sorption Studies of Methanol Exchange in an Alite Paste*, Cement and Concrete Research, Vol. 13, No. 1, pp. 18-22

Parrott L. J. (1984), Materials and Structure, Vol. 17, p. 131

Parrott L. J. and Taylor M. G. (1979), *A Development of the Molybdate Complexing Method for the Analysis of Silicate Mixtures*, Cement and Concrete Research, vol. 9, No. 1, pp. 483-488

Parrott L. J. and Young J. F. (1981), *Effect of Prolonged Drying Upon the Silicate Structure of Hydrated Alite Pastes*, Cement and Concrete Research, vol. 11, No. 1, pp. 11-17

Parrott L. J. and Young J. F. (1982), *Shrinkage and Swelling of Two Hydrated Alite Pastes*, in Fundamental Research on Creep and Shrinkage of Concrete, pp. 35-47.

Parrott L.J. (1985), *Effect of Changes in UK Cements upon Strength and Recommended Curing Times*, Concrete, Vol. 19, pp. 22-24

Parrott L.J., (1981), *Effect of drying history upon the exchange of pore water with methanol and upon subsequent methanol sorption behavior in hydrated alite paste*, Cem. Concr. Res., vol. 11, pp. 651-658.

Parrott L.J., Hansen W. and Berger R. L. (1980), *Effect of drying and rewetting upon the pore structure of hydrated alite paste*, Cem. Concr. Res., vol. 10, No. 5, pp. 647-656.

Pickett G. (1956), *Effect of Aggregate on Shrinkage of Concrete and Hypothesis Concerning Shrinkage*, Journal of The American Ceramic Society, Vol. 52, pp. 581-590

Powers T. C. (1958), *Structure and Physical Properties of Hardened Portland Cement Paste*, Journal of American Ceramic Society, Vol. 41, No. 1, pp. 1-6

Powers T. C. (1961), *Fundamental Aspects of Shrinkage of Concrete*, Revue Matériaux et Construction, No. 544, pp. 79-85

Powers T. C. (1962), *Physical Properties of Cement Paste*, Proceeding of Fourth International Symposium of Cement Chemistry of Cement, Washington, D.C., 1960. National Bureau of Standards Monograph, No. 43, pp. 577-609.

Powers T. C. (1965), *Mechanism of Shrinkage and Reversible Creep of hardened Cement Paste*, Proceeding of International Conference, London, pp. 319-344.

Powers T. C. (1968), *The thermodynamics of volume change and creep*, Matériaux et Constructions, vol. 1, No. 6, pp. 487-507.

Powers T. C. and Brownyard T. L. (1967), *Studies of the Physical Properties of hardened Portland Cement Paste*, Journal of American Concrete Institute, Vol. 43, pp. 933-969.

Powers T. C., Copeland L. E., Hayes J. C. and Mann H. M. (1954), *Permeability of Portland Cement Paste*, Journal of the American Concrete Institute, Vol. 51, pp. 285-298

Ramachandran V. S. and Feldman R. F. (1967), *Length Change Characteristics of Ca(OH)2 Compacts on Exposure to Water Vapor*, Journal of Applied Chemistry, Vol. 17, pp. 328-332

Ramachandran V. S., Feldman R. F. and Beaudoin J.J. (1981), *Microstructure of cement paste: the role of water*, Concrete Science, Treatise on current research, pp. 1-24, pp. 25-53 and pp. 54-90.

Ramachandran V. S., Feldman R. F. and Beaudoin J.J. (1981), *Microstructure and Strength Development*, Concrete Science, Treatise on current research, pp. 25-53.

Rayment D. L. and Majumdar A. J. (1982), *Title*, Cement and Concrete Research, Vol. 12, p. 753

Regourd M., Hornain H. and Mortureux B. (1976), *Evidence of calcium silicoaluminates in hydrated mixtures of tricalcium silicate and tricalcium aluminate*, Cement and Concrete research, Vol. 6, pp. 733-740.

Richardson I. G. and Groves G. W. (1992), *Models for the composition and structure of calcium silicate hydrates (CSH) gel in hardened tricalcium silicate pastes*, Cement and Concrete Research, vol. 22, pp. 1001-1010.

Richardson I. G. and Groves J. W. (1993), *Title*, Journal of Materials Research, Vol. 28, p. 265

Roll F. (1968), *The Relation Between Time-Dependent and Residual Deformation of Unsealed Concrete, Mortar and Paste Under Uniformly Distributed Stress*, Proceeding Conference on Structure of Concrete and Its Behavior Under Load, London, pp. 434-447

Roper H. (1966), *Dimensional Change and Water Sorption Studies of Cement Paste*, Highway Research Bulletin, Special Report, No. 90, pp. 74-83

Roper H. (1968), *Cement Paste Shrinkage-Relationships to Hydration, Young's Modulus and Concrete Shrinkage*, Proceeding Symposium on Chemistry of Cement, Tokyo, 3

Ross, A.D. (1959), *A note on the maturity and creep of concrete*, RILEM Bulletin, pp. 55-57

Roy D. M. and Gouda G. R. (1973), *Porosity-Strength Relation in cementitious materials with very high strength*, Journal of American Ceramic Society, Vol. 56, No. 10, pp. 549-550

Ruetz W. (1968), *A Hypothesis for the Creep of Hardened Cement Paste and the Influence of Simultaneous Shrinkage*, International Conference On the Structure of Concrete, Cement and Concrete Association, London, England, pp. 365-387

Sabri S. and Illston J.M. (1982), *Isothermal Drying Shrinkage and Wetting Swelling of Hardened Cement Paste*, in Fundamental Research on Creep and Shrinkage of Concrete, Edited by Wittmann, pp. 63-72

Scuderi, C.A.; Mason, T.O. and Jennings, H.M. (1991), *Impedance Spectra of Hydrating Cement Pastes*, Journal of Mater. Sci., Vol. 26, pp. 349-353

Sereda P. J., Feldman R. F. and Swenson E. G. (1966), *Effect of Sorbed Water on Some Mechanical Properties of Hydrated Cement Pastes and Compacts*, Highway Research Bulletin, Special Report, No. 90, pp. 58-73

Setzer M. J. and Wittmann F. H. (1974), *Applied Physics*, Vol. 3, p. 403

Slate F. O and Meyers B. L. (1971), *Some Physical Processes Involved in Creep of Concrete*, Proc. Civil Eng. Mat. Conf., London, Wiley-Interscience, Part 1, pp. 769-773

Sluyters-Rehbach M. and Sluyters J. H. (1990), *in Electroanalytical Chemistry*, Vol. 4, Edit. A. J. Bard, Marcel Dekker, New York, pp. 1-125

Soroka I. (1979), *Portland Cement Paste and Concrete*, The MacMillan Press Ltd., 338p.

Spooner D. C. (1972), *The Stress-Strain Relationship for Hardened Cement Pastes in Compression*, Magazine of Concrete Research, Vol. 24, No. 79, pp. 85-92

Spriggs F. P. (1962), *Effect of Porosity on Young's Modulus of Alumina*, Journal of American Ceramic Society, Vol. 45, No. 2, pp. 94-95

Sybertz F. (1989), *Comparison of Different Methods for Testing the Pozzolanic Activity of Fly Ashes*, In: Malhotra, V Edition, Proceeding of the 3rd International Congress on Fly Ash, Silica Fume, Slag, and Natural Pozzolans in Concrete, Trondheim, American Concrete Institute Special Publication 114, Vol. I, pp. 477-497

Sychev M. M. (1974), *Regularities of binding property manifestation*, Proceeding of the Sixth International Congress on the Chemistry of Cement, Moscow, Vol. II, Book 1, pp. 42-57

Taylor H. F. W. (1990), *Cement Chemistry*, Academic Press, 475 p.

Taylor H. F. W. and Newbury D. E. (1984), *Title*, Cement and Concrete Research, Vol. 14, p. 565

Taylor H. F. W. and Turner A. B. (1987), *Reactions of Tricalcium Silicate Paste with Organic Liquids*, Cement and Concrete Research, Vol. 17, No. 4, pp. 613-623

Thomas M. D. A. (1989), *The Suitability of Solvent Exchange Techniques for Studying the Pore Structure of Hardened Cement Paste*, Advances in Cement Research, Vol. 2, No. 5, pp. 29-34

Tien Chao-wu (1984), Electrochemistry Research Methods, Chapter 8, 2nd Edition, Scientific Publisher, China

Uchikawa H., Uchida S. and Hanehara S. (1987), *Title*, Il Cemento, Vol. 84, pp. 117-

Uchikawa H., Uchida S. and Mihara S. (1970), Characterization of Hydrated Ultra Rapid Hardening Cement Pastes, Il Cemento, Vol. 63, No. 1, pp. 59-70.

Ulm, F.J.; Le Maou, F. and Boulay, C. (1999), *Creep and Shrinkage Coupling: New Review of Some Evidence*, Revue Française de Génie Civil, No. 3, Vol. 3-4, pp. 21-37

Verbeck G. J. and Helmuth R. A. (1968), *Structure and Physical Properties of Cement Paste*, Proceeding Symposium on Chemistry of Cement, Tokyo, 3, pp. 1-37

Vernet, C. and Cadoret, G. (1991), *Suivi en continu de l'évolution chimique et mécanique des BHP pendant les premiers jours*, Les Bétons à Hautes Performances: Caractérisation, durabilité, applications, sous la direction d'Yves Malier, Presses de l'école nationale des Ponts et Chaussées, Paris, pp. 115-128

Winslow D.W. and Diamond S. (1974), *Specific Surface of Hardened Portland Cement Paste as Determined by Small-Angle X-ray Scattering*, Journal of The American Ceramic Society, Vol. 57, No. 5, pp. 193-197

Wittmann F. H. (1968), *Surface Tension, Shrinkage and Strength of Hardened Cement Paste*, Materials and Structure, Vol. 1, No. 6, pp. 547-552

Wittmann F. H. (1970), *The Effect of Moisture Content on Creep of Hardened Cement Pastes*, Reol. Acta, Vol. 9, No. 2, pp. 282-287

Wittmann F. H. (1971), *Discussion of Some Factors Influencing Creep of Concrete*, Research Series III-Building, No. 167, The State Institute for Technical Research, Finland

Wittmann F. H. (1973), *Interaction of Hardened Cement Paste and Water*, Journal of American Ceramic Society, Vol. 56, No. 8, pp. 409-415

Wittmann F. H. (1973), *Observation of an Electromechanical Effect of Hydrated Cement Paste*, Cement and Concrete Research, Vol. 3, No. 5, pp. 601-605

Wittmann F. H. (1976), *The structure of hardened cement paste-a basis for better understanding of the materials properties*, in Hydraulic Cement Pastes: Their Structure and Properties, Cement and Concrete Association, Wexham Springs, Slough, UK, pp. 96-117.

Wittmann F. H. (1977), *Principles of Model Describing the Characteristic Properties of Concrete*, Deutcher Ausschuss fur Stahlbeton, No. 290, Wilhelm Ernst u. Sohn, Berlin, pp. 43-101

Wittmann F. H. (1982), *Creep and Shrinkage Mechanisms*, Creep and Shrinkage in Concrete Structures, Edited by Z. P. Bazant and F. H. Wittmann, pp. 129-161

Xi Y. and Jennings H. M. (1992), *Relationships Between Microstructure and Creep and Shrinkage of Cement Paste*, Materials Science of Concrete III. pp. 37-63.

Xie P., Gu P., Xu Z. and Beaudoin J. J. (1993), *A Rationalized AC Impedance Model for Microstructural Characterization of Hydrating Cement Systems*, Cement and Concrete Research, Vol. 23, No. 2, pp. 359-367

Xu Z., Gu P., Xie P. and Beaudoin J. J. (1993), *Application of A.C. Impedance Techniques in Studies of Porous Cementitious Materials (II). Relationship Between ACIS Behavior and the Porous Microstructure*, Cement and Concrete Research, Vol. 25, No. 4, pp. 853-862

Young J. F. (1974), *An Assessment of the Influence of Microstructure on Time-Dependent Deformations of Hardened Cement Paste*, Proceedings, First Australian Conference on Engineering Materials, The University of New South Wales, pp. 3-28.

Young J. F. (1982), *The Microstructure of Hardened Portland Cement Paste*, Creep and Shrinkage in Concrete Structures, Edited by Z.P. Bazant and F. H. Wittmann, John Wiley & Sons Ltd., New-York, pp. 3-22.

Yuan L., Li J. F. and Viehland D. J. (1995), American Ceramic Society, Vol. 78, pp. 3233-3243

Yudenfeund M., Skalny J., Mikhail R. S. and Brunauer S. (1972), *Hardened Portland Cement Paste of Low Porosity II. Exploratory Studies of Dimensional Changes*, Cement and Concrete Research, Vol. 2, No. 3, pp. 331-348.